TECHNISCHE UNIVERSITÄT MÜNCHEN

Fakultät für Medizin

Aberrant cell cycle regulatory ubiquitin networks in B-cell malignancies

Ria Andrea Spallek (M.Sc.)

Vollständiger Abdruck der von der Fakultät für Medizin der Technischen Universität München zur Erlangung des akademischen Grades einer

Doktorin der Naturwissenschaften (Dr. rer. nat.)

genehmigten Dissertation.

Vorsitzender: Prof. Dr. Maximilian Reichert

Prüfer der Dissertation:

1. Prof. Dr. Florian Bassermann
2. Prof. Dr. Bernhard Küster
3. Prof. Dr. Sebastian Theurich

Die Dissertation wurde am 31.03.2022 bei der Technischen Universität München eingereicht und durch die Fakultät für Medizin am 13.12.2022 angenommen.

Table of Contents

Abbreviations ..... *V*

Summary *1*

1 Introduction *3*

1.1 B-cell derived malignancies **3**

1.2 Cells of origin **3**

1.3 B-cell lymphomagenesis **5**

1.3.1 Diffuse Large B-cell Lymphoma (DLBCL) 6

1.3.2 Multiple Myeloma 7

1.4 The Ubiquitin-Proteasome system **11**

1.4.1 E3-Ubiquitin-Ligases 12

1.4.2 KLHL14 14

1.4.3 Deubiquitylases (DUBs) 15

1.4.4 OTUD6B 15

1.5 Cell cycle **16**

1.5.1 Centrosome and microtubule regulation throughout mitosis 18

1.5.2 The DNA damage response (DDR) 21

1.5.3 DNA damage and genomic instability during mitosis 21

1.6 The UPS in NF-κB signaling **24**

1.6.1 UPS dependent pathway activation 24

1.6.2 UPS dependent NF-κB regulation in the nucleus 25

2. Aim of this study *26*

3 Material *27*

3.1 Devices and Instruments **27**

3.2 Consumables **28**

3.3 Chemicals and Reagents **28**

3.4 Commercial Kits **30**

3.5 Enzymes **31**

3.6 Oligonucleotides **31**

3.7 Bacteria **33**

3.8 Standards **33**

3.9 Plasmids **33**

3.10 Antibodies **34**

3.11 Cell Lines **35**

3.12 Tissue Culture Media and Supplements **36**

3.13 Buffers and Solutions **36**

3.14 Software and Databases **38**

4. Methods *39*

4.1. Molecular biology **39**

4.1.1. Molecular cloning 39

4.1.2 Polymerase chain reaction (PCR) 39

4.1.3 Mutagenesis PCR (SNP, two step deletions) ... 40
4.1.4 Agarose gel electrophoresis and gel purification ... 40
4.1.5 Restriction digest and ligation of DNA ... 41
4.1.6 Annealing and ligation of short hairpin RNA-oligonucleotides ... 41
4.1.7 In-fusion cloning ... 41
4.1.8 Transformation of plasmids into bacteria ... 41
4.1.9. Plasmid DNA extraction from bacteria ... 42
4.2 Cell culture and cell-based assays ... 42
4.2.1 Culture of eukaryotic cells ... 42
4.2.2 Freezing and thawing of cells ... 42
4.2.3. Harvesting of cells ... 43
4.2.4 Transient transfection of cells with DNA ... 43
4.2.5 Transient transfection of cells with siRNA ... 43
4.2.6 Production of lentiviral particles and viral transduction of cells ... 43
4.2.7 Doxycycline treatment for transgene expression ... 44
4.2.8 Inhibitor treatment in protein stability assays (Cycloheximide, MG132, MLN4924) ... 44
4.2.9 NF-κB stimulation in various cell lines and primary murine B-cells ... 44
4.2.10 Luciferase assay ... 45
4.2.11 Synchronization of cells in different cell cycle phases ... 45
4.3 Flow cytometry ... 46
4.3.1 Flow cytometry of cells transduced with GFP or RFP ... 46
4.3.2 Cell cycle analysis using flow cytometry ... 46
4.4 Immunofluorescence ... 47
4.4.1 Immunofluorescence of adherent cells ... 47
4.4.2 Immunofluorescence of non- adherent cells ... 47
4.5 Protein Biochemistry ... 48
4.6 Statistical Analysis ... 54
5. Results KLHL14 ... 55
5.1 KLHL14 is a tumor suppressor in B-cell derived malignancies ... 55
5.2 KLHL14 overexpression causes DNA damage and G1 restriction point arrest ... 60
5.3 KLHL14 localizes to the mitotic centrosomes and spindle ... 68
5.3.1 Overexpressed KLHL14 localizes in distinct foci ... 68
5.3.2 Endogenous KLHL14 is recruited to the centrosome in G2/M phase ... 69
5.4 KLHL14 in murine B-cell activation and lymphoma ... 78
5.5 MS based interactome analysis reveals possible KLHL14 substrates ... 82
6. Discussion KLHL14 ... 91
6.1 The tumor suppressive function of KLHL14 in MM does not rely on BCR signaling ... 91
6.2 Prolonged KLHL14 overexpression causes G1/G0 arrest ... 92
6.5 KLHL14 in murine B-cells ... 94
6.6 Implications of KLHL14 in the organization of the cytoskeleton ... 95
7. Results OTUD6B ... 97
7.1. Ectopic expression of LIN28B rescues the G1/S transition defect in OTUD6B depleted cells ... 97
7.2 LIN28B binding at the G1/S transition determines OTUD6B activity ... 99
7.3 Identification and characterization of LIN28B phosphorylation sites ... 100

7.4 CDK9 activity mediates LIN28B and OTUD6B interaction 102
8. Discussion OTUD6B 105
9. Results FBXO21 108
9.1 Previous Data FBXO21 108
9.2 p50 does not interact with FBXO21 and is not destabilized upon cycloheximide treatment 110
9.3 NF-κB1/p50 is not ubiquitylated or degraded in murine BCL-3-/- cells 117
9.4 FBXO21 does not influence NF-κB activity in MCF-7 cells 120
10. Discussion FBXO21 122
10.1 Endogenous p50 does interact with FBXO21 123
10.2 FBXO21 does not influence p50 protein levels or 124
10.3 p50 is not polyubiquitylated in BCL-3 knock out cells 125
11. Acknowledgments 126
12. Publication 126
13. References 127

Abbreviations

°C	degree Celsius
A	alanine
AA	amino acid
ABC	activated B cell-like
AID	activation-induced deaminase
AML	acute myeloid leukemia
AMP	adenosin-5'-monophosphate
April	a proliferation-inducing ligand
ASCT	autologous stem cell transplantation
BAFF	B cell activation factor belonging to the TNF family
BCR	B cell receptor
BM	bone marrow
bp	base pair
BrdU	5-bromo-2′-deoxyuridine
C	cysteine
CD40L	CD40 Ligand
CDK	Cyclin-dependent kinase
cDNA	complementary DNA
Chk	Checkpoint kinase
CHX	cycloheximide
CIP	calf intestinal phosphatase
CKI	CDK inhibitor
CLP	common lymphoid progenitor cell
CP	core particle
CRISPR	clustered regularly interspaced short palindromic repeats
CRL	Cullin-RING ligase
CSR	class switch recombination
Ctrl	control
CUL	Cullin
DLBCL	diffuse large B cell lymphoma
DMSO	dimethyl sulfoxide
DNA	deoxyribonucleic acid
DUB	deubiquitylase
E. coli	Escherichia coli
ESC	embryonic stem cell
EV	empty vector
FACS	fluorescence activated cell sorting
FBXL	F-box and Leu-rich repeat
FBXO	F-box only
FBXW	F-box and WD40 domain
FITC	fluorescein isothiocyanate
FSC	forward scatter
fw	forward
G	glycine
GC	germinal center
GCB	germinal center B cell-like
GFP	green fluorescent protein
H/His	histidine
h, hrs	hour, hours
HA	hemagglutinin
HECT	homologous to E6AP C-terminus
HSC	Hematopoietic stem cell
IF	immunofluorescence
Ig	immunoglobulin
IgH	immunoglobulin heavy chain
IgL	immunoglobulin light chain
IκB	NF-κB inhibitor
IL	interleukin
IP	immunoprecipitation
K	lysine
kb	kilobase
kDa	kilodalton
LE	long exposure
LFQ	label-free quantification
LPS	lipopolysaccharide
LRR	leucine rich repeat
M	molar
MACS	magnetic activated cell sorting
MCL	mantle cell lymphoma
MGUS	monoclonal gammopathy of undetermined significance
min	minute
mM	millimolar
MM	multiple myeloma
mRNA	messenger RNA
MS	mass spectrometry
MT	microtubule
MTOC	microtubule organizing center
MW	molecular weight
n	number
NF-κB	nuclear factor kappa-light-chain-enhancer of activated B cells
nM	nanomolar
NSCLC	non–small cell lung cancer
NT	non-targeting
oligo	oligonucleotide
OTU	ovarian tumor
PAGE	polyacrylamide gel electrophoresis
PC	plasma cell
PCM	pericentriolar material
PCR	polymerase chain reaction
PFA	paraformaldehyde
PI	propidium iodide
PTM	post-translational modification
PVDF	polyvinylidene fluoride
RAG	recombinase-activating gene
RBR	RING-between-RING
RBX1	RING-box protein 1
RING	really interesting new gene
RNA	ribonucleic acid
RNAi	RNA interference
RP	regulatory particle
rpm	revolution per minute
RT	room temperature

rv	reverse
S	serine
S.D.	standard deviation
SCF	SKP1-CUL1-F-box protein
SDS	sodium dodecyl sulfate
SE	short exposure
sec	second
SHM	somatic hypermutation
shRNA	short hairpin RNA
siRNA	small interfering RNA
SKP	S phase kinase-associated protein
SMM	smoldering multiple myeloma
SSC	sideward scatter
TuRC	tubulin ring complex
TF	transcription factor
Ub	ubiquitin
UCH	ubiquitin C-terminal hydrolase
ULP	ubiquitin-like protease
UPS	ubiquitin proteasome system
USP	ubiquitin-specific protease
UV	ultraviolet
V	volt
VS	vinyl sulfone
w/v	weight per volume
WCE	whole cell extract
WT	wildtype

Summary

B-cell derived malignancies are biologically and clinically very heterogeneous disorders, which originate from B-cells at various stages of development and activation (Küppers 2005) and account for approximately 95% of all lymphomas. Most of them, like Diffuse Large B-Cell Lymphoma (DLBCL) as well as Multiple Myeloma (MM), are derived from germinal center or post germinal center B-cells (Demchenko and Kuehl, 2010; Young and Staudt, 2013; Young *et al.*, 2015; Chapuy *et al.*, 2018; Schmitz *et al.*, 2018). Due to the central role of the Ubiquitin Proteasome System (UPS) in NF-κB-signaling, a key signaling pathway in normal differentiation as well as oncogenic transformation processes (Schmitz et al. 2018; Stebegg et al. 2018a), and the substantial responsiveness of MM patients towards proteasomal inhibition (Guerrero-Garcia et al. 2018; Kumar et al. 2017), it is believed that aberrant functions of the UPS may drive and maintain these disease types. Even though the treatment options for B-cell derived malignancies evolved during recent years, most subtypes remain uncurbable and novel therapeutic targets are highly demanded (Frontzek and Lenz 2019; Lange, Lenz, and Burkhardt 2017; Mikhael et al. 2019; Kumar et al. 2017).

Striving to uncover novel UPS members, that are frequently deregulated in hematological malignancies, the CUL3 ubiquitin ligase KLHL14 was identified as a potential tumor suppressor by screening of large patient cohorts. The tumor suppressive functions of the BTB-protein could be validated in various MM as well as DLCBL cell lines, but was not seen in other than B-cell derived tumor entities. The overexpression of KLHL14 resulted in an accumulation of DNA damage followed by a G1/G0 cell cycle arrest and a sensitization of the cells to the CDK4/6 inhibitor palbociclib. Immunofluorescence studies of endogenous KLHL14 in human DLBCL cell lines as well as cells of a genetic lymphoma mouse model, revealed a recruitment of the protein to the centrosomes and the mitotic spindle during mitosis, indicating that the DNA damage detected upon KLHL14 overexpression could stem from errors during this cell cycle phase. Additionally, first attempts to identify ubiquitylation substrates of the CUL3-ligase by mass spectrometric screening, identified multiple mitotic regulators as interactors, further strengthening the hypothesis that KLHL14 exerted its tumor suppressive function during mitosis. During the investigation into the physiological role of KLHL14 during B-cell development and activation, it could be shown that splenic murine B-cells strongly downregulated KLHL14 protein levels upon BCR- and TLR-mediated *ex-vivo* activation, suggesting that KLHL14 acts as a safeguard against untimely B-cell activation and proliferation *in vivo*.

Starting from preliminary work by former lab member C. Paulmann, the second part of this thesis focusses on the mechanism by which the G1/S specific activity of the DUB OTUD6B, which was recently identified as an oncogene in MM, is mediated and whether the substrate LIN28B identified by Paulmann and colleagues was responsible for the described phenotype (Paulmann et.al. under review). Using a rescue experiment, it could be shown that LIN28B, was indeed responsible for the progression of MM cells from G1- to the S-phase of the cell cycle. The interaction of the DUB-substrate pair was demonstrated to be G1/S transition specific and to result in elevated OTUD6B activity, a so far undescribed mechanism of DUB activation. As the interaction of the DUB-substrate pair depended on the phosphorylation of the substrate LIN28B (Paulmann et.al. under review), mass spectrometry-based screens for possible phosphorylation sites on LIN28B and the responsible kinase were performed. The proline directed kinase CDK9 could be identified as an interactor of LIN28B and a mediator of DUB-substrate binding, as pharmacological as well as genetic inactivation of CDK9 resulted

in reduced interaction. Even though multiple phosphorylation sites within the LIN28B protein could be identified and characterized, the exact site responsible for the interaction remains to be determined.

The last part of this thesis was designated to the identify the E3-ubiquitin ligase responsible for the ubiquitylation and proteasomal degradation of NF-κB1/p50 described by Carmody et al. in 2007 (Carmody et al. 2007). Following up on data of the former group members U. Baumann and B. Targosz, the influence of the SCF-complex substrate adaptor FBXO21 on NF-κB1/p50 and NF-κB signaling in general was investigated. Therefore, data implicating the Fbox-protein were reevaluated but no specific interaction between p50 and FBXO21 in an endogenous or semi-endogenous setting could be detected. Neither genetic depletion nor forced expression of FBXO21 led to changes in p50 protein stability or in NF-κB signaling in general as assessed by immunoblot, EMSA and luciferase reporter assays. Additionally, the published ubiquitylation and proteasomal degradation of p50, which was descried to be counteracted by the nuclear IκB BCL3 (Carmody et al. 2007; Collins, Kiely, and Carmody 2014), could not be detected in BCL3 knock out murine embryonic fibroblasts (MEFs), resulting in the presumption that the protein was not polyubiquitylated and degraded in a general cellular context.

Taken together, the data presented in this thesis uncover and characterize KLHL14 as a tumor suppressor exclusive for B-cell derived malignancies even in the absence of active NF-κB signaling, delineate LIN28B and a CDK9 dependent phosphorylation event as activators of the oncogenic DUB OTUD6B driving the G1/S transition in MM cells and finally, refute the hypothesis that NF-κB1/p50 is ubiquitylated and degraded by the proteasome.

1 Introduction

1.1 B-cell derived malignancies

Tumors of the hematopoietic and lymphoid tissues, often referred to as hematologic neoplasms or malignancies, originate from uncontrolled growth and a lack of differentiation of cells of either myeloid or lymphoid origin. While the myeloid branch of the hematopoietic system is responsible for the production of erythrocytes, the cells derived from the other branch of the blood forming system are called lymphocytes and represent the cellular parts of the immune system (Chaplin 2010; Herzog, Reth, and Jumaa 2009). The biologically very heterogeneous disorders originating from the latter account for 6.5% of all cancers worldwide (Tietsche de Moraes Hungria et al. 2019) and make up an estimated 9.8% of newly diagnosed cancer cases in 2021 in the US (ils.org; American cancer society: cancer.org). Approximately 95% of lymphomas originate from B-cells at various stages of development, the rest are of T-cell origin (Küppers 2005).

1.2 Cells of origin

B-cells make up about 15% of lymphocytes in the peripheral blood and are defined by their ability to produce immunoglobulins or antibodies. Immunoglobulins are secreted proteins that specifically recognize and neutralize pathogens via the recognition of pathogen specific molecules called antigens (T. Yoshida et al. 2010). Therefore, the diversity of B-cell antigen receptors (surface immunoglobulin) also known as B-cell receptors (BCRs) is of great importance. During B-cell development from so called common lymphoid progenitors (CLPs) (Blom and Spits 2006), these proteins are generated by random rearrangements of gene segments encoding the immunoglobulin heavy and light chain (IgH and IgL). This reshuffling is possible because the subunits are assembled from genetic loci that contain multiple exons or coding regions that are functionally redundant. Loci for both chains are composed of a series of V elements (variable), followed by D (diversity) segments (in case of the heavy chain), J (joining) segments, and finally C (constant) regions (Chaplin 2010; Blom and Spits 2006). The genetic rearrangements of genetic heavy and light chain occur sequentially and intermitted by different selection and proliferation steps but follow a universal mechanism(Herzog, Reth, and Jumaa 2009). Herein a complex comprised of RAG1 (recombination-activating gene 1) and RAG2 induces DNA double-strand breaks at specific sites in-between the segments that are to be recombined (Herzog, Reth, and Jumaa 2009). These nicks in the DNA are then repaired via non-homologous end joining (NHEJ), thereby excising the unused redundant gene segments. During this process an enzyme called terminal deoxynucleotidyl transferase (TdT) is active and adds random nucleotides to the junctions between the recombined gene parts, in doing so generating additional heterogeneity to the rejoined junctions(Chaplin 2010). In case, this fusion process results in a functional, in-frame transcript the protein Igμ is translated and expressed as part of the pre-B-cell-receptor (pre-BCR) signaling complex. Once functionally assembled and activated, pre-BCR signaling via the tyrosine kinase SYK leads to proliferation of the pre-B-cell (clonal proliferation/ expansion) and the recombination machinery including RAG proteins is downregulated(Melchers 2015).

In a feedback loop, this signaling results in the downregulation of pre-BCR components, which ultimately stops proliferation and enables the recombination of IgL gene cluster(Herzog, Reth, and Jumaa 2009) using the same recombinase machinery as described

for the IgH gene locus. Once the V_L and the J_L gene segments are recombined successfully and paired with the heavy chain, the now immature B-cell expresses an antigen-binding competent B-cell receptor (BCR) of either IgG or IgM class on the cell surface(Chaplin 2010). As these gene rearrangements occur at random and are designated to create as much diversity as possible to ensure antigen recognition, B-cells expressing receptors with autoreactive BCRs can be generated and are subsequently eliminated by negative selection. Interestingly, it is estimated that over 85% of immature B-cells are left to die in the bone marrow, because they recognize endogenous antigens, so called autoantigen (Rolink, Andersson, and Melchers 1998). Once this second hurdle for B-cells with a functional, non-autoreactive BCR is taken, the non-dividing mature B-cells are released into circulation and home to the follicular regions of the secondary lymphoid organs like the spleen and lymph nodes(Melchers 2015; Chaplin 2010).

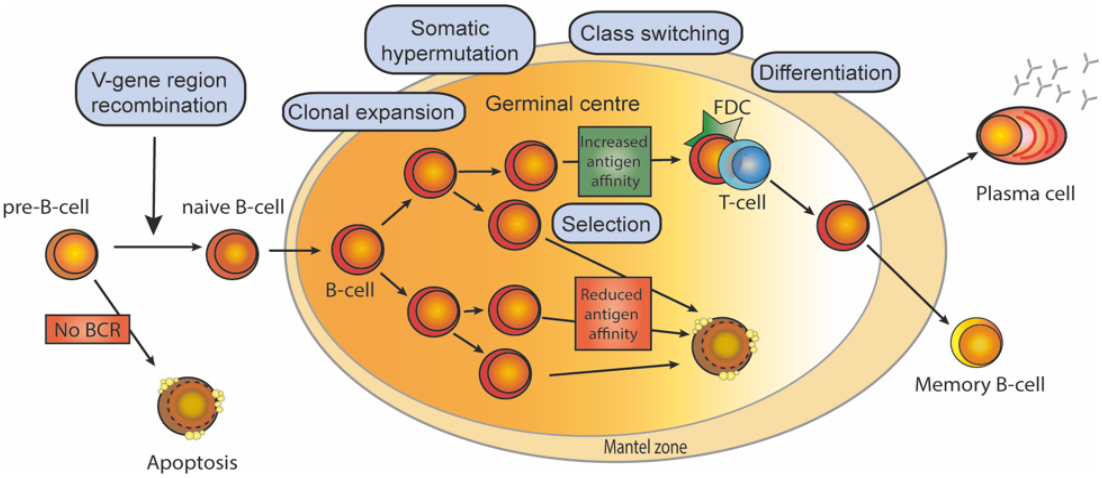

Figure 1. **B-cell differentiation in the germinal-center**. Mature naive B cells form the early germinal centers (GC) in secondary lymphoid organs upon antigen-activation, in which they differentiate and undergo clonal expansion until the mature GC is established. During this proliferation step, somatic hypermutation (SHM) takes place to introduce diversity into the V(D)J region of the rearranged immunoglobulin variable region (IgV) genes. Large parts of these mutations are disadvantageous for the proliferating B-cells, such as those that reduce the antigen affinity of the BCR and will therefore lead to apoptosis of the cells. GC B-cells that happened to acquire favorable mutation that enhance the BCRs affinity for the antigen, will be positively selected with the help of T-cells and follicular dendritic cells (FDCs) in close proximity. A subset of the positively selected GC B-cells undergoes class-switch recombination and differentiate into memory B cells or plasma cells and leave the GCs. (Figure adapted from Basso and Dalla-Favera 2015 and Küppers 2005)

These zones enriched in B-cells enable efficient activation through interactions with antigen presenting cells (APCs) and T-cells and are therefore the main site of activation, somatic mutation, and selection of high-affinity B cells. For this activation, an anatomical microstructure within the secondary lymphoid organs, a so called germinal center (GC) is formed, where B-cells, that encounter an antigen, interact with and stimulate T-cells (Stebegg et al. 2018b; Chaplin 2010). Stimulated by signaling originating from this interaction mainly via CD40, B-cells start to divide and either initiate the germinal center reaction or differentiate into short-lived extrafollicular plasma or memory B cells. Plasma cells are specialized in producing the soluble form of the BCR – so called antibodies – which are secreted and represent the humoral part of the immune system (Figure 1). The initial plasma and memory B-cells have a rather low affinity towards the designated antigens and usually undergo apoptosis within a few days (Stebegg et al. 2018b). Most of the stimulated B-cells will enter the germinal center reaction in which they undergo massive proliferation and somatic hypermutation (SHM) paired with repeated selection to improve their antigen binding capacity, a process called affinity

maturation(De Silva and Klein 2015). Therefore, an enzyme called activation-induced cytidine deaminase (AID) is expressed, that induces random mutations of the variable regions (V_H and V_L) of the IgH and IgL chain genes. The same enzyme enables the BCRs/antibodies to class switch from IgM or IgD to either IgG, IgA or IgE by rearranging the constant (C) region of the IgH gene locus. This change in immunoglobulin isotype allows the generation of antibodies with different effector functions and ultimately leads to the terminal differentiation to long lived plasma cells and memory B-Cells in the bone marrow (Stebegg et al. 2018b; De Silva and Klein 2015; O'Connor et al. 2003).

1.3 B-cell lymphomagenesis

The development of B-cells towards the production of high-affinity antibodies is hallmarked by a sequence of genetic rearrangements and random somatic mutations intermitted by or combined with clonal expansion. This combination of extreme genomic instability and proliferation facilitates the high diversity of B-cells and antibodies on one hand but also poses a great risk for malignant transformation (Figure 2)(Basso and Dalla-Favera 2015). The reasons for this transformation are often but not exclusively chromosomal translocations, in which a proto-oncogene is put under the control of an highly active immunoglobulin promotor causing a permanent, deregulated expression of the oncogene (Küppers 2005). In addition to these chromosomal translocations, SHM driven by AID can cause mutations outside of the immunoglobulin loci, so called aberrant SHM, affecting genes like BCL2, PIM1 and MYD88 and thereby contributing to malignant transformation (Alexandrov et al. 2013; Chapuy et al. 2018). The different stages of B-cell development and activation are defined by a specific type of BCR or differentiation marker on the cells' surface and distinct gene expression patterns.

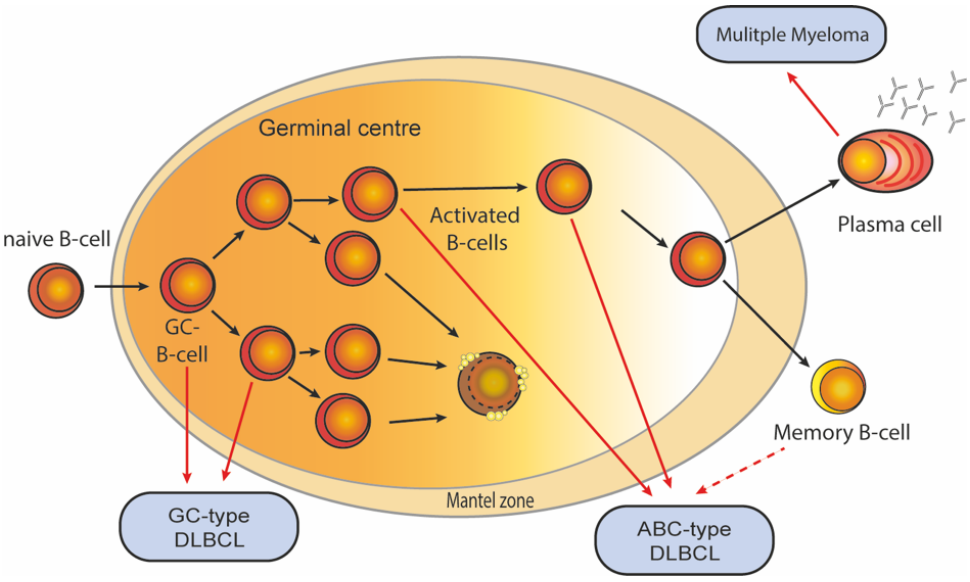

Figure 2. Proposed cellular origins of DLBCLs and Multiple Myeloma. Due to their molecular characteristics, human B-cell malignancies can be matched to a B-cell of origin. Most lymphomas arise from GC or post GC B-cells like DLBCL of the germinal center or the activated B-cell (ABC) type DLBCL, which can be distinguished by their gene expression signatures. Multiple Myeloma derives from plasma cell precursors or terminally differentiated plasma cells, that home to the bone marrow instead of the GCs. Black arrows indicate the B-cell differentiation steps as outlined in Figure 1, while the red arrows assign the different malignancies to a proposed non-transformed counterpart. (Figure adapted from Küppers 2005)

These (surface) markers often remain present after malignant transformation and reflect the different stages B-cell lymphomas arise from (Küppers 2005). Therefore, it is widely believed that most B-cell lymphomas originate from germinal center or post-germinal center B-Cells (Figure 2) (Küppers 2005; Basso and Dalla-Favera 2015).

Whole exome and mRNA sequencing of large patient cohorts have recently helped to define distinct mutational landscapes and mRNA-expression profiles which lead to a refinement of the disease sub-classifications, but also to an understanding of the unprecedented heterogeneity of these tumors(Izzo and Landau 2016; F. C. Chan et al. 2018). Two particular B-cell lymphoma types, that are relevant for this work, are discussed below, including their development, molecular characteristics and treatment options.

1.3.1 Diffuse Large B-cell Lymphoma (DLBCL)

With approximately 40% of newly diagnosed lymphoma cases in adults, DLBCL is considered the most common subtype of non-Hodgkin lymphoma (NHL). The relative 5 year survival is 47.9%(Morton et al. 2006; Han et al. 2008). The cell of origin of this type of lymphoma are large B-cells found in the GC during B-cell development/activation and common pathogenic aberrations include deregulation of BCL6 and chromatin modifiers like EP300, MLL2 and CREBBP. Even though depicted as a single entity, it is important to note that DLBCLs are very heterogenous(Basso and Dalla-Favera 2015). This holds true not only for their clinical progression but also molecular characteristics, mutational landscapes and signaling dependencies. To date massive parallel sequencing efforts are giving further insight into the complex disease pathology, which means that the classification system is still under constant refinement. Historically the most prominent subgroups are called germinal center like (GCB) and activated B-cell like (ABC) DLBCLs. Cases that do not fit the criteria of either subgroup, were previously described as unclassified or not otherwise specified (NOS) and amounted to about 10-20% of cases(Schmitz et al. 2018; Chapuy et al. 2018; King and Bagg 2014). Even though ABC-type DLBCL patients have a significantly inferior prognosis compared to patients with GCB-type DLBCL and pathological mechanisms are clearly distinct, the standard of care treatment for both subtypes remains a combination therapy of rituximab, cyclophosphamide, doxorubicin, vincristine and prednisone (R-CHOP). This therapy leads to a durable remission of the disease in about 60% of DLBCL patients(King and Bagg 2014). In case patients present younger, this therapy regime is complemented with etoposide (R-CHOEP), as these patients can be treated more aggressively (Frontzek and Lenz 2019; Lange, Lenz, and Burkhardt 2017).

GCB-type DLBCLs, which have clinically often a more favorable outcome, originate from Large B-cells residing in the GC light zone (Figure 2). One hallmark of this subgroup is the translocation of the transcription factors MYC and BCL2, putting them under the control of the IgH enhancer element. These aberrations are detected in 10% and 40% of cases respectively. Another frequent mechanism is the gain of function mutation of the methyltransferase EZH2 (mutated in 21% of cases), which leads to transcriptional repression of CDKN1A, IFR4 and PRMDI which further abrogates post-GC differentiation and promotes proliferation(Basso and Dalla-Favera 2015; Schmitz et al. 2018; Chapuy et al. 2018). Novel therapy strategies for the GCB subtype include EZH2-Inhibitors(McCabe et al. 2012) and BCL2 inhibitors like ABT-737 and ABT-199, the latter especially for so called double hit lymphomas, where BCL2 and MYC/BCL6 are deregulated(Kang and Reynolds 2009; Frontzek and Lenz 2019).

ABC-DLBCLs show a gene expression pattern that closely resembles the one of activated B-cells which are already committed to plasma cell differentiation, hinting towards a malignant transformation at this stage of B-cell activation(Alizadeh et al. 2000). The pathogenesis of this subtype is defined by chronic active NFκB signaling, paired with the blockage of terminal plasma cell differentiation(Basso and Dalla-Favera 2015). A hallmark of this subtype seems to be a gain in chromosome 18q, which leads to amplification of lymphoma drivers like BCL2 and MALT1 (Chapuy et al. 2018). NFκB signaling in these cell is mainly driven by aberrant BCR signaling mediated through mutations in CD79A or CD79B (approx. 20% of cases), a gain of function in MYD88 (approx. 35% of cases) and activating mutations in CARD11, that uncouple NFκB activation from BCR stimulation (approx. 10% of cases)(Lenz et al. 2008). While the afore mentioned mutations are activating ones (gain of functions), there are several loss of function mutations contributing to ABC-type DLBCL pathogenesis. In 30% of the cases for example A20, an important negative regulator of this particular pathway, is inactivated(Schmitz et al. 2018; Young et al. 2015; Chapuy et al. 2018). Another important loss of function, which is instrumental for the blockade of terminal plasma cell differentiation, is mediated by the inhibition of BLIMP1 (encoded by the PRMD1 gene)(Basso and Dalla-Favera 2015) via a variety of mechanisms. In approx. 30% of ABC type DLBCL cases the PRDM1 gene is mutated, truncated or biallelically deleted(Mandelbaum et al. 2010), furthermore the dysregulation of BCL6 as discussed above and mutations in SPIB contribute to transcriptional repression of BLIMP1(Basso and Dalla-Favera 2015).

Clinically relevant for the treatment of ABC-type DLBCL seems to be mainly the dependency of the lymphoma cells on NFκB-signaling, as pre-clinical models show that perturbations of it lead to cell death in ABC but not in GCB cells (Frontzek and Lenz 2019). As this pathway is highly dependent on the ubiquitin proteasome system (UPS), one of the first clinical trials, intending to utilize the NFκB-dependency, centered around the proteasome inhibitor bortezomib to block the proteasomal degradation of proteins such as one major inhibitor of the pathway IκBa. Unfortunately, the addition of Bortezomib to R-CHOP therapy failed to improve the patients overall response(Davies et al. 2019). Despite this set back, several other inhibitors are in clinical trials, that are targeting more specific elements of the molecular mechanism leading towards oncogenic NF-κB signaling including the small molecule Ibrutinib, an inhibitor of the Bruton's Tyrosin Kinase (BTK). In this so called PHOENIX trial, the addition of Ibrutinib to R-CHOP resulted in an improved overall survival in a subgroup of younger patients with ABC-DLBCL but induced severe side effects in others study participants (Frontzek and Lenz 2019).

1.3.2 Multiple Myeloma

With an incidence of roughly 32.000 new cases and 13.000 deaths in 2019 in the USA (Siegel, Miller, and Jemal 2019) and an overall 5-Year relative survival rate of 49% (2005 – 2011) (Siegel, Miller, and Jemal 2016), multiple myeloma (MM) represents around 10% of all lymphomas and up to date remains incurable (Rajkumar and Kumar 2016; Küppers 2005).

MM is another hematological cancer arising from post germinal center B-cells (Figure 2). It is characterized by the clonal proliferation of malignant plasma cells in the bone marrow, where normal hematopoiesis and bone formation is disrupted (Palumbo and Anderson 2011). As described before, long-lived plasma cells are terminally differentiated B-cells which can produce high affinity antibodies and are therefore a central part of the humoral immunity. By the time these cells leave the lymph nodes as plasma cell precursors and home to the bone

marrow, a process presumably regulated via CCL12/CXCR4 chemotaxis, these cells are highly proliferative(O'Connor et al. 2003) and enter quiescence when completing terminal differentiation in the bone marrow (Kuehl and Bergsagel 2002; O'Connor et al. 2003). It is believed that these plasma cell precursors are the cells of origin for MM (Figure 2, 3), as they produce rather low amounts of class switched antibodies compared to plasma cells, a fact that also holds true for most transformed MM cells. These low affinity monoclonal antibodies or antibody-fragments are detectable in MM patients' blood and are often referred to as M-Protein (Kuehl and Bergsagel 2002; Kyle and Rajkumar 2009a; Kumar et al. 2017).

Similar to other lymphomas the first transformation events in MM are triggered by the high genomic instability of B-cells during differentiation. The so-called primary translocations in this disease most commonly involve the IgH gene locus on chromosome 14 (q32.33), indicating class switch recombination as the source of the DNA double strand breaks. The transforming dysregulations, resulting from positioning genes under the influence of the Ig enhancer, include oncogenes such as cyclin D1 (on 11q13) in approx. 15-20% of the cases, or D3 (at 6p21), fibroblast growth factor receptor 3 (FGFR3) combined with MMSET (chromosomal location 4q16) and the transcription factor c-MAF (at 20q11) (Palumbo and Anderson 2011; Fonseca et al. 2002; Roodman 2009).

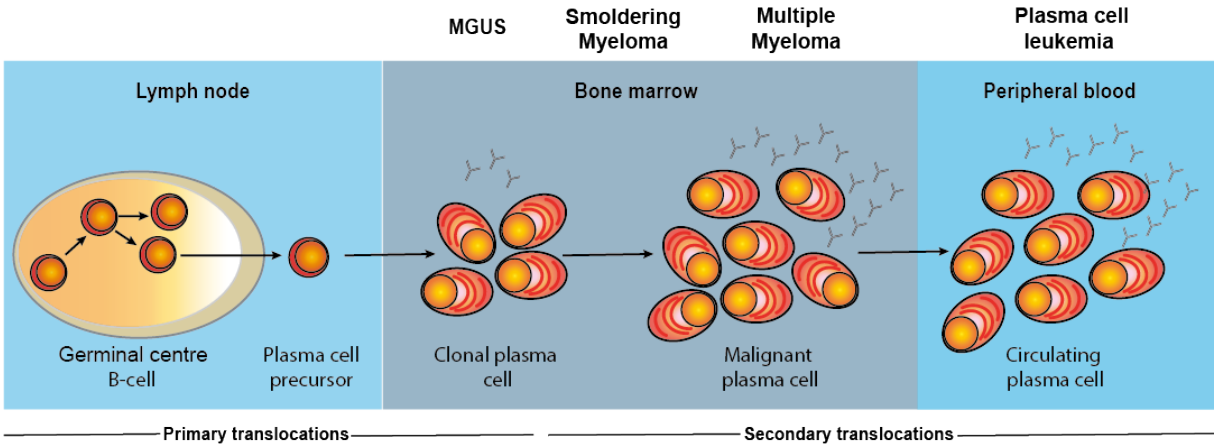

Figure 3. Stages of Multiple Myeloma development. Malignant plasma or MM cells are supposed to originate from plasma cell precursor cells, a type of post-germinal center B-cells, which underwent IgH recombination to produce specific antibodies. This process might result in aberrant genetic translocations putting for example oncogenes under the control of the Ig promotor leading to their overexpression and increased proliferation. Such primary translocations give rise to premalignant monoclonal gammopathy of undetermined significance (MGUS), which progresses via smoldering myeloma to highly proliferative and clinically manifesting MM upon acquisition of secondary translocations. Finally, this can lead to plasma cell leukemia, in which tumor cells enter the peripheral blood (Adapted from Kuehl and Bergsagel 2002; Kumar et al. 2017).

These early gene aberrations result in a pre-malignant lesion called monoclonal gammopathy of undetermined significance (MGUS). MGUS is present in about 4% of all adults over 50 years of age and is believed to precede MM in most cases but is rarely detected as it is almost asymptomatic. Per year, about 1% of MGUS cases proceed towards smoldering myeloma (SMM), which represents an intermediate stage towards highly proliferative, symptomatic MM (Figure 3) (Kyle and Rajkumar 2009b; Rajkumar and Kumar 2016).

The progression from MGUS to MM via SMM is caused by secondary genetic aberrations including additional translocations, chromosomal gains or losses and somatic mutations. The secondary events are believed not to arise from B-cell specific DNA-remodeling mechanisms, as these are no longer active in normal and neoplastic plasma cells (Kuehl and Bergsagel 2002). The risk of progression from MGUS to MM seems to depend on the type of

cytogenetic abnormality – patients carrying the t(4;14) translocation have a median time to progression (TTP) of 2 years, while the transition takes 5 years in patients with the t(11;14) translocation. Other common secondary events are gains of chromosome 1q and the deletions of chromosomes 1p, 17p and 13 (Rajkumar and Kumar 2016). Patients with t(14;16), t(4;14) or del(17p) chromosomal rearrangements have particularly poor prognosis (Fonseca et al. 2002; Palumbo et al. 2015). The monoallelic loss of 13q is a very common abnormality in MM with approximately 50% incidence even though the implications of this isolated event on disease progression is still unclear (Rajkumar and Kumar 2016; Kuehl and Bergsagel 2002). Other common dysregulations, either caused by mutations or translocations, include MYC, RAS, FGFR3 and TP53 (Palumbo and Anderson 2011).

Besides this very heterogenic landscape of cytogenic abnormalities and mutations, the other big contributing factor to MM development, progression and relapse is the bone microenvironment. Plasma cell differentiation and survival as well as the development and survival of MM cells highly depend on the interactions with the extra cellular matrix (ECM), the direct cell-cell contacts and the cytokine milieu of the bone marrow. One of the most important interactions takes place between MM cells and bone marrow stromal cells (BMSCs), but also includes bone marrow endothelial cells (BMECs), osteoclasts and osteoblasts. This interaction not only homes the malignant cells to the BM but also triggers the secretion of cytokines like IL-6, IL-10, VEGF or TNF-a from BMSCs which creates an even more favorable environment for MM cell growth, survival and drug resistance. Moreover the cytokines secreted by MM cells and BMSCs, lead to an imbalance in bone formation by inhibiting the function and formation of bone generating cells (osteoblasts), while activating bone resorbing cells (osteoclasts), leading to one of the hallmarks of manifested MM, namely the lytic bone lesions visible on MRI scans of patients with advanced disease (Oranger et al. 2013; Hideshima et al. 2007; Podar et al. 2001; Roodman 2009).

As afore-mentioned, MM is preceded by the asymptomatic and therefore often undiagnosed MGUS. This disease stage is characterized by less than 10% clonal plasma cells in the BM and less than 3g/dL M-Protein in the serum of patients. The diagnostic criteria for smoldering myeloma are met when the clonal bone marrow plasma cells levels are between 10% and 60% and serum M-protein levels exceed 3g/dL (Kyle and Rajkumar 2009b). These criteria also hold true for MM with the distinction that so-called end-organ damage or tissue impairment caused by the plasma cell disorder must be present. The MM defining events are summarized by the CRAB-criteria, which include hyper**c**alcemia, **r**enal failure, anemia and bone lesions. Hypercalcemia and bone lesions result from the imbalance between osteoblast and osteoclast function as described before, while the anemia is caused by the high burden of MM cells, which displace normal hematopoietic cells in the bone marrow. Renal failure results from the deposition of M-protein in nephrons thereby damaging the tubules of the kidney and the hypercalcemia (Kuehl and Bergsagel 2002; Rajkumar and Kumar 2016; Kyle and Rajkumar 2009b; Palumbo and Anderson 2011).

Staging of MM was carried out using the Durie-Salmon system from 1975 (Raab et al. 2009), which takes the extent of bone lesions, hemoglobin levels, calcium levels and M-protein quantity in serum and urine into account (Durie and Salmon 1975). Since then the staging system continuously evolved towards the now most commonly used revised International Staging System (R-ISS). It defines three risk groups/stages based serum β2-microglobulin, albumin (Greipp et al. 2005) and lactate dehydrogenase (LDH) levels as well as by assessment of cytogenetic aberrations (Palumbo et al. 2015). MGUS and SMM are usually not treated actively as it is not clear, if treatment in these early stages improves prognosis or only leads to a delay in disease progression (Rajkumar and Kumar 2016). Treatment of MM becomes indicated as soon as the disease becomes symptomatic according to the CRAB criteria.

Depending on disease stage, molecular risk group and overall constitution of the patient different therapy regimes are advised. The standard of care used in patients younger than 65-70 years with newly diagnosed MM and little to no comorbidities is a multi-drug chemotherapy consisting of an immunomodulatory drug (IMID), a proteasome inhibitor and a steroid (for example lenalidomide, bortezomib and dexamethasone – VRD), which is followed by a high dose chemotherapy with melphalan, autologous stem cell transplantation (ASCT) (Durie et al. 2018; Rajkumar and Kumar 2016) and maintenance therapy with lenalidomide or bortezomib (McCarthy et al. 2017). Other first line therapy regimes also include classical chemotherapy reagents such as cyclophosphamide and doxorubicin (Palumbo and Anderson 2011). Patients that are older and/or not eligible for ASCT are treated in doublet or triplet regimes consisting of IMIDs (for example lenalidomide or thalidomide) and/or bortezomib with melphalan and/or prednisone (Kumar et al. 2017; Palumbo and Anderson 2011; Greipp et al. 2005; McCarthy et al. 2017). Even though the introduction of IMIDs and proteasome inhibitors and more recently the clinical application of monoclonal antibodies directed against CD38 (Daratumumab) or SLAMF7 (Elotuzumab) has significantly improved the outcomes of MM patients in the last decade, most patients eventually relapse (Rajkumar and Kumar 2016; Mikhael et al. 2019).

Therefore, MM remains an incurable disease with a demand for a better understanding of the disease including new druggable molecular targets, especially for repeatedly relapsing patients.

1.4 The Ubiquitin-Proteasome system

The Ubiquitin proteasome system (UPS) is one of the cells major protein degradation routes. As indicated before it is already being targeted clinically, which gives another inside into its importance in a variety of cellular processes including cell cycle control, cell survival and inflammation. Briefly, it enables the temporal and spatial fine tuning of protein abundance on a post translational level in a flexible and highly coordinated manner. The system uses a in eukaryotes highly conserved 8.5 kDa protein called ubiquitin (Ub) as a post-translational modification, covalently 'tagging' unwanted proteins for degradation by the proteasome. The attachment of Ub occurs in a reaction cascade including three different enzymes (Figure 4). First a Ub monomer is bound to a so-called ubiquitin activating enzyme (E1) in an ATP-dependent manner. This first and only energy consuming step leaves a highly reactive thioester bond between E1 and the Ub-monomer. The thereby activated Ub is subsequently transferred to a conserved cysteine residue on the second enzyme of the cascade, called ubiquitin conjugation enzyme E2. In some cases the Ub is transferred from the E2 enzyme directly to a designated substrate protein but in most cases a coordination step occurs by a substrate/degron-specific E3 enzyme, also known as ubiquitin ligase (Figure 4) (Soltes, Muller, and D'Aversa 2011; Swatek and Komander 2016; Hershko and Ciechanover 1998). The attachment of Ub occurs typically on lysine residues (Lys or K) - less often on the N-terminal methionine - of a substrate protein, where an isopeptide bond is formed between the ε-amino group of the substrate and the free carboxyl-group of the Ub backbone (Ciechanover and Ben-Saadon 2004). This initially attached ubiquitin can either remain in its monomeric form or is itself modified to form polyubiquitin chains. These chains are formed by the attachment of additional Ub molecules to one of the seven lysine residues of the Ub protein. Depending on which lysine is used for chain elongation the Ub chains have different architectures and functions (Figure 5).

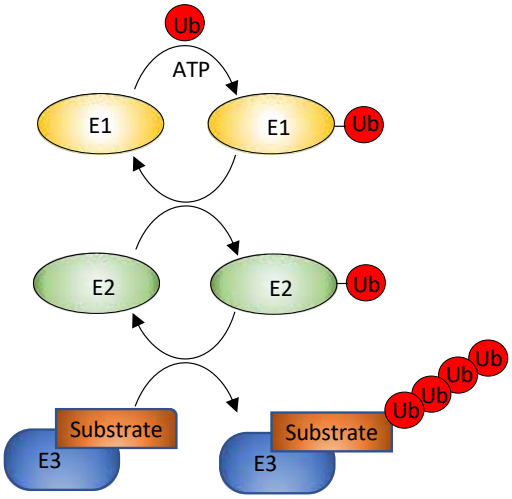

Figure 4: The enzymatic cascade leading to substrate ubiquitylation. First, ubiquitin (Ub) is activated in an ATP-dependent manner and covalently attached to an E1 enzyme via a thiol-ether bond. Next. the ubiquitin molecule is transferred to the catalytic cysteine of an E2 enzyme, which recruits an E3 ligase which mediates the transfer of ubiquitin to a lysine amino acid residue of the substrate protein or a ubiquitin molecule already attached to it.

The most abundant polyubiquitin chain type in mammalian cells has a K48-structure, which destines the modified proteins for proteasomal degradation (Swatek and Komander 2016; Komander and Rape 2012). This degradation is carried out by a macromolecular complex called 26S proteasome. This multiprotein complex with a remarkable size of 2.5 MDa consist of a proteolytic 20S core particle and one or two 19S regulatory particles (Bard et al. 2018; Coux, Tanaka, and Goldberg 1996). The regulatory particles are responsible for the recognition of polyubiquitinated proteins, the removal of the attached Ub, the unfolding of the target protein and the translocation of the resulting polypeptide chain into the core particle (Tomko and Hochstrasser 2013). Within the core particle of the proteasome the polypeptide chain is then cleaved by the proteolytic activity of the ß-subunits and released from the complex as short peptides with a length of 7-9 amino acids. These are subsequently broken down

further by cytoplasmic proteases (Coux, Tanaka, and Goldberg 1996; Kisselev et al. 1999).

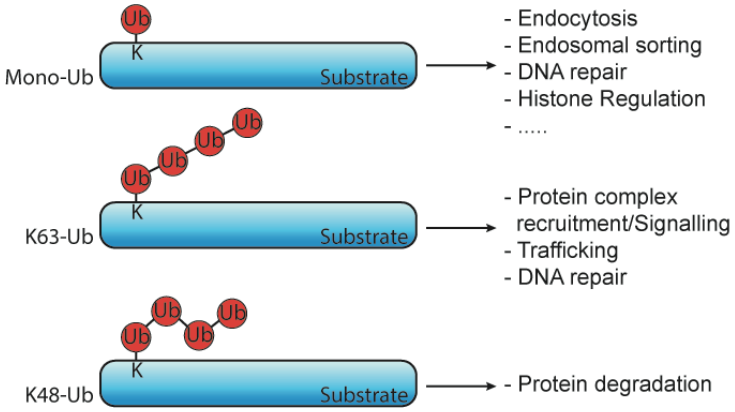

Figure 5: Overview of specific ubiquitin modifications and their cellular outcomes. A substrate protein can be modified by either single ubiquitin (Ub) molecule or with covalently linked polyubiquitin chains, which are connected among others via their K63 or K48 lysine residues, leading to a variety of different cellular outcomes. [Figure adapted from (Haglund and Dikic 2005)].

1.4.1 E3-Ubiquitin-Ligases

The combination of approximately 30 different E2 enzymes and over 600 ubiquitin ligases encoded in the human genome enables the specific ubiquitination of a huge variety of cellular proteins (Soltes, Muller, and D'Aversa 2011; Scheffner, Nuber, and Huibregtse 1995). Interestingly, a protein can be targeted by different ligases and a single E3 ligase can ubiquitinate a multitude of target proteins depending on the cellular context, thereby coupling for example protein phosphorylation to degradation (Skowyra et al. 1997). Not all of these E2/E3 complexes target proteins for degradation. Depending on both the E2 enzyme and E3 ligase a different (poly-) ubiquitin type is assembled, thereby mediating different cellular outcomes of ubiquitination. These other polyubiquitin molecules are build up in linear, K6, K11, K27, K29, K33 and K63 fashion (Swatek and Komander 2016; David et al. 2011; 2010). More recently there are also reports about heterotypic chains showing more than one linkage type leading to an even bigger complexity (Komander 2009; Michel et al. 2017). Of these chain types, linear and the K63-linkage type are the only poly-ubiquitin configurations, besides K48, investigated in great detail. This specific type of PTM is known to have important functions in complex assembly, signal transduction and cellular localization for example in NFκB signaling (Michel et al. 2017; Komander and Rape 2012; Swatek and Komander 2016; Ikeda and Dikic 2008).

In general, all E3 ligases harbor a domain which can bind a ubiquitin charged E2 enzyme and facilitate the transfer of a Ub molecule onto a specific target protein. The different E3 ligases can be subdivided into three classes depending on their mechanism of Ub transfer and the presence of characteristic domains (Buetow and Huang 2016). The so called HECT-E3 ligases transfer Ub in a two-step mechanism. First Ub is transferred from the respective E2 enzyme to an active cysteine on the ligase itself and subsequently to the substrate (Hershko and Ciechanover 1998). The catalytic HECT domain is located at the C-terminal end of the protein, while substrate specificity is determined by the N-terminal part. A group with a similar mechanism of Ub transfer are the RBR-ligases. All of them contain a RING1-IBR-RING2 motif in which the RING1 domain recruits the E2-ubiquitin-complex. The Ub is then transferred to an active cysteine moiety within the RING2-domain, which passes it on to an acceptor cysteine

within the target. The RING domains of this ligase type are structural similar to the motif defining and naming the largest class of E3-ligases – called RING E3s (Petroski and Deshaies 2005). Importantly, the members of this class of E3 do not have inherent catalytic activity but facilitate the recruitment and orientation of an E2-Ub intermediate and a designated ubiquitylation substrate (Willems, Schwab, and Tyers 2004). With approximately 600 members, this highly diverse class can be subdivided further depending on structure and possible complex formation pattern. A big proportion of the multimeric E3-ligases contain one of six different Cullin proteins as a complex scaffold and are therefore named Cullin-RING ligase (CRLs) (Cardozo and Pagano 2004; Sarikas, Hartmann, and Pan 2011).

The most intensively studied SCF-subclass contains Cullin-1 (CUL1) as a scaffold protein, which binds to the RING-domain protein RBX1 via its C-terminus to facilitate the recruitment of an E2-ezmyne. Simultaneously, via its N-terminus CUL1 binds to another adaptor protein, S phase kinase-associated protein 1 (SKP1), which in turn binds to one of 68 different F-box proteins thereby implementing the substrate specificity of the ubiquitylation complex (Figure 6)(Petroski and Deshaies 2005; Jin et al. 2004). All mammalian F-box proteins contain a F-box domain, which enables the interaction with SKP1(Bai et al. 1996), and are further classified by an additional protein-interaction domain for substrate recognition as FBXWs with WD40-domains, FBXLs containing leucine-rich repeats and FBX or FBXOs without a common structural motive (Jin et al. 2004). In order to rapidly integrate a large variety of cellular stimuli, substrate recruitment to SCF-complexes is tightly regulated and relies on short conserved amino acid sequences within a given substrate, so-called degrons. These are often post-translationally modified for example by phosphorylation before recognition by the FBOX-protein (Skaar, Pagan, and Pagano 2013). One of the best characterized FBOX-proteins binding to phosphodegrons is β-transducin repeat-containing protein (β-TrCP/FBXW1), that mediates the K48-ubiquitylation and thereby proteasomal degradation of a big variety of substrates (Cardozo and Pagano 2004) like the canonical NF-κB inhibitor IκBa (Spencer, Jiang, and Chen 1999; Scherer et al. 1995) and the cell cycle regulating phosphatase CDC25A (Bassermann, Eichner, and Pagano 2014; Busino et al. 2003) upon phosphorylation. Another emerging class of CRLs contain Cullin-3 (CUL3) as their molecular scaffold instead of CUL1. These so called CRL3s interact with E2-enzymes by engaging via RBX1 similar to SCF-type complexes but do not rely on SKP1 for substrate adaptor binding

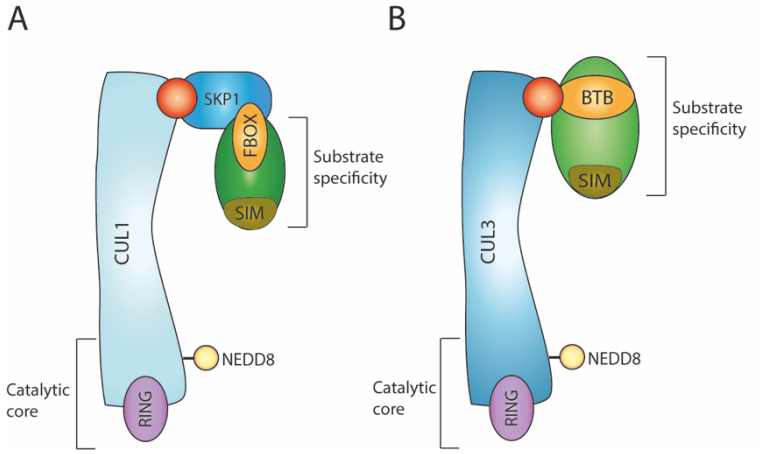

Figure 6: Structural organization of SCF/CRL1 and the CRL3 complexes. CULLIN–RING ligases (CRLs) are comprised of a common catalytic core consisting of a RING protein and a CULLIN-family member. The SCF/CRL1 **(A)** and the CRL3 complexes **(B)** are defined by their scaffold proteins CUL1 and CUL3, respectively and share the RING finger protein RBX1 (ROC1; purple) responsible for E2-interaction. A variable section of the CULLIN (red) mediates the interaction with a specific class of substrate adaptor, in CRL3`s a single-subunit BTB domain (yellow) containing protein (green), while SFC complexes need SKP1 (dark blue) as a bridging factor to the FBOX-protein (green). The recruitment of specific proteins for ubiquitylation by the E2 is mediated by an additional substrate interaction domain (SIM) of the adaptor proteins. [Figure adapted from (Petroski and Deshaies 2005)]

(Figure 6) (Skaar, Pagan, and Pagano 2013; Petroski and Deshaies 2005; Genschik, Sumara, and Lechner 2013). Instead, CUL3 employs BTB proteins as substrate specific adaptors, which contain a BTB domain that is structurally equivalent to SKP1 and confers CUL3 binding(Xu et al. 2003; Sarikas, Hartmann, and Pan 2011; Stogios et al. 2005). More than 150 proteins with BTB domains are encoded in the human genome (Stogios et al. 2005), often in combination with additional protein-protein interaction domains like MATH or Kelch domains, that indicate an involvement of the protein in CUL3-mediated ubiquitylation, even though it remains unclear how many actually act as substrate adaptors *in vivo* (Zhuang et al. 2009; Canning et al. 2013). The most extensively characterized subgroup of BTB-CUL3 adaptor proteins, contain a C-terminal Kelch ß-propeller domain for substrate recognition and are therefore called KLHL-proteins (Canning et al. 2013). These include KEAP1/KLHL19, the E3-ligase regulating the protein levels of the transcription factor NRF2, a master regulator of the anti-oxidative stress response (Kobayashi et al. 2004; McMahon et al. 2003).

Even though other KLHL-substrate pairs have been implicated in a variety of cellular processes like mitotic regulation (Maerki et al. 2009; Sumara et al. 2007; Xu et al. 2003), mTORC1-(J. Chen et al. 2018) and NF-κB-signaling(Choi et al. 2018), most CRL3 ligases are not linked to their substrates to this date.

1.4.2 KLHL14

One of the only rudimentarily characterized KLHL-proteins is KLHL14. It is encoded on chromosome 18q12.1 and was first described as Printor in early onset generalized torsion dystonia (DYT1), a neurological disfunction. The study acknowledged the proteins KLHL-proteins structure as a typical CUL3 substrate adaptor but reported its function to be determined by its interaction with the AAA^+ (ATPases associated with a variety of cellular activities) protein TorsinA in the endoplasmatic reticulum (ER), independent of the ubiquitin system (Giles, Li, and Chin 2009; Valastyan and Lindquist 2011). Furthermore, KLHL14 mRNA was found to be highly expressed in GABApre interneurons, which are essential for the feedback regulation of the sensory-motor synapse (J. Zhang et al. 2017a), and postnatally from E18.5 to P1 in a specific sub-type of corticospinal neurons of the developing murine brain, where it limits axon extension and branching to the cervical cord (Sahni, Itoh, et al. 2021). Other ubiquitin unrelated functions involve reports about a murine long non-coding antisense RNA, whose genomic localization partially overlapped with the KLHL14 gene (Credendino et al. 2017), which might play a role in embryonic development of the intervertebral disc(Kraus et al. 2019). A full body knock out of the protein in mice is embryonically lethal (S. Li et al. 2018).

Importantly, KLHL14 was described to be highly expressed in B-cells (S. Li et al. 2018) and its gene locus subject to aberrant somatic hyper mutation in DLBCL(Choi et al. 2020) and primary CNS lymphoma (PCNSL) (Vater et al. 2015). While heterozygous genetic deletion of KLHL14 did not disturb follicular and marginal zone B-cell development and mature B-cells showed normal class-switch recombination, the development of B-1a peritoneal B-cells was reduced and B-1b cells increased upon KLHL14 reduction. Because proliferation and apoptosis of these cells were not affected by the reduction of KLHL14 expression, the differential development was proposed to stem from differentially active BCR-signaling with stronger activation favoring B1-a B-Cell development (S. Li et al. 2018). In contrast, a recent publication proposed the induction of BCR-dependent NF-κB signaling upon loss of function/destabilizing mutations within the KLHL14 gene. Herein, the authors report KLHL14 as a tumor suppressor in ABC-type DLBCL, that promotes the turnover of immature, glycosylated BCR subunits in the ER in an Cul3-dependent manner, thereby reducing cellular BCR levels (Choi et al. 2020). Furthermore, loss of KLHL14 was reported to correlate with

resistance to the Bruton's tyrosine kinase (BTK) inhibitor ibrutinib (IBR) in ABC-type DLBCL-cell lines (Choi et al. 2020), while others reported a high mutational burden in KLHL14 to be a biomarker for a IBR response in DLBCL patients (Hodkinson et al. 2021). Despite the mounting evidence that the CUL3 and ubiquitylation related functions of KLHL14 play a pivotal role in B-cell development and dysfunction, the underlying molecular mechanisms remains elusive.

1.4.3 Deubiquitylases (DUBs)

As described above, ubiquitylation is a rapid and impactful PTM, which can, like many other PTMs, be reversed or tailored (Komander, Clague, and Urbé 2009). The removal of ubiquitin moieties is carried out by deubiquitylases (DUBs) from six different families, which are defined by their domain structure and catalytic activity (Mevissen and Komander 2017). Most of them are cysteine proteases and catalyze the cleavage of the isopeptide bond formed by the e-amino group of a lysine or methionine and the C-terminus of ubiquitin. Due to their catalytic diads or triads, DUBs are targetable by small molecules, making their inhibition the prime strategy to precisely influence the ubiquitin system clinically. In order to do so, it is of major importance to understand how DUBs recognize potential substrates and establish DUB-substrate pairs with distinct cellular functions (Harrigan et al. 2018). DUBs can either recognize a ubiquitin chain itself for example in a linkage specific manner or interact directly with a substrate protein and subsequently remove ubiquitin from it. While the most of the ubiquitin-specific proteases (UPSs) subclass members for example remove different kinds of ubiquitin linkages from their target proteins, members of the ovarian tumor proteases (OTUs) family seem to have preferences for one or several linkage types (Mevissen et al. 2013; Ritorto et al. 2014).

A DUBs substrate recruitment and activity is tightly regulated, to ensure a precise temporal and spatial response to specific stimuli (Sahtoe and Sixma 2015). Some of this regulation occurs at the transcriptional and translational level (Mevissen and Komander 2017), for example throughout the cell cycle, during which the expression of a specific DUB is induced during the cell cycle phase it controls like USP1 during S-Phase and USP44 in G2/M (Ling Song and Rape 2008; Das et al. 2020). Additional layers of regulation include the regulation of the subcellular localization of either a DUB or its substrate (Urbé et al. 2012; Clague, Coulson, and Urbé 2012), the assembly of the DUB into a larger signaling complex (Komander, Clague, and Urbé 2009; Sahtoe and Sixma 2015) and the direct regulation of a DUBs enzymatic catalytic activity (Mevissen and Komander 2017). The latter is often achieved through PTMs on the protease itself with phosphorylation being the best characterized among them. The OTU class protease DUBA for example needs to be phosphorylated at Ser177 to enter a conformation that allows effective ubiquitin binding and therefore activity (O. W. Huang et al. 2012). A similar activation occurs during the cell cycle, in which CDK-2 phosphorylates USP37 to allow S-phase entry by antagonizing the APC^{CDH1} mediated K48-ubiquitylation of Cyclin A (X. D. Huang et al. 2011).

1.4.4 OTUD6B

Until recently, the two isoforms of OTUD6B, a cysteine protease of the OUT family, were not matched to any ubiquitylation substrate but implicated in the regulation of different cellular processes on a phenotypical level. In non–small cell lung cancer (NSCLC) cells for example the longer isoform 1 of OTUD6B was reported to repress proliferation, while isoform 2 promoted it, but no deubiquitylation targets were proposed (Sobol et al. 2017). Additionally, OTUD6B was long considered enzymatically inactive, as *E. coli* purified recombinant protein

showed proper folding and a reactive Cysteine but lacked cleavage activity towards di-ubiquitin moieties of all linkage types (Mevissen et al. 2013)

Carmen Paulmann (former Richter) recently identified OTUD6B as a novel vulnerability in MM, which's loss lead to a defect in the progression from G1- to the S-Phase of the cell cycle (Paulmann et.al. under review). Furthermore, the RNA-binding protein and suppressor of lethal 7 (let-7) microRNAs LIN28B (Heo et al. 2009; Balzeau et al. 2017) could be identified as a bona-fide deubiquitylation substrate of OTUD6B, proving the DUB to be active in a mammalian cell context. The stabilizing effect of OTUD6B on its substrate could be delineated to the G1/S-transition specifically and could furthermore be shown to be important for MYC stability and activity. Interestingly, Paulmann and colleagues proposed that a phosphorylation event on the LIN28B side was responsible for the G1/S specific interaction of OTUD6B and its substrate (Paulmann et.al. under review), presenting substrate phosphorylation as novel concept for DUB activation and recruitment.

1.5 Cell cycle

The eukaryotic cell cycle describes the process in which cells propagate and while there is a variety of cellular mechanisms in place to ensure an error free division, the replication and distribution of a cells genome bares great potential for malignant transformation (Borg and Dixit 2017; Kastan and Bartek 2004). The cell cycle is subdivided into four stages, which are tightly controlled by the so-called cell cycle checkpoints, that ensure the genomic integrity and fitness of the emerging daughter cells. Each cell cycle phase is defined by the activity of a specific Cyclin-dependent Kinase (CDK), which depend on the interaction with their respective Cyclin counterpart and the absence of a CDK-inhibitor (CKI) (Figure 7) (Fisher et al. 2012; Skaar and Pagano 2009; Bassermann, Eichner, and Pagano 2014). While the expression of CDKs is comparatively constant, Cyclins as well as CKI are stimulus dependent periodically synthesized and degraded by the proteasome, ensuring the unidirectionality of the cell cycle (Skaar, Pagan, and Pagano 2013; Hochegger, Takeda, and Hunt 2008).

Cells in G1 need a variety of extra- and intracellular stimuli to commit to cell division by entering the cell cycle. In response to these stimuli CDK4/6 together with the D Cyclins drive the transcriptional program to allow cells to prepare for DNA replication during S-phase (Tchakarska and Sola 2020). A main prerequisite for this is the integrity of the DNA and other cellular compartments. If for example excessive DNA-damage is detected, the restriction point is triggered and the cells arrest in G1 to either repair the damage or eventually undergo apoptosis(Barnum and O'Connell 2014). Once the restriction point is passed, cells progress from G1 into S-phase, a transition that is mediated by CDK1/Cyclin E complexes, which are exclusively formed during the onset of DNA-synthesis. As S-phase progresses, Cyclin E is rapidly ubiquitylation by FBXW7 and subsequently degraded (Borg and Dixit 2017), which allows the complex formation of Cyclin A with CDK1/2. The CDK1/2-Cyclin A activity is essential not only for S-phase progression, but also in the late phases of DNA replication for the transition towards mitosis, a phase known as G2-phase (Malumbres and Barbacid 2009). Both Cyclin/CDK complexes that drive S-phase, can be inhibited by phosphorylation upon sensing of various stresses, which are detected for example via ATM/ATR and the checkpoint kinases Chk1/2, leading to stalling of S-phase progression (intra-S-checkpoint) and delayed G2-mitosis transition (M; G2/M checkpoint), depending on when the stress occurs (Bassermann, Eichner, and Pagano 2014; Borg and Dixit 2017; Kastan and Bartek 2004).

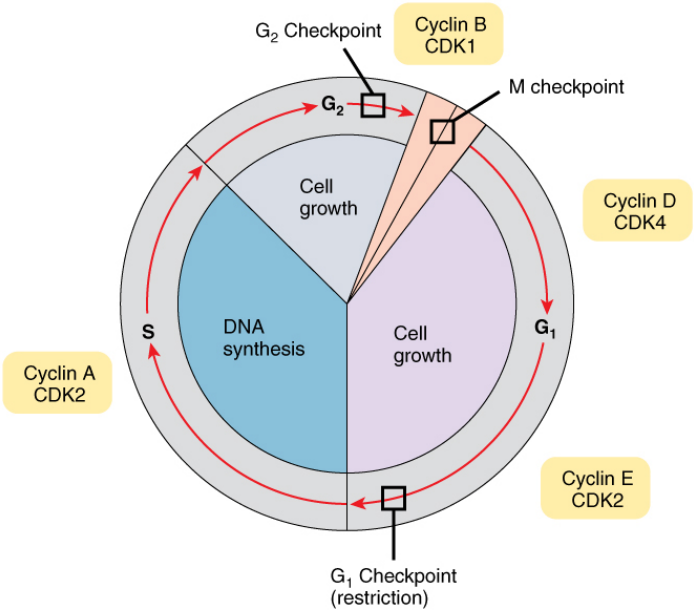

Figure 7. Overview of the cell cycle. The mammalian cell cycle is defined by four phases: G1, S, G2 and mitosis (M). So-called cycle checkpoints tightly control the progression of cycling cells through a given phase to avoid division without the necessary mitogenic signals and the propagation of damaged DNA to daughter cells. The different cell cycle phases are defined by the activity of specific Cyclin-dependent kinases (CDKs), that are mediated by complex formation with their respective Cyclin (indicated in yellow boxes). Cyclin E-CDK2 drives the G1/S-transition and therefore becomes activated in late G1 phase, while progression through and completion of the S phase is driven by the Cyclin A-CDK2/CDK1 complex. Activation of Cyclin B-CDK1 regulates mitotic entry, which needs to be abrogated for the exit from this cell cycle phase. [Figure from Textbook OpenStax Anatomy and Physiology (Version 8.25) Published May 18, 2016]

In the absence or after recovery from replication stress and DNA damage, A-type Cyclins levels decline, allowing CDK1/Cyclin B and polo-like kinase 1 (PLK1) activity to trigger mitotic entry (Joukov and De Nicolo 2018), which includes chromosome condensation, buildup of the mitotic spindle and the breakdown of the nuclear envelope(P. Wang, Malumbres, and Archambault 2014). This first phase of mitosis is called prophase and is succeeded by prometaphase during which the microtubules (MTs) of the mitotic spindle are attached to the chromosomes. The so called spindle assembly checkpoint (SAC) is crucial to ensure the accurate segregation of the sister chromatids during mitosis by preventing the progression towards anaphase until all chromosomes are attached to the mitotic spindle (Lara-Gonzalez, Westhorpe, and Taylor 2012). The attachment of the microtubules of the mitotic spindle occurs at the kinetochores, which are formed by multi component complexes at the centromeres of sister chromatids. Complex assembly starts in late pro-phase with Bub1 binding, which then recruits Mad1 and Mad2. The interaction triggers conformational changes in Mad2, which leads to the assembly of the mitotic checkpoint complex (MCC), which contains Cdc20, an important activator of the APC/C ubiquitin ligase complex. Thereby the ubiquitylation activity of APC/C, which controls the proteasomal degradation of secruin and Cyclin B, is severely reduced and cells cannot progress to anaphase (Nitta et al. 2004; Lara-Gonzalez, Westhorpe, and Taylor 2012). The SAC is satisfied and the MCC disassembled, when all kinetochores are stably bound by microtubules anchored at opposing spindle poles and a mechanical tension is sensed for example by the Aurora-B kinase. This kinase is part of the chromosomal passenger complex (CPC), which regulates essential steps of mitotic signaling and kinetochore organization throughout mitosis (Trivedi and Stukenberg 2020), at the meta- to anaphase transition especially the depolymerization of incorrectly attached microtubules. Even though not fully understood, the tension sensing mechanism involves a change of Aurora-B substrate accessibility that is triggered by the kinetochore deformation attributed to the attachment to mitotic spindle in a bipolar fashion (Lampson and Cheeseman 2011). The tension-mediated model explains the possibility to mechanistically differentiate between correct bi-polar MT attachment, the attachment of both sister kinetochores to microtubules originating from a single pole (syntelic attachment) and the attachment of a single kinetochore to both spindle poles (merotelic

attachment).
As soon as all kinetochores are correctly attached and aligned on the spindle equator, also known as metaphase plate, the SAC is completed and the anaphase-promoting complex (APC/C) targets Cyclin B and secruin for ubiquitylation and degradation (M T Hayashi and Karlseder 2013; Bassermann, Eichner, and Pagano 2014; Lara-Gonzalez, Westhorpe, and Taylor 2012). The degradation of the latter, releases a protease called separase to allow chromosome segregation during anaphase (Lara-Gonzalez, Westhorpe, and Taylor 2012). After migrating towards the spindle poles, the chromosomes start to de-condensate at the beginning of telophase and the nuclear envelopes are established around the replicated/daughter chromosomes. The cellular division is completed by cytokinesis, during which the cytoplasm of the two daughter cells is separated by the assembly a contractile actin myosin ring that mediates the cleavage process towards abscission of the plasma membranes (Fededa and Gerlich 2012).

1.5.1 Centrosome and microtubule regulation throughout mitosis

While Aurora-B is essential for the regulation of the SAC and during telophase and cytokinesis, Aurora-A plays an essential role on the other side of the mitotic spindle formation, at the spindle poles, where the so-called centrosomes reside. In proliferating cells, centrosomes act as the prime microtubule organizing centers (MTOCs) with a variety of cellular functions beyond mitosis like intracellular transport, motility and cellular polarity (Tillery et al. 2018). Their variety of functions is mainly but not exclusively related to their ability to nucleate, anchor and stabilize MTs within their pericentriolar material (PCM) in which the mother and daughter centrioles reside. A key regulator for MT nucleation within the PCM is a specific kind of tubulin called γ-tubulin, which is, together with different γ-tubulin complex proteins (GCPs), assembled into ring complexes called γ-tubulin ring complex (γ-TuRC) and serves as a nucleation template for MT formation (Muroyama and Lechler 2017; Schatten 2008; Tillery et al. 2018).

During interphase, the centrosome usually organizes the MT network in a way suitable for intracellular transport and other structural purposes (Muroyama and Lechler 2017), while a pair of centrosomes with increased MT nucleation activity mediates the buildup of the bipolar mitotic spindle during mitosis. As having more than two centrosomes during mitosis can result in multipolar spindles, a possible cause for the mis-segregation of the genetic material, centrosomes are duplicated only once during S-phase. First, centriole duplication is initiated during the G1/S-transition and continues in a PLK4-dependent fashion during S-phase, resulting in two centrosomes consisting of a mother and a daughter centriole(Bettencourt-Dias and Glover 2007; Gouveia et al. 2019).

Next upon mitotic entry, centrosome maturation sets in by expansion of the PCM around the mother centriole(W. J. Wang et al. 2011), which includes a massive increase in γ-TuRC and MT nucleation capacity (Schatten 2008). The maturation process is dependent on the activity of two distinct kinases – PLK1 and Aurora-A (Joukov and De Nicolo 2018). Aurora-A expression increases during G2-phase, which leads to its accumulation in the nucleus (E. Willems et al. 2018). After breakdown of the nuclear envelope, the kinase is tethered to mitotic centrosomes and activated by its interaction with CEP192, which while present at the centrosomes throughout the cell cycle, accumulates in the PCM during G2-phase and enables autophosphorylation of Aurora-A at Thr288. Aurora-A subsequently phosphorylates PLK1 at Thr210, leading to its activation and the enhanced binding to CEP192. This kinase cascade ultimately results in the phosphorylation of CEP192, which generates attachment sites for γ -TuRC, its adaptor protein NEDD1 and cytoskeleton-associated protein 5 (CKAP5), facilitating

MT nucleation and anchorage to establish the mitotic spindle. Despite maturation, the two centrosomes need to migrate to the opposite poles of the cells to ensure bipolarity of the spindle apparatus. This movement depends on the interaction of either the MT motor protein kinesin-5 (Eg5/ KIF11) and kinesin-12 (KIF15) (Joukov and De Nicolo 2018) or kinesin-13 (MCAK/KIF2C) and kinesin-8 (KIF18b) with Aurora-A, PLK1 and Cep192 (van Heesbeen et al. 2017; Joukov, Walter, and De Nicolo 2014). Upon recruitment of kinesin-5 to the MT network between the two centrosomes and its phosphorylation (Dutertre, Descamps, and Prigent 2002), kinesin-5 mediates the sliding of antiparallel MT, forcing the centrosomes apart to form the spindle poles at opposite sides of the cells (Nikonova et al. 2013; Dutertre, Descamps, and Prigent 2002; E. Willems et al. 2018; Joukov and De Nicolo 2018). Furthermore, Aurora-A inhibits MT depolymerases, promotes MT polymerization and stability to aid in mitotic spindle formation and stabilization (E. Willems et al. 2018; Dutertre, Descamps, and Prigent 2002). Defects in the centrosome separation machinery can lead to the formation of a monopolar spindle, which is unable to segregate the chromosomes (van Heesbeen et al. 2017).

A process called disengagement in late mitosis on the other hand, prevents centriole over duplication and the occurrence of multipolar mitotic spindles (Nigg and Raff 2009; Tsou and Stearns 2006). Therefore, the cysteine protease separase, cleaves the cohesin protein complexes that links the replicated centrioles, in an Aurora-A and PLK1-dependent cascade to allow the protein complexes to separate (Joukov, Walter, and De Nicolo 2014). Disengagement of the centrioles during mitosis is a prerequisite for the duplication of the centrioles in the S-phase, thus limiting centrosome duplication to a single round per cell cycle (Tsou and Stearns 2006). Furthermore, it provides a direct temporal link to the SAC, as the APC/C-triggered release of separase is involved in both sister chromatid and centrosome separation, effectively coupling the DNA-replication and centrosome cycle during mitosis (Bettencourt-Dias and Glover 2007; Tsou and Stearns 2006). During anaphase, the APC/C mediated degradation of Cyclin B by the proteasome leads to a decline in CDK1 activity (Bassermann, Eichner, and Pagano 2014; Skaar and Pagano 2009) and the reorganization of the mitotic spindle is initiated. An important factor of this reorganization process is protein required for cytokinesis 1 (PRC1), which is no longer inhibited by CDK1-phosporylation as anaphase progresses and assists MT bundling to build an array of antiparallel MTs between the segregating chromosomes called spindle midzone or central spindle (Fededa and Gerlich 2012). Furthermore, the central spindle enriches in a MT-associated protein like the centralspindlin complex, which contains the kinesin motor protein MKLP1, which in turn helps recruits the CPC including Aurora B to the spindle midzone. This translocation depends on the absence of CDK1-mediated phosphorylation on MKLP1 and the CPC component INCENP, MKLP2 activity and the removal of Aurora-B from inner anaphase centromere (Trivedi and Stukenberg 2020).

Even though the exact mechanism remains elusive, a variety of CRL ligase complexes containing CUL3 in combination with KLHL21 (Maerki et al. 2009), KLHL9 and KLHL13 (Sumara et al. 2007), probably in combination with the p97-ATPase (Ramadan et al. 2007) and the ubiquitin binding protein UBASH3B (Krupina et al. 2016) are necessary for the relocation of Aurora B (Trivedi and Stukenberg 2020).

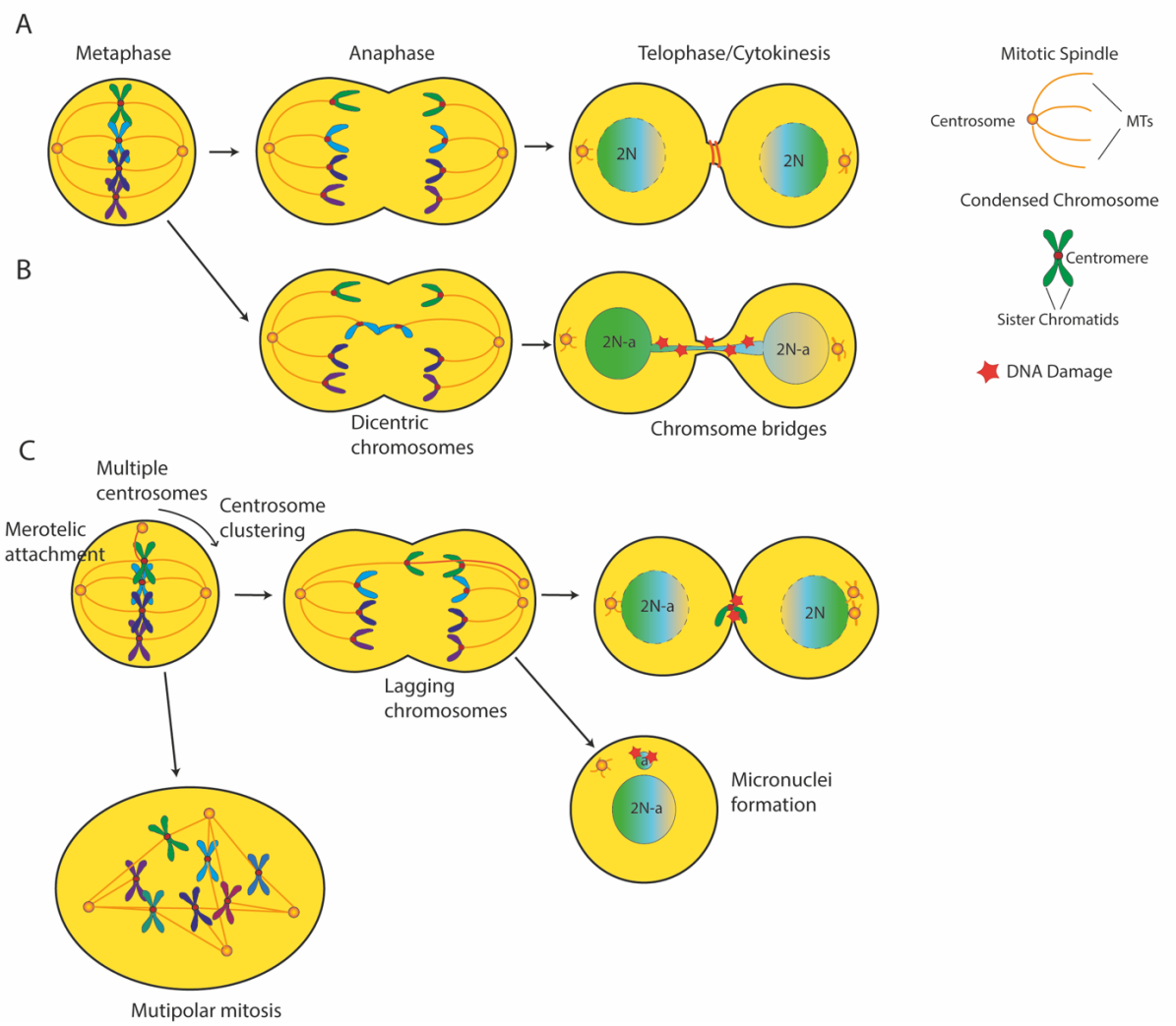

Figure 8. DNA damage induction by chromosome segregation and mitotic errors. **A**, Undisturbed mitotic division. During metaphase, condensed chromosomes line up at the metaphase plate and attach to a network of microtubules (MT) anchored at the centrosomes – the mitotic spindle. At this stage, unattached kinetochores activate an inhibitory SAC signal, which in hinders progression to anaphase. Upon SAC satisfaction, sister chromatids are separated by cleavage of securin and cells progress to anaphase, during which chromatids are pulled to the opposite spindle poles. Once the spindle midzone is free, the cleavage furrow starts to ingress and cytokinesis and abscission separate the resulting daughter cells. During this time, chromosomes start to decondense and new nuclear envelopes are formed. **B**, Fusion of two chromosomes upon telomere crisis generates dicentric chromosomes, which can, when attached to opposite spindle poles, result in a chromatin bridge that connects resulting daughter nuclei. The newly formed nuclear membrane surrounding the bridging DNA is disrupted in the next interphase and the exposed DNA is severely damaged by cytoplasmic nucleases while separating the daughter cells. **C**, Additional centrosomes may lead to a permanent or transient multipolar spindle and lagging chromosomes. Even if centrosome clustering prevents a multipolar cell division, the abnormal numbers of centrosomes increase the rate of merotelic attachments, where the same sister kinetochore is bound to MTs pulling from opposite spindle poles. These chromosomes can be held back at the spindle midzone during anaphase and may therefore be mis-segregated or incorporated into micronuclei, where they may acquire DNA damage in the interphase of the subsequent cell cycle. Additionally, lagging chromosomes can be trapped in the ingressing cleavage furrow, resulting in DNA damage. [Figure adapted from (Levine and Holland, 2018)]

These first events of cytokinesis and telophase, are overlapping with and followed by the assembly of a contractile actomyosin ring, assembled from actin filaments and active myosin II after activation of RhoA-GTP by ECT2. This Rho-GEF is tethered to the central spindle by centralspindlin subunit upon PLK1 phosphorylation and after CDK1 inactivation, thereby

synchronizing cytokinesis even tighter with chromosome segregation (Fededa and Gerlich 2012). After assembly of the ring structure, it contracts creating a cleavage furrow in the attached plasma membrane until an intercellular bridge of only a couple of micrometers remains. Aurora-B activity at the midbody is maintained until the division plane is free of unsegregated chromatin to avoid DNA damage of lagging chromosomes and chromosome bridges, that become trapped in the cleavage furrow, by phosphorylating and stabilizing MKLP1 and a regulatory subunit of the endosomal sorting complex (ESCRT)-III, thus preventing cleavage furrow ingression (Steigemann et al. 2009; Williams et al. 2021). Upon Aurora-B inactivation by dephosphorylation and proteasomal degradation at the end of telophase/mitotic exit (S. Stewart and Fang 2005; Steigemann et al. 2009), the endosomal sorting complex (ESCRT)-III, which is essential for abscission and accumulated close to the midbody after PLK1 is degraded and thereby inactivated during late telophase, triggers the formation of so-called 17 nm filaments (Fededa and Gerlich 2012; Gatta and Carlton 2019; Carlton and Martin-Serrano 2007). These membrane-associated structures form helices on the intercellular bridge bring the opposing plasma membranes into direct contact, leading to their fission (Fededa and Gerlich 2012), resulting in the physical separation of two daughter cells (Figure 8).

1.5.2 The DNA damage response (DDR)

DNA single and especially double strand breaks pose a major risk to genomic integrity and cells with detected unresolved DNA damage are prevented from proliferation. Those strand breaks are recognized by damage ‘sensors’ like the MRN (Mre11/Rad50/Nbs1) complex or Ku70-Ku80 heterodimers in case of DNA double strand breaks (DSB) or RPA (replication protein A) and ATRIP for single strand breaks (Falck, Coates, and Jackson 2005). These complexes tether the phosphatidylinositol-3-kinase-like kinases (PIKKs) ATM and ATR, which mediate the phosphorylation of Ser-139 on histone H2XA, resulting in well described gamma-H2AX-foci at the sites of the DNA damage (M T Hayashi and Karlseder 2013; Malumbres and Barbacid 2009). These foci amplify the DDR in a positive feedback loop via MDC1 (Stucki et al. 2005) and TOPBP1 (Cimprich and Cortez 2008) respectively. ATM and ATR furthermore initiate DNA repair mechanisms, in case of ATR by stalling the replication fork during S-phase and activating the checkpoint kinases CHK1/2 (Cimprich and Cortez 2008; Falck, Coates, and Jackson 2005; Barnum and O’Connell 2014; M T Hayashi and Karlseder 2013). Consequently, CHK1 and CHK2 phosphorylate the phosphatase Cdc25A, as well as the transcription factor p53 and its negative regulator MDM2 among others. This leads to the ß-TrCP-mediated ubiquitylation and subsequent proteasomal degradation of both Cdc25A and MDM2, which together with the p53 transcriptional program delays cell cycle progression at the G1/S-, G2/M- or intra-S checkpoints (Bassermann, Eichner, and Pagano 2014; Borg and Dixit 2017; Inuzuka et al. 2010). This delay enables the cell to either repair the detected DNA damage or triggers cellular senescence (Giunta and Jackson 2011; B. S. Zhou and Elledge 2000; Bartek and Lukas 2003).

1.5.3 DNA damage and genomic instability during mitosis

As outlined above, a multitude of mechanism ensure error free segregation of the duplicated genetic material during cell division in non-transformed cells. The interplay between the pathways is immense and the disruption or dysregulation of a single component can lead to the propagation of damaged DNA and genomic instability, which has been established as a

hallmark of cancer (Negrini, Gorgoulis, and Halazonetis 2010) and becomes apparent, as between 70 and 80% of solid and around 70% of hematopoietic tumors in humans are believed to have an altered number of chromosomes – a state called aneuploidy (Duijf, Schultz, and Benezra 2013; Potapova and Gorbsky 2017). Indeed, mitotic errors can cause aneuploidy (Potapova and Gorbsky 2017), structural chromosomal rearrangements like translocations, deletions and amplifications (Levine and Holland 2018), as well as DNA-double strand breaks (Thompson, Gatenby, and Sidi 2019) with transformative potential. In already checkpoint compromised cells like cancer cells, these events can potentially drive cancer evolution (Giam and Rancati 2015; Sansregret and Swanton 2017; Negrini, Gorgoulis, and Halazonetis 2010).

During mitosis, the activation of the DDR pathways downstream of ATM and ATR are impaired due to the inhibitory effects of CDK1 and PLK1 on CHK1/2, RNF8 and 53BP1 (Thompson, Gatenby, and Sidi 2019; M T Hayashi and Karlseder 2013; Giunta and Jackson 2011). It is widely believed that the suppression of DNA repair mechanisms especially of NHEJ, is a cellular mechanism to prevent telomere fusions and other DNA translocations while sister chromatids are in close proximity during mitosis. Cells with moderate DNA damage acquired during mitosis or the preceding S/G2 phases, are thus thought to progress through mitosis, followed by restriction point activation and DNA damage repair during the subsequent G1 phase (Giunta and Jackson 2011). Extensive DNA damage on the other hand is believed to lead to prolonged mitosis and subsequent cell death within the cell cycle phase, a process called mitotic catastrophe, in a SAC dependent but ATM independent process (M T Hayashi and Karlseder 2013; Thompson, Gatenby, and Sidi 2019; Manchado, Guillamot, and Malumbres 2012; Nitta et al. 2004). Another outcome of prolonged mitosis is the propagation of damaged DNA to the next cell cycle phase, as APC/C background activity while the SAC is activated can be sufficient to mediate Cyclin B degradation and mitotic exit. This leads to the completion of mitosis by cells, prior to proper spindle assembly, a process called mitotic slippage (S. Zhang et al. 2020; Molina et al. 2020). This phenomenon poses a great risk to the genomic integrity to the resulting daughter cells as the chromosomes might not be segregated correctly.

While mutations that inactivate the SAC completely exist in cancer cells with high tolerance for DNA-damage, these mechanisms are not believed to have a great effect on genomic instability in general, as the onset of anaphase before all kinetochores are attached to the mitotic spindle usually results in a very severe miss-segregation of chromosomes and subsequent reduction of cellular fitness and cell death (Levine and Holland 2018; Sansregret and Swanton 2017). However, there are mitotic errors that are not reliably detected by a possibly compromised checkpoint, evolve from prolonged arrest in metaphase itself like telomere deprotection and DNA damage followed by mitotic slippage (Uetake and Sluder 2010; Demidenko et al. 2008) or occur at later stages of mitosis (Trivedi and Stukenberg 2020; Potapova and Gorbsky 2017; M T Hayashi and Karlseder 2013; Levine and Holland 2018; Uetake and Sluder 2010). One of the infrequent detected errors are merotelic kinetochore attachments in which the kinetochore of a chromatid is attached to different spindle poles. These miss-attachments can stem from alterations in Aurora A/B and/or PLK1 activity, leading to a hyper-stabilization of kinetochore-MT interactions regardless of the attachments nature, alterations in kinetochore structure or the establishment of multipolar mitotic spindles (Figure 8) (Adams, Carmena, and Earnshaw 2001; Trivedi and Stukenberg 2020; Levine and Holland 2018).

Multipolar mitotic spindles can be caused in a couple of different ways but are often a direct result of centrosome amplifications (Sansregret and Swanton 2017). Even though, replication of the centrioles is tightly controlled during S- and M-phases (Tsou and Stearns 2006; W. J. Wang et al. 2011), increased expression and activity of PLK4 (Nigg and Raff 2009)

or a decrease of its inhibitor FAM46C (Kazazian et al. 2020) can lead to the generation of multiple centrosomes during S-phase. Furthermore, the amplification can result from a cytokinesis and abscission failure in a previous cell division (M T Hayashi and Karlseder 2013; Fededa and Gerlich 2012), from virus mediated or spontaneous cell fusion, or endoreplication of the DNA and the centrioles (Levine and Holland 2018; Nigg and Raff 2009). Such multipolar cell divisions can result in more than two daughter cells with only fractions of the replicated genome per cell. While polyploid cells like cancer cell might be able to compensate the loss, most cells show severely compromised viability and eventually undergo apoptosis. Additionally, a process called centrosome clustering, in which multiple centrosomes move to the opposite cellular poles in close proximity to build a bipolar spindle, can prevent the cells from severe chromosome losses (Levine and Holland 2018; Leber et al. 2010) but favor merotelic attachments, as the clustering of the centrosomes occurs randomly. Merotelic as well as syntelic attached kinetochores are prone to produce lagging chromosomes, which remain on the division plane during cytokinesis and telophase. Thereby the DNA material can either interfere with cytokinesis and abscission by either triggering the abscission checkpoint in an Aurora-B dependent manner (Steigemann et al. 2009) or cause DNA damage (M T Hayashi and Karlseder 2013).

Chromosomes that failed to leave the spindle midzone, become trapped in the ingressing cleavage furrow leading to DNA damage including double strand breaks, ATM-dependent DDR in the following G1-phase and potentially unbalanced translocations (Janssen et al. 2011). Furthermore, lagging chromosomes can be engulfed by a new nuclear membrane before reuniting with the chromosome mass forming so called micronuclei. These can acquire DNA damage in the next cell cycles due to delayed DNA replication extending to the next mitotic cycle, which leads to the condensation of replicating DNA and thereby DNA fragmentation (Crasta et al. 2012; C. Z. Zhang et al. 2015). Additionally, the nuclear envelope of the micronuclei is reported to be defective in nuclear- cytoplasmic transport (Potapova and Gorbsky 2017) and to rupture spontaneously, due to changes in lamina organization, exposing the chromatin to cytoplasmic stressors (Hatch et al. 2013). Another source for cytoplasmic DNA exposure is the establishment of a so-called chromatin bridge. In this special case, unresolved ultra-fine DNA bridges (UFBs) resulting from sister chromatid non-disjunction(Y. W. Chan, Fugger, and West 2018) or dicentric chromosomes, sister chromatids with fused telomeres due to telomere shortening and deprotection, establish a stable connection between the two daughter nuclei, that either leads to cytokinesis failure or persists until early G1-phase (Dewhurst 2020; Thompson, Gatenby, and Sidi 2019; Makoto T. Hayashi et al. 2015). Upon rupture of the newly build nuclear envelope along the chromosome bridge and exposure of the chromatin to cytoplasmic nucleases, the bridge is resolved but results in randomly fragmented and later rearranged chromosome stretches with clusters of APOBEC-mediated mutagenesis and induction of the DDR (Maciejowski et al. 2015; Dewhurst 2020).

The mechanisms causing DNA damage during mitosis are diverse and at the same time the detection during cell division is limited, leading to cells that exit mitosis in the presence of DNA damage (Uetake and Sluder 2010). Furthermore, a lot of mitotic errors lead to DNA damage and the corresponding DDR in the next cell cycle(s) and can thereby induce cells to arrest in the subsequent G1-phase, especially in p53 competent cells (Uetake and Sluder 2010; Maciejowski et al. 2015; Fong et al. 2016; Janssen et al. 2011; Demidenko et al. 2008; Levine and Holland 2018).

1.6 The UPS in NF-κB signaling

1.6.1 UPS dependent pathway activation

Nuclear Factor kappa B (NF-κB) signaling has been studied extensively and was found to be a master regulator of gene expression present in almost every cell type (Karin and Ben-Neriah 2000). A variety of stimuli like pathogen-derived particles, UV-radiation and cytokines induces DNA binding of transcription factors leading to the induction of either the so called canonical/classical or the non-canonical/alternative NF-κB pathway (Kanarek and Ben-Neriah 2012). The family of NF-κB transcriptions factors is comprised of p65 (RelA), RelB, c-Rel, p50/p105 (NF-kB1) and p52/p100 (NF-kB2), which form various dimers in their active, DNA-binding form to tailor a transcriptional response to the various stimuli (Q. Zhang, Lenardo, and Baltimore 2017).

In resting cells, the different NF-κB transcription subunits are sequestered in the cytoplasm due to their interaction with members of the IκB family(Hayden and Ghosh 2004). Upon stimulation of the classical NF-κB pathway, by for example exposure to the cytokine TNF-a, the ß-subunit of the IκB kinase (IKK) complex gets activated and phosphorylates a subset of IκB proteins - IκBa, IκBb and IκBe. These are then recognized by the E3-ubiqutin ligase ß-TrCP/FBXW1 (Kanarek and Ben-Neriah 2012) and degraded by the 26S-proteasome, which exposes the nuclear localization sequences (NLS) of the NF-κB TFs and allows them to translocate to the nucleus (Hayden and Ghosh 2008). Due to this mechanism of activation, which is independent of de-novo protein synthesis (Sen and Baltimore 1986a) the transcriptional response that follows is very rapid. The UPS is not only responsible for the degradation of the IκB proteins but also for the generation of p50 and p52 to form their respective precursor proteins, which act as additional IκB-proteins through their interaction with their processed counterparts (Karin and Ben-Neriah 2000). NF-κB1/p50 is processed continuously by limited proteolysis of the precursor protein p105 through the 26S-proteasome following ubiquitylation by KIP1 ubiquitination-promoting complex (KPC) (Kravtsova-Ivantsiv et al. 2015). Upon stimulation of the canonical NF-κB pathway, this processing is enhanced and together with the induction of complete ß-TrCP-mediated degradation of p105 and the degradation of the classical IκBs described above, allows for rapid translocation of the NF-κB TF subunits to the nucleus (Kanarek and Ben-Neriah 2012). In contrast to the continuous processing of p105, the generation of p52 from p100, a central part of the non-canonical pathway, is stimulation dependent in most cell types (Sun 2011). NF-κB2/p100 not only acts as a precursor but also as the major IκB(-like) protein of the non-canonical signaling pathway by sequestering RelB in the cytoplasm.

Unlike the canonical, the non-canonical pathway depends on protein de novo synthesis (Hayden and Ghosh 2008). The NF-κB-inducing kinase (NIK), which is the central regulator of this branch of the pathway, is constantly synthesized and targeted by TRAF3/2 and the cIAP1/2 ubiquitin ligase complex for degradation by the 26S-proteasome (Vallabhapurapu et al. 2008). Upon stimulation of CD40, BAFFR or RANK, the TRAF2/3 are recruited to the crosslinked receptors, where they are in turn ubiquitylated by cIAP2/3 and proteasomaly degraded. Thereby newly synthetized NIK can accumulate (Sun 2011) and recruits and activates IKKa, which then phosphorylates p100, leading to its ubiquitylation by ß-TrCP and subsequent degradation. This generates p52 homodimers as well as p52:RelB heterodimers, which are able to translocate to the nucleus (Hayden and Ghosh 2004) an trigger a transcriptional response.

1.6.2 UPS dependent NF-κB regulation in the nucleus

To halt this transcriptional response and prevent cellular exhaustion, hypo-responsiveness, tissue damage and various diseases (Durand and Baldwin 2017), NF-κB signaling needs to be properly terminated. One mechanism that involves the UPS, centers around the protein A20. It harbors deubiquitylation as well as E3-ligase activity, which is induced as a negative feedback loop and mediates the removal of a variety of K63-linked ubiquitin chains implicated in the recruitment of receptor complexes upstream of the IKK complex (Q. Zhang, Lenardo, and Baltimore 2017), but also targets the kinase receptor-interacting protein 1 (RIP1) for proteasomal degradation (Harhaj and Dixit 2012), disassembling the signaling complexes. Additionally, the activating NF-κB transcription factor dimers need to be removed from IκB enhancers of the DNA (Karin and Ben-Neriah 2000). Thus newly translated IκBa and IκBe, also directly induced upon NF-κB stimulation in a feedback loop, are able to translocate to the nucleus, bind to the DNA-bound transcription factors and shuttle them back to the cytoplasm (Hayden and Ghosh 2008; Ruland 2011).

More recently, another level of regulation/termination of NF-κB in the nucleus has emerged. This involves the K48-polyubiquitylation and subsequent proteasomal degradation of DNA-bound NF-κB-subunits for example of the NF-κB-subunit p65 (Ryo et al. 2003). Over the years several E3-ligases have been described to target this particular subunit (Tanaka, Grusby, and Kaisho 2007; Shin et al. 2017; Maine et al. 2007; Jodo et al. 2020). One example is PDLIM2, which shuttles p65/Rel-A to promyelocytic leukemia nuclear bodies prior to polyubiquitylation (Tanaka, Grusby, and Kaisho 2007). The other described E3-ligase complex is comprised of SOCS1, Cullin-2 (CUL2) and COMMD1, also known as EC2S complex, in which COMMD1 mediates the interaction between Rel-A and SOCS1/CUL2 upon stimulation with proinflammatory cytokines (Maine et al. 2007).

A similar concept was reported for the removal of transcription inhibiting p50 homodimers from the DNA in the absence of BCL3 (Carmody et al. 2007; Collins, Kiely, and Carmody 2014). The rationale behind this was, that B-cells, macrophages and dendritic cells from BCL-3 knock out mice produced higher levels of cytokines, when treated with different Toll-like receptor (TLR) ligands, indicating a hyperactivation of NF-κB-signaling. As p50:p50 complexes lack a TAD domain, they are believed to repress expression either by blocking activatory dimers from binding kB-promotor regions or by recruiting histone deacetylases (HDACs) (Smale 2012) and are reported to interact with the BCL3 (Palmer and Chen 2008). Carmody et al. therefore investigated whether altered p50 DNA binding was responsible for the NF-κB hyperactivation in BCL-3 knock out mice and found the lack of BCL3 interaction with DNA-bound p50 homodimers to enable the K48-polyubiquitylation and degradation of nuclear NF-κB1 (Carmody et al. 2007). A responsible E3 ubiquitin ligase was not implicated.

2. Aim of this study

B-cell derived tumors originate from uncontrolled growth and a lack of terminal differentiation at various stages of a B-cell`s development and make up approximately 95% of all lymphomas (Küppers 2005). Even though the treatment options for B-cell malignancies evolved during recent years, most subtypes remain uncurbable and novel therapeutic targets are highly demanded (Frontzek and Lenz 2019; Lange, Lenz, and Burkhardt 2017; Mikhael et al. 2019; Kumar et al. 2017). A subset of B-cell lymphomas like ABC-type DLBCL as well as MM originate from post-germinal center B-cells (Basso and Dalla-Favera 2015) and are therefore characterized by chronically active NF-κB-signaling (Schmitz et al. 2018; Young et al. 2015; Phelan et al. 2018; Davis et al. 2010; Demchenko and Michael Kuehl 2010; Chapuy et al. 2018). The strong dependency of this cellular signaling pathway on the UPS (Hayden and Ghosh 2008) and the substantial responsiveness of especially MM patients towards proteasomal inhibition (Guerrero-Garcia et al. 2018; Kumar et al. 2017), resulted in the theory that aberrant functions of the UPS drive and maintain these disease types (Bianchi et al. 2009). As most patients eventually become resistant to proteasomal inhibitors like bortezomib and carfilzomib (Saavedra-Garcia, Martini, and Auner 2019), the identification and in depth characterization of novel dependencies from the UPS for example DUB/E3-ligase-substrate pairs might provide novel therapeutic targets for drug development even in resistant patients.

The aims of this study were therefore (I) to identify and characterizes novel disease relevant members of the UPS starting from MM and MCL patient samples, (II) to delineate the mechanism by which the activity of the DUB OTUD6B is timed to the G1/S transition to mediate its oncogenic function in MM and (III) to evaluate the functional relevance of the SCF-complex substrate adaptor FBXO21 in the proteasomal degradation of NF-κB inhibitory p50-homodimers.

3 Material

3.1 Devices and Instruments

Device	Supplier
Aqualine water bath	Lauda-Brinkmann
Axiovert 40 CFL with HBO50	Carl Zeiss
Mini-Sub® Cell GT system for agarose electrophoresis	Bio-Rad Laboratories
BioSAFE SC-smart CHRONOS 220	Cryotherm
BransonSonifier 250	Heinemann
Centrifuge 5417R with rotor F453011	Eppendorf
Centrifuge 5424 with rotor FA452411	Eppendorf
Concentrator plus	Eppendorf
Curix 60	Agfa
ENVAIReco safe Comfort Sterilwerkbänke	ENVAIR
FACS Accrui C6 plus	BD Biosciences
FACSCalibur	BD Biosciences
Fridges and lab freezers	Liebherr
GEL IX IMAGER 20	INTAS
GloMax Explorer Multimode Microplate Reader	Promega
HERAcell 150i CO2 incubator	Thermo Fisher Scientific
HERAfreeze	Thermo Fisher Scientific
HERASafe KS safety cabinet	Thermo Fisher Scientific
Hypercassette™	Amersham Biosciences
Innova® 40 shaker for bacteria	New Brunswick Scientific
Invitrogen Chamber for Ready Gels	Invitrogen
LTQ Orbitrap Velos mass spectrometer	Thermo Fisher Scientific
Magnetic thermo stirrer RCT basic	IKA Laboratory Equipment
Mastercycler nexus	Eppendorf
Mini-PROTEAN Tetra cell SDS electrophoresis system	Bio-Rad Laboratories
Mithras LB 940 Multimode Microplate Reader	BERTHOLD TECHNOLOGIES
Multifuge 3SR+	Thermo Fisher Scientific
NanoPhotometer	Implen
Neubauer chamber	Marienfeld
Novex Mini cell system for precast NuPAGE gels	Thermo Fisher Scientific
peqSTAR Thermocycler	Peqlab Biotechnology
Pipetman neo	Gilson
Polymax 1040 platform shaker	Heidolph Instruments
PowerPac Basic power supply	Bio-Rad Laboratories
PowerPac HC power supply	Bio-Rad Laboratories
Precision balance 572-37	Kern & Son
Quintix® Analytical Balance	Sartorius
Scanner V850 Pro	Epson
SevenCompact pH/Ion pH-meter	Mettler-Toledo
SP8 confocal microscope	Leica Microsystems
Thermo block MBT250	Kleinfeld Labortechnik
Thermomixer compact	Eppendorf
Tube rotator	Fröbel Labortechnik
Tumbling roller mixer RM5	Neolab

3.2 Consumables

Consumable	Supplier
3mm CHR paper (Whatman)	GE Healthcare
Biodyne™ B Nylon Membrane	Thermo Fisher Scientific
Cell culture flasks	Greiner Bio-One
Cell culture plates	Biochrom/Falcon/Techno
Cell scraper	Sarstedt
CL-XPosure™ Films	Thermo Fisher Scientific
Glass Vover slips for microscope slides	Sarstedt
Hypodermic needles	Braun
Immobilon-P PVDF transfer membrane	Merck Millipore
Pipette tips	Sarstedt
SafeSeal tubes	Sarstedt
Serological pipettes	Greiner Bio-One
Syringe filters	TPP/Biochrom
Syringes	Braun
UVette routine pack	Eppendorf
x-well chamber slides on PCA detachable	Sarstedt

3.3 Chemicals and Reagents

Chemical/reagent	Supplier
16 % Formaldehyde, methanol free	Thermo Fisher Scientific
ß-Mercaptoethanol	Sigma-Aldrich
2-Propanol	Carl Roth
3x FLAG Peptide	Sigma-Aldrich
5- Bromo-2′-deoxyuridine (BrdU)	Sigma-Aldrich
Acetic acid glacial	Carl Roth
Acetone	Carl Roth
C&L fixer solution type F	Christiansen and Linhardt
C&L developer solution type E	Christiansen and Linhardt
Agarose NEEO	Carl Roth
Albumin Fraction V (BSA)	Carl Roth
Ammonium persulfate (APS)	Sigma-Aldrich
Ampicillin sodium salt	Sigma-Aldrich
Anti-FLAG M2 Affinity Gel	Sigma-Aldrich
Anti-HA-Agarose	Sigma-Aldrich
Aprotinin from bovine lung	Sigma-Aldrich
Aqua ad injectable, sterile	B. Braun Melsungen
Bacto Agar	BD Diagnostics
Bacto Tryptone	BD Diagnostics
Bacto Yeast Extract	BD Diagnostics
BES buffered saline	Sigma-Aldrich
ß-Glycerolphosphate disodium salt hydrate (G-2-P)	Sigma-Aldrich
Blasticidin S HCl	Thermo Fisher Scientific
Boric acid	Sigma-Aldrich
Bortezomib	Janssen-Cilag
Brilliant Blue R 250	Carl Roth
Bromphenol Blue	Sigma-Aldrich
Calcium chloride dihydrate	Sigma-Aldrich.
CD40L (murine)	Thermo Fisher Scientific
Cycloheximide (CHX)	Sigma-Aldrich
Deoxycholic acid sodium salt	Sigma-Aldrich
Di-sodium hydrogene phosphate dihydrate	Merck Milliprore

Dimethylsulfoxid (DMSO)	Carl Roth
Disodium Phosphate	Carl-Roth
DL-Dithiothreitol	Sigma-Aldrich
DNA Loading Dye (6x)	Thermo Fisher Scientific
dNTP Mix, 10 mM each	Thermo Fisher Scientific
Dodecylsulfate-Na-salt (in pellets, SDS))	SERVA
Doxycyline Monohydrat	Sigma-Aldrich
Ethanol	Merck
Ethylene-bis(oxyethylenenitrilo)tetraacetic acid (EGTA)	Sigma-Aldrich
Ethylenediaminetetraacetic acid (EDTA)	Sigma-Aldrich
FACS Clean	BD Biosciences
FACS Flow	BD Biosciences
FACS Rinse	BD Biosciences
Formaldehyd (16 % w/v) (PFA)	Thermo Fisher Scientific
Fluoride ion solution (NaF)	Sigma-Aldrich
Gelatin from cold water fish skin	Sigma-Aldrich
GelRed Nucleic Acid Gel Stain	Biotium
Gibco™ Trypan Blue Solution, 0.4%	Thermo Fisher Scientific
Glucose	Sigma-Aldrich
Glutathione Sepharose 4B	GE Healthcare
Glycerol	Sigma-Aldrich
Glycin	Carl Roth
Guanidinium Chloride	Sigma-Aldrich
HA-ubiquitin-vinyl sulfone (HA-Ub-VS)	BostonBiochem
Hexadimethrine bromide (polybrene)	Sigma-Aldrich
Hexanucleotide Mix, 10x conc.	Roche
Hoechst3342	Sigma-Aldrich
Hydrochloric acid 32%	Carl Roth
Hydrochloric acid fuming 37%	Carl Roth
IgM (murine)	Thermo Fisher Scientific
IL-4 (murine)	Thermo Fisher Scientific
Imidazole	Sigma-Aldrich
Kanamycin sulfate	Sigma-Aldrich
LDC000067	Selleckchem
Leupeptin	Sigma-Aldrich
Lipofectamine 2000 Reagent	Thermo Fischer Scientific
Lipofectamine RNAiMAX Reagent	Thermo Fischer Scientific
Lipopolysaccharide	Thermo Fisher Scientific
Magnesium chloride anhydrous	Sigma-Aldrich
Magnesium sulfate anhydrous	Sigma-Aldrich
Methanol	J. T. Baker
MG132	Biotechne/Tocris Bioscience
MLN4294	Biotechne/Tocris Bioscience
N-(2-Hydroxyethyl)piperazine-N-2-ethane sulfonic acid (HEPES)	SERVA
N-p-Tosyl-L-phenylalanine chloromethyl ketone(TPCK)	Sigma-Aldrich
N,N,N`,N``-tetramethyl-ethylenediamine (TEMED)	Sigma-Aldrich
Ni-NTA Agarose	Qiagen
Nocodazole	Sigma-Aldrich
Nonidet P-40 substitute (10%)	Roche
NuPAGE MES SDS Running buffer (20x)	Thermo Fisher Scientific
Nα-Tosyl-L-lysine chloromethyl ketone hydrochloride (TLCK)	Sigma-Aldrich
Okadaic Acid Prorocentrum sp.	Calbiochem
Palbociclib	Sigma-Aldrich
PBS Dulbecco, powder	Merck Millipore/Biochrome
Penicillin-Streptomycin (10.000 U/ml)	Thermo Fisher Scientific
Phenylmethanesulfonylfluoride solution (PMSF)	Sigma-Aldrich

PI/RNase staining buffer	BD Pharmingen
Poly-D-Lysin hydrobromide	Sigma-Aldrich
Poly-L-Lysin solution 0.1%	Sigma-Aldrich
Ponceau S solution	Sigma-Aldrich
Potassium chloride	Sigma-Aldrich
ProLong™ Diamond Antifade Mountant	Thermo Fisher Scientific
Propidium iodide (PI)	Sigma-Aldrich
Protein A Sepharose CL-4B	GE Healthcare
Protein G Agarose, Fast Flow	Sigma-Aldrich
Protein G Sepharose 4 Fast Flow	GE Healthcare
Puromycin	Thermo Fisher Scientific
RNaseOUT Recombinant Ribonuclease Inhibitor	Thermo Fisher Scientific
Rotiphorese NF-Acrylamide/Bis-solution 40% (29:1)	Carl Roth
Saponin	Sigma-Aldrich
SERVA DNA Stain Clear G	SERVA Electrophoresis
Skim Milk Power	Sigma-Aldrich
SOC Medium	New England Biolabs
Sodium acetate	Merck
Sodium azide	Merck
Sodium carbonate	Merck
Sodium chloride	Carl Roth
Sodium dihydrogen phosphate monohydrate	Merck
Sodium fluoride	Sigma-Aldrich
Sodium hydroxide solution 45%	Carl Roth
Sodium orthovanadate	Sigma-Aldrich
Sodium phosphate dibasic	Sigma-Aldrich
Sodium tetraborate	Sigma-Aldrich
Sodium thiosulfate pentahydrate	Sigma-Aldrich
Strep-Tactin Superflow	IBA Lifesciences
Succore	Sigma-Aldrich
SuperSignal West Femto Maximum Sensitivity Substrate	Thermo Fisher Scientific
SuperSignal West Pico Chemiluminescent Substrate	Thermo Fisher Scientific
TRIS-acetat-EDTA (TAE) buffer (50x)	Thermo Fisher Scientific
Thymidine	Sigma-Aldrich
TNF-a (murine)	PeproTech
TNF-a (rec., human)	PeproTech
Trichloroacetic acid solution (TCA)	Sigma-Aldrich
TRIS	Carl Roth
Triton X-100	Sigma-Aldrich
Trypsin inhibitor from soybean	Sigma-Aldrich
Trypsin-EDTA (0.5%), no phenol red	Thermo Fisher Scientific
Tween 20	Sigma-Aldrich
UltraPure TBE buffer (10x)	Thermo Fisher Scientific
Urea	Sigma-Aldrich
Water	Sigma-Aldrich

3.4 Commercial Kits

Kit	**Supplier**
96® AQueous One Solution Cell Proliferation Assay	Promega
DC Protein Assay	Bio-Rad Laboratories
GeneJET Gel Extraction Kit	Thermo Fisher Scientific
In-Fusion® HD Cloning Kit	Takara Bio USA
LightShift™ Chemiluminescent EMSA Kit	Thermo Fisher Scientific
LightShift™ EMSA Optimization and Control Kit	Thermo Fisher Scientific
Nano-Glo Dual-Luciferase Assay system	Promega

NucleoBond Xtra Midi	MACHEREY-NAGEL
peqGOLD Plasmid Miniprep Kit	Peqlab
Pierce™ Silver staining kit	Thermo Fisher Scientific
QIAquick PCR Purification Kit	Qiagen
QIAshredder	Qiagen
Rapid DNA Dephos & Ligation Kit	Roche
RNeasy Mini Kit	Qiagen
B Cell Isolation Kit, mouse	Miltenyi Biotech

3.5 Enzymes

Enzyme	**Manufacturer**
AgeI (BshTI)	Thermo Fisher Scientific
Alkaline Phosphatase, Calf Intestinal (CIP)	New England Biolabs
Antarctic Phosphatase	New England Biolabs
BamHI	Thermo Fisher Scientific
BsmBI	New England Biolabs
EcoRI	Thermo Fisher Scientific
DpnI	Thermo Fisher Scientific
KpnI	Thermo Fisher Scientific
NheI	Thermo Fisher Scientific
NotI	Thermo Fisher Scientific
Q5 DNA-polymerase	New England Biolabs
SalI	Thermo Fisher Scientific
XbaI	Thermo Fisher Scientific
XhoI	Thermo Fisher Scientific
MluI	Thermo Fisher Scientific

3.6 Oligonucleotides

Oligonucleotide	**Sequence (5'-3')**
Cloning Oligonucleotides	
FBXO21_XhoI_FWD	GCCCTCGAGGCCACCATGGCCGAATTCTTACTCATCTATGT TCTC
FBXO21_EcoRI_RV	GCCGAATTCTTACTCATCTATGTTCTC
FBXO21_NheI_FWD	GCCGCTAGCGCCACCATGGCGGCGGCAGCAGTCGACAGC
FBXO21_XhoI_RV	GCCCTCGAGTTACTCATCTATGTTCTC
KLHL14_NheI_FWD	GCC GCTAGC TCCAGATCCGGGGACAGG
KLHL14_SalI_RV	GCCGTCGACTTATTTGTTGTATGGTAC
KLHL14_XbaI_FWD	GCCTCTAGAGCCACCATGTCCAGATCCGGG
KLHL14_BamHI_RV	GCCGGATCCTTATTTGTTGTA
KLHL14_XbaI_FLAG_FWD	GCCTCTAGAGCCACCATGGACTACAAAGACGATGACGA CAAGTCCAGATCCGGG
KLHL14_AgeI_FWD	GCCACCGGTGCCACCATGTCCAGATCCGGGGACAGGA
KLHL14_MluI_RV	GCCACGCGTTTATTTGTTGTATGGTAC
KLHL14_AgeI_FLAG_FWD	GCCACCGGTGCCACCATGGACTACAAAGACGATGACGAC AAGTCCAGATCCGGGGA
KLHL14_SalI_del_KELCH6_RV	GCCGTCGACTTAGCTGTCATCAAGCACTGCAC
KLHL14_SalI_del_KELCH5-6_RV	GCCGTCGACTTAGCGATCATTCATTACA
KLHL14_SalI_del_KELCH4-6_RV	GCCGTCGACTTACCCATTGTGCA
KLHL14_SalI_del_KELCH3-6_RV	GCCGTCGACTTACTTGTCCAACCGA
KLHL14_SalI_del_KELCH2-6_RV	GCCGTCGACTTAGTTTTCCACCTC
KLHL14_SalI_del_KELCH_RV	GCCGTCGACTTATTTCTTGTTAGAGCGAATT
KLHL14_del_BTB_C-term_FWD	GCAGCTGTTTGACACGGTGGAGGA
KLHL14_del_BTB_N-term_RV	TCCTCCACCGTGTCAAACAGCTGCTTC
KLHL14_del_BACK_C-term_FWD	CAACAAGTACCTGTCAGTGGATTTCA

KLHL14_del_BACK_N-term_RV	TGAAATCCACTGACAGGTACTTGTTG
KLHL14_del_BTB_BACK_Cterm_F	GAAGCAGCTGTTTTCAGTGGATTTCA
KLHL14_del_BTB_BACK_Nterm_R	TGAAATCCACTGAAAACAGCTGCTTC
LIN28B_XbaI_FLAG_FWD	GCCTCTAGAGCCACCATGGATTACAAGGATGACG
LIN28B_BamHI_RV	CCGGGATCCTTATGTCTTTTTCCTTTTTTGAACTGAAGG

In-Fusion Cloning Primer

IF_BLASTresis_FWD	CCACCGGAGCTTACCATGGCCAAGCCTTTGTCTCAAGA
IF_BLASTresis_RV	GTCGTGGGGCGGGCGTTAGCCCTCCCACACATAACCAG
IF_PuroReplace_FWD	CGCCCGCCCCACGACCCGCAGC
IF_PuroReplace_RV	GGTAAGCTCCGGTGGATCCCCCTGG

Mutagenesis primer

LIN28B_S105A_FWD	GTAACAGGACCTGGTGGGGCCCCCTGTTTAGGAAGTGAAG
LIN28B_S105A_RV	CTTCTTTCACTTCCTAAACAGGGGGCCCCACCAGGTCCTGT
LIN28B_T202A_FWD	GGCATGGCTGTGCATCACCACCGTT
LIN28B_T202A_RV	AACGGTGGTGATGCACAGCCATGCC
LIN28B_S203A_FWD	GGCGGGCATGGCTGTACAGCACCACCGTTTCCTCAGG
LIN28B_S203A_RV	CCTCCTGAGGAAACGGTGGTGCTGTACAGCCATGCCC
LIN28B_S218A_FWD	ATCTCAGAACGGGCAGGCAGGTCAC
LIN28B_S218A_RV	GTGACCTGCCTGCCCGTTCTGAGAT
LIN28B_S221A_FWD	CTCAGAACGGTCAGGCAGGGCACCTCAAGAAGCTTCCTCC ACG
LIN28B_S221A_RV	CTTCGTGGAGGAAGCTTCTTGAGGTGCCCTGCCTGACCGT TCT
LIN28B_202/203A_FWD	GGCGGGCATGGCTGTGCAGCACCACCGTTTCCTCAGG
LIN28B_202/203A_RV	CCTGAGGAAACGGTGGTGCTGCACAGCCATGCCCGCC
LIN28B_S218/221A_FWD	CTCAGAACGGGCAGGCAGGGCACCTCAAGAAGC
LIN28B_S218/221A_RV	GCTTCTTGAGGTGCCCTGCCTGCCCGTTCTGAG

shRNA sequences

shFBXO21_#1_FWD	CCGGACTGGTGTGTATCCTAAATATCTCGAGATATT TAGGATACACACCAGTTTTTTG
shFBXO21_#1_RV	AATTCAAAAAACTGGTGTGTATCCTAAATATCTCGAGATATT TAGGATACACACCAGT
shLIN28B_FWD	CCGGGCCTTGAGTCAATACGGGTAACTCGGTTACCCGTAT TGACTCAAGGCTTTTTG
shLIN28B_RV	AATTCAAAAAGCCTTGAGTCAATACGGGTAACTCGAGTT ACCCGTATTGACTCAAGGC
shCDK9_FWD	CCGGCCGCTGCAAGGGTAGTATATACTCGAGTATATACTAC CCTT GCAGCGGTTTTTG
shCDK9_FWD	AATTCAAAAACCGCTGCAAGGGTAGTATATACTCGAGTATA TACTACCCTTGCAGCGG
shCtrl_FWD	CCGGCCTAAGGTTAAGTCGCCCTCGCTCGAGCGAGGGCG ACTTAACCTTAGGTTTTTG
shCtrl_RV	AATTCAAAAACCTAAGGTTAAGTCGCCCTCGCTCGAGCGA GGGCGACTTAACCTTAGG

Sequencng Primer

pTRIPZ_Seq_rv	GCGGGCCGCTGTCCTGAG
pTRIPZ_Seq_fw	GTCGAGGTAGGCGTGT
pHIV seq_FWD	TGG AAT TTG CCC TTT TTG AG
pHIV seq_RV	AGG AAC TGC TTC CTT CAC GA

siRNA constructs

Target	*Order number*	*Kind*
FBXO21	L-012917-00-0005	SMARTPool
Lin28B	L-028584-01-0005	SMARTPool
LIN28A	L-018411-01-0005	SMARTPool
Non-targeting Control	D-001810-10-05	SMARTPool

3.7 Bacteria

Bacteria strain	Supplier
NEB 5-alpha competent *E. coli*	New England Biolabs

3.8 Standards

Standard	Supplier
GeneRuler 1 kb DNA Ladder	Thermo Fisher Scientific
PageRuler Plus Prestained Protein Ladder	Thermo Fisher Scientific

3.9 Plasmids

Plasmid	Origin
pcDNA3.1-(+) zeo	Thermo Fisher Scientific
pcDNA3.1-C-FLAG-murine_p50	Addgene (#20018), S. Smale
pcDNA3.1-FBXO21	Prof. F. Bassermann
pcDNA3.1-FLAG-human_p50	U. Baumann
pcDNA3.1-FLAG-STREP-FBXO21	U. Baumann
pcDNA3.1-GFP-FBXO21	U. Baumann
pcDNA3.1-N-FLAG	Prof. F. Bassermann
pcDNA3.1-N-FLAG-A20	Prof. F. Bassermann
pcDNA3.1-N-FLAG-BTRC	Prof. F. Bassermann
pcDNA3.1-N-FLAG-CENT	C. Paulmann
pcDNA3.1-N-FLAG-FBXO21	R. Spallek, this study
pcDNA3.1-N-FLAG-IKKa	R. Spallek, this study
pcDNA3.1-N-FLAG-KLHL14	R. Spallek, this study
pcDNA3.1-N-FLAG-KLHL14_deltaBACK	R. Spallek, this study
pcDNA3.1-N-FLAG-KLHL14_deltaBTB	R. Spallek, this study
pcDNA3.1-N-FLAG-KLHL14_deltaBTB_BACK	R. Spallek, this study
pcDNA3.1-N-FLAG-KLHL14_deltaKELCH	R. Spallek, this study
pcDNA3.1-N-FLAG-KLHL14_deltaKELCH2-6	R. Spallek, this study
pcDNA3.1-N-FLAG-KLHL14_deltaKELCH3-6	R. Spallek, this study
pcDNA3.1-N-FLAG-KLHL14_deltaKELCH4-6	R. Spallek, this study
pcDNA3.1-N-FLAG-KLHL14_deltaKELCH5-6	R. Spallek, this study
pcDNA3.1-N-FLAG-KLHL14_deltaKELCH6	R. Spallek, this study
pcDNA3.1-N-FLAG-LIN28B	C. Paulmann
pcDNA3.1-N-FLAG-LIN28B_S105A	R. Spallek, this study
pcDNA3.1-N-FLAG-LIN28B_S105A_T202A_S218A	R. Spallek, this study
pcDNA3.1-N-FLAG-LIN28B_S105A_T202A_T203A_S218A_S221A	R. Spallek, this study
pcDNA3.1-N-FLAG-LIN28B_S203A	R. Spallek, this study
pcDNA3.1-N-FLAG-LIN28B_S218A	R. Spallek, this study
pcDNA3.1-N-FLAG-LIN28B_S221A	R. Spallek, this study
pcDNA3.1-N-FLAG-LIN28B_T202A	R. Spallek, this study
pcDNA3.1-N-FLAG-LIN28B_T203A_S221A	R. Spallek, this study
pcDNA3.1-N-FLAG-PKCd	U. Baumann
pcDNA3.1-N-FLAG-SKP1	D. Brockelt
pcDNA3.1-N-FLAG-Tti1	B. Targosz
pCR-Flag-IKKalpha	Addgene (#15467), H. Nakano
pHIV-EGFP-KLHL14	R. Spallek, this study
pHIV-EGFP-N-FLAG-KLHL14	R. Spallek, this study
pHIV-EGFP-N-FLAG-KLHL14_deltaBACK	R. Spallek, this study
pHIV-EGFP-N-FLAG-KLHL14_deltaBTB	R. Spallek, this study
pHIV-EGFP-N-FLAG-KLHL14_deltaBTB_BACK	R. Spallek, this study

pHIV-EGFP-N-FLAG-KLHL14_deltaKELCH	R. Spallek, this study
pHIV-Puro-FLAG-LIN28B	C. Paulmann
pHIV-Puro-FLAG-LIN28B	C. Paulmann
pLenti-Blast-6xHIS-Ubiquitin-WT	R. Spallek, this study
pLenti-Puro-6xHIS-Ubiquitin-WT	M. Dietachmeyr
pLKO.1 TRC cloning vector	Addgene (#10878), D. Root
pLKO.1-Puro-sh_scramble	Addgene (#1864), D. Sabatini
pLKO.1-Puro-shFBXO21	R. Spallek, this study
pLKO.1-RFP-sh_scramble	M. Heider, AG Bassermann
pLKO.1-RFP-shCDK9	C. Paulmann
pLKO.1-RFP-shLIN28B	R. Spallek, this study
pLKO.1-RFP-shOTUD6B-2	C. Paulmann
pMD2.G	Addgene (#12259), D. Trono
pMSCV	Clontech
pMSCV_FBXO21	R. Spallek, this study
pRK5-HA-Ubiquitin-WT	Addgene (#17608), T. Dawson
psPAX2	Addgene (#12260), D. Trono
pTRIPZ	Thermo Fisher Scientific
pTRIPZ-KLHL14	R. Spallek, this study
pTRIPZ-LIN28B	C. Paulmann
pTRIPZ-N-FLAG-KLHL14	R. Spallek, this study
pTRIPZ-RFP_only	R. Spallek, this study

3.10 Antibodies

Antibody (clone)	Species	Dilution(Application)	Supplier (Catalog#)
Centrin-3 (SS12)	Mouse	1:1000 (WB), 1:400 (IF)	Santa Cruz Biotech.(#sc-100933)
CUL1 (2H4C9)	Mouse	1:500 (WB)	Sigma-Aldrich (#32-2400)
a-tubulin (DM1A)	Mouse	1:400 (IF)	Sigma-Aldrich (#T9026)
a/ß-tubulin	Rabbit	1:1000 (WB), 1:400 (IF)	Cell Signaling Technology (#2148)
BCL-3	Rabbit	1:300 (WB)	Santa Cruz Biotechnology (#sc-185)
c-Rel	Rabbit	1:1000 (WB)	Cell Signaling Technology (#4727)
CDK9 (C12F7)	Rabbit	1:1000 (WB)	Cell Signaling Technology (#2316T)
Centrin-2	Rabbit	1:1000 (WB)	Santa Cruz Biotech. (#sc-27793)
Cyclin A (H-432)	Mouse	1:1000 (WB)	Santa Cruz Biotechnology (#sc-751)
Cyclin B1	Rabbit	1:500 (WB)	Cell Signaling Technology (#4138)
Cyclin D1 (G124-326)	Mouse	1:500 (WB)	BD Biosciences (#554180)
Cyclin E (HE12)	Mouse	1:1000 (WB)	Santa Cruz Biotechnology (#sc-247)
FBXO21 (OTI2C7)	Mouse	1:1000 (WB)	Origene (#TA504013)
FLAG	Rabbit	1:1000 (WB), 1:800 (IF)	Sigma-Aldrich (#F7425)
FLAG-M2	Mouse	1:1000 (WB)	Sigma (#F3165)
GFP (B-2)	Mouse	1:1000 (WB)	Santa Cruz Biotech (#sc-9996)
HA	Rabbit	1:1000 (WB)	Cell Signaling Technology (#3724)
Histone H2B	Rabbit	1:1000 (WB)	Merck (#07-371)
HSP90 (C45G5)	Rabbit	1:500 (WB)	Cell Signaling Technology (#4877S)
IκBa (L35A5)	Mouse	1:500 (WB)	Cell Signaling Technology (#4814S)
IκBzeta	Rabbit	1:1000 (WB)	Cell Signaling Technology (#9244S)
IKKa	Rabbit	1:1000 (WB)	Cell Signaling Technology (#2682S)
KLHL14	Rabbit	1:1000 (WB)	Proteintech (#16693-1-AP)
KLHL9/13 (D-4)	Mouse	1:1000 (WB)	Santa Cruz Biotech (#sc-166486)
LIN28B	Rabbit	1:1000-10000 (WB)	Cell Signaling Technology (#4196)
MCL1	Rabbit	1:1000 (WB)	Cell Signaling Technology (#4572)
NF-κB1 (p105/p50)	Rabbit	1:1000 (WB)	Cell Signaling Technology (#3035S)
NPM1 (FC-61991)	Mouse	1:1000 (WB)	Invitrogen (#32-5200)
NUDCD3 (H-10)	Mouse	1:1000 (WB)	Santa Cruz Biotech (#sc-514016)
OTUD6B	Rabbit	1:1000 (WB)	Abcam (#ab127714)
p-GSK-3f3 (S9)	Rabbit	1:1000 (WB)	Cell Signaling Technology (#9322)

p-H2A.X (S139)	Mouse	1:1000 (WB)	Santa Cruz Biotech (#sc-517348)
p-Histone H3 (S10)	Rabbit	1:1000 (WB)	Cell Signaling Technology (#9701)
p-IκBa (5A5)	Mouse	1:500 (WB)	Cell Signaling Technology (#9246S)
p-IKKa (16A6)	Rabbit	1:1000 (WB)	Cell Signaling Technology (#2697T)
p-p53 (S15)	Rabbit	1:1000 (WB)	Cell Signaling Technology (#9284)
p27 (G173-524)	Mouse	1:500 (WB)	BD Biosciences (#554069)
p53	Rabbit	1:1000 (WB)	Cell Signaling Technology (#9282)
p65 (D14E12)	Rabbit	1:500 (WB)	Cell Signaling Technology (#8242S)
PLK1 (PL6/PL2)	mouse	1:500 (WB)	Thermo Fisher Scientific (#33-1700)
RelB (D7D7W)	Rabbit	1:1000 (WB)	Cell Signaling Technology(#10544S)
SKP1	Rabbit	1:1000 (WB)	Santa Cruz Biotech (#sc-7163)
ß-actin (AC-15)	Mouse	1:5000 (WB)	Sigma-Aldrich (#A-1978)
Ubiquitin (P4D1)	Mouse	1:1000 (WB)	Santa Cruz Biotech (#sc-8017)
BrdU-FITC (B44)	Mouse	1:50 (FACS)	BD Biosciences
pHH3(Ser28) Alexa-Fluor 647 (HTA28)	Rat	1:400 (IF)	BD Biosciences (#558217)
anti-mouse IgG – Alexa Fluor 488	Goat	1:1000 (IF)	Invitrogen (#A11001)
anti-mouse IgG – Alexa Fluor 594	Goat	1:1000 (IF)	Invitrogen (#A11005)
anti-rabbit IgG – Alexa Fluor 488	Goat	1:1000 (IF)	Invitrogen (#A11008)
anti-rabbit IgG – Alexa Fluor 594	Goat	1:1000 (IF)	Invitrogen (#A11012)
ECL anti-mouse IgG, HRP-linked	Sheep	1:30.000 (WB)	GE Healthcare (#NA931)
ECL anti-protein-A, HRP-linked	Sheep	1:5000 (WB)	GE Healthcare
ECL anti-rabbit IgG, HRP-linked	Donkey	1:30.000 (WB)	GE Healthcare (#NA934)

3.11 Cell Lines

Cell line	Type	Supplier	Medium
A549	human lung carcinoma	ATCC (CCL-185)	DMEM + 10% FBS
AMO-1	human MM	DSMZ (ACC-538)	RPMI + 10% FBS (h.i.)
Granta-519	human MCL	kind gift of Prof. M. Dreyling	RPMI + 10% FBS (h.i.)
H1437	human lung carcinoma	ATCC (CRL-5872)	RPMI + 10% FBS (h.i.)
H929	human MM	DSMZ (ACC-163)	RPMI + 10% FBS (h.i.)
HBL-1	human DLBCL	kind gift of Prof. D. Krappmann	RPMI + 20% FBS (h.i.)
HCC44	human lung carcinoma	DSMZ (ACC 534)	RPMI + 10% FBS (h.i.)
HEK293T	human embryonic kidney	ATCC (CRL-3216)	DMEM + 10% NCS
HT	human DLBCL	DSMZ (ACC 567)	RPMI + 20% FBS (h.i.)
INA-6	human MM	DSMZ (ACC 862)	RPMI + 20% FBS (h.i.)+ IL-6
Jeko	human MCL	DSMZ (ACC 553)	RPMI + 10% FBS (h.i.)
JJN3	human MM	DSMZ (ACC-541)	RPMI + 10% FBS (h.i.)
KMS12BM	human MM	DSMZ (ACC-551)	RPMI + 10% FBS (h.i.)
L363	human MM	DSMZ (ACC-49)	RPMI + 10% FBS (h.i.)
LP-1	human MM	DSMZ (ACC-41)	IMDM + 10% FBS (h.i.)
MHH-PreB1	human DLBCL	DSMZ (ACC 354)	RPMI + 10% FBS (h.i.)
Mino	human MCL	DSMZ (ACC 687)	RPMI + 10% FBS (h.i.)

MM1.S	human MM	ATCC (CRL-2974)	RPMI + 10% FBS (h.i.)
Molm13	human AML	DSMZ (ACC 554)	RPMI + 10% FBS (h.i.)
Oci-AML2	human AML	DSMZ (ACC 99)	alpha MEM+ 10% FBS (h.i.)
Oci-AML3	human AML	DSMZ (ACC 582)	alpha MEM+ 10% FBS (h.i.)
Oci-LY1	human AML	DSMZ (ACC 722)	IMDM + 20% FBS (h.i.)
OCI-LY10	human AML	kind gift of Prof. M. Schmidt-Supprian	IMDM + 20% FBS (h.i.)
OCI-LY7	human DLBCL	DSMZ (ACC-688)	IMDM + 20% FBS (h.i.)
Oci-LY3	human DLBCL	DSMZ (ACC 761)	RPMI + 20% FBS (h.i.)
RIVA/ RI-1	human DLBCL	DSMZ (ACC 585)	RPMI + 20% FBS (h.i.)
RPMI8226	human MM	DSMZ (ACC-402)	RPMI + 10% FBS (h.i.)
TMD8	human DLBCL	kind gift of Prof. D. Krappmann	RPMI + 10% FBS (h.i.) + Sodium Pyruvate
U266	human MM	DSMZ (ACC-9)	RPMI + 10% FBS (h.i.)
U2OS	human osteosarcoma	ATCC (HTB-96)	McCoy's 5A+ 10% FBS (h.i.)
Z138	human MCL	ATCC (CRL-3001)	IMDM + 10% FBS (h.i.)

3.12 Tissue Culture Media and Supplements

Product	**Supplier**
Dulbecco's Modified Eagle's Medium (DMEM)	Thermo Fisher Scientific
FBS superior	Merck Millipore/Biochrom
HBSS (Hank's Balanced Salt Solution) 10X	Thermo Fisher Scientific
HEPES Buffer Solution (1M)	Thermo Fisher Scientific
Interleukin 6 (IL-6), human	Thermo Fisher Scientific
Iscove's Modified Dulbecco's Media (IMDM)	Thermo Fisher Scientific
McCoy's 5A Medium Modified	Thermo Fisher Scientific
Newborn Calf Serum (NCS)	Merck Millipore/Biochrom
Opti-MEM I, reduced serum media	Thermo Fisher Scientific
Phosphate buffered saline (PBS), 10X, sterile	Thermo Fisher Scientific
Penicillin/ Streptomycin (100X)	Thermo Fisher Scientific
RPMI 1640 GlutaMAX medium	Thermo Fisher Scientific
Sodium Pyruvate (100 mM; 100X)	Thermo Fisher Scientific
Trypan Blue Stain (0,4%)	Thermo Fisher Scientific
Trypsin-EDTA (10X) solution	Merck Millipore/Biochrom

3.13 Buffers and Solutions

Buffer / solution	
DUB Activity Assay Buffer	50 mM TRIS pH 7.4 5 mM MgCl2 250 mM Sucrose 2 mM ATP 1 mM DTT
FACS Buffer	PBS (1x) 3% FBS

Fractionation Buffer A	10 mM HEPES (pH 7.9) 10 mM KCl 1.5 mM $MgCl_2$ 0.34 M Succrose 10% Glycerol 0,1% TRITON X-100
Fractionation Buffer B	10 mM HEPES (pH 7.9) 10 mM KCl 1.5 mM $MgCl_2$ 0.34 M Succrose 10% Glycerol
Fractionation Buffer C	3 mM EDTA 0,2 mM EGTA
Freezing medium	90% FBS (heat inactivated) 10% DMSO
HIS-Ubi Buffer A (pH 8.0)	6 M Guanidinium Chlorid 0.1 M Na_2HPO_4 20 mM Imidazol (pH 8.0) (Freshly added!)
HIS-Ubi Urea Buffer (pH 6.3)	8 M Urea 300 mM NaCl 0.05% NP40 50 mM Na_2HPO_4 50 mM TRIS (pH 6.3) 20 mM Imidazol (pH 8.0) (Freshly added!)
HIS-Ubi Elution Buffer	30% Glycerol 0.72 M β-mercaptoethanol 150 mM TRIS (pH 6.3) 300 mM Imidazol (pH 8.0) (Freshly added!)
IF Blocking Buffer	PBS (1x) 0.25% gelatin from cold water fish skin 0.01% Saponin
IF Permeabilization Buffer	PBS (1x) 0.1% Triton-X
IF Staining Buffer	PBS (1x) 0.5% BSA 0.01% saponin
Inhibitors in WB Lysis Buffers	1 µg/mL aprotinin 1 mM DTT 10 mM G-2-P 1 µg/mL leupeptin 0.1 mM PMSF 0.1 mM Na_3VO_4 10 µg/mL soybean trypsin inhibitor 5 µg/mL TLCK 10 µg/mL TPCK

Laemmli Buffer (5x)	300 mM TRIS (pH 6.8) 10% SDS 5% β-mercaptoethanol 0.05% bromphenolblue 50% glycerol
Luria-Bertani (LB) medium (1x)	1% Bacto Tryptone 0.5% Bacto Yeast Extract 170 mM NaCl
LB-agar plates	1.5% Bacto Agar LB medium
Lysis Buffer (150 mM NaCl)	50 mM TRIS (pH 7.5) 150 mM NaCl 0.1% NP40 5 mM EDTA 5 mM $MgCl_2$ 5% Glycerol
Lysis Buffer (250 mM NaCl)	50 mM TRIS (pH 7.5) 250 mM NaCl 0.1% Triton X-100 1 mM EDTA 50 mM NaF
SDS Running Buffer (10×)	250 mM TRIS (pH 7.5) 1.92 M glycine 1% SDS
Stripping Buffer	62.5 mM TRIS (pH 6.8) 2% SDS 0.867% β-mercaptoethanol
Transfer Buffer (10x)	48 mM TRIS (pH 7.5) 20% methanol 39 mM glycine
Washing Buffer	PBS (1x) 0.1% Tween20

3.14 Software and Databases

Software/database	**Supplier**
Basic local alignment search tool	NCBI
FlowJo v10	Tree Star
CellQuest Pro	BD Biosciences
Gene Expression Omnibus	NCBI
GeneCardsSuite	Weizmann Institute of Science
GPP Web Portal	Broad Institute
IMARIS Viewer	Oxford Instruments
Immgen database	Immunological Genome Project
Oncomine	Thermo Fisher Scientific
Prism	Graph Pad Software
Serial Cloner	Open Source
The human protein atlas	http://www.proteinatlas.org

4. Methods

4.1. Molecular biology

4.1.1. Molecular cloning

To modify the expression of a specific gene within target cells, expression vectors are commonly used. These circular dsDNA stands can be engineered using molecular cloning. Herein a so-called insert (a cDNA for overexpression, a shRNA-stretch for reduction of expression etc.) can be either synthetically synthesized or amplified by PCR from template DNA and subsequently stably integrated into a DNA-vector (plasmid). Therefore, insert and plasmid are cut with bacteria derived restriction enzymes, merged by an enzymatic reaction (ligation) into a circular DNA construct and subsequently amplified in bacteria. Using modifications of this workflow a variety of changes can be introduced into given DNA sequences including point mutations and deletions of bigger regions in a gene of interest.

4.1.2 Polymerase chain reaction (PCR)

After designing the appropriate primers to generate the desired expression constructs, PCRs were used to amplify a gene of interest from a DNA template. For each primer pair the annealing temperature cycles was set 5-10°C below the primers respective melting temperature. The Elongation time was adjusted to the length of the expected DNA-product and the elongation rate of the NEB Q5-polymerase (20-30sec/kb) stated by the manufacturer. The general composition and setup of the PCRs are outlined below.

Reagent/compound	**Amount**
DNA-Template	20-100 ng
Forward primer (10 µM)	2.5 µL
Reverse primer (10 µM)	2.5 µL
dNTPs (10 mM)	1 µL
Q5-Reaction Buffer (5x)	10 µL
Q5 High GC Enhancer (5x)	10 µL
Q5-High-Fidelity Polymerase	0.5 µL
Nuclease free dH2O	To 50 µL

Program step	**Temperature**	**Time**	**Repetitions**
Initial Denaturation	98°C	30 sec	-
Denaturation	98°C	20 sec	35 Cycles
Annealing	X	30 sec	
Elongation	72°C	X	
Final Elongation	72°C	2 min	-
Storage	8°C	∞	-

PCR fragments were subjected to agarose gel electrophoresis and gel purification (see 4.1.4) to confirm the proper size of the PCR product.

4.1.3 Mutagenesis PCR (SNP, two step deletions)

To generate mutant versions of a certain gene, sets or primers were designed to generate gene fragments lacking the desired region in a first PCR step. Following gel purification (see 4.1.4) these fragments were used as templates in a following fusion PCR.
The first set of primers enables the performance of a PCR from the start codon (P1(start)), that runs right up to the domain or stretch of DNA that is supposed to be deleted. The reverse primer for this PCR contains approximately 15 base pairs of this sequence and then continues with a similar number of base pairs matching the DNA sequence right after the undesired DNA stretch (Pdel(rev)), creating an overlap. The second set of primers contains the reverse complement of the described domain deletion primer (Pdel(fwd)) and one including the stop codon (P2(stop)). By amplifying parts of the gene of interest in two separate PCRs using this strategy, two DNA oligomers were created with matching overhangs but lacking the domain in question. The partially overlapping fragments were then used as the input for a 'fusion PCR' in an equimolar fashion, using the primers covering start (P1(start)) and stop (P1(stop)) codon for amplification. The fused PCR product was then inserted into a plasmid via restriction cloning as described in 4.1.5.

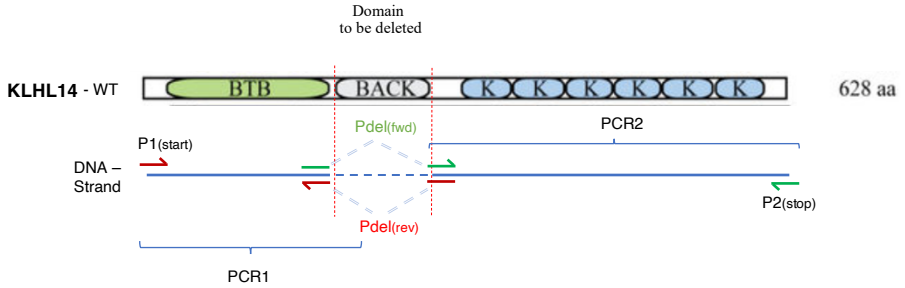

For the generation of point mutations, thus exchanging only a limited number of amino acids, usually a single one site directed mutagenesis was used. Complementary primers were designed with a length of 25-30 bp with the desired base pair changes close to the center of the sequence. These primers were used to amplify not only a fragment of cDNA but the whole plasmid by PCR. The PCR protocol used was reduced in cycle numbers to only 16 and the elongation temperature to 68°C. After the amplification step, methylated template DNA stemming from bacteria was removed by enzymatic digest. Briefly, the PCR reaction was topped up with the corresponding buffer and incubated with 1 µL DpnI enzyme at 37°C for 60min. The resulting plasmid was subsequently transformed into bacteria and processed like described in 4.1.8.

4.1.4 Agarose gel electrophoresis and gel purification

Following PCRs (apart from site directed mutagenesis see 4.1.3), the resulting DNA fragments were analyzed using gel electrophoresis. Therefore, 0.7-2% agarose gels were produced by dissolving the appropriate amount of agarose in TAE buffer by heating. The liquid agarose was cooled down for a couple of minutes and mixed with *DNA Stain Clear G* according to the manufacturer's instructions. The still liquid agarose was then poured into a gel chamber, a comb inserted and allowed to solidify. The resulting gel was transferred to a gel running chamber and covered in TAE buffer. Before loading the DNA into the wells, the DNA was mixed with 6xDNA-loading dye and run next to a 1kb DNA ladder at 100V for 30-45 min. The DNA was visualized using UV-light and analyzed for size. If desired, DNA fragments were excised and extracted using a *GeneJet Gel Extraction Kit* according to the manufacturer's protocol.

4.1.5 Restriction digest and ligation of DNA

One basic principle of molecular cloning is the site-specific cut or digest of DNA by bacterial enzymes and the subsequent fusion or ligation to a different piece of DNA for example an expression vector. During the restriction digest an enzyme recognizes and cleaves a specific DNA sequence resulting in defined 5'- or 3'- single strand overhangs (sticky ends) or blunt ends. DNA fragments cut with enzymes producing compatible ends, can later be fused by an enzymatic reaction called ligation. For restriction digests an appropriate amount of plasmid DNA (1-6 µg) or gel-purified PCR product (see 4.1.4) was mixed with the desired restriction enzyme (amount calculated from the number of units per µL supplied by the manufacturer) and its corresponding buffer. The reaction mix was then incubated for up to 1h at 37°C. For the simultaneous digestion with multiple enzymes, buffer conditions were chosen as recommended by the manufacturer. After the digest, plasmids were analyzed by gel electrophoreses and gel purified (see 4.1.4), whereas smaller PCR products or inserts were separated from the digestion mixture by *GeneJet Gel Extraction Kit* according to the manufacturer's protocol. Subsequently, the *Rapid DNA Dephos & Ligation Kit* was used to ligate insert and plasmid DNA in a molar ratio of 3:1, using 50 ng of digested plasmid DNA, according to manufacturer's protocol.

4.1.6 Annealing and ligation of short hairpin RNA-oligonucleotides

Oligonucleotides for the generation of short hairpin (shRNA) expression constructs were designed using the GPP-Web Portal (https://portals.broadinstitute.org/gpp/public/resources) and ordered from Eurofins Genomics (Ebersberg, Germany). Diluted and mixed Oligos were annealed and subsequently ligated into pLKO.1 TRC cloning. The annealing mixture was composed of 1 µL of forward and reverse oligonucleotide each (100 µM) and Buffer G in a total volume of 50 µL. This mixture was incubated in a beaker of boiling water and set to cool down overnight. 2 µL of the annealed oligos were ligated with 50 ng of the pLKO.1 TRC cloning vector cut with AgeI and EcoRI and transformed into NEB5a chemically competent bacteria (4.1.8).

4.1.7 In-fusion cloning

Another way to generate new expression vectors, either completely without or with a reduced number of restriction digestion/ligation steps, is via so-called in fusion cloning or Gibson assembly. In this case the *In-Fusion® HD Cloning Kit* was used. Therein PCR products are generated from different DNA templates with homologous ends similar to the ones used for domain deletions described in 4.1.8 – usually an insert and a linearized vector/plasmid with 15bp homologous ends. These fragments are then used in an enzymatic fusion reaction resulting in a seamless new DNA construct. Therefor the appropriate primer pairs were designed, insert and linearized vectors were generated via PCR (as described 4.1.3), fragments of appropriate size gel-purified and the In-Fusion reaction set up with 50 ng insert and 100 ng linearized vector according to the manufacturer's protocol.

4.1.8 Transformation of plasmids into bacteria

After ligation, In-Fusion reaction or site directed mutagenesis the resulting DNA constructs were transformed into bacteria for amplification and/or insert screening. For this purpose, 15-20 µL of chemically competent *NEB® 5-alpha Competent E. coli* were mixed with

1.5-2 µL ligation or 100 ng DNA and incubated on ice for 20 min, followed by a 45 sec heat shock at 45°C. After an additional 2 min incubation on ice, bacteria were supplemented with 200 µL SOC-media and incubated at 37°C shaking at 500 rpm for 20 min. To allow for selection of a plasmid carrying bacterial colony, transformed bacteria were then plated on LB agar plates containing antibiotics, matching the plasmid encoded antibiotic resistance, usually ampicillin or kanamycin. Agar plates were then incubated at 37°C overnight. Single colonies were picked and inoculated in LB medium containing the respective antibiotic and incubated at 37°C and 250 rpm shaking overnight.

4.1.9. Plasmid DNA extraction from bacteria

Purification of plasmid from bacteria was carried out using two different commercial kits. For volumes up to 5 mL the *peqGOLD Plasmid Miniprep Kit* was used, while purifications from up to 200 mL of overnight cultures were done with *NucleoBond® Xtra Midi Kit*, both according to the manufacturer's protocol. In case the sequence identity of a plasmid was not clear, for example after molecular cloning, the resulting plasmids were analyzed by test digest and/or sequencing at Eurofins Genomics (Ebersberg, Germany), using promoter or gene specific primers.

4.2 Cell culture and cell-based assays

4.2.1 Culture of eukaryotic cells

Mammalian cell cultures were handled in biological safety cabinets (HERAsafe®, Thermo Fisher Scientific). Cultured cells and cell lines were grown in a humidified incubator (HERAcell 150i CO2 incubator, Thermo Fisher Scientific) at 37°C with 5% CO2. All cell lines were grown in media containing 1% penicillin/streptomycin and GlutaMax supplement if not indicated otherwise. The respective media composition per cell line can be found in the material section, where the cell line used are listed. Heat inactivation of serum (FBS or FCS) was achieved by incubation for 60 min at 65°C. Adherent cells were kept on cell culture treated dishes and sub-cultured at 70-80% confluence. After a PBS wash, cells were detached by incubation with trypsin at 37°C for 3-10 min. Trypsin was then quenched by addition of full growth medium, the resulting single cell suspension pelleted by centrifugation at 1200 rpm for 4 min and a proportion of cells were transferred to a new plate in fresh medium. Suspension cells were grown in appropriately sized cell culture flasks till densities between 1-10 x10^5 cells/mL were reached and then split every 2-3 days at a ratio of 1:4-1:10. To determine the number of cells in culture, an aliquot of the cell solution was mixed in a 1:1 ratio with trypan blue and live cells were counted in a Neubauer counting chamber.

4.2.2 Freezing and thawing of cells

Cryopreservation of mammalian cells was achieved by resuspending pellets of 1x10^6 exponentially growing cells in 1mL of FBS supplemented with 10% DMSO, an agent which prevents crystallization and thereby cell damage at low temperatures. To reduce damage to the cells even further, cells aliquoted in cryotubes were transferred to a -80°C freezer inside of an isopropanol containing freezing device, assuring a cooling rate of 1°C per min. After 1-2 days at -80°C, frozen cells were transferred to liquid nitrogen for long term storage.
To thaw cells, frozen vials were incubated at 37°C for 1-2min, resuspended in a 10-fold volume of growth medium, pelleted by centrifugation and plated in an appropriate culture vessel.

4.2.3. Harvesting of cells

For subsequent protein-, RNA- or DNA extraction, supernatants of adherent cultured cells were removed and cells detached from culture plates by scraping in PBS. The obtained suspensions or collected non-adherent cells were pelleted by centrifugation at 1200 rpm for 4 min and washed in PBS to remove remaining culture medium. Supernatant was removed and cell pellets were either used immediately for cell lysis (e.g. *In-vivo*-Ubiquitylations or fractionations) or frozen at -80°C.

4.2.4 Transient transfection of cells with DNA

Transient HEK293T cell transfection with plasmid DNA was carried out using the calcium phosphate method described previously (Graham and Van der EB 1973; Kingston, Chen, and Okayama 1999). In brief, for a 10 cm cell-culture plate at 50-70% confluence, 10 µg of DNA were dissolved in 450 µL sterile dH_2O and 50 µL of 2.5 M $CaCl_2$ were added. After mixing thoroughly and incubation at RT for 5 min, 500 µL BES buffer were added dropwise while constantly vortexing. After additional 20min at RT, the DNA calcium phosphate solution was dripped onto the cells. Cells were incubated with the formed DNA-Calcium complexes for 4-24h and subsequently analyzed or processed further.

For all adherent cell lines but HEK293T used in this study, *Lipofecatmine2000* was used a transfection reagent according to the manufacturer`s protocol. In short, equal amounts of serum-free Opti-MEM were mixed with DNA and Lipofectamine 2000 reagent in separate reaction and incubated for 5 min at room temperature. The DNA-containing solution was then added to the Lipofectamin2000 dilution and everything was mixed by repeated uptake with a pipette. After 20 min incubation at RT, the transfection mix was added onto cells in P/S-free medium. Medium was renewed after 3-4h. In order to achieve good transfection results while retaining low cytotoxicity a DNA to Lipofectamine ratio of 1:3 was determined as optimal while amounts of DNA were adapted depending on the transfected plasmid(s). Cells were transfected at 50-70% confluence.

4.2.5 Transient transfection of cells with siRNA

Transiently reduced expression or knockdown of a protein of interest was achieved by transfection of adherent cells with siRNA using *Lipofectamine RNAiMAX* transfection reagent according to the manufacturer's protocol. These short dsRNA strands induce RNA interference by exploiting a cell intrinsic system of post-transcriptional gene regulation (Elbashir et al. 2001). Similar as for Plasmid-transfections described in 4.2.4. siRNA and RNAiMAX reagent were diluted in serum-free Opti-MEM separately and incubated for 5 min at RT. The siRNA- was then added to the Lipofectamine-solution and everything was mixed by pipetting. After 10-20 min incubation at RT, the siRNA-transfection mix was added dropwise onto 50% confluent cells in P/S-free medium. Knockdown efficiency was evaluated 2-3 days after transfection by immunoblot analysis (see 4.5.3 and 4.5.5).

4.2.6 Production of lentiviral particles and viral transduction of cells

Lenti- or Retroviral transduction of cells is a method that allows the stable expression of a desired DNA stretch by permanently integrating it into a cell's genome. Lentiviral particles were produced by transfection of HEK293T cells in a 10 cm format using the calcium phosphate method (see 4.2.4) to deliver 15 µg packaging plasmid (psPAX2), 5 µg envelope

plasmid (pMD2.G) and 20 µg of plasmid of interest (e.g. shRNA-, pHIV- or similar suitable construct). 24h after transfection, the plates medium was replaced by 6-10 mL OpitMEM, which was harvested as viral supernatant another 24h later. To clear the supernatant from cell debris, it was passed through a 0.45 µm filter and used either directly or stored at -80°C for future use.

In order to infect adherent cell lines, cells were plated at 50% confluence in a 10cm dish and were allowed to attach to the plate overnight. The following day the cells growth medium was replaced with fresh medium containing 50% viral supernatant supplemented with 8 µg/mL polybrene. After 24 hrs of growth the viral supernatant was removed and cells were washed twice with 10 mL PBS before being cultured with appropriate growth medium. If suspension cell lines were to be infected, 1x10^6 cells per well were plated in a 6 well plate with 1-2 mL full growth medium. 1-2mL of viral supernatant were added, again supplemented with 4-8 µg/mL polybrene. The plate was subjected to centrifugation between 300 and 700g for 30-60 min depending on the cell line before being transferred back to the incubator. The next day, the viral supernatant was removed by centrifugation, cells were washed twice in PBS transferred to flasks in their respective full growth medium. To generate a homogenous population, transfected cells were subjected to FACS (see 4.3) – in case the transduce DNA contained a fluorescence marker - or to antibiotic selection. Depending on the antibiotic resistance carried by the transferred vector Blasticidin (final concentration 10 µg/mL) or Puromycin (final concentration 1-4 µg/mL) was used to select for transgene expressing cells.

4.2.7 Doxycycline treatment for transgene expression

To induce the expression of a transgene at a specific time point after viral transduction, a doxycycline inducible system was applied. Herein a plasmid with the transgene or shRNA of interest under the control of a doxycycline inducible promotor is stably integrated into cells. After selection for the plasmid, transgene expression can be induced by the addition of doxycycline into the cell's growth medium. In this study, 1 µg/mL of the antibiotic was used. For prolonged transgene expression, doxycycline was renewed every 48h.

4.2.8 Inhibitor treatment in protein stability assays (Cycloheximide, MG132, MLN4924)

Analysis of protein stability and turnover is of central interest when working with ubiquitin ligases and DUBs as these might influence these processes. Cycloheximide is a natural occurring compound that inhibits eukaryotic mRNA translation and can therefore be used to prevent protein de novo synthesis which allows the assessment of a proteins halt life time. Cycloheximide was dissolved in 100% ethanol to create a stock solution of 100 mg/mL right before use. Cells were then treated with 100-200 µg/mL for different time points depending on the proteins of interest. To check whether the destabilization was proteasome dependent or not, the proteasome inhibitor MG132 or the neddylation inhibitor MLN4294 were added on top of the cycloheximide for the indicated time points at concentrations of 10 µM and 2 µM respectively.

4.2.9 NF-κB stimulation in various cell lines and primary murine B-cells

The NF-κB-pathway can be triggered by a variety of internal and external stimuli. In this study, TNF-a (10 ng/mL), IL-1ß (10 ng/mL) or LPS (10-100 ng/mL) were added to cells either in full growth or starvation medium for the indicated time points to achieve NF-κB activation in a time resolved manner. Murine B-cells were stimulated *ex vivo* after MACS-purification using

LPS (10 µg/mL), IL4 (10 ng/mL), Fab(2(IgM)) (10 µg/mL), CD40L (1 µg/mL) or combinations of those for the indicated time points.

4.2.10 Luciferase assay

In order to assess the (time resolved) NF-κB-activation in cells a so-called luciferase reporter assay was performed. The *Nano-Glo Dual-Luciferase Assay system* with a reporter luciferase specific for NF-κB activity was used according to the manufacturers instruction.
In this dual vector system, one vector encodes a firefly luciferase which is driven by a NF-κB-response element, making the expression level of this luciferase relative to the pathways activity. On a second plasmid a so-called nanoLuc luciferase is driven by a constitutively active PGK promoter, which allows the monitoring of transfections efficiencies in every single well transfected. Briefly, $2.5x10^5$ cells per well were seeded into an opaque 96 well plate in full growth medium. The next day cells were transfected with a lipofectamine2000 transfection mix (see 4.2.4) containing the NF-κB-Firefly luciferase reporter construct (50 ng/well) and the nanoLuc-Luciferase construct (10 ng/well). After transfections, cells were either cultivated in full growth or starvation medium (only 0.5% FBS) for the indicated time before the luciferase assay was performed. Next, cells were either stimulated with TNF-a (10 ng/mL) for the indicated time points or put forward to the assay directly. For the assay, medium was reduced to 50 µL per well, 50 µL of Firefly luciferase Substrate (Promega) was added and mixed by pipetting. After 10 min of incubation, luminescence was measured using a Mithras plate reader (Berthold) with a gain of 1 second per well before the firefly luminescence was quenched by addition of 50 µL Stop-and-Glow solution. After incubation for another 10 min, nanoLuc luminescence was detected in the same way as before to determine transfection efficiency. Conditions were measured in triplicates.

4.2.11 Synchronization of cells in different cell cycle phases

For the analysis of events in specific phases of the cell cycle, cells were synchronized at G1-, G1/S-phase or mitosis respectively. By release of the synchronized cell population from the forced blockage, the transition through the subsequent cells cycle phases could be monitored.

Synchronization in G1/S and G1 phase
A double thymidine block was applied for the synchronization of cells at the entry of S phase. An excess of the DNA nucleoside thymidine added to cell culture medium interferes with the cellular production of deoxynucleotides and thereby inhibits DNA synthesis. Cycling cells are thereby arrested in or just before entering S-phase. By releasing cells after a first block and re-administering the nucleoside, cells can homogeneously be sequestered at the G1/S transition. Briefly, thymidine powder was dissolved in sterile PBS at 25 mg/mL right before use. 2 mM (0.5 mg/mL) thymidine were added to the cell cultures for 24 hrs, before performing a thymidine washout to release cells from S-Phase. To achieve this, cells were incubated for 10 min twice with PBS and once with medium, before they were cultured in full growth medium for 12 hrs. After this, the medium was supplemented with thymidine for another 24 hrs, thereby arresting cells at the G1/S transition. To analyze cells in S and G2/M phase, thymidine was washed out as described before and cells were sampled at the indicated time points.
To induce a cell cycle arrest at the restriction point in late G1 phase, cells were treated for 24 hrs with the cyclin-dependent kinase (CDK) 4/6 inhibitor palbociclib, at a final concentration of

1 µM. A release into S phase was achieved through palbociclib removal by washout in the same manner as described for thymidine.

Synchronization in mitosis

The treatment of cells with the spindle poison nocodazole, which depolymerizes microtubules, leads to a cell cycle arrest in the pro-metaphase of mitosis.

To obtain a homogenous mitotic population, cells were first treated with 0.5 mg/mL thymidine for 24h to stall them in S phase. After thymidine washout as described above or after plating into fresh full growth medium, cells were cultured in full growth medium containing 500 ng/mL nocodazole for 14-16 hrs. When working with adherent cells, mitotic cells were collected by mitotic shake off. As cells in mitosis round up and detach from the culture plate, these can be singled out by rocking the dish and subsequently collecting the cells that were shaken off into suspension. For non-adherent cells, this discrimination is not possible. Therefore, synchronization conditions were carefully optimized to achieve at least 90% of mitotic cells in a population as measured by flow-cytometry based cell cycle analysis (see 4.3.2). After this synchronization, cells were either collected for analysis or released from mitosis by washing them two times with PBS and once with medium for 10 min each. These were then plated in fresh full growth medium and samples taken at indicated time points.

4.3 Flow cytometry

Flow cytometry is a versatile technique, which enables not only the analysis of size and granularity on a single cell level but also the detection of fluorescent labels, attached to cells during a staining/labeling process. This labeling can either be done by expression of a fluorescent protein like GFP, the incorporation of a fluorescent dye or the binding of a fluorescently labeled antibody. A single cells suspension of processed cell is then analyzed using laser light for excitation and a suitable detection module for the emission signal. Data presented in this study were either obtained at a BD FACS Calibur or a BD Acccuri C6 plus and analyzed using the software FlowJo v8 or V10.

4.3.1 Flow cytometry of cells transduced with GFP or RFP

In case the percentage of cells transduced with a viral vector containing RFP or GFP as a selection marker was to be determined, cells from the growing culture were collected at the indicated time points. These were then washed with 2 mL PBS, resuspended in PBS and analyzed using one of the mentioned flow cytometers.

4.3.2 Cell cycle analysis using flow cytometry

One way to analyze the cell cycle stage of cell is via monitoring its DNA content. Consequently, the DNA intercalating fluorescent dye propidium iodide (PI) is used to discriminate between cells in G0/G1 phase and G2/M phase cells. The latter population has a DNA content of 4N as compared for 2N for cells in G0/G1 and therefore exhibits distinctively higher fluorescence when labeled with PI and measured by flow cytometry at around 617 nm emission. During S- or Synthesis phase, cells duplicate their genomic DNA for the upcoming division and hence show an intermediate amount of DNA and PI signal. Throughout this study PI/RNase staining buffer (BD Pharmingen) was used for PI staining according to the manufacturer´s protocol. To resolve the S-phase population further, cells were incubated for 40min with the uridine derivate bromodeoxyuridine (BrdU), which is incorporated during DNA

replication in S-phase. After fixation of the cells in 70% ice cold ethanol, the derivate was stained with mouse anti-BrdU-FITC conjugate antibodies (BD Bioscience) according to the manufacturer's instructions, stained with 1ug/mL PI (Sigma) for 15 min at RT and analyzed by flow cytometry.

4.4 Immunofluorescence

Using a fluorescence microscope and specific antibodies, the localization of proteins within a cell can be determined. For this to work, cells are attached to and fixed on a suitable slide, permeabilized and stained with antibodies, that are either directly coupled with a fluorescent dye or are later visualized by incubation with a coupled secondary antibody.

4.4.1 Immunofluorescence of adherent cells

When using adherent cells in immunofluorescence, cells were seeded in detachable multi-well chamber slides made of PCA. If desired, cells were transfected with the indicated constructs using Lipofectamine2000 (see 4.2.6) and cultured for another 24-38 hrs. Cells were then fixed with 4% PFA for 10 min at RT, washed extensively with PBS, permeabilized with 0.1% Triton-X-100 in PBS, washed extensively with PBS again and blocked for 1 h at RT with blocking buffer. Primary antibodies were diluted in staining buffer and added to the wells for overnight incubation at 4°C. The next day, wells were washed three times with PBS and incubated with secondary antibodies diluted in staining buffer for 1 h at RT in the dark. Antibody dilutions used are listed in the material section 3.10. The antibody solution was then replaced by PBS with 0.3 µg/mL Hoechst3342 (Sigma) for another 15 min incubation under the same conditions. After three subsequent washes with PBS, chambers were detached, cells mounted with ProLong Diamond Antifade Mountant (Thermo Fisher Scientific) and sealed with a cover slip. Slides were stored in the dark for at least 24h before imaging using a Leica SP8 WLL. Subsequent analysis was done using the IMARIS viewer software version 9.7 (Oxford Instruments Group)

4.4.2 Immunofluorescence of non- adherent cells

For imaging non-adherent cells, the chamber slides first had to be coated to provide an attachable surface for the cells prior to fixation. For this two different ploy-lysins were used.
For MM cells, detachable multi-well chamber slides were coated with poly-D-lysin (1 mg/mL in ddH_2O) for 1 h at RT. After coating, slides were washed with PBS and set to dry completely. Cells were counted ($2x10^5$ per 8-well chamber), washed twice with PBS and resuspended in HBSS. After plating, cells were allowed to attach for 20-120 min at 37°C depending on the cell line. For DLBCL cells, the same multi-well slides were coated with poly-L-lysin (0.01% in ddH_2O) for 1 h at RT and washed once with PBS. These slides were kept moist at all times. Cells were counted and $2x10^5$ per 8-well chamber seeded in full growth medium. Cells were allowed to attach for 15-30 min at 30 min at 37°C. Afterwards, irrespective of attachment strategy used, cells were fixed and stained as described for adherent cells.

4.5 Protein Biochemistry

4.5.1 Cell lysis

To analyze the protein content of a cell population or protein-protein interactions within it, cells need to be lysed by disruption of their membranes.
Harvested cell pellets were resuspended in suitable buffers containing high amounts of salts and/or detergents. To prevent degradation of proteins or changes in post-translational modifications, specific protease and phosphatase inhibitors were added. If not further specified, ice cold 150 mM NaCl lysis buffer supplemented with DTT, protease (PMSF, TLCK, TPCK, PIN) and phosphatase inhibitors (Nava, Glycerol-2-Phospate) was added, cell pellets resuspended and incubated for 20 min on ice. Lysates were cleared of DNA and membrane debris by centrifugation at 14.000 rpm at 4°C for 20 min. Subsequently protein concentrations of the cleared supernatants were measured using a modified Lowry assay (Lowry et al. 1951) in form of the Bio-Rad DC protein assay according to the manufacturer's instructions. Protein containing supernatants were either denatured by addition of Lämmli buffer and heating to 95°C for 10min or used for examples in immunoprecipitations.

4.5.2 Sub-Cellular fractionations

Another method to determine the location of a protein within a cell apart from immunofluorescence is called sub-cellular fractionation. Herein, cells are lysed stepwise in specialized low salt buffers to obtain lysates containing the proteins of specific cellular compartment only. These lysates can then be analyzed using for example immunoblot analysis (4.5.5) or EMSA (4.5.6). In this study cells were fractionated into the cytoplasmic, nuclear (soluble) and the chromatin/membrane fractions. For that, cells were washed with 2 mL ice cold PBS and resuspended/harvested in fractionation Buffer A without prior freezing. After incubation on ice for 5 min, lysates were centrifuged at 1700g for 10 min at 4°C. The resulting supernatant contained the proteins of the cytosolic fraction and was kept on ice. The left-over pellets were washed twice with Buffer B without disrupting it to avoid rupture of the nuclear membrane. These pellets were then incubated in Buffer C for 30 min on ice prior to centrifugation at 1700g for 10 min at 4°C. The resulting supernatant represents the soluble nuclear fraction and was kept on ice. The still clearly visible pellets were washed once with Buffer C and then dissolved in a lysis/assay buffer of choice (Buffer C, EMSA-Buffer or 150 mM lysis buffer). All lysis buffers were supplemented with the described protease and phosphatase buffers right before use. To break down the DNA within this chromatin fraction, samples were either subjected to sonication or incubated with benzonase (Sigma).

4.5.3. SDS polyacrylamide gel electrophoresis (SDS-PAGE)

SDS PAGE (SDS polyacrylamide gel electrophoresis) is a method which allows for the separation of proteins in a complex mixture based on their protein mass. By addition of SDS, denatured proteins are coated in negatively detergent molecules, which allows them to move through a polyacrylamide gel with a speed specific for their mass but not their inherent charge, as soon an electric field is applied. SDS-acrylamide gels were cast using Mini-PROTEAN® Tetra Electrophoresis System. A standard gel consisted of a smaller upper part, a so-called stacking gel containing 3.9 % acrylamide, and a lower separating gel containing 5 - 12 % acrylamide, depending on the size of the proteins of interest, were used.

Reagent per gel in mL	Separating Gel (10 mL)				Stacking Gel (5 mL)
	5%	8%	10%	12%	
Acrylamide 40% (29:1)	1.25	2.0	2.5	3.0	1.25
H2O	to 10 ml				to 5 ml
Separating Buffer	2.5				-
Stacking Buffer	-				1.25
SDS (10%)	0.1				0.05
APS (10%)	0.1				0.05
TEMED	0.004				0.005

After polymerization, 10-25 µg of denatured protein sample were loaded into the pockets of a gel assembled in a running buffer filled chamber next to a protein ladder and resolved at 80-120V. After electrophoreses gels were incubated in Coomassie or silver stain (4.5.4) to visualize proteins within the gel or transferred to a membrane for immunoblot analysis (4.5.5).

4.5.4. Coomassie- and Silver-staining

Proteins can be visualized directly within an acrylamide gel using silver- or Coomassie staining. Both methods stain proteins based on charges present in the amino acid chains. The less sensitive Coomassie interacts with the positive amine groups through Van der Waals interactions and helps to visualizes ≥50 ng protein, while the reduction of silver ions to elementary silver by negatively charged residues detects down to 1 ng of protein.
For a Coomassie staining, gels were incubated in Coomassie staining solution for at least 1 h or overnight while shaking. Access dye was removed by repeated washes with Coomassie destaining solution. Silver stains were carried out using the Thermo Scientific Pierce Silver Stain Kit according to the manufacturer's instructions.

4.5.5. Immunoblot Analysis (Western blot)

Immunoblot analysis is a method used to detect specific membrane-bound proteins using antibodies raised against them.
Proteins separated by SDS-PAGE were transferred to either polyvinylidene difluoride or nitrocellulose membranes. While the latter were used without activation, PVFD membranes were activated in methanol for 1 min before assembly into a Mini Trans-Blot® cell from Bio-Rad. Using pre-cooled transfer buffer, electroblotting was carried out either at 100V for 80 min or over-night at 30V. Membranes were cut if necessary, to analyze different proteins of different molecular weights on the same membrane and blocked for 30-60 min in 5% milk in PBS-T at RT. The blocked membranes where then incubated in primary antibody at 4°C over night. The next day excessive antibodies were removed by three subsequent washes with PBS-T for 10 min each. For chemiluminescent detection the blots were then incubated with the respective horse-radish peroxidase (HRP) coupled secondary antibody diluted in 5% milk/PBS-T for 1.5 hrs at RT. After another round of three washes at 10 min each in PBS-T, blots were incubated with enhanced chemiluminescent (ECL) solution (Pierce™ ECL Western Blotting Substrate; Thermo Fisher Scientific) and exposed to photosensitive films (Amersham HyperfilmT^M ECL). An automatic film developer machine (Curix 60, Agfa) was used to visualize protein bands.

4.5.6. Electrophoretic Mobility Shift Assay (EMSA) and native PAGE

Some proteins like transcription factors exert their function by binding to specific stretches of nucleic acids (DNA or RNA). Electrophoretic Mobility Shift Assays (EMSAs) can

be used to visualize these interactions by incubation of pre-labeled nucleic acid oligomers with protein lysates followed by native PAGE. In general protein-nucleic acid-complexes travel a lot slower through a respective acrylamide gel than free nucleic acids, allowing for the analysis of DNA or RNA binding components within a given lysate.
In this study EMSA was used to determine the binding of NF-κB transcription factors to their corresponding consensus sequences. NF-κB-specific dsDNA-oligos with or without a 5'-biotin attached were ordered from Eurofins Genomics (Ebersberg, Germany) and total nuclear extracts (see 4.5.2) prepared. The DNA oligo probes were diluted to 1 pmol/µL and nuclear extracts adjusted to 1 µg/µL to use with the LightShift Chemiluminescent EMSA Kit (Thermo Fisher Scientific) in the following reaction:

Components (µL)	Negative Control	Test-Sample	Specific Competitor
Nuclease free H_2O	to 20	to 20	to 20
5x gel shift binding buffer	4	4	4
Poly dI-dC (1 µg/µL)	1	1	1
Nuclear extract (1 µg/µL)	-	1	1
Unlabeled specific competitor (100 pmol/µL)	-	-	2
Labeled DNA probe (1 pmol/µL)	2	2	2

Binding reactions were incubated at RT for 20–30 min, before addition of 2 µL of 10x loading buffer (without SDS, provided by the kit) to each reaction. The reactions were then loaded onto a native acrylamide gel with the following composition:

Reagent per gel in mL	Native Gel
Acrylamide 40% (29:1)	1.25
dH2O	to 10 mL
5xTBE	2
APS (10%)	0.1
TEMED	0.004

After electrophoresis at 80V for 1 h or 2/3 of the gel, gels were transferred onto nylon membranes (Biodyne™ B Nylon Membrane, Thermo Fisher Scientific) in 0.5x pre-cooled TBE buffer for 30 min at 100V. Samples were then crosslinked to the membrane by UV exposure on a transilluminator equipped with 312 nm bulbs for 10–15 min. Detection of biotin labeled DNA-strands was performed using the chemiluminescent nucleic acid detection module of the kit. Finally, after incubation with enhanced chemiluminescent (ECL) solution (Pierce™ ECL Western Blotting Substrate; Thermo Fisher) photosensitive films (Amersham HyperfilmT^M ECL) were exposed to the membranes and an automatic film developer machine (Curix 60, Agfa) was used to visualize protein bands.

4.5.7. Stripping of membranes

In case a PVDF or nitrocellulose membrane was supposed to be re-analyzed with a

different antibody, the antibodies previously bound to it, were removed by incubation with a denaturing buffer containing SDS and ß-mercaptoethanol for 40 min at RT, followed by four washes with PBS with 15 min each. Afterwards membranes were again blocked in 5% milk/PBS-T and incubated with new primary antibody.

4.5.8. Immunoprecipitation (IP)

Immunoprecipitation (IP) is a method used to purify proteins in solution using specific antibodies raised against a protein or protein-tag of interest. These antibodies are either covalently coupled to agarose beads or used together with protein A or G conjugated beads which bind rabbit or mouse antibodies, respectively. By incubation with a lysate, these antibodies will bind a specific protein if present, which later can be sedimented with the agarose by centrifugation. IPs were performed either from whole cell extracts (WCE) using standard lysis buffers (see 4.5.1) or from fractionated samples (see 4.5.2).
For IPs of Flag- or HA-tagged proteins, lysates were incubated with Flag-M2 or HA-7 agarose beads (both Sigma) respectively. Before use, the beads were washed three times in lysis buffer and diluted 1:1 with the buffer to retain a slurry suspension. Per 500 µL sample of cell lysate, 20 µL of slurry beads were added and incubated for 1.5-2 hrs at 4°C on a rotating wheel. Beads were then sedimented at low centrifugation speed and washed three times with lysis buffer to reduce unspecific binding. If unspecific binding was causing problems in further analyses, a pre-clear was done using plain agarose beads. These ‘empty beads’ were added to every lysate before the actual IP-beads for 30min at 4°C, removed from the lysates and discarded. Furthermore Flag-M2- or HA-7-beads were blocked for 10 min in 2% BSA (w/v) before addition to the lysates to further reduce unspecific binding to the agarose material. If not further specified, beads were eluted by addition of 40 µL of 2x Lämmli buffer and cooked at 95°C for 10 min.

For IPs of endogenous, untagged proteins, 1-2 mg protein in 500 µL lysis buffer, where incubated with 1-4 µg control IgG or protein specific antibody overnight at 4°C on a rotating wheel. The next day samples were supplemented with 20-40 µL protein A or G coupled agarose, depending on the species the antibody was raised in, and incubated for another 60 min at 4°C. Beads were then washed and eluted as descried for FLAG/HA-IPs.
Finally, samples of WCE and IPs were analyzed by SDS-PAGE and immunoblot (see 4.5.5).

4.5.9. Protein-purification for mass spectrometric analysis (TAP und Flag)

Mass spectrometry is a method commonly used to identify unknow interaction partners of purified proteins. Therefore, either FLAG-IPs similar to the ones described above (see 4.5.8) or so-called Tandem Affinity Purifications (TAPs) were performed, followed by a FLAG-peptide- or acid-based elution of the purified proteins from the beads with subsequent MS/MS measurement (see 4.5.10) of proteins presents in the eluates.
In this work TAPs as well as FLAG-IPs were utilized to identify interaction partners of FBXO21. For the TAP approach, which promises a greater specificity by combining to subsequent affinity binding steps, FBXO21 was cloned into a N-terminal tandem-Strep-single-Flag-tag construct (Gloeckner et al. 2007). This construct and a respective empty-vector control were transfected into approximately $2x10^9$ 293T cells with a confluence of 60-70% and harvested 24 hrs later. Lysis was performed in 150 mM standard lysis buffer as described above including the passage of each lysate through 22G and 26G syringe needles to ensure complete rupture of all cell organelles. The cleared supernatants were incubated with Strep-Tactin Superflow resin (IBA Lifesciences) for 2 hrs at 4°C on a rolling wheel. After three washes in lysis buffer, bound

proteins were eluted using desthiobiotin elution buffer twice for 10 min each at RT. Next, eluates were supplemented with Flag-M2 beads for 1.5 hrs at 4°C, followed by two washes in lysis buffer and one in 1x TBS. For the finale elution of bound proteins, samples were incubated with 1 mg/ml 3xFlag-peptide (Sigma) in TBS in three consecutive elution steps for 10 min at RT each. Matching eluates were pooled, a small sample taken for quality control and remaining samples precipitated with 20% (v/v) Tri-chloric acidic acid (TCA) over night. The next day, precipitated proteins were sedimented by centrifugation at 14.000 rpm for 15 min at 4°C, washed twice with ice cold acetone and dried in a speed-vac. Quality control samples were analyzed by SDS-PAGE followed by silver staining and/or immunoblot.

Additionally, single FLAG purifications were performed to identify (unknown) interactors of FBXO21, KLHL14 and LIN28B. For that, FBXO21 was cloned into a pcDNA3.1 vector with an N-terminal FLAG-tag and purified from $1x10^9$ 293T cells alongside an empty-vector control. The same was done for KLHL14. This protein was additionally cloned into the doxycycline inducible vector pTRIPZ and transduced into MM1.S cells alongside an empty vector control. $5x10^9$ of these cells were then either left asynchronous or arrested in mitosis (see 4.2.11) and transgene expression induced for 18 hrs before sample collection. LIN28B was cloned into pHIV including an N-terminal FLAG-tag and lentivirally transduced into MM1.S cells, again alongside an empty vector control and selected for transgene expression. The selected cells were then either left asynchronous, arrested in mitosis or at G1/S using a double thymidine block (see 4.2.11) before harvesting. The samples for the single FLAG-purifications were done in the same way as for the TAP described above but without the incubation with and elution from Strep-Tactin Superflow resin. Furthermore, only the FBXO21 samples were eluted with FLAG-peptide, while the latter were separated from the beads using acidified glycine. For that the protein bound beads were washed an additional time with 0.2 M Glycine pH 7.0, before three sequential elution steps with 2.5 bead-bed volumes of 0.2 M Glycine (pH 3.5)/HCl for 5 min at RT each. The eluates were pooled per sample and quenched with 50 µL TRIS (pH 6.0)/HCl. TCA precipitation and quality control were performed as described for the TAP. All samples were sent to, processed and analyzed by collaborators at the Department of Proteomics and Bioanalytics at TUM for mass spectrometric analysis or the Bavarian Center for Biomolecular Mass Spectrometry at the University hospital rechts der Isar (BayBioMS@MRI) as indicated (see 4.5.10).

4.5.10 Mass spectrometric analysis

Sample preparation and mass spectrometric analyses of the TAP and FLAG-purification of FBXO21 were performed by Susan Klaeger (Department of Proteomics and Bioanalytics, TUM). KLHL14 and LIN28B samples were processed and analyzed by Jana Zecha (Department of Proteomics and Bioanalytics, TUM) and Julia Mergner/Piero Giansanti of the BayBioMS@MRI.

In general, dried proteins were reconstituted, reduced with DTT and alkylated with chloroacetamide (CAA). Half of the sample was run on a 4-12% BIS-TRIS NuPAGE gel, where in-gel trypsin digestion of proteins was performed. Tryptic peptides were extracted, dried and reconstituted in buffer containing 0.1% formic acid (FA) and analyzed by nano LC-MS/MS on an Eksigent NanoLC-ultra 1D+ system or a Dionex Ultimate 3000 UHPLC+ system coupled to a Q Exactive HF mass spectrometer (Thermo Fisher Scientific) as described previously(Baumann et al. 2014; Eichner 2016; Fung et al. 2018). Peptide and protein identification and quantification were performed using MaxQuant by searching the MS2 spectra against the human reference proteome supplemented with common contaminants.

Difference in sample preparations (as far as known) are listed below:

Purified protein	FBXO21	FBXO21	KLHL14	KLHL14	LIN28B	LIN28B
Type of purification	TAP	Single FLAG	Single FLAG	Single FLAG	Single FLAG	Single FLAG
Cell type, number, treatment	$2x10^9$ HEK 293T cells	$1x10^9$ HEK 293T cells	$5x10^8$ MM1.S cells	$5x10^8$ mitotic MM1.S cells	$5x10^8$ asynchronous and G1/S arrested MM1.S cells	$5x10^8$ asynchronous, mitotic and G1/S arrested MM1.S cells
Analysis type	Interactome	Interactome	Interactome	Interactome	Interactome	Phosphosites
Type of Gel	Long gel; fractionated	Long gel; fractionated	Short gel	Short gel	Short gel	Long Gel, 35kDa LIN28B band cut out
Replicates per sample	1	1	3	3	1	1
MaxQuant Verison	v1.5.3.30	v1.5.3.30	v1.6.3.2	v1.6.3.3	v1.6.3.3	v1.6.3.3
Operator	Susan Klaeger	Susan Kläger	Piero Giansanti	Julia Mergner	Jana Zecha/ Julia Mergner	Jana Zecha/ Julia Mergner

4.5.11 In vivo ubiquitylation assay

One method to analyze the ubiquitylation status of a protein under specific conditions in a cellular context is a so-called *in vivo* ubiquitylation assay. For this purpose, cells plated on 6 cm dishes were transfected with plasmids encoding 0.3-1 µg HA-tagged ubiquitin or one of its variants, 1-2.5 µg FLAG-tagged substrate-candidate and 1-2.5 µg E3-ligase or DUB of interest or respective controls using Lipofectamine2000 (see 4.2.4). 20-24 hrs after transfection cells were treated with 10 µM MG132 for 3-4 hours if indicated to enrich for proteins which might otherwise be degraded by the proteasome and harvested and lysed in 100 µL ice cold 250 mM NaCl lysis buffer supplemented with protease and phosphatase inhibitors without prior freezing. After 10 min of incubation on ice, lysates were cleared by centrifugation and supernatants denatured by addition of 1% SDS (v/v), 6 mM EDTA, 0.1% NP-40 and heating to 95°C for 10 min. Samples were allowed to reach room temperature and diluted with 900 µL 250 mM NaCl lysis buffer supplemented with 1% Triton X-100 (Sigma) and incubated on ice for 15min. Finally, a FLAG-IP was performed as descried in 4.5.8.

4.5.12 DUB activity assays

For assessment of DUB activity towards HA-ubiquitin vinyl sulfone (HA-Ub-VS), cells were lysed in DUB activity buffer for 20 min on ice and lysates subsequently clarified by centrifugation for 20 min at 4°C and full speed. Equal amounts of protein were mixed with 5 µM HA-Ub-VS (Boston Biochem #U-212) and subsequently incubated at 37°C for 45 min. The reactions were stopped and lysates denatured by the addition of 1% SDS and subsequent boiling at 95°C for 5 min. After cooling to room temperature, samples were diluted with DUB activity buffer to a final volume of 500 µL. Active DUBs modified by HA-Ub-VS were immunoprecipitated by HA agarose as described in 4.5.8.

4.5.13 His-Ubiquitin purification

Apart from the descried *in vivo* ubiquitylation, ubiquitinated proteins were purified from cells stably expressing 6xHis-tagged ubiquitin. If indicated, cells were treated with MG132 to block proteasomal degradation and harvested as described. Pellets were then lysed in His-Ubi

buffer A described in Wang et. al. (B. Wang et al. 2017b), sonicated at 40% output with a pulse length of 1 second using a sonicator for 12 cycles to disrupt membranes and DNA complexes and incubated on ice for 30 min. Per $1x10^7$ cells (for MM/DLBCL cells) lysed in 1 mL, 200 µL Ni-NTA beads (Quiagen) were washed twice with His-Ubi buffer A and incubated with the respective lysates for 3h at RT on a rolling wheel. Beads were spun down at 300g for 5 min, allowed to settle and supernatants removed. The Ni-NTA beads where then washed once with His-Ubi buffer A and five times with Urea buffer, before finally eluting the proteins either using Lämmli or by three subsequent elution steps with 2 bed volumes of His-Ubi elution buffer (B. Wang et al. 2017b) for 15 min at RT each. In case, the elution buffer was used, eluates were pooled and precipitated with TCA as described in 4.5.9.

4.5.14 Protein dephosphorylation

The Dephosphorylation of proteins was carried out by treatment of lysates with Calf Intestine Phosphatase (CIP; NEB). Cells were lysed and processed in 150 mM NaCl lysis buffer without phosphatase inhibitors (Nava, G2P) and 5 mM $MgCl_2$, complemented with 10 units CIP per 500 µL and incubated at RT for 15 min.

4.5.15 Benzonase treatment of lysates

For the digestion of DNA and complete lysis of chromatin and nuclear fractions, cell lysates were supplemented with 1 µL benzonase (Sigma) per 500 µL and 5 mM $MgCl_2$ and incubated on ice for 30 min before further processing.

4.6 Statistical Analysis

The statistical evaluations of data sets were performed by log-rank (Mantel-Cox) test, paired or unpaired two tailed Student's t-test, Pearson’s correlation or linear regression or one-way ANOVA, according to assumptions of the test using GraphPad Prism (GraphPad Prism 9) software. P-values were adjusted using the Bonferroni-Dunn method integrated in the Prism software for multiple testing. The error bars shown represent the mean ± s.d., unless specified otherwise. The number of biological replicates is specified in the figure and/or its legend. The P values presented, in case a statistically significant difference was found, depict: * $P < 0.05$, ** $P < 0.01$, *** $P < 0.001$ and **** $P < 0.0001$.

5. Results KLHL14

Despite recent advances in the characterization of ubiquitin modifiers like DUBs and E3-ligases, most of them are not linked to a specific substrate yet and their role in a (patho-) physiological context remains elusive. Therefore, RNAseq data of patients with different hematological malignancies were screened for deregulated members of the UPS to identify novel, interesting ligase candidates for in depth phenotypic and mechanistic characterization.

5.1 KLHL14 is a tumor suppressor in B-cell derived malignancies

B-cell derived malignancies like DLBCL, MCL and MM are clonal hematopoietic disorders, which are characterized by excessive proliferation, abnormal self-renewal and impaired differentiation. Despite recent advances in therapy, they remain mostly incurable. High response rates towards proteasome inhibitors like bortezomib especially in MM suggest a central function of the UPS in these diseases beyond the induction of proteolytic stress (Kumar et al. 2017; Guerrero-Garcia et al. 2018).

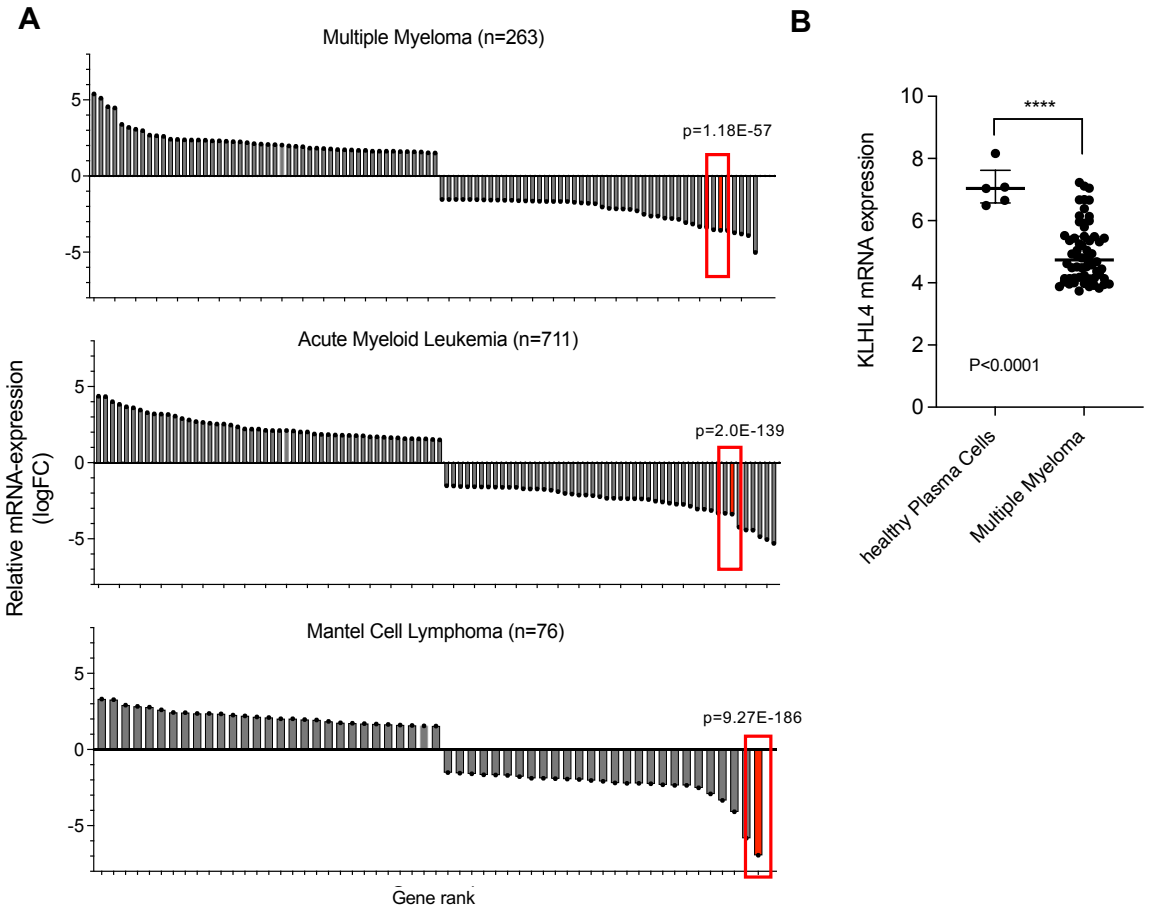

Figure 9. KLHL14 mRNA levels are significantly downregulated in MM, AML and MCL patient samples
A, Waterfall plots of the relative fold change in mRNA expression of significantly downregulated ($P < 0.05$) UPS components in MM (n=263), AML (n=711) and MCL (n=76) patient samples when compared to bone marrow cells of healthy control donors (n=64). Data and analysis were provided by T. Haferlach (MLL Munich), sorted from highest to lowest log-fold change in mRNA levels and plotted according to gene rank. KLHL14 mRNA fold-change is marked in red and the adjusted p-value indicated. **B,** Data of the GSE16558 dataset were re-analyzed for relative KLHL14 mRNA-expression in healthy plasma cells (n=5) and MM patient samples (n=60). **** P < 0.0001, by Student's t-test.

As the identities of the involved components of the UPS remain elusive, we screened RNAseq data provided by T. Haferlach (MLL Munich) from patients with various hematological malignancies for deregulated components of the UPS. Data from 263 MM, 711 acute myeloid leukemia (AML) and 76 mantel cell lymphoma (MCL) patients were analyzed and the orphan E3-ligase KLHL14 was identified as significantly downregulated in all three disorders when compared to healthy control donors (n=64) (Fig. 9A). Furthermore, KLHL14 ranked among the seven candidates with the most severe reduction in mRNA levels in this dataset (Fig. 9A). This downregulation could be confirmed by analyzing publicly available Affymetrix mRNA expression data (GSE16558)(Gutiérrez et al. 2010) for KLHL14 levels (REF_ID: 8022817), which were significantly lower in MM patients (n=60) compared to normal plasma cells from healthy donors (n=5), hinting towards an involvement of the protein as a tumor suppressor (Fig. 9B).

Next, cell line panels representing the three different disease entities were analyzed by immunoblot to verify that the mRNA downregulation observed in the patient data was reflected on protein level in the available cell line models (Fig. 10). DLBCL cell line samples were used for comparison as these cells are known to have high levels of KLHL14 protein (Choi et al. 2020; S. Li et al. 2018) and blotted alongside whole cell lysates of MCL (Fig. 10A), AML (Fig. 10B) and MM (Fig. 10C) cell line lysates, confirming low KLHL14 protein abundance in all cell lines tested.

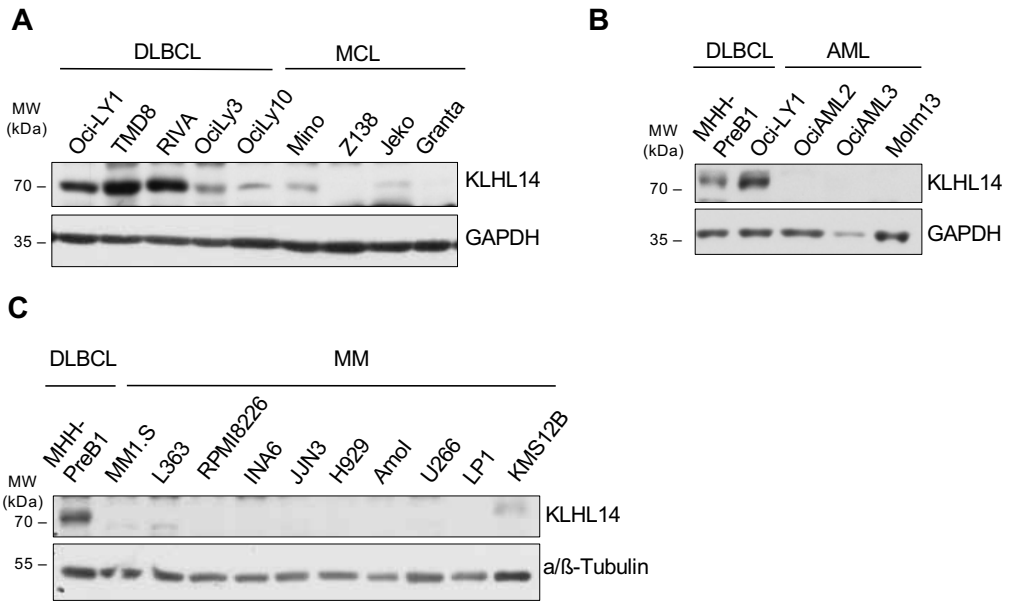

Figure 10. KLHL14 protein levels are low in MCL, AML and MM when compared to DLBCL cell lines. A-C, Immunoblot analysis of whole cell extracts (WCEs) from various MCL (**A**), AML (**B**), MM (**C**) and DLBCL (**A-C**) cell lines for KLHL14 protein expression using the indicated antibodies. GAPDH and a/ß-Tubulin served as loading controls.

In order to verify that KLHL14 acts a tumor suppressor, KLHL14 was lentivirally overexpressed using a pHIV-IRES-GFP derived construct or empty control vector in cell lines of different origins with a multiplicity of infection (MOI) of 0.30-0.50. GFP positive cells in the mixed population were monitored by flow cytometry over a period of 14 days (Fig. 11). While the amount of GFP+ empty vector control cells stayed constant over time in all cell lines, KLHL14 expressing GFP+ cells significantly dropped out of the population in DLBCL and MM cells but not in AML and lung adenocarcinoma lines (Fig. 11A).

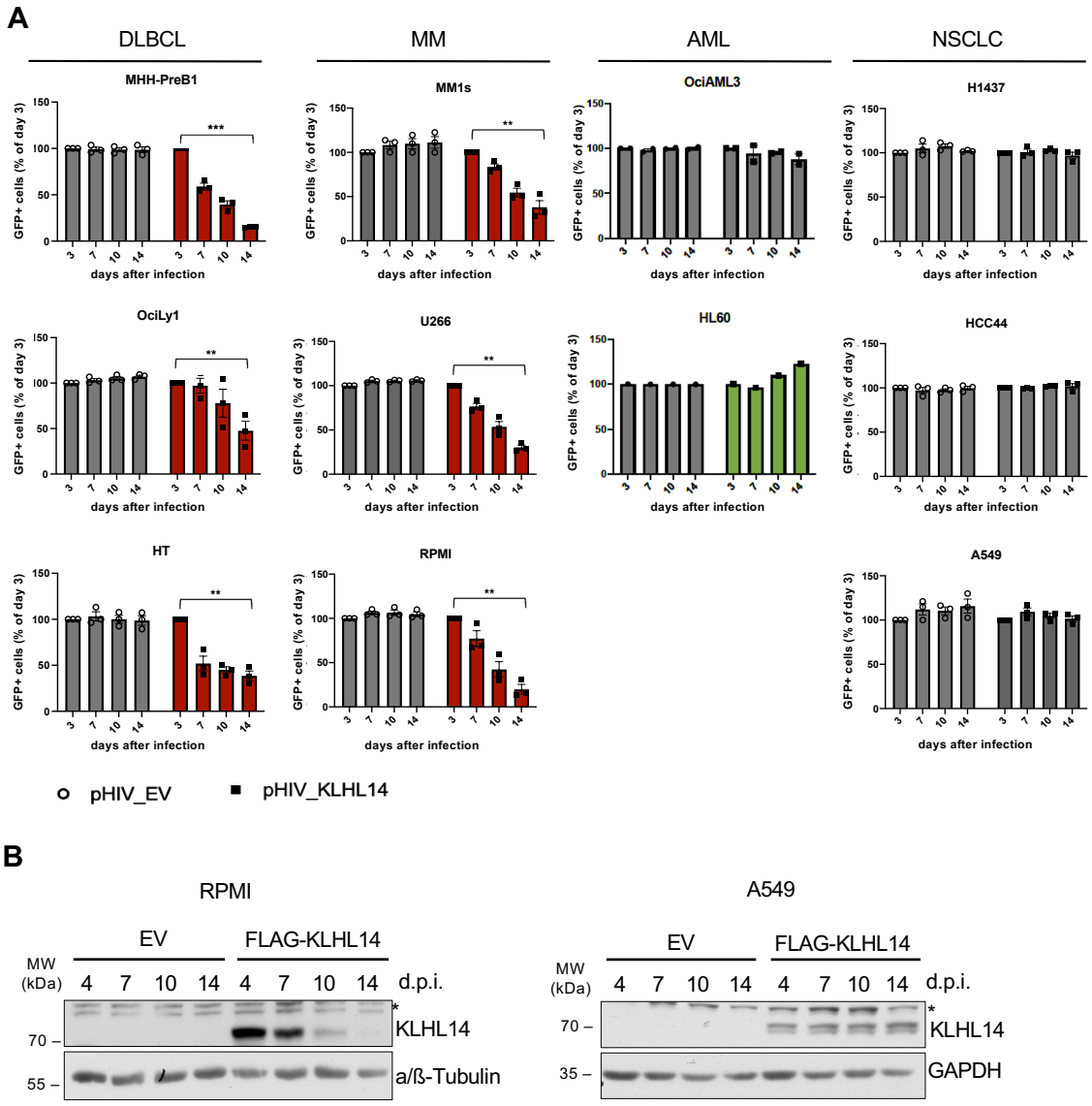

Figure 11. KLHL14 overexpression suppresses proliferation in B-cell derived cell. A, Proliferation analysis of various DLBCL, MM, AML and NSCLC cell lines infected with pHIV-KLHL14-IRES-GFP or empty vector control (MOI 0.3-0.5). The ratio of pHIV-expressing/ GFP positive to uninfected cells was measure by flow cytometry at the indicated time points post infection. Results are depicted as percentage of day 3. red- reduction over time >80%; green increase over time >120% (n = 3 independent experiments for all but HL60 (n=1) and OciAML3 (n=2); mean ± S.D.). **, P < 0.01; ***, P < 0.001; by Students T-Test. **B,** Immunoblot analysis of whole cell extracts (WCEs) collected from a representative time course in RPMI8226 and A549 cells as described in A. The indicated antibodies were used and GAPDH and a/ß-Tubulin served as loading controls. d.p.i. – days post infection, EV – empty vector.

The reduction in abundance of KLHL14 expressing cells in the mixed population was confirmed by immunoblot analysis of samples taken at the indicated time points after infection, which were analyzed for the protein's expression. The immunoblots showed a reduction of KLHL14 protein expression over time in MM- and DLBCL cells, while levels stayed constant in AML and lung adenocarcinoma cells as exemplified for RPMI8226 (MM) and A549 (NSCLC) cells (Fig. 11B).

In an intend to establish whether full length KLHL14 was needed to exert its tumor suppressive functions, different deletion mutants of the protein (Fig. 12A) were created by deletion cloning and tested for their expression in HEK293T cells followed by immunoblot analysis. This showed that the KLHL14 deletion variants could be expressed in HEK293T cells.

While the included FLAG-tag was detected at varying levels throughout, the KLHL14 antibody failed to visualize the variant of the protein in which both the BTB- and BACK-domains were deleted indicating that these included the antibody binding site (Fig. 12B). The deletion of the CUL3-binding domains (BTB and BACK) should interfere with CUL3 binding, while the stepwise deletion of the KELCH domains might reduce substrate recognition. Both mutant types should therefore cause a loss of function of KLHL14 and abolish the antiproliferative effect of KLHL14-WT.

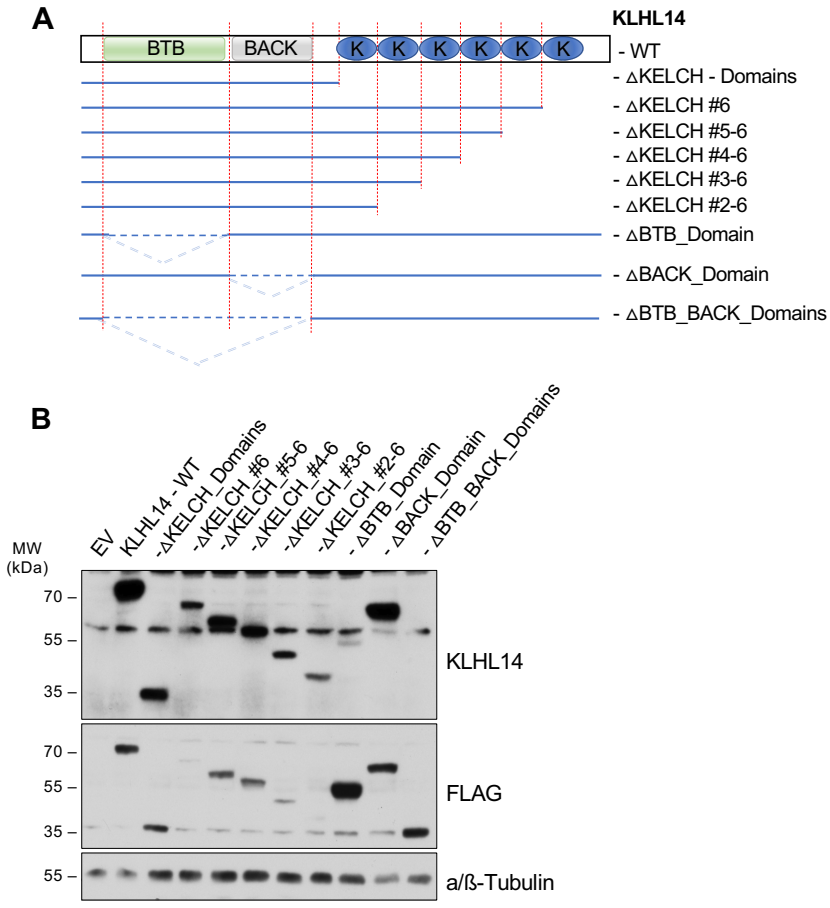

Figure 12. Generation and test of expression of KLHL14 deletion mutants. A, Schematic overview of KLHL14 wildtype (WT) and created deletion mutants. Δ, delta; KELCH, Kelch fold domain. **B**, Immunoblot analysis of HEK293T cells that were transfected with pcDNA3.1 expressing KLHL14-WT, one of the indicated deletion mutants depicted in (A) or empty vector (EV) control using the $CaCl_2$ method. Blots were analyzed with the indicated antibodies and a/ß-Tubulin served as a loading control.

To test this hypothesis, a growth competition assay was performed again. Indeed, when lentivirally overexpressing the deltaBTB- and deltaKELCH-domain variants of KLHL14 alongside the WT protein or an empty vector control in various MM cell lines as described above, the deletion variants did not drop out of a mixed population over time as measured by flow cytometry (Fig. 13A). The expression of all three transgenes was again confirmed by immunoblot analysis (Fig. 13B). Even though the protein expression levels of the different variants were not as high as the one for KLHL14-WT, this indicated that only the full-length protein exerts tumor-suppressive functions in the MM cell lines tested.

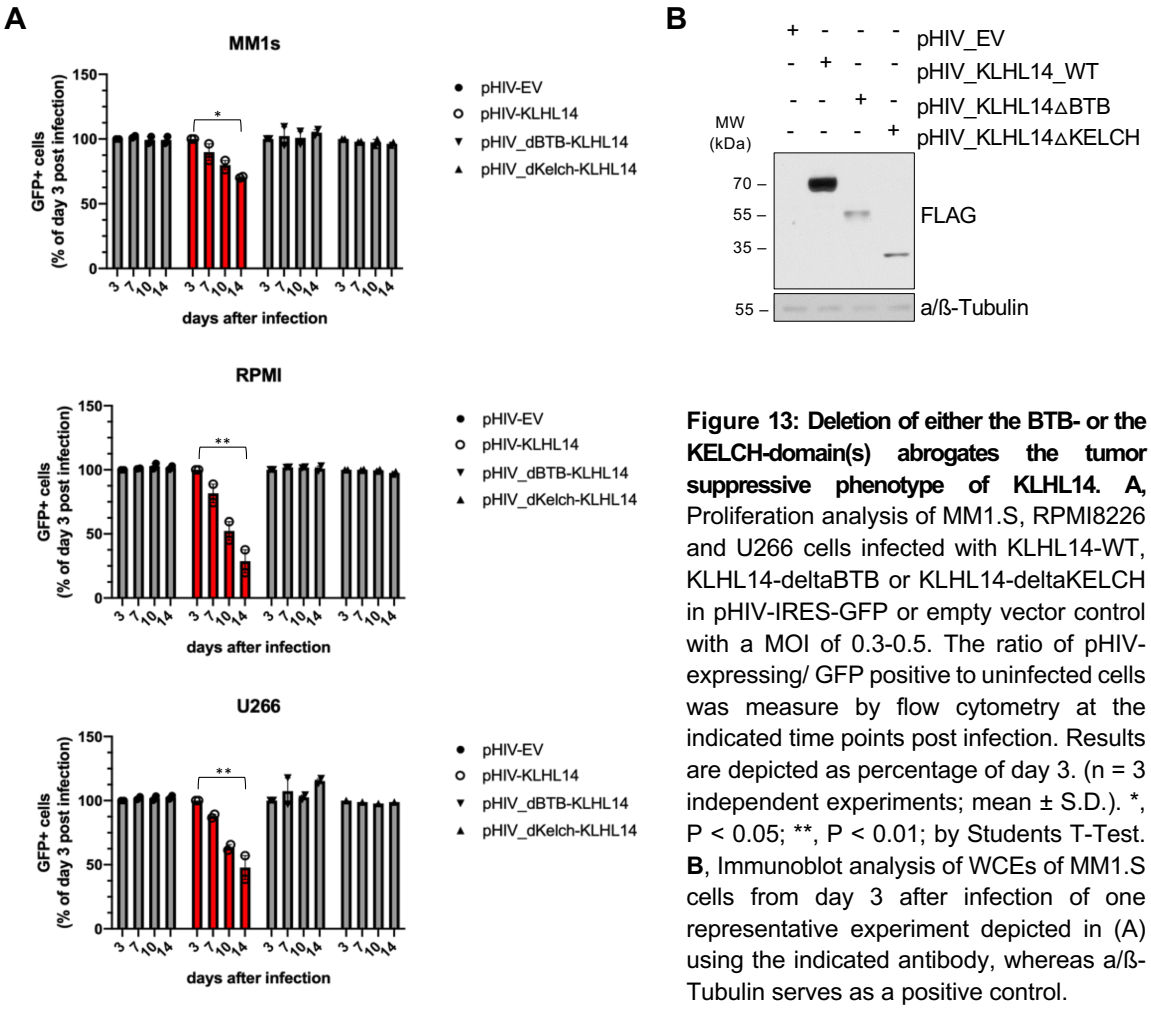

Figure 13: Deletion of either the BTB- or the KELCH-domain(s) abrogates the tumor suppressive phenotype of KLHL14. A, Proliferation analysis of MM1.S, RPMI8226 and U266 cells infected with KLHL14-WT, KLHL14-deltaBTB or KLHL14-deltaKELCH in pHIV-IRES-GFP or empty vector control with a MOI of 0.3-0.5. The ratio of pHIV-expressing/ GFP positive to uninfected cells was measure by flow cytometry at the indicated time points post infection. Results are depicted as percentage of day 3. (n = 3 independent experiments; mean ± S.D.). *, $P < 0.05$; **, $P < 0.01$; by Students T-Test. **B**, Immunoblot analysis of WCEs of MM1.S cells from day 3 after infection of one representative experiment depicted in (A) using the indicated antibody, whereas a/ß-Tubulin serves as a positive control.

After confirming the tumor suppressive effects of KLHL14 in the described growth competition assays, a system for doxycycline inducible overexpression of the protein or a respective control was established. The pTRIPZ-vector system, which was originally designed to express RFP as an easily detectable marker protein followed by a miRNA, was chosen, in which either RFP was retained and the miRNA insertion site removed or both were replaced by (FLAG-) KLHL14. The RFP expressing construct was used as the empty vector (EV) control. After lentiviral transduction and puromycin selection of pTRIPZ-positive MM1.S cells to create a stable cell line, uninduced pTRIPZ-RFP and pTRIPZ-KLHL14 cells were tested for possible differences in growth kinetics. Cell counting assays over 5 days revealed that there was no major difference in proliferation rates in the resulting MM1.S transgenic cell lines (Fig. 14A). When the transgene expression of either RFP or KLHL14 was induced by doxycycline addition, the MM1.S expressing KLHL14 proliferated significantly slower than their uninduced counterparts and the RFP control cells (Fig. 14B).

Taken together, the data described above show that full length KLHL14 acts as a tumor suppressor in MM and other B-cell derived malignancies but not in cell lines of other origins.

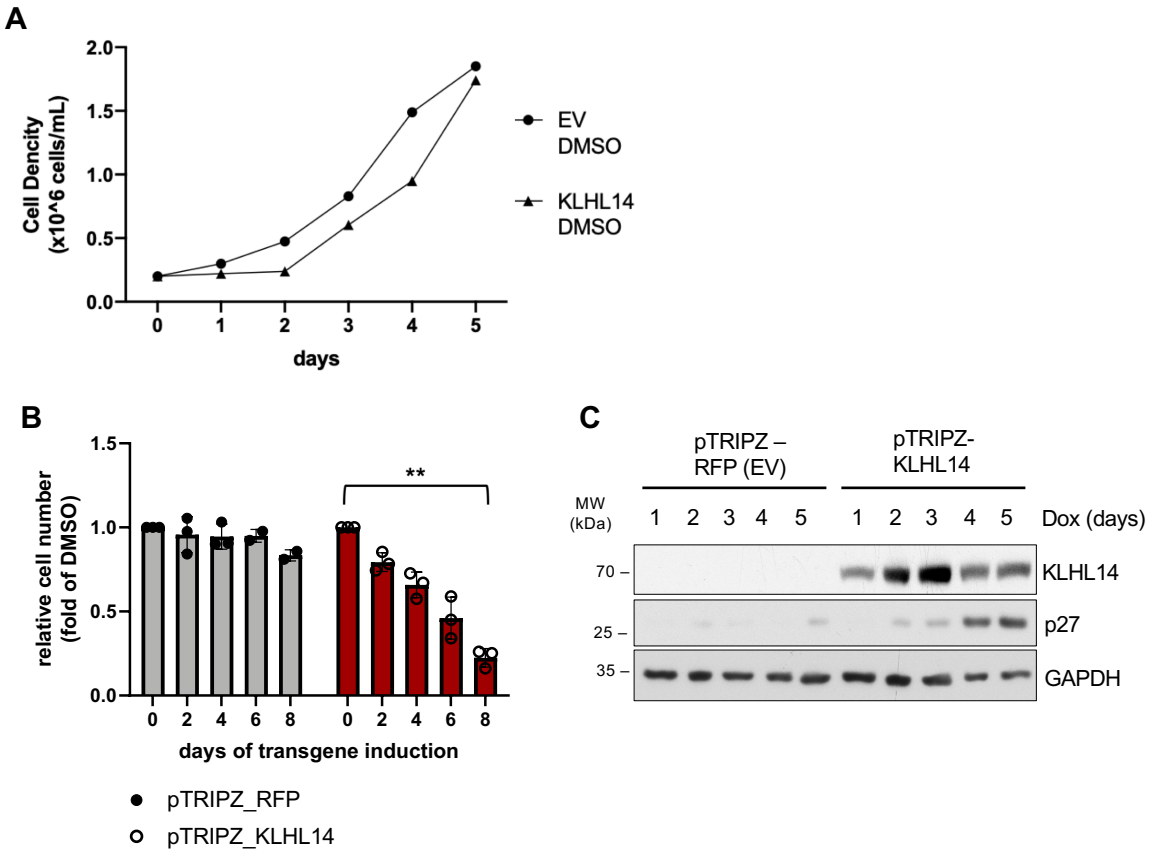

Figure 14: Doxycycline induced KLHL14 overexpression suppresses proliferation in MM1.S cells A, Proliferation analysis of DMSO treated/uninduced MM1.S cells, that were lentivirally transduced with pTRIPZ-RFP(EV) or pTRIPZ-KLHL14. After infection, cells were selected with increasing amounts of puromycin (0.3 µg/mL to 1 µg/mL) for construct expression, seeded into fresh medium at 0.25x10^6 cells/mL and counted over a course of 5 days (n= 1). **B**, Proliferation analysis of MM1.S cells stably expressing pTRIPZ-RFP or pTRIPZ-KLHL14 upon transgene induction. Cells were seeded at 0.25x10^6 cells/mL, treated with doxycycline at 1 µg/mL or DMSO for 8 consequent days and counted ever second. Cell numbers are depicted as fold of DMSO control and normalized to day 0. (n= 3 independent experiments; mean ± S.D.). **, P < 0.01; by Students T-Test. **C** Immunoblot analysis of WCEs collected from a representative time course treatment of MM1.S cells as described in **B**. The indicated antibodies were used and GAPDH served as loading control.

5.2 KLHL14 overexpression causes DNA damage and G1 restriction point arrest

One reason for impaired proliferation without the immediate induction of cell death, could be the arrest of cells in a specific cell cycle phase. Therefore, MM cells with or without ectopic expression were subjected to cell cycle analysis by flow cytometry and immunoblot.

Both types of analysis showed that, the prolonged expression of KLHL14 resulted in a gradual increase in p27 protein, a prominent indicator of G1-cell cycle arrest, as seen by immunoblot analysis of MM1.S cells expressing the transgene for up to 5 days (Fig. 14C). In order to verify this observation a PI/BrdU cell cycle analysis was performed in MM1.S cells, in which KLHL14 or RFP expressing was induced by doxycycline addition for up to 8 days. On the day of the assay, BrdU was added for 45 min, cells were processed as described previously (Bassermann et al. 2005) and analyzed for BrdU incorporation and PI/DNA content by flow cytometry (Fig. 15A).

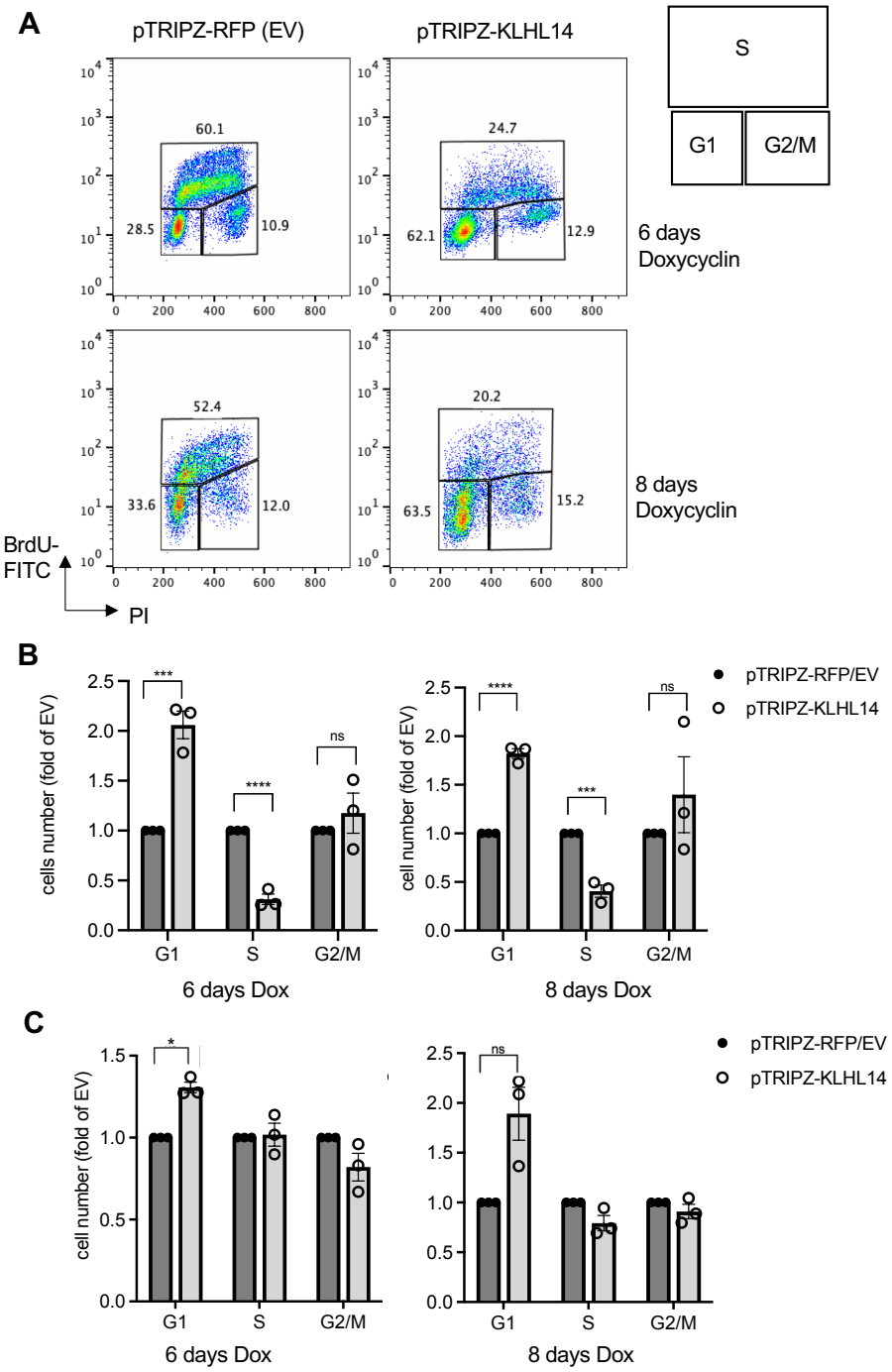

Figure 15: Ectopic expression of KLHL14 leads to a G1 cell cycle arrest. A, BrdU/PI flow cytometric cell cycle analysis of MM1.S cells upon KLHL14 expression. Transgene expression was induced in MM1.S cells stably expressing pTRIPZ-KLHL14 or -EV by doxycycline addition (1 µg/mL) for 6 (upper panel) and 8 (lower panel) days respectively. Cells were then supplemented with BrdU for 45 min, fixed in ethanol, labelled with FITC-conjugated anti-BrdU antibody and DNA was stained with propidium iodide (PI). Data are depicted as graphs of BrdU-FITC signal (FL1-H) versus PI staining (FL2-A, DNA content). **B,** Cell cycle distribution of KLHL14 and RFP overexpressing MM1.S cells**.** Quantification of cells per cell cycle phase analyzed in **A** (G1, S, G2-M) presented as fold change of EV-control (n = 3 independent experiments, mean ± S.D.). **C**, Quantification of a PI/BrdU cell cycle analysis in MHH-PreB1 cells, which were treated as in (A) and analyzed for the presenting cell cycle distribution plotted as fold change of EV-control (n = 3 independent experiments, mean ± S.D.). ns, not significant; *, $P < 0.05$; ***, $P < 0.001$, ****, $P < 0.001$; by Students t-test.

This analysis showed a significant drop of cells from the S-phase population (BrdU/FITC-high), accompanied by a significant enrichment in G1 cells (BrdU/FITC low, PI-low) when KLHL14 was overexpressed for 6 and 8 days respectively (Fig. 15A, B). A similar trend could be observed for the DLBCL cell line MHH-PreB1 after prolonged KLHL14 expression, even though the effect was not constantly significant (Fig. 15C), suggesting a similar mechanism by which the KLHL14 interferes with cell cycle progression in MM and in DLBCL cells.

The flow cytometric data were also reflected by immunoblot analysis of MM1.S cells with prolonged transgene expression for up to 8 days, which showed a decrease in the mitotic marker Cyclin B1 and the G1/S-transition marker Cyclin E with the cooccurrence of p27 and Cyclin D1 induction (Fig. 16A), indicating a cell cycle arrest in early to mid G1-phase or even a permanent exit of the cell cycle into G0/quiescence (Cassimere, Mauvais, and Denicourt 2016). The tumor suppressive effects of KLHL14 in MM cells stem therefore from the induction of a cell cycle arrest in G1-phase by a so far unidentified mechanism.

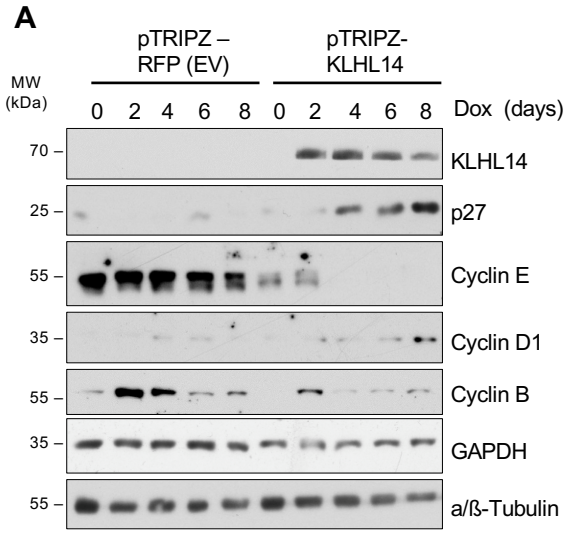

Figure 16: Prolonged KLHL14 overexpression induced a G1/G0 cell cycle arrest. A, Immunoblot analysis of MM1.S cells stably expressing pTRIPZ-KLHL14 or -RFP/EV upon doxycycline (1µg/mL) mediated transgene induction. Samples of doxycycline treated cells were taken at the indicated time points and WCE analyzed by immunoblot using the indicated antibodies. a/ß-Tubulin and GAPDH served as loading controls.

The involvement of KLHL14 in cell cycle regulation prompted the question, if the ligase's expression levels were regulated in a cell cycle dependent manner, as known for other components of the UPS like SKP2 (Wei et al. 2004). MM1.S or MHH-PreB1 WT cells were hence arrested at the G1/S transition using a double thymidine block or in G2/M with a sequential thymidine and nocodazole treatment. Both arrested populations were subsequently released by wash out and samples takes for immunoblot analysis at the time points indicated in figure 17.

While the arrest and release worked well in both cell lines according to the cells cycle markers analyzed as controls, MM1.S cells (Fig. 17A), which don't have detectable amounts of KLHL14 protein when analyzed as an asynchronous cell population, did not show a KLHL14 induction in any cell cycle phase and the protein's levels were stable throughout the time course in MHH-PreB1 (Fig. 17B) cells. This indicated that the proteins function within the cell cycle was not regulated by differential expression but might be mediated for example by phase specific post translational modifications (PTM) or differential localization of the ligase and its substrate.

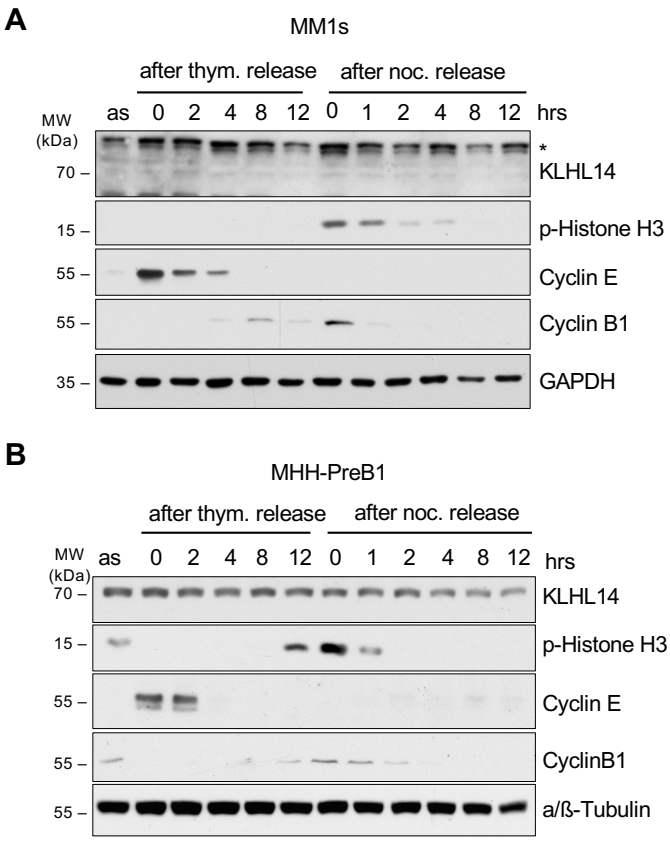

Figure 17: KLHL14 protein levels are not cell cycle regulated. A, B Cell cycle analysis of KLHL14 protein levels by immunoblot. MM1.S (A) and MHH-PreB1 (B) cells were synchronized at G1/S transition by a double thymidine block or in G2/M by a single thymidine block for 24 hrs followed by a release for 12 hrs into nocodazole. Synchronized cells were released and harvested at the indicated time points. WCEs of asynchronous cells and the collected time course samples were subjected to immunoblot analysis using the indicated antibodies. a/ß-Tubulin and GAPDH served as loading controls.

The observed G1 arrest can stem from a variety of reasons like errors in mitosis followed by mitotic slippage, persistent nutrient deprivation or a lack of mitogenic signals(B. S. Zhou and Elledge 2000). To address the immanent question of the origin of the cell cycle arrest, KLHL14 or RFP transgene expression was induced in MM1.S pTRIPZ cells for different durations, cells were arrested at the G1/S transition using a double thymidine block and subsequently released for 8 hrs. By analyzing the DNA content of the cells using PI flow cytometry at the indicated time points, their progression from G1/S towards S-phase could be monitored (Fig. 18A). Ectopic KLHL14 expression had little to no effect on progression into S-Phase until day 5 of transgene induction as indicated by the percentage of cells that remained in G1 after thymidine wash out (Fig. 18C). At day 6 to 8 after KLHL14 induction, the cells entered permanent G1 arrest, as seen in earlier experiments (Fig. 15A, B), so the failure to enter S-phase and initiate DNA-synthesis at the late time points is probably not a direct effect on the transition process. Furthermore, there seemed to be no general defect at the G1/S-transition, even though the experiment remains to be repeated.

Subsequently, a string of experiments was set up to investigate whether the overexpression of the ligase had an effect earlier in G1 for example on the restriction point. Thus, ectopic expression was triggered by doxycycline addition in pTRIPZ-KLHL14 or pTRIPZ-RFP transduced MM1.S cells for up to five days as described above, but this time cells were synchronized at the restriction point using the CDK4/6 inhibitor palbociclib. The DNA content of the cells before and 10 hrs after palbociclib wash out was then analyzed by PI staining and flow cytometry (Fig. 18B). Remarkably, the forced expression of KLHL14 lead to an impaired release from the cell cycle block after just 48 hrs. The impairment intensified after longer doxycycline treatment and led to an almost complete lack of cells leaving G1-phase after palbociclib mediated restriction point arrest (Fig. 18D), hinting towards a mechanism of G1 arrest in which KLHL14 overexpression triggers the restriction point and sensitizes the cells to CDK4/6 inhibition.

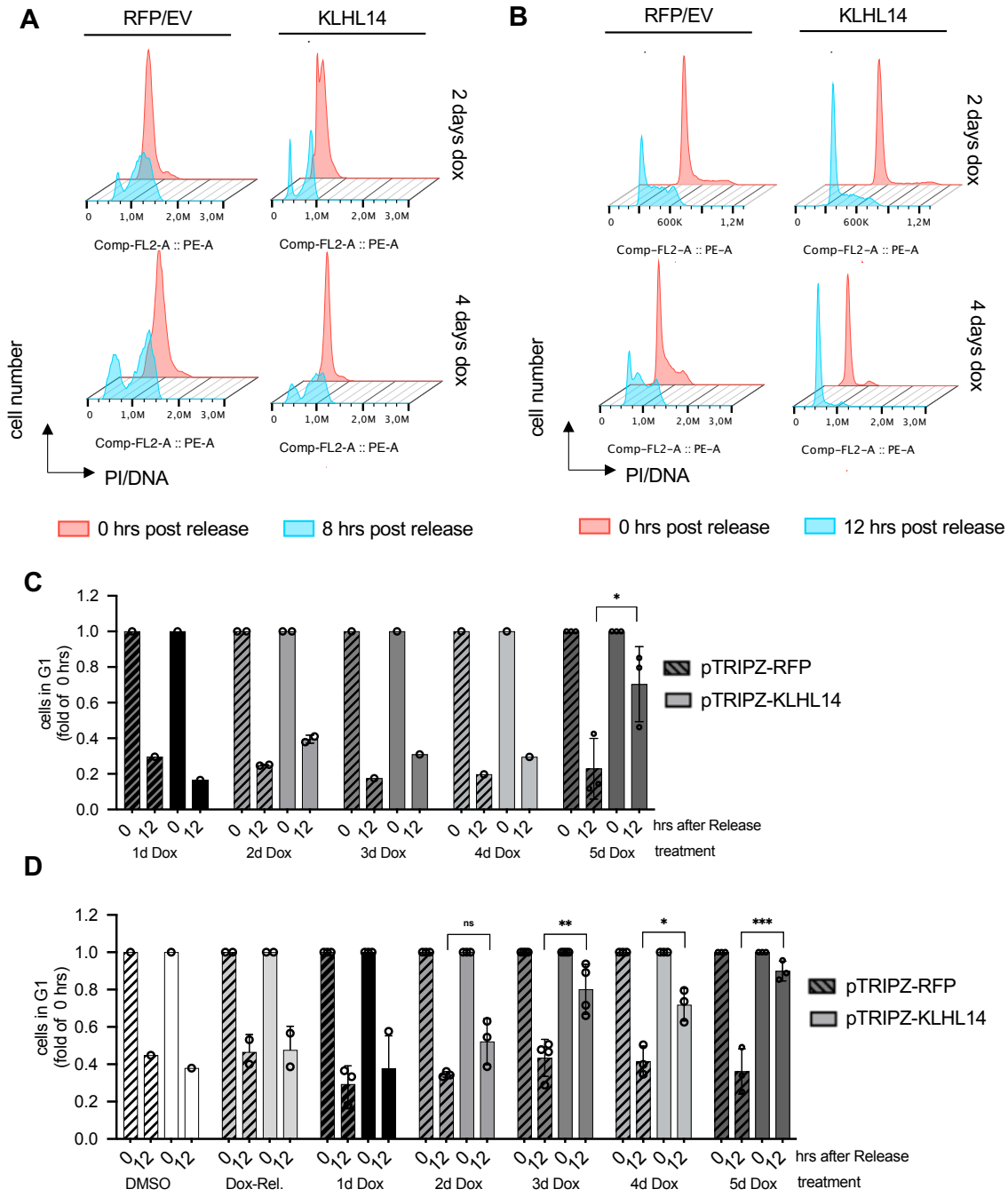

Figure 18: KLHL14 overexpression sensitizes MM1.S cells to palbociclib. A, Flow cytometric analysis of PI stained MM1.S cells with doxycycline induced KLHL14 or RFP expression before and after release from G1/S block. MM1.S cells stably expressing pTRIPZ-KLHL14 or -EV were treated with doxycycline (1 µg/mL) for the indicated durations to mediated transgene induction, synchronized at G1/S phase by a double thymidine block (red) and subsequently released for 8 hrs (blue). DNA was stained with propidium iodide (PI) and results are depicted as histogram analysis of FL2-A (PI) signal intensity. **B,** Flow cytometric analysis of PI stained MM1.S cells with doxycycline induced KLHL14 or RFP expression before and after release from a palbociclib mediated G1 arrest. Cells were treated and analyzed as in (A) but synchronized in G1-phase using palbociclib (1 µM) followed by release for 12 hrs. **C,** Quantification of G1/S-release experiments as described in (A) showing the cells in G1 normalized to 0 hrs release with 1-5 days of transgene induction (n=3 independent experiments for 5-days dox, n=2 for 2 days, all other time points: n=1). **D,** Quantification of the G1-release experiments as described in (B) showing cells in G1 normalized to 0 hrs release including days 0-5 of transgene induction (n=3 independent experiments for 1- 5-days dox, all other time points: n=1). ns, not significant; *, $P < 0.05$; **, $P < 0.01$, ***, $P < 0.001$; by Students t-test.

This further indicated that the KLHL14 expression exerted a so far undefined effect on the cells early on, which needed to accumulate before a permanent G1 arrest set in eventually, because cells were not able to satisfy the restriction point.

A major trigger of the restriction point is DNA damage (Borg and Dixit 2017; Bassermann, Eichner, and Pagano 2014). To investigate the hypothesis that KLHL14 triggered the restriction point by inducing increasing amounts of DNA damage or interfering with DNA damage repair during prolonged expression, doxycycline was again used to prompt KLHL14 expression in MM1.S cells stably transduced with the pTRIPZ system. Samples from the treated cells were taken for up to 8 days and WCEs analyzed by immunoblot, which revealed that DNA damage markers like yH2A.X and p-p53 were indeed detectable in KLHL14 overexpression samples from day 4 on. This marker induction was accompanied by the already established upregulation of the CDKI p27 (Fig. 19A). Furthermore, Caspase-3 cleavage was detected in these cells, implicating that cells eventually die from prolonged G1-arrest.

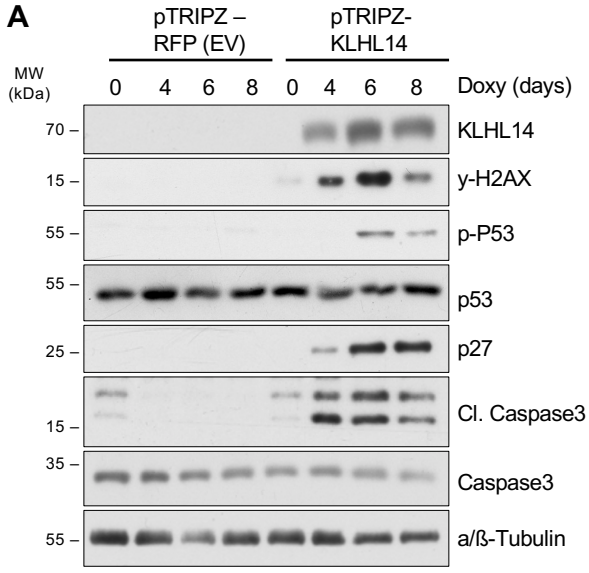

Figure 19: Prolonged KLHL14 expression induces DNA damage and apoptosis in MM 1.S cells. A, Immunoblot analysis of MM1.S cells stably expressing pTRIPZ-KLHL14 or -EV upon doxycycline (1 µg/mL) mediated transgene induction. Samples of doxycycline treated cells were harvested at the indicated time points after doxycycline addition and WCEs analyzed by immunoblot using the indicated antibodies. a/ß-Tubulin served as loading control.

DNA damage, followed by arrest in the subsequent G1 phase can be triggered by errors during mitosis or by prolonged mitosis (Fong et al. 2016; M T Hayashi and Karlseder 2013) and was therefore considered as a possible reason for the upregulation of DNA damage markers observed. As the KLHL14-mediated G1-arrest only occurred in B-Cell derived entities, which are difficult to handle in live cell imaging to determine the time a cell spends in mitosis, cell cycle analysis by PI staining and flow cytometry was used to determine the transgenes effect on G2/M duration. Accordingly, cells with and without KLHL14 overexpression were synchronized in G2/M by sequential thymidine and nocodazole block for MM1.S or nocodazole block only for Oci-LY1 cells. Samples for PI staining and immunoblot analysis were taken before and at the indicated time points after the drug was washed out and analyzed by flow cytometry and immunoblot respectively.

MM1.S cells readily progressed from the mitotic arrest into G1-phase and mostly completed mitosis at 4 hrs post release. The presence of KLHL14 lead to a marginally faster progression of the cells from mitosis, but over all very comparable dynamics of mitotic progression were observed (Fig. 20A). Analysis of the respective protein samples showed a similar trend of a full but slightly faster exit from G2/M arrest as indicated by an earlier

downregulation of pHH3 and Cyclin B1 in KLHL14 overexpressing compared to control cells (Fig. 20A, right panel).

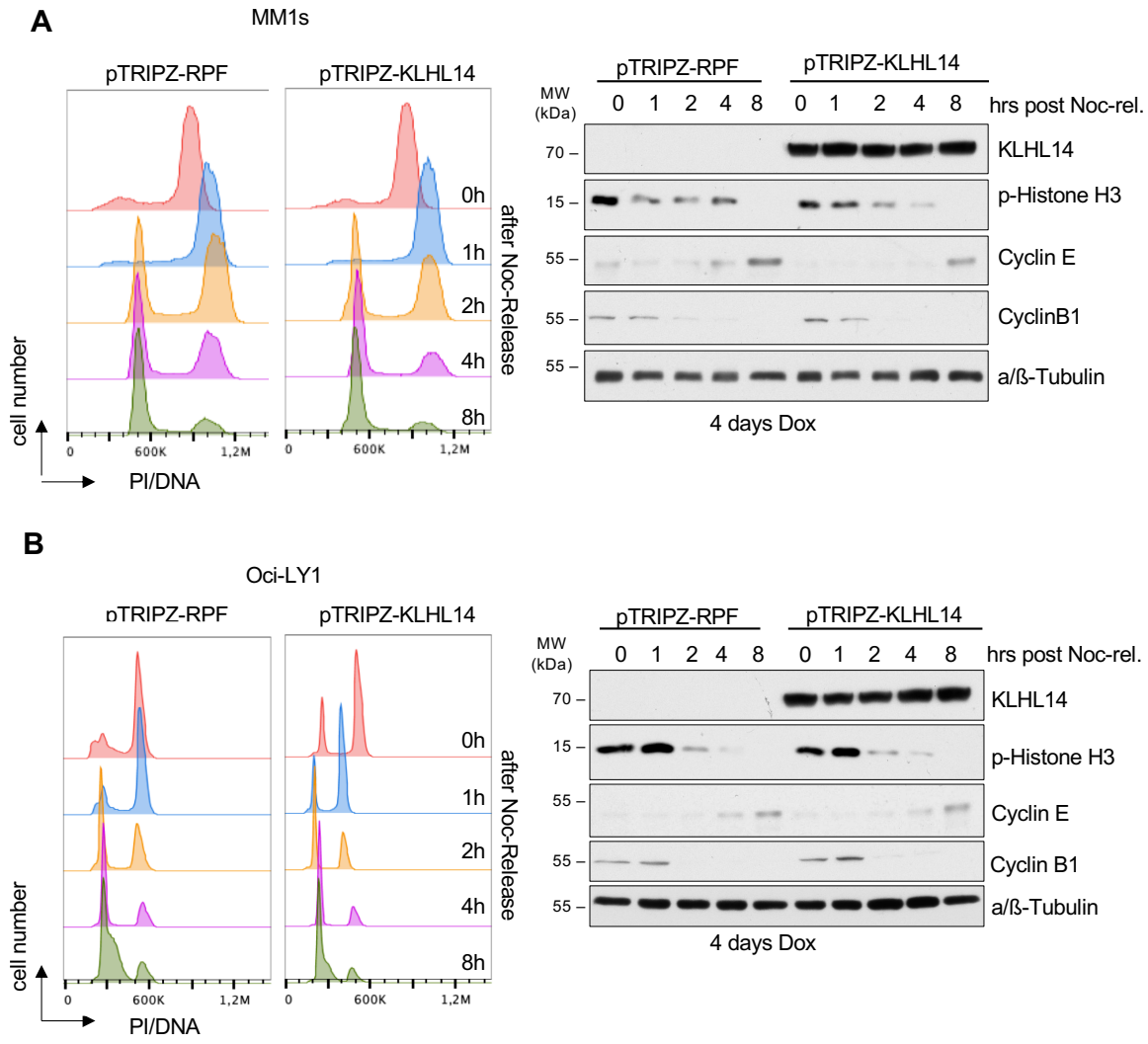

Figure 20: The duration of mitosis is unchanged in KLHL14 overexpressing cells. A, Cell cycle analysis of MM1.S cells with doxycycline induced KLHL14 or RFP expression before and after release from a G2/M block. MM1.S cells stably expressing pTRIPZ-KLHL14 or -EV were treated with doxycycline (1 µg/mL) for 4 days to mediate transgene induction and cells were synchronized in G2/M by sequential thymidine and nocodazole treatments. Samples for PI/flow cytometry (left) and immunoblot analysis (right) were taken before and at the indicated time points after released. For flow cytometry analysis, DNA was stained with propidium iodide (PI). Results are depicted as histograms of FL2-A (PI) signal intensity (left). For immunoblot analysis, WCEs were generated and analyzed using the indicated antibodies (right). a/ß-Tubulin served as a loading control. **B,** Cell cycle analysis of Oci-LY1 cells with doxycycline induced KLHL14 or RFP expression before and after release from a G2/M block. Samples were processed as described in (A). Noc-rel. – Nocodazole Release.

The same effect was visible using the DLBCL cell line Oci-LY1, even though the synchronization of the cells in G2/M was not as good as in the MM1.S cell lines to start with, especially in the KLHL14 overexpression line. The latter might be caused by prolonged transgene presence, which already lead to a permanent G1 arrest in a subset of cells by the time of the experiment (Fig. 20B). Interestingly, the late time points of this mitotic release show Oci-LY1-RFP cells starting to leave G1 phase and progress into S-phase after 8 hrs post wash out (Fig.20B, green graph), while their KLHL14 overexpressing counterparts are still represented as a narrow G1/2N peak. To follow up on this observation, a similar cell cycle

analysis experiment was performed using Oci-LY1 and MHH-PreB1 cells after just four days of either RFP or KLHL14 induction to ensure a good synchronization in G2/M. Again, cells were synchronized in and released from G2/M while samples for PI staining were taken at the indicated time points for up to 12 hrs to monitor cell populations that progressed from the subsequent G1-cell cycle phase (Fig. 21A).

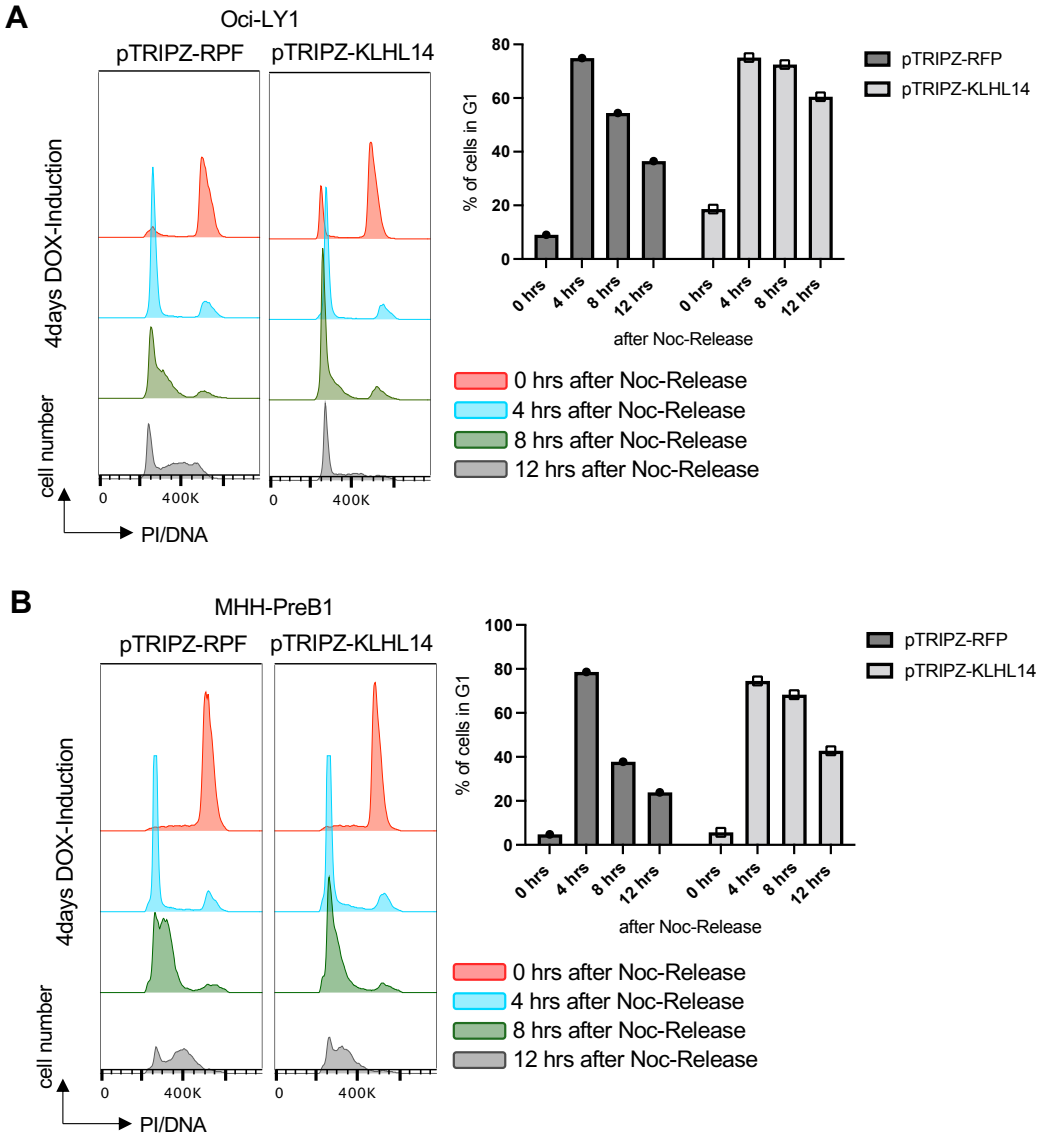

Figure 21: DLBCL cells overexpressing KLHL14 show a prolonged G1-phase after nocodazole release. **A,B,** PI/Flow cytometry-based cell cycle analysis of Oci-LY1 (A) and MHH-PreB1 (B) cells with doxycycline induced KLHL14 or RFP expression before (left panels) and after release (right panels) from a G2/M arrest and quantification thereof. Cells stably expressing pTRIPZ-KLHL14 or -EV were treated with doxycycline (1 µg/mL) for 4 days to mediated transgene induction and synchronized in G2/M by nocodazole treatment (MM1.S) or nocodazole block. Samples for PI/flow cytometry were taken before and at the indicated time points after release, DNA was stained with propidium iodide (PI) and analyzed. Results are depicted as histogram analysis of FL2-A (PI) signal intensity. Quantifications show percentages of cell in G1-phase at the indicated time points. Noc-Release – Nocodazole Release

The flow cytometric evaluation of these samples showed that Oci-LY1 and MHH-PreB1 control cells readily shifted from G2/M to G1 and into S-phase and G2/M phase 12 hrs after the removal of nocodazole, while the KLHL14 expressing cells showed a prolonged G1 (Fig. 21). Unfortunately, none of the MM cell lines tested progressed from G1 at 12 hrs post wash out,

making longer release times necessary to reproduce the effect seen in Oci-LY1 and other DLBCL lines in MM cell line models, which at the time of this thesis was not performed.

In conclusion, the overserved DNA damage in KLHL14 overexpressing cells might occur during the late time points during mitosis or in the subsequent G1, as overexpressing cells showed no signs of a delayed mitotic exit or mitotic slippage which would be a sign of an active/unsatisfied spindle assembly checkpoint.

5.3 KLHL14 localizes to the mitotic centrosomes and spindle

5.3.1 Overexpressed KLHL14 localizes in distinct foci

The indications that the DNA damage, which triggered the arrest at the restriction point in KLHL14 overexpressing B-cell derived cells, might be caused by errors or stress in mitosis, prompted the need for immunofluorescence (IF) studies in these cells.

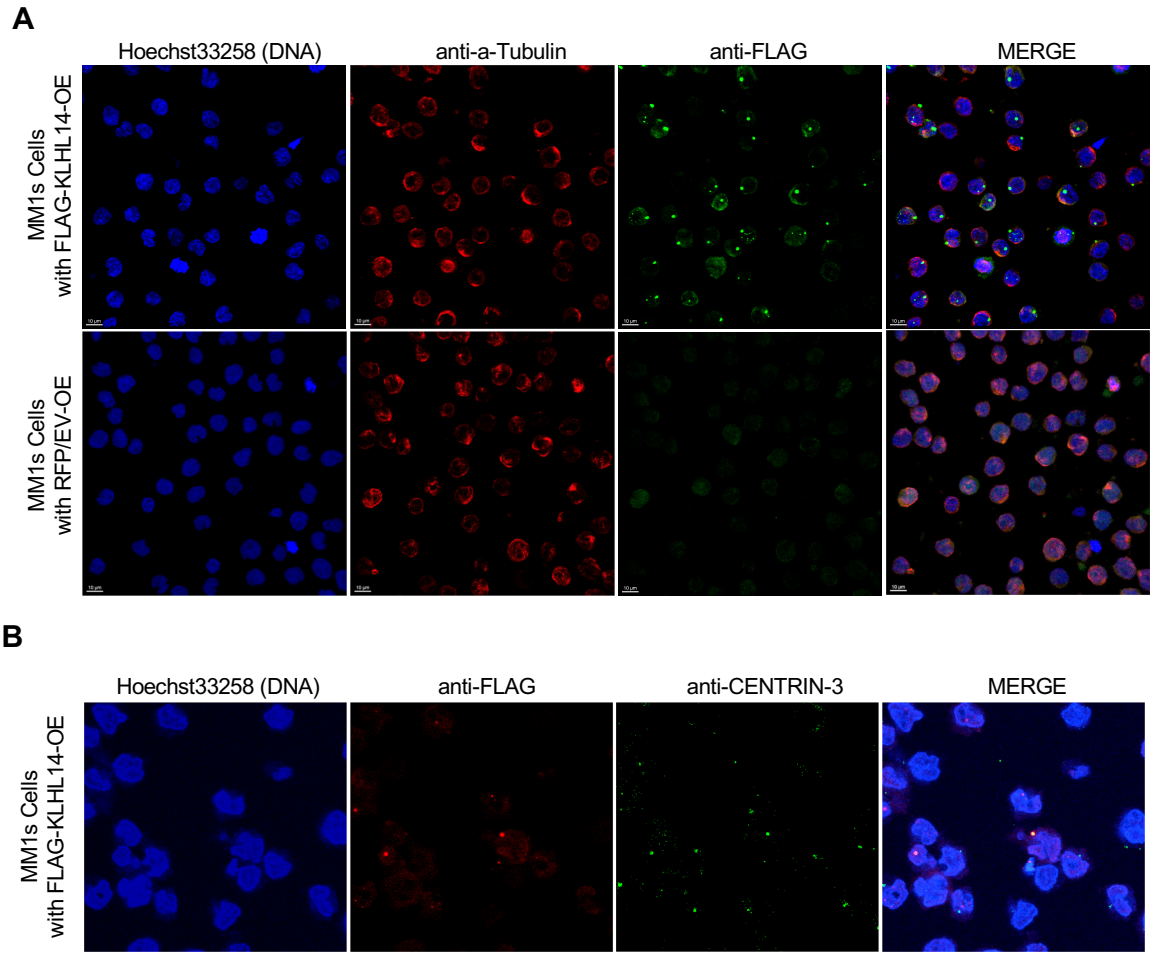

Figure 22: Overexpressed KLHL14 localizes to distinct cytoplasmic foci. A, Representative images of immunofluorescence analyses of MM1.S cells with doxycycline induced FLAG-KLHL14 (upper panel) or RFP (lower panel) expression. Cells stably expressing pTRIPZ-FLAG-KLHL14 or -EV were treated with doxycycline (1 µg/mL) for 24 hrs to mediated transgene expression, attached on poly-D-lysin coated chamber slides in HBSS and fixed with 4% PFA. Slides were stained with anti-FLAG (KLHL14, green), anti-a-Tubulin (red) and the respective Alexa-Fluor-488 and -594 coupled secondary antibodies in a two-step procedure. DNA was stained with HOECHST33258 (blue) and images were acquired by confocal microscopy. Scale bars represent 10 µm. **B**, Representative images of immunofluorescence analyses of MM1.S cells expressing pTRIPZ-FLAG-KLHL14 treated as described in (A) but stained with anti-FLAG (KLHL14, red) and anti-CENTRIN-3 (green) antibodies.

First, MM1.S cells stably expressing either the pTRIPZ-RFP or -FLAG-KLHL14 construct were treated with doxycycline for 24 hrs and then attached on poly-D-lysine coated chamber slides. The cells were then fixed with 4% PFA and incubated with anti-FLAG and anti-Tubulin primary antibodies produced in rabbit and mouse respectively. After addition of fluorophore coupled species specific secondary antibodies, DNA staining by HOECHST33258 (Sigma) and mounting, the slides were imaged using a LEICA-SF8 confocal microscope (Figure 22).

These first images revealed that KLHL14 localized into very distinct dot like structures or foci, resembling a centrosomal localization at microtubule organizing centers (MTOC)(Sanchez and Feldman 2017; Tillery et al. 2018) when overexpressed in MM1.S cells (Fig. 22A). Indeed, when co-staining the centrosomal protein CENTRIN-3 instead of Tubulin in the same cellular setup, not all but many KLHL14 (FLAG) foci co-localized with it, indicating at least a partial MTOC or centrosomal localization of overexpressed KLHL14 (Fig 22B). These data indicate, that KLHL14 might be recruited to the centrosomes of the cells during specific cell cycle phases.

5.3.2 Endogenous KLHL14 is recruited to the centrosome in G2/M phase

The partial localization of overexpressed KLHL14 to the centrosomes in MM cells lead to the hypothesis, that the protein was either involved in centrosome duplication and maturation (Bettencourt-Dias and Glover 2007) or recruited specifically to the centrosomes as part of the pericentrosomal material during mitosis(Gouveia et al. 2019). As the ectopic expression of a protein can lead to its miss-localization or aggregation within cells, endogenous KLHL14 protein was studied by immunofluorescence.

Therefore, the GCB-type DLBCL cell line Oci-LY1, which has been found to express detectable levels of KLHL14 protein (Fig. 10) and can be synchronized in a specific cell cycle phase, was chosen to study the dynamics of the endogenous protein during different cell cycle phases. The cells were either used as an asynchronous population supplemented with DMSO, arrested in G1 using palbociclib or in G2/M by addition of nocodazole, attached on poly-L-lysine coated chamber slides and stained with a primary antibody raised against KLHL14. Co-staining with an anti-CENTRIN-3 antibody enabled the monitoring of the two endogenous proteins in the different cells cycle phases (Fig. 23A). The subsequent analysis of the fluorescence images taken of the asynchronous cell population (Fig. 23A, upper panel) revealed only a very limited amount of KLHL14 condensates, that looked similar to the overexpressed version of the protein. Interestingly, these condensates were found around the centrosomes of cells that were undergoing chromosome condensation or segregation during meta-/anaphase as shown in the close up in figure 23B.

In contrast, the intense dot-like staining was almost completely absent from cells arrested in G1 by palbociclib treatment (Fig. 21A middle panel). In case a localized signal could be found, it did not appear in proximity to CENTRIN-3 signal (Fig. 21B). When cells were arrested in G2/M in the other hand, a distinct and almost punctual KLHL14 signal was detected in close proximity to CENTRIN-3 in almost every cell, indicating a recruitment of the CUL3-ligase to the spindle poles/centrosomes in G2/M phase (Fig. 21 A,B).

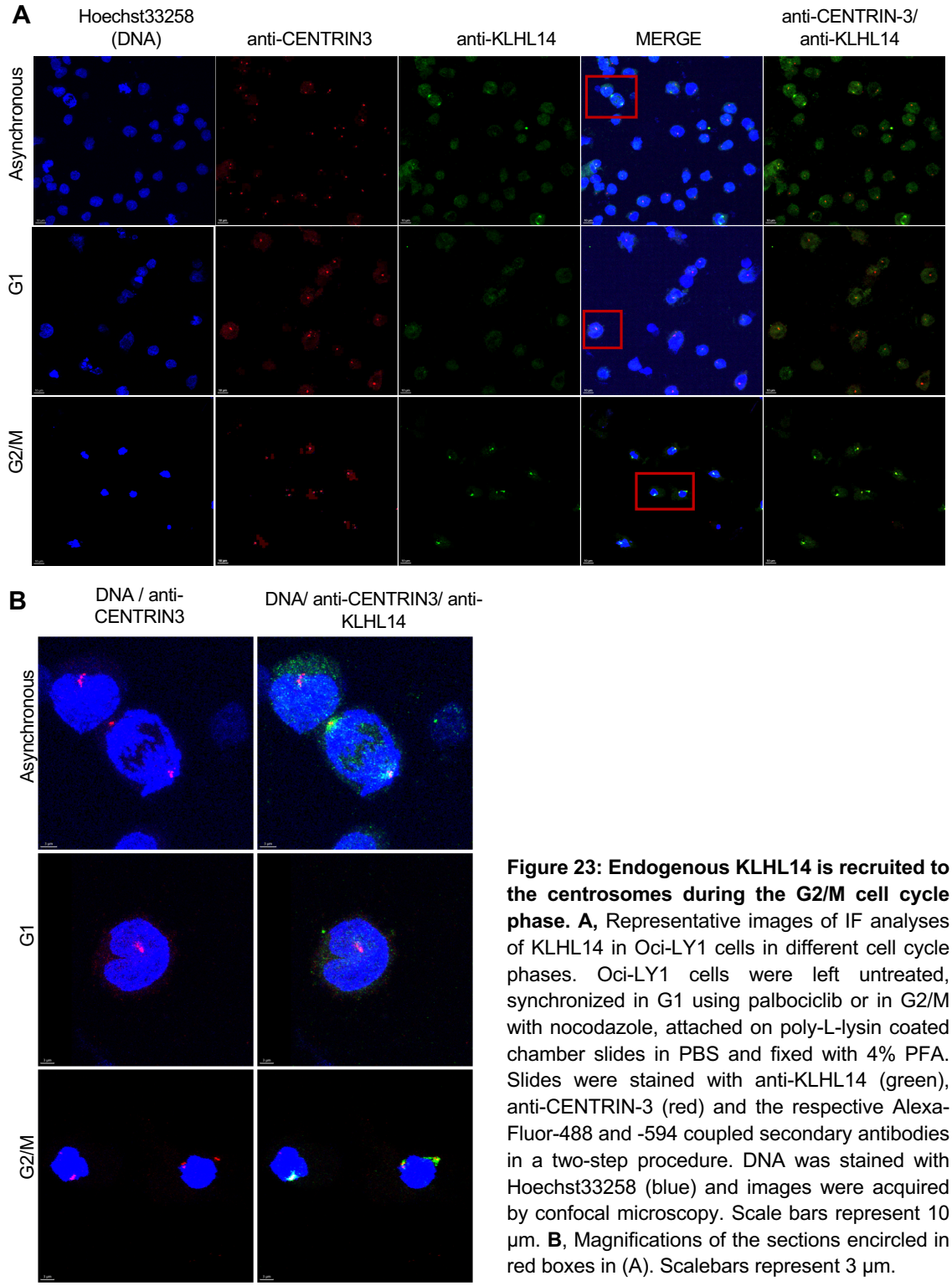

Figure 23: Endogenous KLHL14 is recruited to the centrosomes during the G2/M cell cycle phase. A, Representative images of IF analyses of KLHL14 in Oci-LY1 cells in different cell cycle phases. Oci-LY1 cells were left untreated, synchronized in G1 using palbociclib or in G2/M with nocodazole, attached on poly-L-lysin coated chamber slides in PBS and fixed with 4% PFA. Slides were stained with anti-KLHL14 (green), anti-CENTRIN-3 (red) and the respective Alexa-Fluor-488 and -594 coupled secondary antibodies in a two-step procedure. DNA was stained with Hoechst33258 (blue) and images were acquired by confocal microscopy. Scale bars represent 10 µm. **B**, Magnifications of the sections encircled in red boxes in (A). Scalebars represent 3 µm.

The Quantification of the foci formation and their CENTRIN-3 co-localization from 5 different confocal images and at least 50 cells per condition revealed an 8-fold increase in KLHL14 condensates upon G2/M synchronization of the cells (from 9% in asynchronous to 72% in nocodazole treated samples). Furthermore, almost 95% of these structures clustered around the centrosomes as indicated by its close proximity to CENTRIN-3. In case cells were arrested in G1, 95% of cells showed a diffuse cytoplasmic KLHL14 fluorescence signal and none of the observed condensates co-localized with the CENTRIN-3 staining (Fig. 24A). The synchronization within the indicated cell cycle phases was confirmed by immunoblot and PI/

flow cytometry-based cell cycle analysis of cell aliquots taken prior to attaching the cells on chamber slides (Fig. 24B-D). The flow cytometry data revealed a correlation between the number of CENTRIN-3 colocalizing KLHL14 foci and the number of cells that were in G2/M according to the DNA content measured (Fig 24A-C). Importantly, total KLHL14 protein levels did not change upon synchronization of Oci-LY1 cells in G1 or G2/M phases (Fig. 24D), corroborating data generated in the MHH-PreB1 DLBCL cell line (Fig. 17).

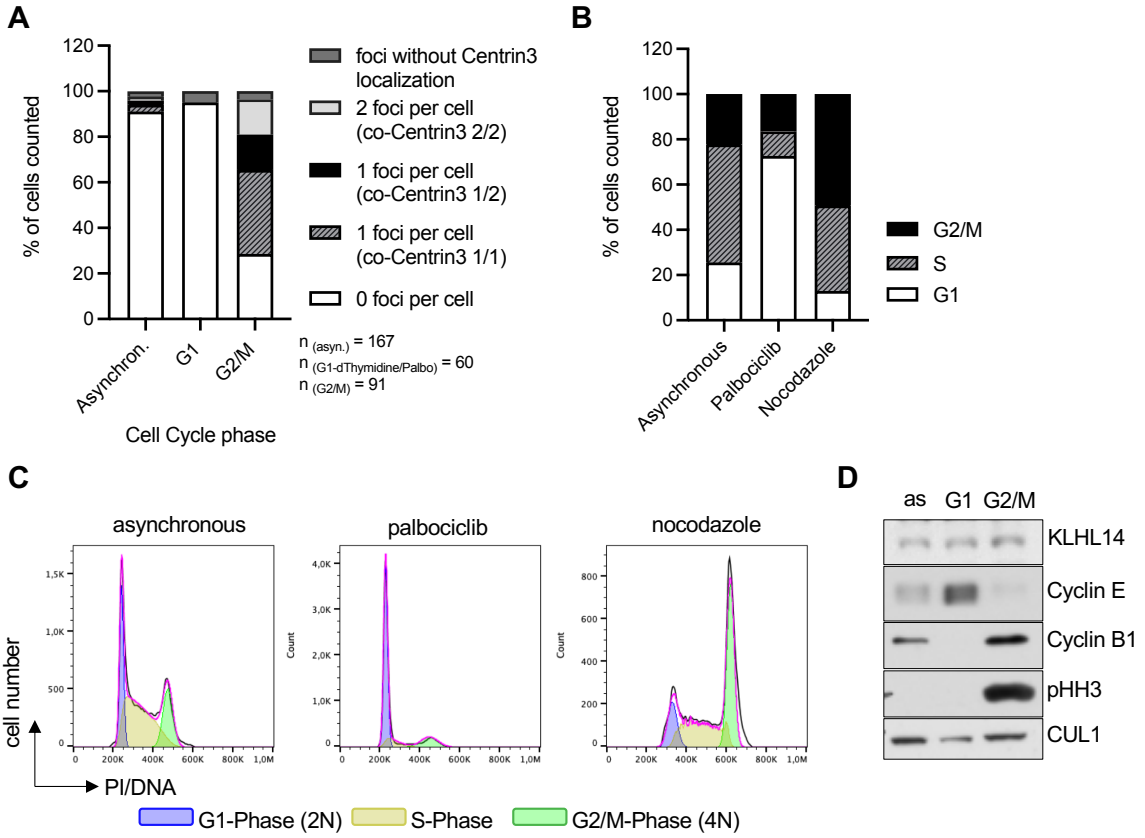

Figure 24: Endogenous KLHL14 co-localizes with CENTRIN-3 in G2/M cells. A, Quantification of the KLHL14 foci from two independent experiments preformed as described for Fig. 23. KLHL14 foci were counted in 5 representative images from different areas of the slide, grouped according to their co-localization with the centrosomal marker CENTRIN-3 and plotted as percentages of total cells counted per condition. **B, C,** PI/Flow cytometry-based cell cycle analysis of the Oci-LY1 cells used for IF in (A) and Fig. 23. **B,** Quantification of cell per cell cycle phase plotted as percentage of all cells measured per treatment condition. **C**, FACS blots representing the PI stained DNA content of the Oci-LY1 cells quantified in (B). The distribution of cells in the different cell cycle phases was determined by the Dean-Jett-Fox method implemented in the FlowJo V10 software without setting constraints. Results are depicted as histogram analysis of FL2-A (PI) signal intensity. **D,** Immunoblot analysis of Oci-LY1 cells used for IF in (A) and Fig. 15. Cells were harvested at the time of fixation, WCEs were prepared and analyzed for KLHL14 and cell cycle marker expression using the indicated antibodies. CUL1 served as a loading control. asynch./as – asynchron, N – chromosome number.

To avoid possible cell line artefacts by focusing on a particular model cell line, the experimental setup of G2/M synchronization followed by indirect immunofluorescence as described for Oci-LY1 cells was performed in additional DLBCL cell lines. Due to their comparably high KLHL14 protein expression detected by immunoblotting (Fig. 10), HBL1, RIVA, Oci-LY3 and MHH-PreB1 were used to analyze KLHL14 foci formation and their co-localization with CENTRIN-3 in asynchronous and G2/M- arrested cells by immunofluorescence (Fig. 25).

Interestingly, 60% of HBL1 cells showed foci formation in asynchronous cells, of which 51% did not localize to the centrosomes. The percentage of foci co-localizing with CENTRIN-3 did not correlate with the percentage of G2/M phase cells as measured in PI flow cytometry

(Fig. 25A, B, very left panels). Upon nocodazole treatment the number of cells with the distinct staining pattern not only increased further, but the CENTRIN-3/KLHL14 co-localization increased 5.5-fold from 9 to 50% of all cells counted. When analyzing untreated and therefore asynchronous RIVA, Oci-LY3 and MHH-PreB1 cells, KLHL14 foci could be found in between 5 (MHH-PreB1) and 13% (RIVA) of cells mainly at the centrosomes (Fig. 25A), which is approximately the percentage of cells in G2/M in asynchronous populations (Fig. 25B). The percentage of dot like staining and co-localization with CENTRIN-3 signal increased between 3.8 (RIVA) and 14-fold (MHH-PreB1) upon synchronization, hinting towards the specific recruitment of endogenous KLHL14 in human DLBCL-cells during mitosis.

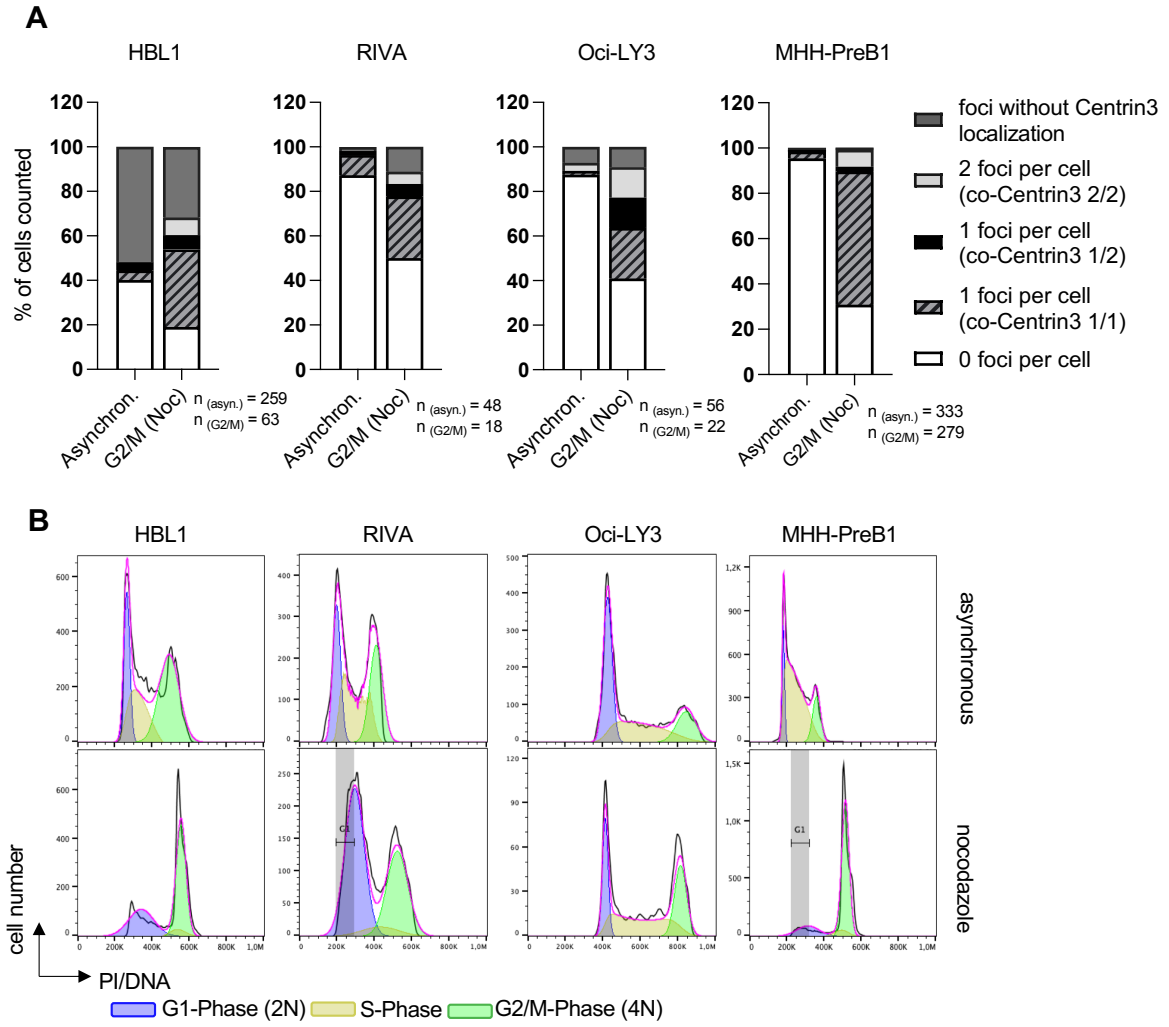

Figure 25: Recruitment of KLHL14 to the centrosomes during G2/M arrest occurs in various DLBCL cell lines. A, Quantification of KLHL14 foci detected by IF in various asynchronous and G2/M arrested DLBCL cells lines. HBL-1, RIVA, Oci-LY3 and MHH-PreB1 cells were either left untreated or synchronized in G2/M using nocodazole, attached on poly-L-lysin coated chamber slides in PBS and fixed with 4% PFA. Slides were stained with anti-KLHL14, anti-CENTRIN-3 and Hoechst33258 (DNA) prior to imaging using a confocal microscope. KLHL14 foci were counted in 5 representative images from different areas of the slide, grouped according to their co-localization with the centrosomal marker CENTRIN-3 and plotted as percentages of total cells counted per condition. **B,** PI/Flow cytometry-based cell cycle analysis of the cells used for IF in (A). Samples of the respective cell line and condition were taken prior fixation on IF-slides and subjected to PI/flow cytometry analysis. The distribution of cells in the different cell cycle phases was determined by the Dean-Jett-Fox method implemented in the FlowJo V10 software with (RIVA, MHH-PreB1) or without constraining the G1 population. Results are depicted as histogram analysis of FL2-A (PI) signal intensity.

Even though the synchronization of cells used for immunofluorescence experiments was always controlled by PI-flow cytometry and immunoblot analyses and slides were only imaged if high percentages of synchronized cells were detected, not all cells that attached to a slide were in the desired cell cycle phase. In order to discriminate mitotic cells during microscopy or picture evaluation, an Alexa-647-coupeled p-Histone-H3 (pHH3) (Ser28) antibody produced in rat (BD bioscience) was added to the staining panels.

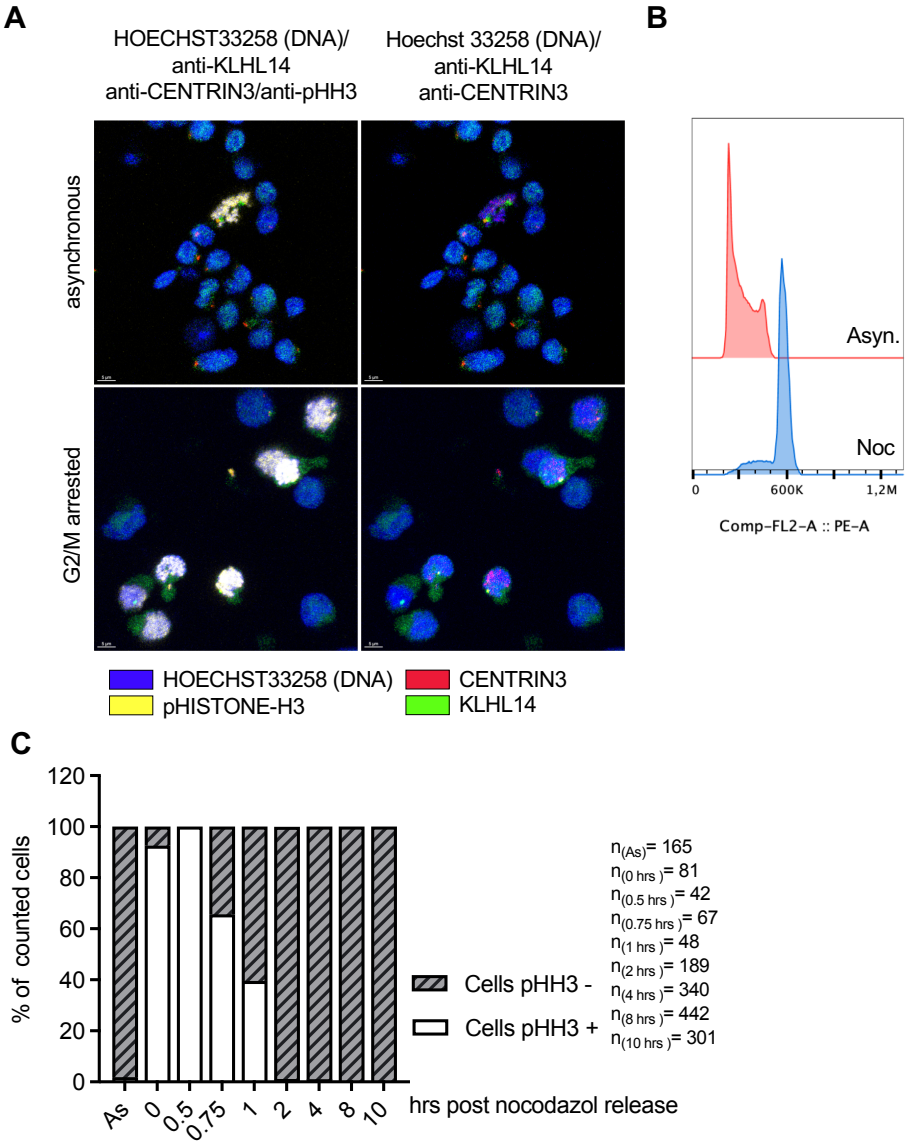

Figure 26: Test of a directly coupled pHH3-antibody to identify mitotic cells by IF. A-C, Analysis of a nocodazole release time course in MHH-PreB1 cells by IF. Cells were left untreated or synchronized in G2/M using nocodazole and attached on poly-L-lysin coated chamber slides before or at the indicated time point after release from G2/M. Cells were fixed with 4% PFA and slides were stained with anti-KLHL14 (green), anti-CENTRIN-3 (red), anti-pHH3(Ser28)-AlexaFluor647 (yellow) and the respective fluorophore coupled secondary antibodies in a two-step procedure. DNA was stained with Hoechst33258 (blue) and images were acquired by confocal microscopy. **A**, Representative IF images of asynchronous and nocodazole arrested (0 hrs time point) MHH-PreB1 cells of the release time course. Scale bars represent 5 µm. **B**, Cell cycle analysis of MHH-PreB1 cells used for IF in (A). Cells were synchronized as described above and samples taken at the time of fixation on IF slides. DNA-content was stained using PI and analyzed by flow cytometry. Results are depicted as histogram analysis of FL2-A (PI) signal intensity. **C,** Quantification of pHH3 positive cells at the different time points of the nocodazole release time course described in (A) depicted as percentage of cells counted per condition.

First tests in MHH-PreB1 DLBCL cells revealed that the antibody indeed stained only the chromatin of cells, that were determined to be in meta/-anaphase by their characteristic condensation and segregation of aligned chromosomes, presence of the mitotic spindle and high DNA content. Additionally, the amount of pHH3 positive cells could be highly enriched by nocodazole mediated G2/M synchronization (Fig. 26A). This corresponded with the number of cells in G2/M as determined by analysis of the cell's DNA content by PI staining and subsequent flow cytometry (Fig. 26B). Quantification of pHH3 positive MHH-PreB1 cells, that were synchronized in G2/M using nocodazole, subsequently released by wash out and analyzed by immunofluorescence at the indicated time points before and after release, showed a decrease of mitotic cells over time, consistent with a presumed mitotic exit within 2 hrs after removal of the drug (Fig. 26C). As this antibody stained mitotic cells reliably, it was included in all subsequent imaging experiments to more accurately identify mitotic cells. Due to its varying expression levels during mitosis and strong overlap with DNA, that hinder the proper visualization of other proteins stained within a given cell, the pHH3 staining will only be shown in pictures if necessary.

The question remained, whether the treatment with the microtubule depolymerizing agent nocodazole prompted a permanent KLHL14 aggregation at the centrosomes or if the release from mitotic arrest by removal of the drug would cause a shift or even loss of the prominent staining pattern. The evaluation of the KLHL14 signal detected by immunofluorescence of the mitotic release time course in MHH-PreB1 cells described above, uncovered that by the time most cells exited from mitosis approximately 2 hrs after nocodazole removal, only 7% of cells showed KLHL14 foci. The fraction of cells showing the distinct staining pattern, did not increase to more than 5% during later time points after the mitotic release, when cells were presumably progressing through G1- and into S-phase (Fig. 27).

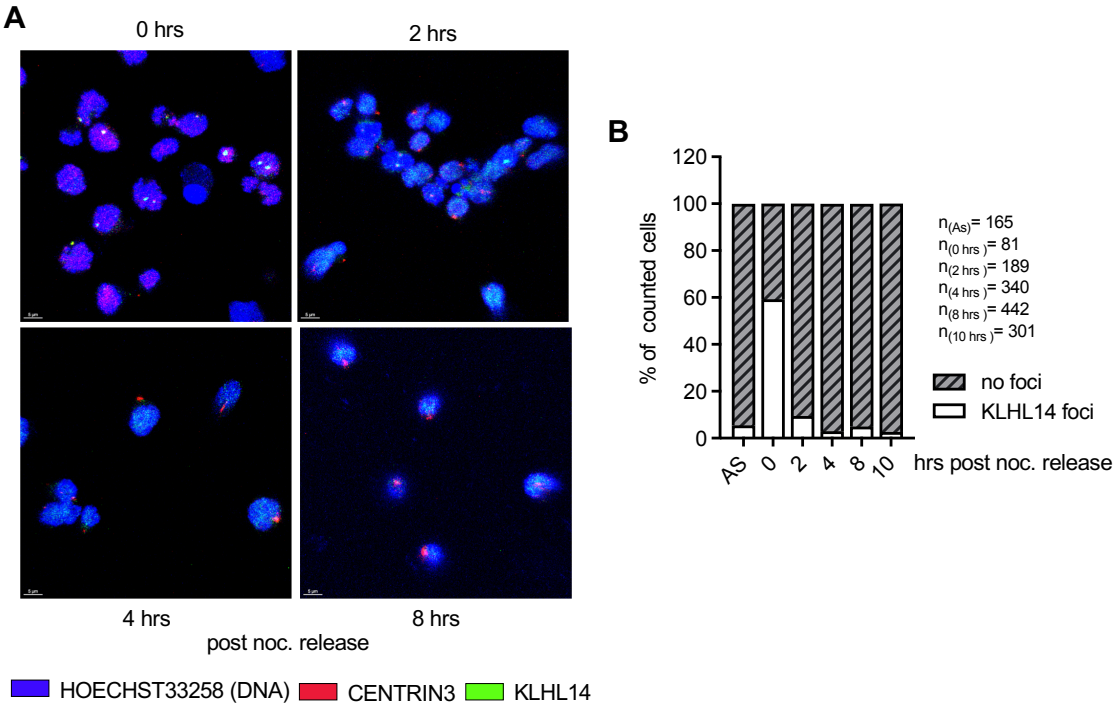

Figure 27: KLHL14 does not localize to the centrosomes after mitotic exit. A, Representative IF images of different time points of the nocodazole release time course in MHH-PreB1 cells as described in figure 18. Scale bars represent 5 µm. **B**, Quantification of KLHL14 foci per cell during the mitotic release time course experiment described in figure 26, depicted as percentage of cells with at least one KLHL14 condensate per cell at the indicated time point.

Next, IF images of the earlier time points of the nocodazole wash out/release experiment where examined in more detail to monitor KLHL14 dynamics from Pro-/Metaphase to cytokinesis and abscission. The different cell cycle phases were distinguished by their characteristic DNA and a-Tubulin arrangement. Briefly, during metaphase, chromosomes are condensed and aligned at the metaphase plate. At the Meta-to-Anaphase transition, microtubules have formed the characteristic bipolar mitotic spindle attached to two opposite spindle poles of the cell, that pulls the sister chromatids the opposite poles during anaphase (Lara-Gonzalez, Westhorpe, and Taylor 2012). Cells in both cell cycle phases could be identified in the samples fixed on poly-L-lysin coated slides 30 or 45 min after nocodazole wash out.

Interestingly, the fluorescence signal representing KLHL14 was found to co-localize with the a-Tubulin signal of the spindle apparatus with a clear polarization towards the spindle poles (Fig. 28A, left panel). In telophase the condensed chromosomes have reached the centromeres/spindle poles, new nuclear membranes form around them and finally the cytoplasm is divided (Fededa and Gerlich 2012). Even though cells in telophase/cytokinesis and abscission were not observed frequently in the conducted experiments or could not be unambiguously identified, the few examples of cells in those mitotic phases, showed less well-defined a-Tubulin/KLHL14 co-staining at the spindle midbody (middle panel), that was further reduced during progressing abscission (right panel) (Fig. 28A).

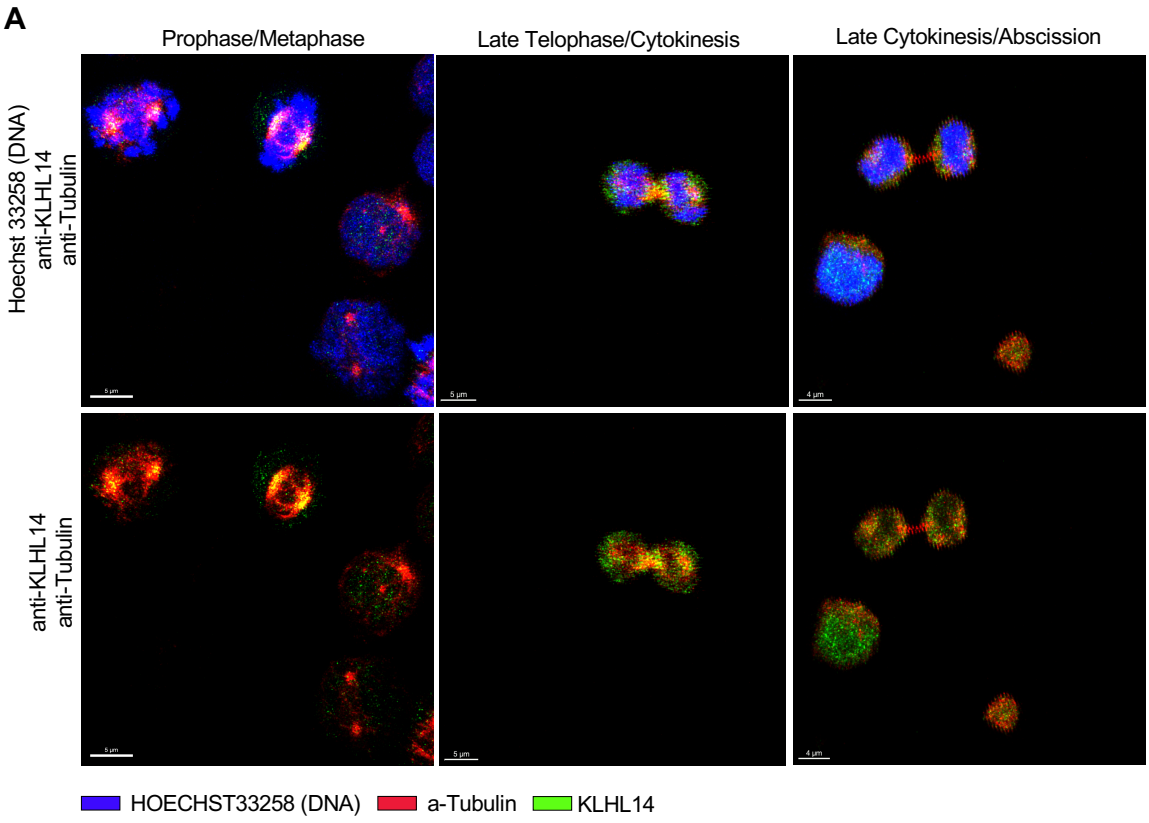

Figure 28: KLHL14 localizes to the mitotic spindle and the spindle midbody. A, Representative IF images of MHH-PreB1 cells in different phases of mitosis. Pictures of MHH-PreB1 cells fixed early during the nocodazole release time course experiment described in figure 26 were searched for cells in the different stages of cell division. The different stages of mitosis were identified by their characteristic interplay between DNA und a-Tubulin signal. Confocal images show maximum projection overlays of DNA (blue), a-Tubulin (red) and KLHL14 (green) signals (upper panel) or a-Tubulin and KLHL14 signals only (lower panel) for better visualization. Scale bars represent 5 µm.

To ensure that the observed staining patterns were indeed mitosis specific, MHH-PreB1 cells were additionally arrested in G1 by palbociclib treatment, released from the cell cycle block by wash out and attached to poly-L-lysine coated slides at the indicated time points. The cells were then stained by indirect immunofluorescence for endogenous KLHL14, a-Tubulin and pHH3. HOECHST-33258 was again used as a DNA stain. The imaging of the resulting slides revealed KLHL14 condensates in between 1.5 and 3.8% of non-mitotic (pHH3 negative) cells counted. This number fluctuated during the release time course from 2.7% in G1 arrested cells to 3.8% at 4 hrs and 2.7% after 10 hrs of palbociclib wash out (Fig. 29). This indicated that the distinct KLHL14 foci formation does not occur during G1- or S-phases, but is restricted to G2/M.

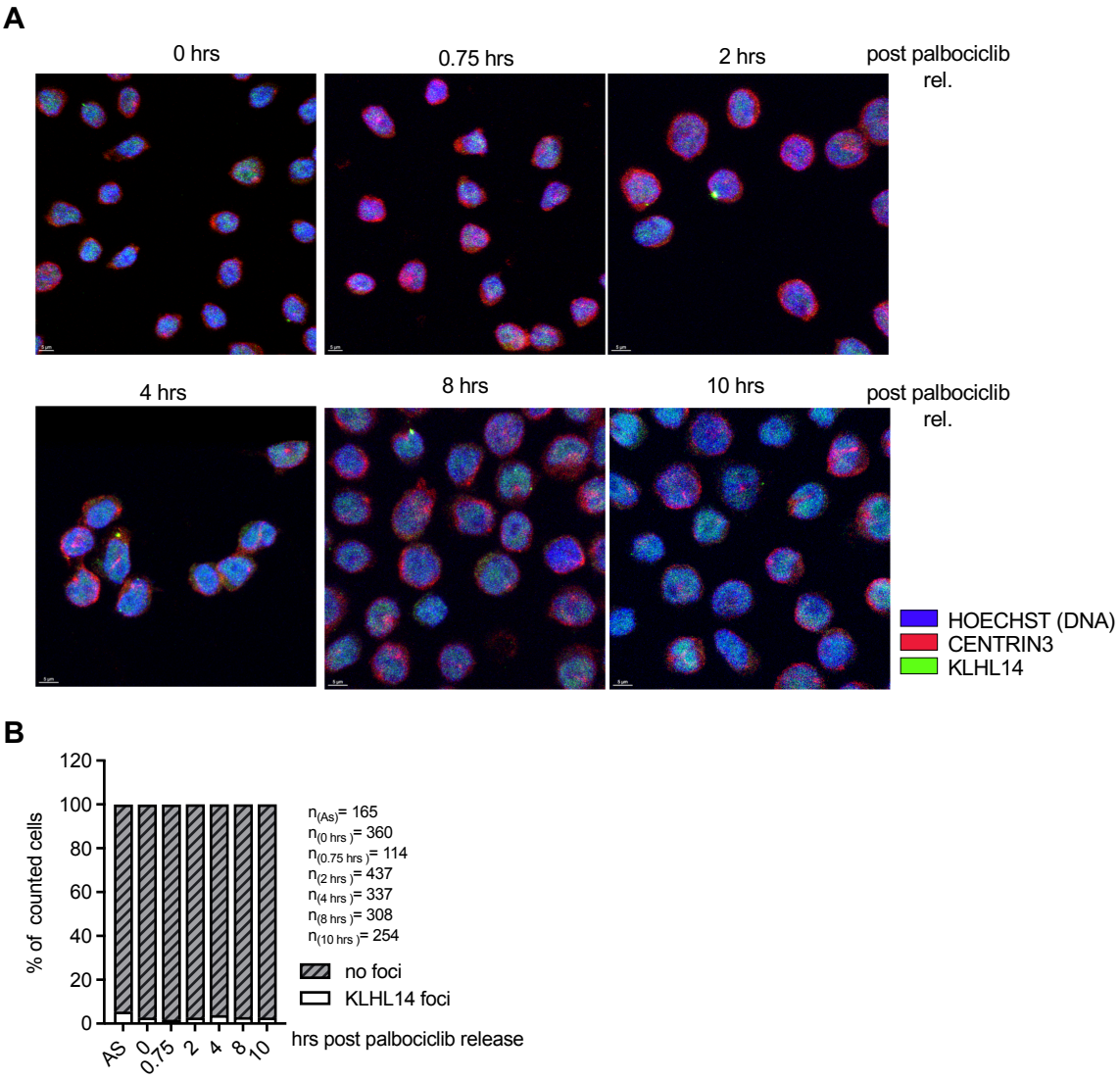

Figure 29: KLHL14 foci are mitosis specific. A, Representative IF images of MHH-PreB1 cells at different time points after G1 release. MHH-PreB1 cells were arrested at the G1 restriction point by administering palbociclib for 24 hrs, attached on poly-L-lysin coated chamber slides and fixes with 4% PFA at the indicated time points before or after release from the cell cycle block. Slides were stained with anti-KLHL14 (green), anti-CENTRIN-3 (red), anti-pHH3(Ser28)-AlexaFluor-647 (not shown) and the respective fluorophore coupled secondary antibodies. DNA was stained with Hoechst33258 (blue) and images were acquired by confocal microscopy. Scale bars represent 5 µm. **B**, Quantification of KLHL14 foci in pHH3 negative cells detected in five representative images per timepoint of the experiments described in (A). Data are blotted as percentage of all cells counted.

Figure 30 depicts examples, where KLHL14 foci were detected in non-mitotic cells as determined by the absence of pHH3 signal. When looking at the individual fluorescence channels of these images in more detail, it becomes apparent that the structures co-occur with

accumulations of a-Tubulin (white arrows), which are not necessarily the MTOCs of asynchronous cells, as these are clearly visible as separate areas with Tubulin assemblies (blue arrows) (Fig. 30). These imaging data indicate that endogenous KLHL14 is specifically recruited to functionally distinct Tubulin assemblies like the mitotic spindle or the spindle midbody, further feeding the hypothesis that KLHL14 exerts its function during cell division.

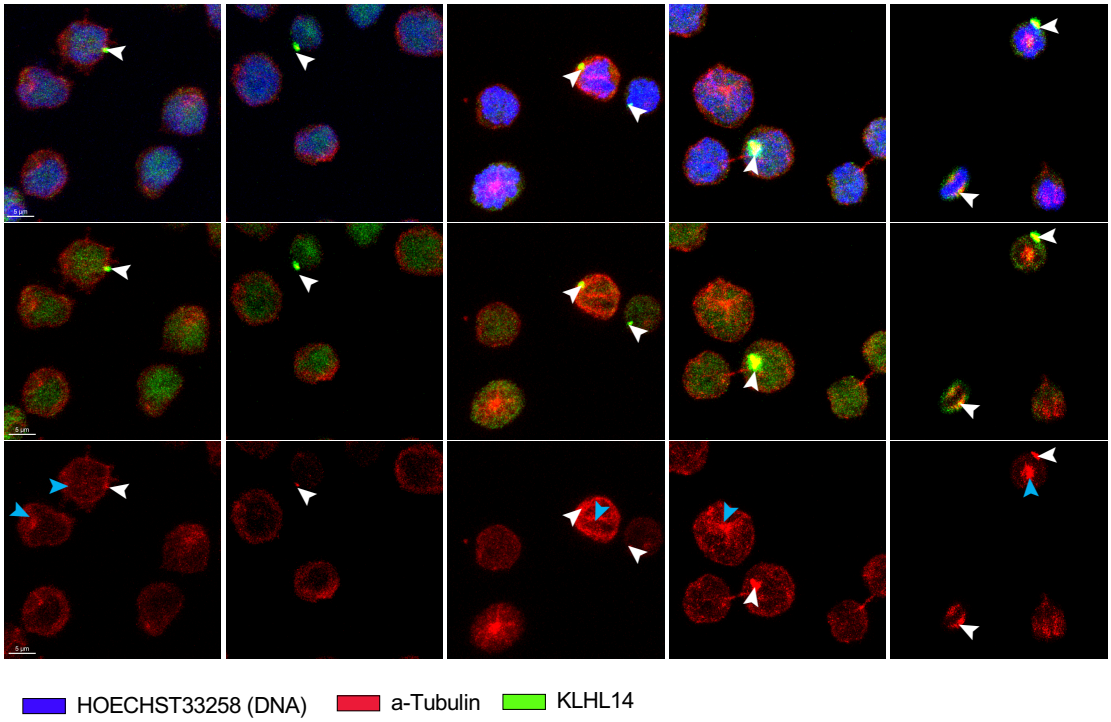

Figure 30: Foci of endogenous KLHL14 in non-mitotic cells colocalize with a-Tubulin accumulations. Representative IF images of non-mitotic MHH-PreB1 cells with visible KLHL14 foci formation. Pictures of the G1 release time course in MHH-PreB1 cells described in Figure 29 were analyzed for pHH3 negative cells with KLHL14 condensates. Confocal images show maximum projection overlays of DNA (blue), a-Tubulin (red) and KLHL14 (green) signals (upper panel), a-Tubulin and KLHL14 signals (middle panel) and a-Tubulin signal only (lower panel) for better visualization. White arrows indicate the positions of KLHL14 condensates and blue arrows tubulin accumulations and MTOCs without KLHL14 co-localization. Scale bars represent 5 µm.

Having established mitosis as the cell cycle phase, where KLHL14 most likely mediated its tumor suppressor function, possible effects of KLHL14 overexpression on mitosis in MM1.S cells were analyzed using immunofluorescence. Thus, the doxycycline inducible pTRIPZ vector system was used to trigger ectopic RFP or KLHL14 expression in MM1.S by doxycycline addition. Cells were subsequently arrested in G2/M by sequential thymidine and nocodazole blocks and prepared for immunofluorescence imaging at different time points after nocodazole wash out. The slides were stained with the established antibody panel consisting of anti-a-Tubulin, anti-FLAG (KLHL14), anti-pHH3 and HOECHST33258 (DNA). Five pictures per time point were taken and examined for cells in the different phases of mitosis, which were again identified by their characteristic a-Tubulin/DNA interplay and pHH3 signal.

KLHL14 localization was studied to establish whether the overexpressed protein showed a distinct localization during the different stages of mitosis. The KLHL14 foci appeared in a variety of staining pattern throughout all stages of mitosis, as exemplified in Figure 31. Some cells showed single KLHL14 accumulations, while others had multiple foci of different sizes. Neither size nor cellular localization correlated with the mitotic stage of the cells analyzed (Fig. 31A).

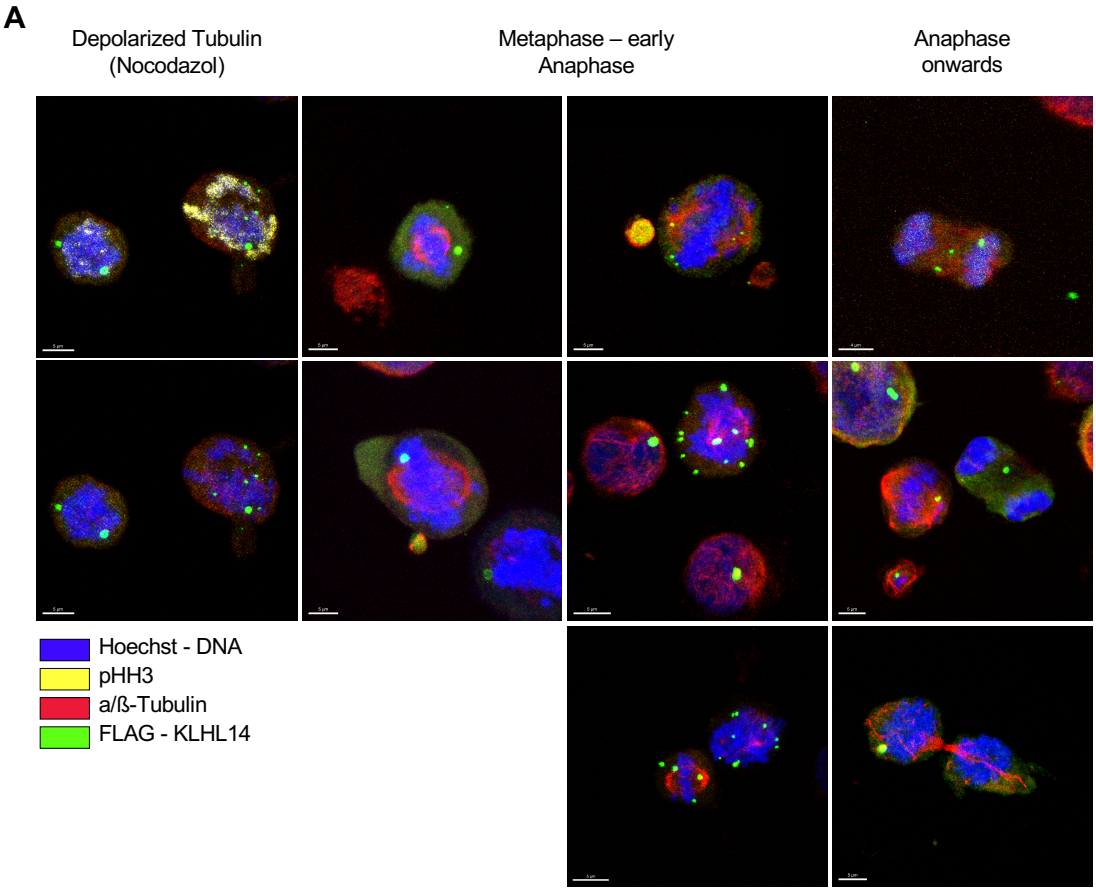

Figure 31: Overexpressed KLHL14 foci do not localize to specific sites during mitosis. A, Representative images of IF analyses of MM1.S cells with doxycycline induced FLAG-KLHL14 expression during different stages of mitosis. Cells stably expressing pTRIPZ-FLAG-KLHL14 were arrested in G2/M using a sequential thymidine and nocodazole block and were treated with doxycycline (1 µg/mL) for the last 24 hrs of the synchronization procedure to mediate transgene expression. Cells were then released from the G2/M block and attached on poly-D-lysin coated chamber slides at different time points before and after release. After fixation with 4% PFA, slides were stained with anti-FLAG (KLHL14, green), anti-a-Tubulin (red), anti-pHH3(Ser28)-AlexaFluor-647 (yellow, shown only in the upper left picture) and the respective fluorophore secondary antibodies in a two-step procedure. DNA was stained with Hoechst33258 (blue) and images were acquired by confocal microscopy. Cells within the different mitotic phases were identified by pHH3 staining and their characteristic interplay between DNA and a-Tubulin. Scale bars represent 5 µm.

Taken together, the imaging experiments conducted for this study, show that endogenous KLHL14 is specifically recruited to the mitotic spindle or the spindle midbody, further indicating that KLHL14 exerts its function during cell division. Throughout G1 and S-phase of the cell cycle KLHL14-foci co-inside with other, so far uncharacterized, Tubulin accumulations at very low numbers. The overexpressed protein localizes into dot-like structures independent of the cell cycle phase of a given cell but without any apparent changes in cellular morphology or mitotic defects.

5.4 KLHL14 in murine B-cell activation and lymphoma

Another intriguing question was, which function KLHL14 had in a physiological setting during B-cell development and differentiation. Gene expression analysis of publicly available mRNA data from different stages of murine B-cell development and activation

(http://rstats.immgen.org), showed that common lymphoid progenitors (CLPs) and proB-cells, both located in the bone marrow, expressed only low levels of KLHL14, while there was a sharp increase in expression in follicular and marginal zone B-cells. Levels in B1-peritoneal and germinal center B-cells were still comparably high, while plasma cell mRNA levels dropped notably below the level of proB-cells (Fig. 32A). Additionally, datamining revealed that the expression of the E3-ligase might be driven by the transcription factor (TF) PAX5, which is essential in B-cell development and activation (Revilla-I-Domingo et al. 2012). In figure 32 KLHL14 mRNA levels are shown obtained by RNAseq from murine PAX5 knock out B-cells (GSE10489) by Cresson and colleagues 2018 (Cresson et al. 2018), in which an empty vector control or one of the two isoforms of the TF were re-expressed. The B-cells from both mice show a significant increase of KLHL14 mRNA levels upon re-expression, which might either be an effect of un-impaired B-cell differentiation or caused by direct regulation of the KLHL14 gene by PAX5 (Fig. 32B).

Next, KLHL14 mRNA quantity was evaluated in Affymetrix data from a XBP1.S driven transgenic MM mouse model (GSE6980; Probe-ID: 1428837_at) (Carrasco et al. 2007). Herein, a significant reduction of mRNA expression from WT splenic B-cells, to XBP1s-transgenic B-cells and finally the transgenic tumor cells indicated that KLHL14 might also act as a tumor suppressor in this particular mouse model (Fig. 32C).

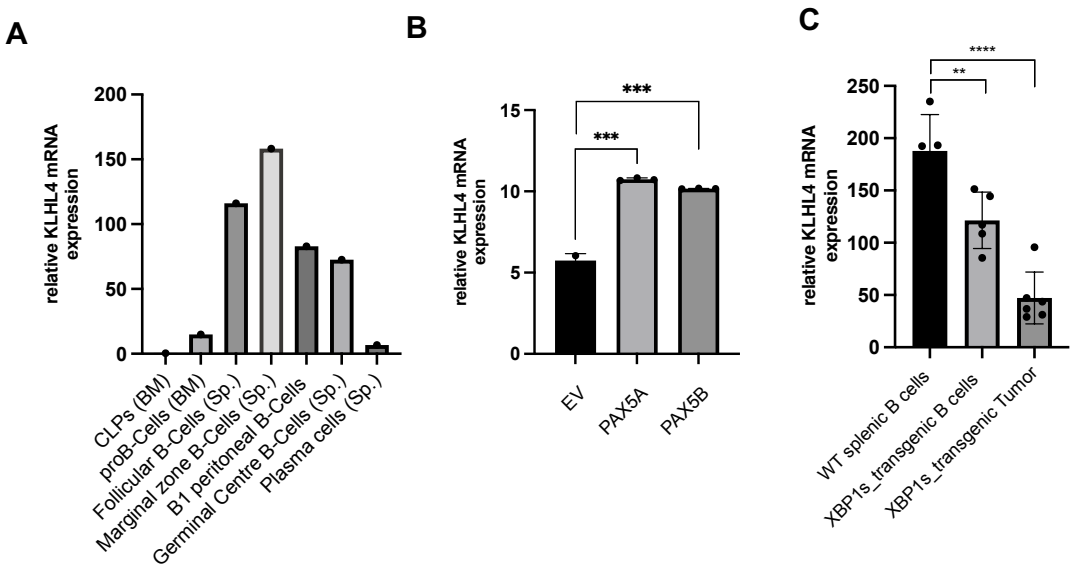

Figure 32. KLHL14 mRNA levels are differentially regulated in different murine B-cells types. A, KLHL14 gene expression analysis in different murine B-cells populations. RNAseq and Affymetrix data available on http://rstats.immgen.org were analyzed for KLHL14 mRNA expression. CPLs, common lymphoid progenitors; BM, bone marrow; Sp., Spleen. **B,** RNAseq data of the GSE104890 dataset were analyzed for KLHL14 mRNA levels obtained from murine PAX5 knock out B-cells, in which either EV, PAX5A or PAX5B were re-expressed**.** EV, empty vector**. C,** Relative KLHL14 mRNA levels (Probe-ID: 1428837_at) were evaluated in the GSE6980 Affymetrix data set from a transgenic MM mouse model, in which tumor formation is driven by XBP1.S overexpression. WT, wild type. **, $P < 0.01$; ***, $P < 0.001$ ****, $P < 0.0001$; by Student's t-test corrected for multiple testing.

From the expression data, it became apparent that KLHL14 was expressed highest, when B-cells are homing to the microenvironments where they are set to be activated – the lymphoid organs like the spleen and the peritoneal cavity, while cells that are not highly proliferative in a physiological context like proB-cells and plasma cells only show low mRNA levels of the E3-ligase (Fig. 32A). Thus, KLHL14 might suppress the expansion of unstimulated B-cells. Upon encounter of an activation signal, for example antigen contact, KLHL14 would need to be downregulated to enable rapid proliferation of the activated B-cells.

To test this hypothesis, MACS-purified CD19/B220-positive splenic murine B-cells (provided by S. Keppler and J. Gadjalova; AG Keppler, TUM) were left untreated or stimulated with lipopolysaccharide (LPS) (10 µg/mL) for 24 hrs and analyzed by immunoblot. As expected, LPS stimulation led to an induction of G2/M markers and the downregulation of G1-specific proteins which reflected the activation and proliferation of the cells (Lu and Munford 2016; Coutinho et al. 1974). KLHL14 protein levels also decreased upon LPS stimulation (Fig. 33A-D).

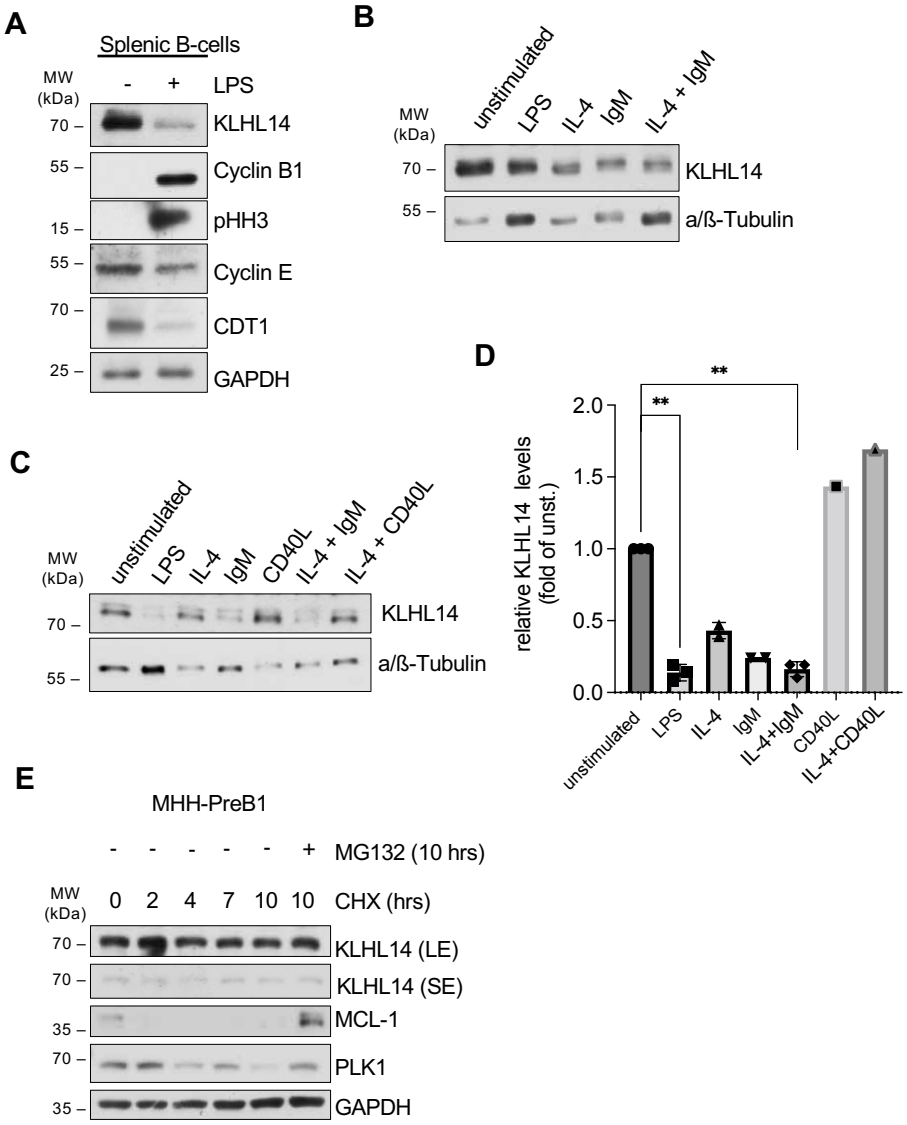

Figure 33. KLHL14 protein is downregulated by BCR and TLR signaling. A-D, Immunoblot analysis of splenic murine B-cells upon stimulation**.** MACS-purified CD19/B220-positive purified primary murine B-cells were left untreated or stimulated with **A**, lipopolysaccharides (LPS, 10µg/mL) **B**, lipopolysaccharides (LPS, 10µg/mL), IL-4 (10 ng/mL), IgM (F(ab)2) (10 µg/mL) or a combination of the latter two or **C,** lipopolysaccharides (LPS, 10 µg/mL), IL-4 (10 ng/mL), IgM (F(ab)2) (10 µg/mL), IL-4+IgM, CD40-Ligand (CD40L, 1 µg/mL) or CD40L+IL-4. WCEs were prepared and analyzed by immunoblot using the indicated antibodies. **D,** Quantification of the KLHL14 protein levels upon stimulation. Optical densities were determined using the ImageStudioLite software, normalized to the respective a/ß-Tubulin or GAPDH input control and plotted as fold of the unstimulated condition. (n=3 independent experiments for LPS and IL-4+IgM stimulations; n=2 independent experiments for IgM and IL-4 only stimulations and n=1 for CD40L and CD40L+IL-4 stimulation). **E**, Half live analysis of KLHL14 protein in MHH-PreB1 cells. Cells were left untreated, treated with CHX (200 µg/mL) or CHX and MG132 (10 µM) for the indicated times and the resulting WCEs analyzed by immunoblot using the indicated antibodies. **, $P < 0.01$; by Student's t-test corrected for multiple testing.

In a next step, purified splenic B-cells were left either unstimulated or incubated with IL-4 (10 ng/mL), IgM (F(ab)2) (10 µg/mL) or both to investigate whether full BCR stimulation was necessary for KLHL14 downregulation (Hodgkin et al. 1991; Wortis et al. 1995). Treatment with LPS was included as a positive control. Analysis of KLHL14 protein levels by immunoblot revealed that even though stimulation with IL-4 and IgM alone caused KLHL14 downregulation, only complete activation of the BCR by co-treatment with IgM and IL-4 led to a reduction in protein levels comparable to the one caused by LPS stimulation (Fig. 33B-D). When incubating the cells with CD40-Ligand (CD40L, 1 µg/mL) or CD40L and IL-4, mimicking activation in a T-cell dependent manner (Elgueta et al. 2009; Kooten, Banchereau, and Gene 2000), KLHL14 levels increased 1.4- and 1.7-fold, respectively (Fig. 33C,D), which remains to be confirmed in replication experiments though. This would suggest, that the observed KLHL14 downregulation of the first 24 hrs of B-cell activation occurs through TLR and BCR signaling but not upon CD40 stimulation. This dynamic behavior prompted the question, whether KLHL14 was also unstable in human DLBCL cells as these cells proliferate independent of specific BCR stimulation. To address this, MHH-PreB1 DLBCL cells were subjected to a cycloheximide time course, in which translation was inhibited for up to 10 hrs. One condition included MG132 to test for proteasomal degradation. Immunoblot analysis showed that the short lived protein MCL1(D. P. Stewart et al. 2010) readily declined with prolonged addition of the ribosome inhibitor, which was rescued by proteasomal inhibition. KLHL14 was stable throughout the time course, indicating that the protein is either stable in DLBCL cells or degradation is stimulus dependent (Fig. 33E).

As for the prominent immunofluorescence staining pattern of KLHL14 so far only cell lines were used, the next step was to reproduce the experiments in primary murine B-cells. But primary splenic B-cells did not tolerate incubation with nocodazole, so an enrichment of G2/M-phase cells was not possible. To overcome this technical issue, MACS purified splenic B-cells from $Rosa26^{LSL\text{-}CARD11\text{-}CA}$ mice, which express a constitutive active mutant of CARD11 in Cre recombinase positive cells (Knies et al. 2015; Rosenbaum et al. 2019), were *ex-vivo* treated with recombinant tatCre recombinase protein to induce transgene expression and proliferation (performed by A. Kratzert, AG Ruland, TUM). The resulting B-cells strongly resemble ABC-type DLBCL cells (Knies et al. 2015). 24 hrs post recombination induction, the cells were treated with nocodazole to induce an arrest in mitosis and were immobilized on poly-L-lysine coated slides. Indirect immunofluorescence studies revealed KLHL14 condensates in a limited number of untreated control cells, which could be increased from 4 to 36% by nocodazole mediated G2/M arrest (Fig. 34A, B). This correlated with the increase of the G2/M population from 8 to 41% by nocodazole incubation, as determined by PI DNA-staining and flow cytometry-based cell cycle analysis (Fig. 34C, D).

The data acquired in naïve murine B-cells provide a mechanistic explanation on how splenic B-cells, which are poised to proliferate massively upon activation, deal with the expression of a tumor suppressor and nominate KLHL14 as a safeguard against unphysiologically B-cell activation and proliferation without a respective stimulus. The immunofluorescence data generated in CARD11-dirven murine B-cell lymphoma model further solidifies the hypothesis, that KLHL14 is functionally relevant in B-cells during G2/M cell cycle phases and that the observed condensation of KLHL14 is not a DLBCL cell line artefact

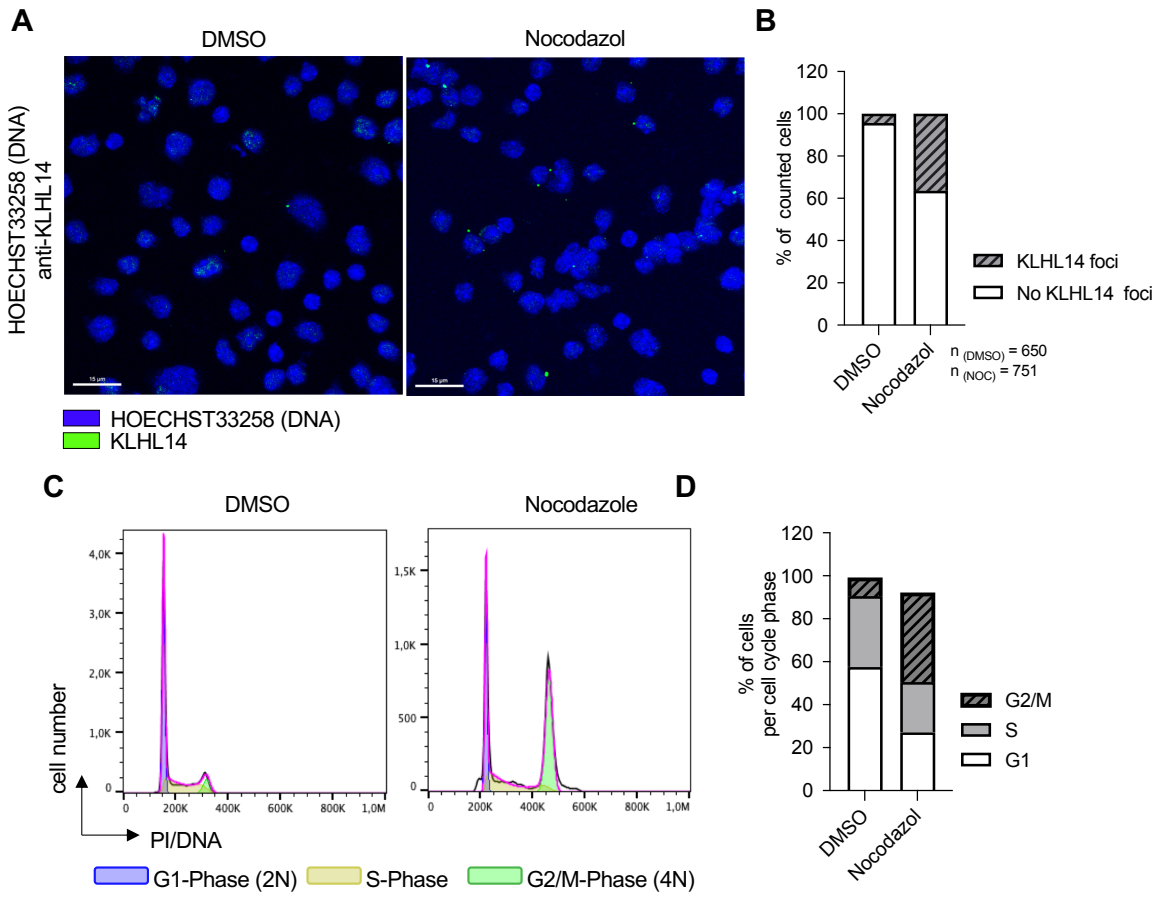

Figure 34: KLHL14 foci are found in mitotically enriched murine B-cell lymphoma cells.
A-D, Analysis of KLHL14 foci in cells of a genetic murine B-cell-lymphoma model. Purified splenic B-cells from Rosa26$^{LSL\text{-}CARD11\text{-}CA}$ mice were treated *ex vivo* with recombinant tatCre to induce expression of a chronically active mutant of CARD11 and drive lymphomagenesis (performed by A. Kratzert, AG Ruland, TUM). 24hrs later cells were treated with nocodazole for 12 hrs and analyzed. **A,** Representative IF images of untreated or nocodazole treated murine B-cell-lymphoma cells attached on poly-L-lysine coated chamber slide, fixed with 4% PFA and stained with anti-KLHL14 antibody (green), the corresponding secondary antibody and Hoechst33258 (DNA, blue). Pictures were taken by confocal microscopy. Scale bars represent 15 µm. **B,** Quantification of cells with at least one KLHL14 accumulation per cell, detected in five representative images from different areas of the slide of the experiment described in (A). Numbers are plotted as percentage of all cells counted. **C-D,** Cell cycle analysis of untreated and nocodazole treated murine B-cell-lymphoma cells. Cells were harvested, DNA stained with PI and analyzed by flow cytometry. **C,** Results of the cell cycle analysis are depicted as histograms of FL2-A (PI) signal intensity. The distribution of cells in the different cell cycle phases was determined by the Dean-Jett-Fox method implemented in the FlowJo V10 software without constraints. **D,** Quantification of the cell cycle distribution depicted in (C) depicted as percentage of cells per cell cycle phase.

5.5 MS based interactome analysis reveals possible KLHL14 substrates

Ubiquitin ligases (and DUBs) exert their biological function by post-translationally modifying their substrate proteins. Thus, one of the most important tasks that remained was to match KLHL14 with its ubiquitylation substrate(s).

First steps in this process involved an unbiased MS-based interactome screen. As the tumor suppressor function of the E3 ligase seemed to be limited to B-Cell derived malignancies, KLHL14 was purified from the human MM cell line MM1.S. To ensure a homogenous population of transgene expressing cells, the doxycycline inducible system, described previously, was used to induce FLAG-KLHL14 or RFP expression in 5x10^8 MM1.S

cells for 24 hrs. Samples were harvested in biological triplicates and FLAG-IPs performed using M2-FLAG-Affinity gel. Bound proteins were eluted with acidified 0.2M glycine, of which 5% were used for quality control, while the rest was precipitated with 20% TCA, dried and send for mass spectrometry analysis to the BayBioMS@MRI core facility. Silver gel and WB analysis of the quality control samples revealed a good and even enrichment of the FLAG-tagged bait among all three replicates (Fig. 35A, B). The denatured proteins send for MS/MS analysis were resuspended, reduced, alkylated and in gel trypsin digested. Peptides were then dissolved in 0.1% formic acid (FA) plus 2% acetonitrile (ACN) and analyzed by MS/MS as described previously. Peptide and protein identification were carried out using the MaxQuant software version 1.6.3.3.

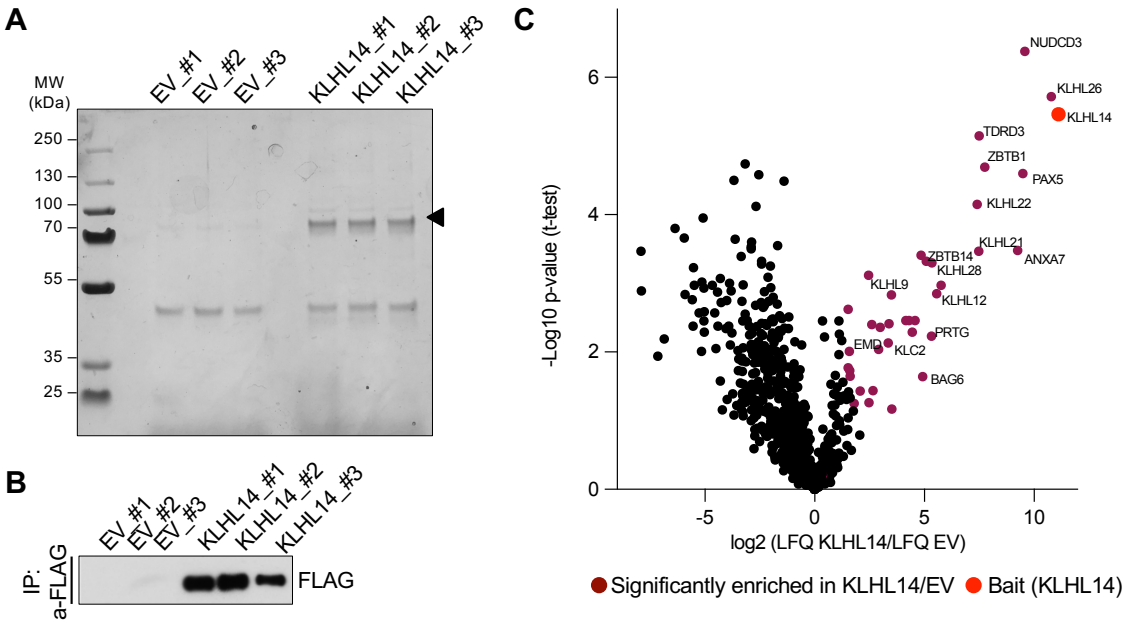

Figure 35: KLHL14 interactome analysis obtained by mass spectrometry. A, Silver stained gel of FLAG-purified KLHL14. Expression of N-terminal tagged KLHL14 or empty vector (EV) control was induced in $5x10^8$ MM1.S cells stably transduced with pTRIPZ-FLAG-KLHL14 or -RFP (EV) by doxycycline addition for 24 hrs. For the last 4 hrs MG132 (10 µM) was added to enrich for ubiquitylated proteins. Samples were harvested in biological triplicates, IPs performed using FLAG-M2-Affinity gel and subsequently eluted from beads with acidified glycine. 2.5% of each replicate were separated by SDS-PAGE and proteins visualized by silver staining. The arrowhead points to the band at the expected size of KLHL14. **B**, Immunoblot analysis of FLAG-purified KLHL14. 2.5% of the elution from each replicate were used for immunoblot analysis using the indicated antibodies. **C,** Mass spectrometric analysis of samples described in (A). Co-purified proteins were identified by mass spectrometry and log2 ratios of averaged KLHL14/EV LFQ values were plotted against the negative Log10 of the calculated p-value. Significantly enriched KLHL14 interactors (FDR < 0.05; S0 = 1 by Students T-test) are depicted in magenta. [MS data for **C** provided BayBioMS@MRI core facility, Dr. P. Giansanti and Prof. B. Küster].

After removal of known non-human contaminants, a list of 710 protein groups identified in at least two out of three replicate samples was obtained. If a protein was not identified in one respective sample, missing values were imputed from a normal distribution. Of all proteins identified, 64 were more than two-fold enriched in the KLHL14 sample, 37 of them significantly (FDR < 0.05; S0 = 1) (Fig. 35C). The significantly enriched interactors included a large proportion (8 out of 37) of proteins containing a BTB-domain like KLHL26, KLHL21 and ZBTB14. Though this interaction could be attributed to the BTB-fold of KLHL14, which acts as a general protein interaction domain unrelated to CRL3 complex formation for example in ion channel assembly or transcriptional repression (Stogios et al. 2005), the detected BTB-domain proteins like KLHL9, KLHL21 and KLHL22 have all been implicated in mitotic regulation

(Genschik, Sumara, and Lechner 2013) and might thus provide a direct link to the role of KLHL14 in mitosis. The other functional cluster of proteins detected by MS/MS included proteins involved in the UPS including proteasomal subunit like PSMB/As, UBL4A and ADRM1, which are frequently co-purified with components of the UPS (Fig. 35C).

To further narrow down the list of potential ubiquitylation substrate candidates, a more functional MS/MS based screen was set up, in which all ubiquitylated proteins of a given population were purified from cells with and without KLHL14 overexpression. For this purpose, MM1.S cells were lentivirally transduced with a 6xHis-tagged Ubiquitin expression construct, that contained a blasticidin resistance gene by which MM1.S cells were selected for transgene expression. Then, these cells were lentivirally infected with either pTRIPZ-RFP or -KLHL14 and selected for vector expression by puromycin. After testing the two resulting cell lines for equal His-Ubiquitin expression, cells were expanded to 10^9 cells per condition. Next, RFP or KLHL14 transgene expression was induced by doxycycline addition. For the last 4 hrs before sample collection MG132 was supplemented to enrich for ubiquitylated proteins that might otherwise be degraded by the proteasome. MM1.S-WT cells were treated in the same manner as described for the His-Ubiquitin expressing cells to act as a negative control.

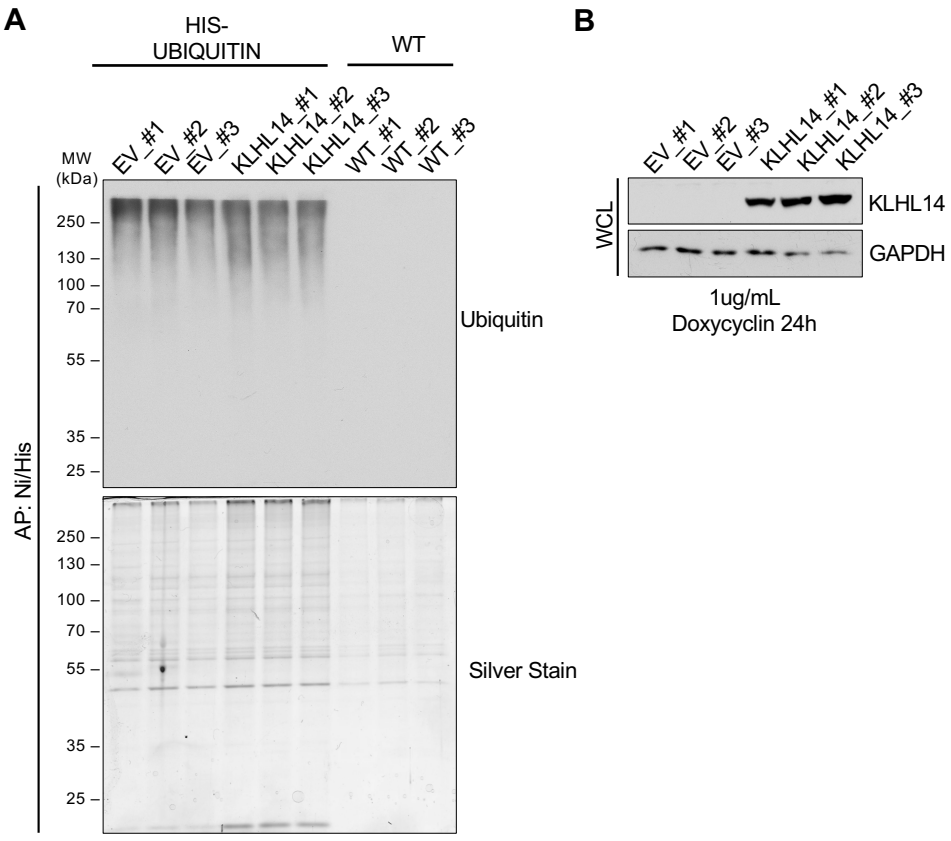

Figure 36: Purification of ubiquitylated proteins from 6xHis-Ubiquitin expressing cells with or without KLHL14 overexpression. A, Immunoblot and silver stain analysis of HIS-ubiquitin purifications from EV or KLHL14 overexpressing cells. Expression of KLHL14 or empty vector (EV) control was induced in 10^9 MM1.S cells stably transduced with 6xHis-tagged Ubiquitin and pTRIPZ-KLHL14 or –RFP (EV) by doxycycline addition for 20 hrs. For the last 4 hrs MG132 (10 μM) was added. MM1.S WT cells were treated identically to serve as a negative control. Samples were harvested in biological triplicates, APs performed using Ni-NTA-agarose and bound proteins subsequently eluted from beads. 5% of each replicate were separated by SDS-PAGE and proteins analyzed by immunoblot using the indicated antibodies (upper panel) and silver staining (lower panel). **B**, Immunoblot analysis of unbound fraction of the HIS-Ubiquitin samples after affinity purification described in (A). 2.5% of the HIS-ubiquitin expressing WCEs were collected after AP with Ni-NTA-agarose, subjected to SDS-PAGE and analyzed using the indicated antibodies. GAPDH served as loading control.

The purification of ubiquitylated proteins from three independent biological replicates was carried out by Histidine pull down with Nickle-(Ni)-NTA-agarose under denaturing conditions. After extensive washes, bead bound proteins were eluted(B. Wang et al. 2017a; Dietachmayr et al. 2020), precipitated with 20% TCA and 2.5% used for immunoblot and silver stain analysis (Fig. 36A).

The latter revealed an equal amount of precipitated protein in His-Ubiquitin expressing replicates and a clear decrease of purified proteins in the WT cells. On the corresponding immunoblot, ubiquitin was only detected in the HIS-Ubiquitin samples. This verified that the proteins detected in the eluates from WT cells by silver staining represented proteins that bound un-specifically to the agarose beads (Fig. 36A). Immunoblot analysis of the unbound fraction of the HIS-Ubiquitin samples after affinity purification confirmed the sample identity and sufficient KLHL14 expression (Fig. 36B).

The remaining 97.5% of purified proteins were then sent to the BayBioMS@MRI core facility, where samples were TMT-labeled and analyzed by MS/MS. Following measurement, data processing and analysis by P. Giansanti (BayBioMS@MRI), a list containing 1672 proteins groups identified in at least one or three replicates in KLHL14 or EV samples was obtained. As expected, the proteins purified from WT cells contributed the strongest to the differences in the data set as depicted by principal component analysis (PCA) - component one explains 82.6% of the variances and clearly distinguishes between WT and HIS-Ubiquitin samples (EV and KLHL14). Compared to that, only a minor difference could be detected between EV and KLHL14 samples with component three of the PCA being the main contributor (3.8%) (Fig. 37A, provided by P. Giansanti). Further analysis and statistical testing were thus performed between EV and KLHL14 samples only, with an imputation of 1000 for missing values. Of the 1672 proteins measured by mass spectrometry, 13 were significantly altered between the conditions (FDR <0.05, S=0.3, FC~2). 11 of them were purified significantly less, while only the overexpressed ligase KLHL14 and FAM46C were significantly enriched in the KLHL14 vs control samples (Fig. 37B). Interestingly, FAM46C was recently reported as a tumor suppressor in MM and colorectal cancer with roles in regulating mRNA stability (Mroczek et al. 2017), the unfolded protein response and autophagy (Manfrini et al. 2020) and in inhibiting PLK4 activity (Kazazian et al. 2020), but was not identified in the interactome screen performed in MM1.S cells (Fig. 35B).

In order not to exclude relevant but not significantly regulated ubiquitylated proteins, the cut off for a meaningful enrichment in the HIS-affinity purification was set to 1.5-fold between the KLHL14 and control samples. This resulted in a list of 69 proteins with potentially higher ubiquitin attachment. When correlating these with the KLHL14 interactome obtained from MM1.S, only ADRM1, RAD23B and GID8 were found in both screening results. When additionally, cross validating the remaining candidates with proteins known to be detected in affinity-based MS/MS screens using the CRAPOME database (https://reprint-apms.org), peptides of all of them were detected frequently in this kind of experimental set ups - ADRM1 in 196, RAD23B in 79 and GID8 in 48 of 716 cases.

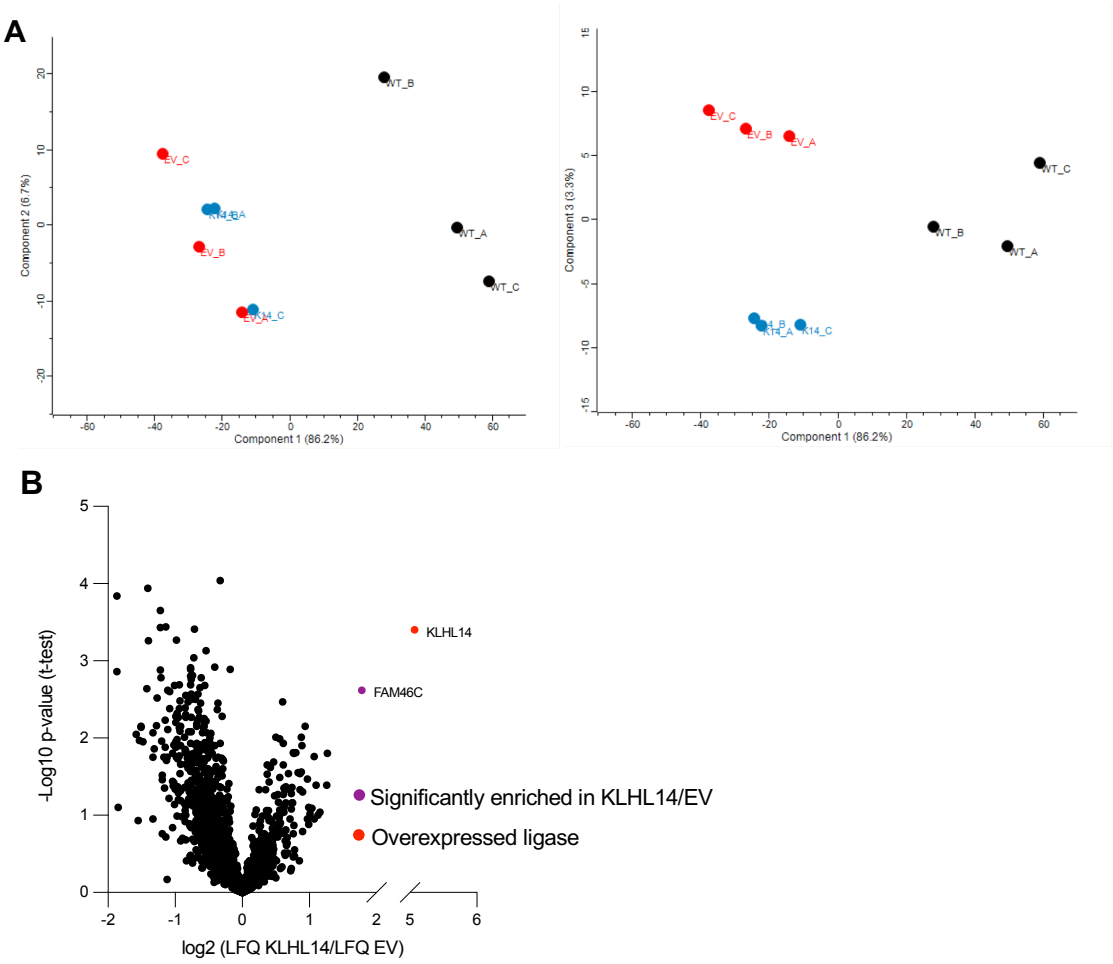

Figure 37: Mass spectrometric analysis of ubiquitylated proteins from KLHL14 expressing cells. Purified proteins from WT, His-Ubiquitin-EV and -KLHL14 expressing cells described in figure 28 were TMT-labeled and analyzed by mass spectrometry. **A**, Observation plots of a principal component analysis (PCA) of the Ni-NTA purifications from WT and HIS-ubiquitin MM1.S cells. Left side: Two-dimensional (2D) subspace for the His-ubiquitin data including the two major variance contributors PC1 and PC2. Component 1 is defined by the differences between WT and His-UBI-expressing samples and explains 82.6% of the overall variances. Right side: 2D subspace of the His-ubiquitin data depicting the variances between EV and KLHL14 expressing cells. PC3 explains the variance between KLHL14 and EV expressing His-UBI cells and contributes to the overall variance in the data set with 3.8%. WT – black; His-Ubi-EV - red and His-Ubi-KLHL14 - blue. [PCA and visualization by P. Giansanti, BayBioMS@MRI core facility]. **B**, Volcano plot of proteins identified by MS analysis in the His-Ubiquitin purifications. Log2 ratios of averaged KLHL14/EV LFQ values plotted against the negative Log10 of the calculated p-value. Proteins significantly enriched in the KLHL14 expression samples (FDR < 0.05; S0 = 0.3, FC=2 by Students T-test) are depicted in magenta. KLHL14 is marked in red. [Sample preparation, measurement and analysis provided BayBioMS@MRI core facility, P. Giansanti and Prof. B. Küster].

The low number of proteins that were identified as significantly changed in both the HIS-Ubiquitin- and the FLAG-purifications together with the possible implications of KLHL14 in mitosis, prompted the question whether possible substrates of the E3-ligase could not be detected because cells were not synchronized in a specific cell cycle phase. This might hold true especially for the analysis of ubiquitylated proteins, as only approximately 10-20% of MM1.S cells are in mitosis in an asynchronous population, making it very unlikely to detect differentially ubiquitylated proteins, if the ubiquitylation event is restricted to this cell cycle phase. Therefore, the interactome analysis was repeated as described above but from 10^9 mitotically synchronized MM1.S cells in biological triplicates. Silver staining and immunoblot analysis was used to confirm sufficient enrichment of FLAG-KLHL14 as compared to control

samples (Fig. 38A), before sending the precipitated proteins for processing, mass spectrometry and data evaluation to the BayBioMS@MRI core facility. Bioinformatic work up, performed as described above, by J. Mergner resulted in a list of 1796 identified protein groups. A total of 150 proteins were co-purified over 2-fold more with FLAG-KLHL14 compared to the control samples, 15 proteins of those significantly (FDR<0.05, S0=0.1) (Fig. 38A, B). Of the significantly enriched hits, NUDCD3, KLHL12, -21, -22, -26 and ZBTB14 were also identified as significant interactors in asynchronous cells (Fig. 38B).

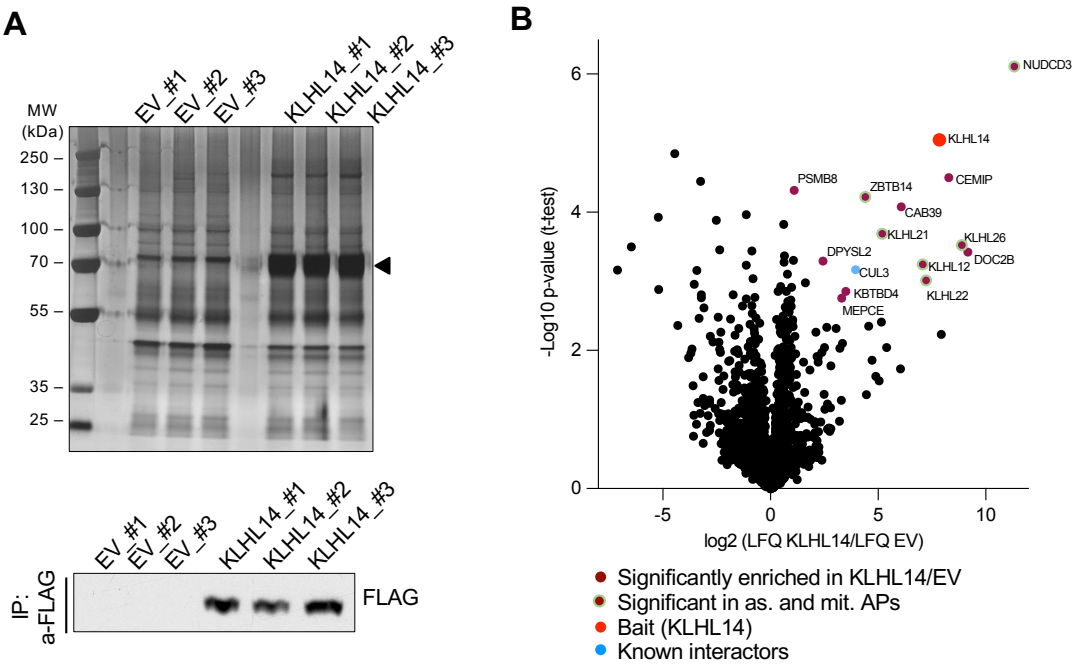

Figure 38: Interactome of KLHL14 from G2/M arrested MM1.S cells obtained by Mass spectrometry. A, Silver stained gel and immunoblot analysis of FLAG-purified KLHL14. 10^9 MM1.S cells stably transduced with pTRIPZ-FLAG-KLHL14 or – RFP were arrested in mitosis by a sequential thymidine and nocodazole treatment and expression of FLAG-KLHL14 or –RFP was induced in by doxycycline addition for the 24 hrs during the synchronization proceedings. For the last 4 hrs MG132 (10 µM) was added to enrich for ubiquitylated proteins. Samples were harvested in biological triplicates, IPs performed using FLAG-M2-Affinity gel and subsequently eluted from beads with acidified glycine. 2.5% of each replicate were separated by SDS-PAGE and proteins visualized by silver staining. The arrowhead points to the band at the expected size of KLHL14. Immunoblot analysis of FLAG-purified KLHL14. 2.5% of the elution from each replicate were used for immunoblot analysis using the indicated antibodies. **B,** Mass spectrometric analysis of samples described in (A). Co-purified proteins were identified by mass spectrometry and log2 ratios of averaged KLHL14/EV LFQ values were plotted against the negative Log10 of the calculated p-value. Significantly enriched KLHL14 interactors (FDR < 0.05; S0 =0.1 by Students T-test) are depicted in magenta. [MS data for **B** provided BayBioMS@MRI core facility, Dr. J. Mergner and Prof. B. Küster].

When comparing the two-fold enriched proteins from asynchronous and mitotically synchronized MM1.S, it becomes apparent, that more possible interaction partners were co-purified in mitotically arrested cells (150 versus 68). This might be due to a higher overall amount of identified protein groups in these samples or the changes in the full proteome caused by the synchronization (Fig. 39A). The overlap between the two groups is comprised of the 21 proteins depicted in Fig. 39B and is dominated by BTB/POZ interaction domain containing ones (10 of 21). Analysis of publicly available databases (https://string-db.org) shows a central interaction network of the KLHL-proteins detected by MS/MS, which might explain the repeated pull down of the whole cluster (Fig. 39B).

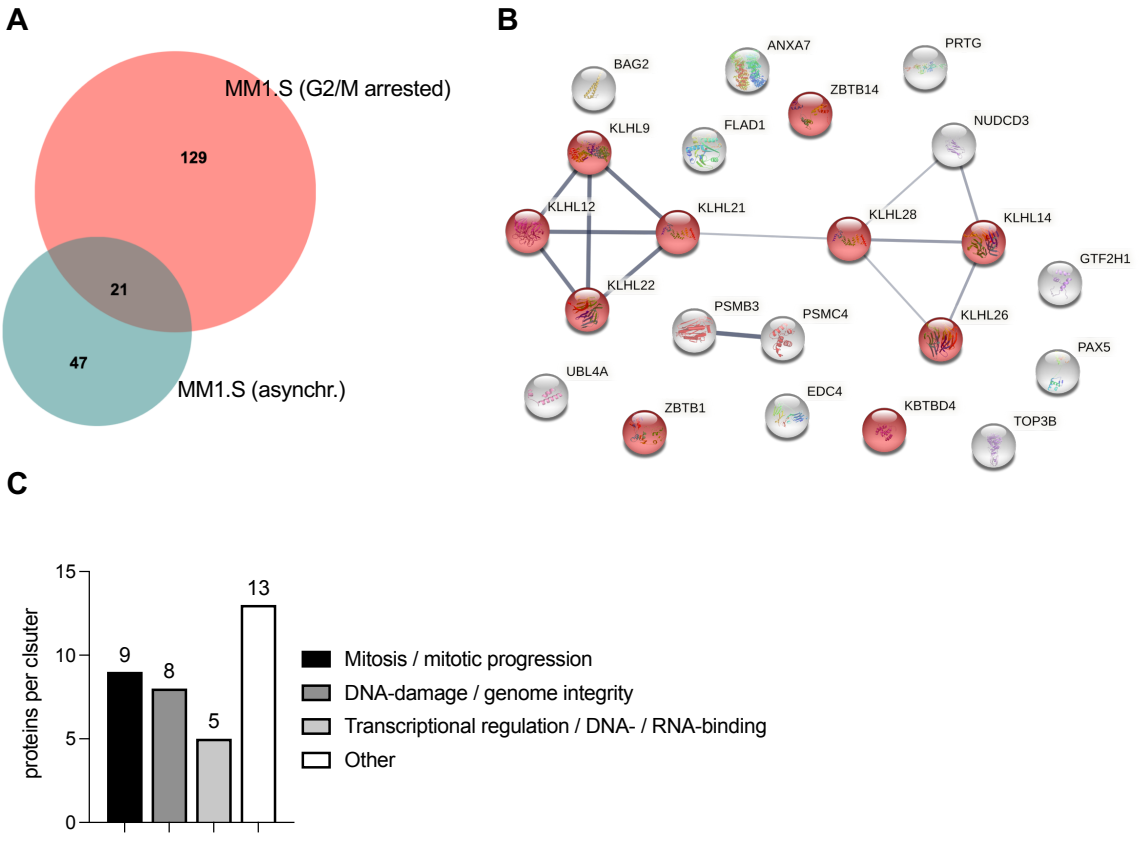

Figure 39: The KLHL14-Interactome is enriched in mitosis related proteins. A, Venn-diagram of proteins co-purified with KLHL14 from asynchronous and G2/M arrested MM1.S cells. Proteins identified by MS to be more than 2-fold enriched in KLHL14 vs EV IP samples from G2/M arrested (Figure 37) and asynchronous MM1.S cells (Figure 34) were analyzed for overlaps using https://www.biovenn.nl. Circle sizes represent the amount of proteins identified in each condition. Red: Interactors from G2/M arrested cells; Blue: Interactors from asynchronous cells. **B**, Physical network of proteins identified as interactors in both G2/M and asynchronous cells. The 21 proteins found to interact with KLHL14 in both G2/M and asynchronous cells in (A) were used as input material for a network analysis on https://string-db.org. Each circle represents a protein and grey lines in-between indicate physical interaction. Line thickness represents a database generated confidence score. Proteins containing a BTB-domain are depicted in red. **C,** Functional clustering of the 35 top hits in the interactome analysis of the G2/M arrested MM1.S cells. Literature research was performed for the 35 most promising substrate candidates identified by MS-based interactome screening. Proteins where then clustered according to their described functions/implications and the most prominent clusters depicted with number of assigned proteins.

Literature search of the top 35 hits that remained as promising substrate candidates after comparison with CRAPOME database, revealed that 48,57% were implicated directly or indirectly in mitotic processes (9/35) or DNA-damage response (8/35). This further solidifies the hypothesis that KLHL14 was involved in one of these processes (Fig. 39C). As the HIS-UBI-purification was not analyzed by mass spectrometry by the time of submission of this thesis, the cross validation of the interactome of KLHL14 from mitotic cells is still pending.

Due to the strong enrichment of mitotic regulators in the interactome of KLHL14 and its prominent subcellular localization hinting towards this cell cycle phase, validation experiments were started for some of the detected interactors. Thus, semi-endogenous FLAG-IPs were conducted from lysates of asynchronous or G2/M arrested MM1.S cells with doxycycline induced overexpression of FLAG-KLHL14 or empty vector control, which were then analyzed by immunoblot for endogenous NUDCD3 and KLHL9/13 using the indicated antibodies. The latter is described to detect both KLHL9 and KLHL13 due to their high sequence similarity and can therefore not be used to discriminate between the two proteins.

Both KLHL9/13 and NUDCD3 were co-purified with KLHL14 in in asynchronous as well as in G2/M arrested cells (Fig 40A). The KLHL9/13 antibody produced a distinct double band in the IP-samples (indicated by the red arrow), which might either result from of a differential binding of the two different KLHL-proteins detected by the antibody or post translational modifications on one or both of the proteins, which are known to be phosphorylated and ubiquitylated (according to phosphosite.org). The interaction between KLHL14 and the lower of the two bands was reduced in G2/M arrested samples (Fig. 40A, B). Dephosphorylation of the lysates by calf intestine phosphatase (CIP) treatment prior to FLAG-IP, neither enhanced KLHL14 binding to the lower band in mitosis nor altered the double band pattern. To confirm the successful dephosphorylation of the lysates immunoblots of the WCEs were probed for pGSK3b and pHH3, which showed a decrease of signal when treated with CIP consistent with the loss of the PTM. This indicated that the interaction itself, as well as the differences in molecular weight of the bound proteins are independent of the phosphorylation status of the proteins involved (Fig. 40B).

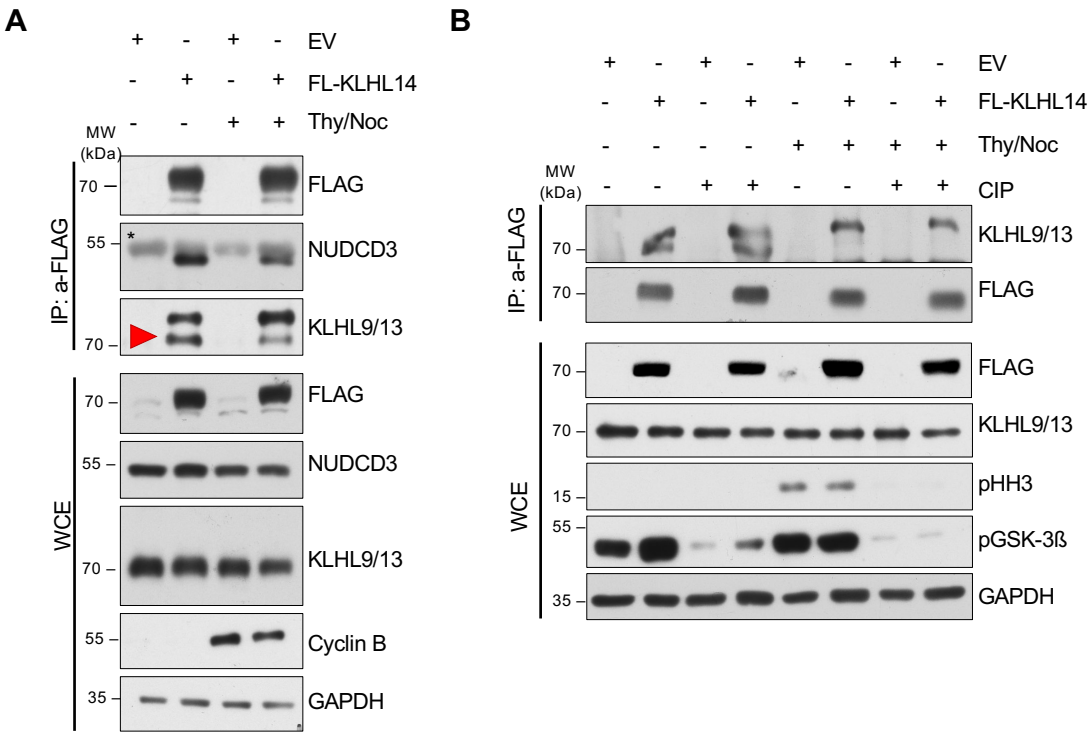

Figure 40: KLHL14 binds to KLHL9/13 and NUDCD3. A, B Immunoprecipitation (IP) of FLAG-KLHL14 from asynchronous and G2/M arrested MM1.S cells. MM1.S cells stably transduced with pTRIPZ-FLAG-KLHL14 or –RFP (empty vector, EV) were either left untreated or were arrested in mitosis by a sequential thymidine and nocodazole treatment. Expression of FLAG-KLHL14 or –RFP was induced by doxycycline addition for 24 hrs. The resulting WCEs were either left untreated **(A)** or incubated for 30min at RT with vehicle or calf intestine phosphatase (CIP) **(B)** prior to FLAG-IP. WCEs and IPs were subsequently analyzed by immunoblotting using the indicated antibodies. GAPDH served as loading control.

Next, the stability of the substrate candidates was tested in cycloheximide chase experiments. MM1.S cells with and without KLHL14 overexpression were treated with cycloheximide for the indicated time points for up to 10 hrs, including one condition in which MG132 was added to test for proteasomal degradation and WCE subjected to immunoblot analysis. The successful inhibition of both the ribosome and the proteasome was confirmed by analysis of MCL1 levels, a protein known to have short half-life due to proteasomal degradation (D. P. Stewart et al. 2010). Even though the NUDCD3 levels seemed to be a bit lower in KLHL14 overexpression samples, neither this protein, nor KLHL9/13 were destabilized upon inhibition of protein

synthesis, regardless of the overexpression of the E3-ligase (Fig. 41A).

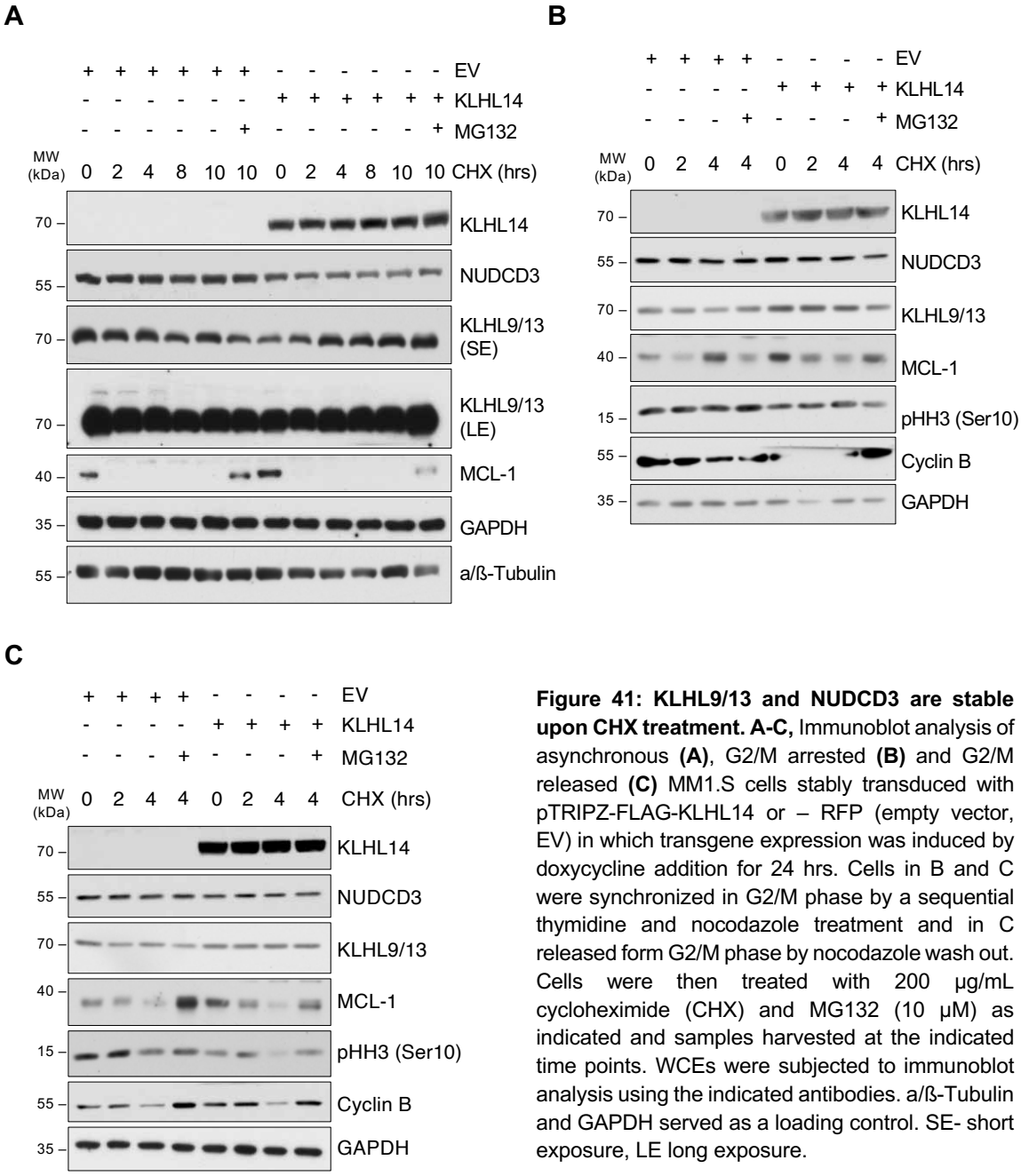

Figure 41: KLHL9/13 and NUDCD3 are stable upon CHX treatment. A-C, Immunoblot analysis of asynchronous **(A)**, G2/M arrested **(B)** and G2/M released **(C)** MM1.S cells stably transduced with pTRIPZ-FLAG-KLHL14 or – RFP (empty vector, EV) in which transgene expression was induced by doxycycline addition for 24 hrs. Cells in B and C were synchronized in G2/M phase by a sequential thymidine and nocodazole treatment and in C released form G2/M phase by nocodazole wash out. Cells were then treated with 200 µg/mL cycloheximide (CHX) and MG132 (10 µM) as indicated and samples harvested at the indicated time points. WCEs were subjected to immunoblot analysis using the indicated antibodies. a/ß-Tubulin and GAPDH served as a loading control. SE- short exposure, LE long exposure.

As described above, the antibody used to detect the KLHL-proteins does not distinguish between the two, which might mask the effect on either of the two. In order to investigate whether the proteins were destabilized in or throughout mitosis, MM1.S cells were arrested in G2/M by sequential thymidine and nocodazole cell cycle blocks and transgene expression induced for 24 hrs by doxycycline addition. These cells were then either subjected to cycloheximide treatment while keeping up the nocodazole block (Fig. 41B) or released from G2/M by wash out during which the ribosome inhibitor was added (Fig. 41C). In both conditions, KLHL9/13 and NUDCD3 protein levels were stable throughout the course of the time as seen by immunoblot, while the control proteins MCL1 and CyclinB1 were readily degraded.

Taken together, interactome analysis of KLHL14 by mass-spectrometry identified a high number of interactors that are described in the context of cell cycle or mitotic regulation. The interaction of KLHL14 with a subset of promising substrate candidates could be validated in a semi-endogenous immunoprecipitation setting and immunoblot analysis but no proteasomal degradation of the proteins was observed at this point.

6. Discussion KLHL14

Multiple myeloma (MM) is the second most common hematological malignancy and remains incurable (Mikhael et al. 2019). While the pathophysiology of MM is only partially understood, the substantial responsiveness of MM patients to proteasomal inhibitors (PIs) like bortezomib or carfilzomib hints towards a central role of the ubiquitin proteasome system (UPS) (Guerrero-Garcia et al. 2018; Kumar et al. 2017). We therefore screened patient cohorts for deregulated components of the UPS and identified the BTB-domain proteins KLHL14 as an interesting candidate (Fig 9-11). Over the recent years, multiple publications reported functions of the BTB- and KELCH-domain containing protein either in neuron (Giles, Li, and Chin 2009; Valastyan and Lindquist 2011; Juliet Zhang et al. 2017b; Sahni, Itoh, et al. 2021) or B-cell(S. Li et al. 2018; Choi et al. 2020; Vater et al. 2015; Hodkinson et al. 2021) development and disfunction. While the publications discussing the proteins implications in neurons did not report any involvement of the ubiquitin system (Giles, Li, and Chin 2009; Valastyan and Lindquist 2011; Juliet Zhang et al. 2017b; Sahni, Itoh, et al. 2021), the most recent paper link KLHL14 to the UPS in B-cells. Therein, Choi and colleagues report KLHL14 as a tumor suppressor in the ABC-subtype of DLBCL due to its negative regulation of BCR abundance and signaling (Choi et al. 2020).

6.1 The tumor suppressive function of KLHL14 in MM does not rely on BCR signaling

The hypothesis that KLHL14 might be a relevant tumor suppressor in MM, was based on the significant downregulation of KLHL14 mRNA in patient samples from two independent cohorts (Fig. 9) and could be experimentally confirmed in a panel of different MM cell lines (Fig. 10). Furthermore, recently published data that the protein has tumor suppressive functions in DLBCL could be confirmed (Fig. 11). In DLBCL and PCNSL KLHL14 is encoded in a genomic locus that undergoes aberrant somatic hypermutation (Vater et al. 2015; Reddy et al. 2017), but the clinical and mechanistic significance of these mutations remained elusive. Choi and colleagues reported that truncation instead of missense mutations in KLHL14 leading to a destabilization of the protein were significantly more frequent in the gene, than in proteins with a similar mutational load in a specific subtype of ABC-type DLBCL (Choi et al. 2020) but not in a more general context. Furthermore, they stated that KLHL14 accelerated the turnover of immature BCR subunits, thereby reducing the surface expression of the receptor complex and restricting NF-κB signaling (Choi et al. 2020), which these type of cancer cells rely on for survival(Phelan et al. 2018). Even though this explanation sounds plausible for this specific subtype of DLBCL cells, the mechanism by which KLHL14 exerts its function in MM is most likely a different one.

First, MM cells indeed have a gene expression signature typical for active NF-κB signaling, which is crucial for cell survival (Demchenko and Kuehl 2010), but signaling through the BCR expressed on the cells surface is an undescribed and unlikely cause. MM derives from the malignant transformation of plasma cells or plasma cell precursors (Kumar et al. 2017)

and while the paradigm that fully differentiated plasma cells do not express a functional BCR on their surface, as they switch towards secretion of the Ig molecules as antibodies, was challenged during recent years (Blanc et al. 2016; Pinto et al. 2013; Wiedemann et al. 2021), the BCR surface expression is strongly reduced and the cells do not rely on BCR signaling for survival (T. Yoshida et al. 2010). A re-expression of cell surface BCR during the malignant transformation from plasma to MM cells is not described in the literature (Y. Tai and Anderson 2012) or monitored clinically (personal communication) and it is therefore assumed that BCR signaling does not contribute to MM maintenance and survival (Y. Tai and Anderson 2012). Additionally, the mutational pattern in MM patients does not hint towards functional defects of the BCR genes as major drivers of MM (Demchenko and Kuehl 2010). In contrast, ligands produced in the bone marrow microenvironment like IL-6, BAFF and APRIL are responsible for NF-κB activation, survival and proliferation of MGUS as well as MM cells (Utley et al. 2020; Y. T. Tai et al. 2016).

Second, MM cells are sensitive to proteotoxic stress, as they secrete large amounts of antibodies or antibody fragments (Nikesitch et al. 2018), and the response of MM patients to proteasome inhibitors like bortezomib can be attributed in part to the inhibition of the unfolded proteins response (UPR) (Wirth et al. 2020; Obeng et al. 2006), that clears the antibody fragments from the ER in an UPS dependent process called ER-associated protein degradation (ERAD) (Ron and Walter 2007). The enhanced degradation of immature BCR subunits, in MM probably antibody fragments as well, or any glycosylated protein within the ER as postulated for DLBCL (Choi et al. 2020), might therefore be rather beneficial for MM cells, as it would reduce the cells ER protein load. Additionally, the interaction of KLHL14 with the ER related proteins p97 and TorsinA reported in HeLa and SH-SY5Y neuroblastoma cells (Giles, Li, and Chin 2009), could not be detected in MM cells by MS-based interaction screening (Fig. 35, 37). In contrast to the proclaimed ER localization of overexpressed KLHL14 in TMD8 cells(Choi et al. 2020), we could visualize the recruitment of endogenous KLHL14 to the mitotic spindle during cell division in DLBCL lines (Fig. 23-25, 28), the formation of KLHL14 foci in primary murine B-cell tumors (Fig. 34) and a distinctive dot like pattern of overexpressed protein MM1.S cells (Fig. 22). B- and B-cell-derived lymphoma cells are rather small and consist of a large nucleus with a halo of cytoplasm around it when viewed under a microscope. The co-localization with the ER marker LRMP as well as BCR components reported by Choi and colleagues might therefore be an artefact of the strong overexpression of the E3-ligase in the presented immunofluorescence pictures (Choi et al. 2020). Taken together, this implies that KLHL14 does not play a role in ER-associated protein turnover in MM cells.

Third, the cell lines used to demonstrate that KLHL14 exerts tumor suppressive functions in DLBCL in this study were of the GCB-type (Fig. 11), which do not rely on chronic active BCR and NF-κB signaling for survival(Young et al. 2015; Young and Staudt 2013). In line with the data generated in MM cell lines, this suggests that the tumor suppressive function of KLHL14 in B-cell derived malignancies cannot be explained exclusively by its negative regulation of BCR stability or might even be completely BCR independent.

6.2 Prolonged KLHL14 overexpression causes G1/G0 arrest

Ectopic KLHL14 overexpression caused a significant amount of MM1.S cells to arrest in G1 phase after approximately six days of transgene induction. A similar, even though not consistently significant, trend could be detected in the MHH-PreB1 DLBCL cell line (Fig. 15). Immunoblot based cell cycle analysis corroborated these findings (Fig. 16) and further indicated, that the cell cycle arrest did either not occur at the G1/S boundary but earlier in G1 or lead cells to enter G0 or quiescence, as indicated by low Cyclin E levels(Hwang and

Clurman 2005). In line with these findings, preliminary results showed that MM1.S expressing KLHL14 progressed readily from a thymidine mediated cell cycle arrest at the G1/S transition, until the onset of the permanent G1-arrest discussed earlier was observed after prolonged transgene expression (Fig. 18). In contrast, cells stalled at the restriction point by palbociclib (Bonelli et al. 2019) were impaired in their ability to progress towards S-phase after just 48 hrs of KLHL14 overexpression and were almost completely incapable of overcoming the G1 arrest by day three of transgene expression (Fig. 18), suggesting that KLHL14 triggered the restriction point. This can involve a variety of stimuli including missing mitogenic signals and DNA damage (Kastan and Bartek 2004). A clue came from unperturbed cycling MM1.S cells, where expression of well-established DNA-damage markers (Ciccia and Elledge 2010) increased gradually with prolonged KLHL14 overexpression, linking the accumulation of DNA damage to increasing sensitization of MM1.S cells to CDK4/6 inhibition by palbociclib (Fig. 19). Interestingly, this induction went along with an increase in CDK inhibitor (CKI) p27 protein levels. This seems counter intuitive at first, as the dominant cellular response to DNA damage during G1 involves the enhanced transcription of the CKI p21 to delay S-phase entry (Kastan and Bartek 2004), while p27 has been implicated mostly in G1/G0 induction in response to anti-proliferative signals or terminal differentiation (Denicourt and Dowdy 2004). More recently though, p27 was reported to be stabilized upon prolonged exposure of cells to DNA-damage, especially DSBs, and to be required to maintain the G1 arrest in those cells (Cuadrado et al. 2009; Liontos et al. 2010; Cassimere, Mauvais, and Denicourt 2016). Furthermore, mice genetically depleted of the CKI harbor an increased susceptibility to chemical carcinogen or gamma-radiation induced tumor formation (Fero et al. 1998).

Together, this indicates that DNA damage can indeed be the cause for the observed sensitization towards palbociclib, G1/G0 arrest and induction of p27 observed in KLHL14 overexpressing cells. Whether ectopic expression of the BTB-protein directly causes the damage or impairs cellular repair mechanisms remains to be investigated.

DNA damage can occur in every cell cycle phase and its timing and severity strongly influences the cellular outcome(Chao et al. 2017). It was therefore of great importance to investigate the source of DNA damage in KLHL14 overexpressing cells. The regulation of endogenous KLHL14 in DLBCL cells throughout the cell cycle with its prominent localization to the spindle poles/centrosomes during nocodazole mediated G2/M arrest (Fig. 23-25) and during the different stages of mitosis (Fig. 28), hints towards a possible role of KLHL14 in the regulation of cell division. The staining pattern resembles the dynamics of well described components of the PCM like Aurora-A (Barr and Gergely 2007) and a large proportion of potential interactors/substrates have mitosis-related functions (Fig. 35, 38-39). NUDCD3, also known as NudCL, for example is part of the dynein MT motor complex (Asante, Stevenson, and Stephens 2014) and mediates the stability of the dynein intermediate chain. Deregulation of the protein leads to aggregation followed by the degradation of this specific dynein chain, mis-localization of the dynein complex from kinetochores, spindle MTs and poles and ultimately mitotic defects (Cai et al. 2009; T. Zhou et al. 2006). The low number of KLHL14 foci visible in other cell cycle phases than mitosis (Fig. 29) were found in cellular regions with a/ß-tubulin accumulation, however these did not necessarily coincide with a clearly visible MTOC (Fig. 30). This demonstrates that KLHL14 does not localizes to regions with high tubulin content per se but rather needs a specific trigger for accumulation. Possible explanations for the rare cases of KLHL14 foci in interphase cells remain speculative until experimental follow up, but include the establishment of non-centrosomal MTOCs, where the recruitment of proteins similar to the PCM takes place (Sanchez and Feldman 2017), the recruitment of dynein complexes in order to resolve patches of aggregated proteins (Ripon et al. 2020) or the

presence of midbody derivatives or midbody rings from previous divisions(M T Hayashi and Karlseder 2013; Pohl and Jentsch 2009).

Defects in every mitotic phase like spindle attachment (Ruchaud, Carmena, and Earnshaw 2007), centrosome and chromosome segregation (Nigg and Raff 2009) and cytokinesis/abscission (Fededa and Gerlich 2012) can lead to varying amounts of DNA damage (Thompson, Gatenby, and Sidi 2019; Crasta et al. 2012; M T Hayashi and Karlseder 2013; Janssen et al. 2011) and cell cycle arrest in the subsequent cell cycle phases (Uetake and Sluder 2010; Maciejowski et al. 2015; Fong et al. 2016; Janssen et al. 2011; Demidenko et al. 2008; Levine and Holland 2018). Interestingly, cells that overexpress KLHL14 did not enter mitotic arrest or showed a severely prolonged G2/M phases when released from a nocodazole block (Fig. 20). In case of the DLBCL cell lines MHH-PreB1 and Oci-LY1, the progression of these cells from the subsequent G1 was gravely delayed when KLHL14 was overexpressed, indicative of an active restriction point (Fig. 21). Cells of the MM cell line MM1.S did not re-enter S-phase 10 hrs after the removal of nocodazole in this experimental setup independent of the expressed construct, which might either stem from serious defects caused by the treatment with the depolymerizing drug or a generally slower cell cycle progression, hindering a comparison between the entities with the data acquired to this date. It would therefore be interesting to test whether the two DLBCL cell lines are more tolerant to or could repair DNA-damage more efficiently than MM1.S cells and whether KLHL14 induced DNA damage in already quiescent cells, that do not undergo mitosis.

The overexpression of KLHL14 in asynchronous MM1.S cells lead to the accumulation of the protein in dot-like structures, that partially co-localized with the centrosomal-marker protein CENTRIN-3 (Fig. 22) comparable to endogenous protein after G2/M-arrest (Fig. 23). Upon arrest and release of these cells, the dot-like structures remained and were distributed without a recognizable systematic throughout the mitotic cells (Fig. 31). Mitotic spindles were anchored independently from the KLHL14 foci and no differences in multipolar spindle formation could be determined (Fig. 31). Unfortunately, the analysis of suspension cells during mitosis remains challenging, as distinguishing between slide attachment artefacts and physiological effects is difficult, when for example attempting to determine the abundance of micronuclei or mis-aligned/attached chromosomes. Further experiments will therefore be necessary to microscopically investigate the effects of KLHL14 on mitosis in more detail.

6.5 KLHL14 in murine B-cells

The characterization of KLHL14 as a tumor suppressor in B-cell derived malignancies promoted questions on the function of the protein in non-transformed cells. The gene expression profile of KLHL14 during B-cell development and activation (Fig. 32A), the implication of PAX5 as a potential transcription factor (Fig. 32B) and its severe downregulation upon B-cell activation by LPS and IgM/IL-4 but not CD40L/IL-4 stimulation (Fig. 33A-D), points towards a role of KLHL14 in hindering unstimulated B-cells from proliferation. We reasoned that the loss of KLHL14 might therefore result in B-cells that could be activated with weaker TLR or BCR stimuli (Elgueta et al. 2009; Kooten, Banchereau, and Gene 2000).

A study investigating the role of KLHL14 in murine B-cell development determined that mice with a heterozygous loss of KLHL14 showed normal marginal zone or follicular B-cell development and unchanged IgG class switching upon *ex-vivo* stimulation (S. Li et al. 2018), suggesting that a reduction of the protein is not sufficient to cause differences in B-cell activation or differentiation. Fetal liver cells isolated from WT or KLHL14 knock out embryos transplanted into Rag-/- mice (Mombaerts et al. 1992) and the subsequent stimulation of extracted splenic B-cells showed a trend towards more proliferation of KLH14 -/- cells after 48

hrs for a subset of stimulation conditions. Interestingly, these trends could be observed upon stimulation with LPS and IL-4/IgM only (S. Li et al. 2018), which correspond to the conditions leading to the strongest downregulation of KLHL14 in explanted WT B-cells in this study (Fig. 33A-D). The stimulus dependent downregulation of KLHL14 therefore seems be a result of T-cell independent B-cell activation via the classical NF-κB pathway (Elgueta et al. 2009; Kooten, Banchereau, and Gene 2000) and the loss of KLHL14 might indeed have functional consequences.

The study of Li et al (S. Li et al. 2018) further reports the reduction of B1a B-cells upon deletion of KLHL14, arguing that the loss of the protein resulted in weaker BCR signaling and therefore a polarization towards the B1b sub-class of peritoneal B-cells (S. Li et al. 2018; Hoffmann et al. 2007; Berland and Wortis 2002). Importantly, Li and colleagues did not actually investigate differences in BCR signaling in those cells and did not report differences in antibody serum levels (S. Li et al. 2018), which would be expected in mice with generally reduced B1a levels (Hoffmann et al. 2007; Berland and Wortis 2002). The only functional marker used to identify B1a cells in these mice was CD5 surface expression, which can be downregulated due to a variety of reasons including the differentiation towards plasma cells (Calame 2001; Khodadadi et al. 2019) for examples due to enhanced BCR signaling or spontaneous activation. A differentiation towards antibody producing plasma cells (Calame 2001) could be an explanation for the missing differences in serum immunoglobulins. Monitoring the whole B-cell compartment upon immunization of these mice with agents inducing a T-cell-independent B-cell activation thus might give further inside into functional consequences of KLHL14 loss in peritoneal B1/B2 and B-cells in general.

In conclusion, the mere reduction of KLHL14 appears to be insufficient to cause changes in B-cell activation and proliferation, while a complete loss of the protein can potentially result in functional differences. In an *ex vivo* setup KLHL14 WT and KO B-Cells could be stimulated with decreasing doses of the described stimuli to provide an insight into whether there are indeed differences in the signaling threshold, that needs to be overcome to fully activate those cells. *In vivo* studies using either a transplant model of *ex vivo* modified murine B-cells or a conditional genetic deletion of KLHL14 for example in MB1+ (E Hobeika et al. 2006; Elias Hobeika et al. 2015) or CD19+ cells (Rickert, Roes, and Rajewsky 1997) would also be beneficial for the understanding of the role of KLHL14 in murine B-cell activation and differentiation. Genetically modified animals could also potentially be crossed to murine B-Cell lymphoma models (Meyer, Koul, and Pasqualucci 2021) to investigate whether KLHL14 has tumor suppressive potential *in vivo.*

6.6 Implications of KLHL14 in the organization of the cytoskeleton

Two publications connected KLHL14 with the epithelial-to-mesenchymal transition (EMT) (Di Lollo et al. 2020; Z. Chen, Wu, and Liu 2020), which relies heavily on the remodeling of the cytoskeleton to establish a polar morphology and motility (Bettencourt-Dias and Glover 2007; Leggett et al. 2021; Yilmaz and Christofori 2009). In the first, the protein is suggested as a marker for poor prognosis in ovarian cancer patients, nominating it as an oncogene in this cancer type. In different ovarian cancer cell lines, the depletion of KLHL14 lead to reduced proliferation, migration and invasiveness as well as an enrichment in G1-cells and an induction of apoptosis (Z. Chen, Wu, and Liu 2020). It would therefore be interesting to monitor the localization and protein levels of KLHL14 in those cells throughout the different cell cycle phases to establish whether the protein has a similar function in ovarian carcinoma cells and why these cells are dependent on the protein. The other publication, identifies KLHL14 mRNA as exclusively expressed in a subset of stem cells from the placenta (Miki et al. 2005) called

amniotic epithelial cells, if these cells were kept in their epithelial state (Di Lollo et al. 2020). As these cells retain their stemness and potential to differentiate into more mesenchymal cells upon stimulation (Miki et al. 2005), the role of KLHL14 in these cells might be rather similar to the one in unstimulated B-cells, that are restricted from uncontrolled proliferation and differentiation as well.

The other descriptions of KLHL14 are centered around its spatial and temporal mRNA expression during the development of corticospinal neurons (Sahni, Itoh, et al. 2021; Sahni, Shnider, et al. 2021) and in GABAergic inhibitory interneurons (J. Zhang et al. 2017a) as well as the proteins role in a neurological disorder called early onset generalized dystonia (DYT1) (Giles, Li, and Chin 2009). In line with the data presented in this study and discussed above, centrosomal/MTOC positioning as well as directional MT and actin dynamics determine axonal growth, synapsis formation and the migration of the neuron within the vertebrate brain (Higginbotham and Gleeson 2007; Meka, Scharrenberg, and Calderon de Anda 2020; Solecki et al. 2006; Lüders 2021) during development of post mitotic neurons. KLHL14 might be influencing these processes in a similar fashion as during mitosis in actively cycling B-cell lymphoma and MM cells. In the context of neurological disorders, the protein first found to interact with KLHL14 – TorsinA (Giles, Li, and Chin 2009) was recently described to be essential for the rearward movement of the nucleus during centrosome orientation (Saunders et al. 2017) to establish polarity and efficient migration in fibroblasts (Gomes, Jani, and Gundersen 2005; Gundersen and Worman 2013). Defects in the directional migration and centrosome orientation were uncovered in DYT1 dystonia patients derived fibroblasts, that carry disease relevant mutations in TorsinA (Nery et al. 2014), which were reported to interfere with its KLHL14 interaction (Giles, Li, and Chin 2009), highlighting a possible link between KLHL14, MTOC/centrosome related defects and the neurological dysfunction.

Even though only the 2009 performed study by Giles and colleagues discussed in this section aimed to describe the functions of the translated KLHL14 protein, instead of phenotypically describing its loss *in vitro* or *in vivo*, it is intriguing to note that in all of these processes, the cytoskeletal organization of MT and actin fibers plays a central role. It is therefore very well possible, that KLHL14 influences the establishment on cellular polarity, cellular migration and mitosis by affecting the MTOC/centrosome or the MT network including dynein trafficking.

7. Results OTUD6B

The data presented and discussed in this part of the thesis, are part and the follow up of a project in Prof. Dr. Florian Bassermann's (TUM) research group initiated by C. Paulmann (Richter). Data presented below are part of a manuscript, which is currently under (Paulmann et. al; under review). For comprehensive reasons, contributions by Carmen Paulmann and other collaborators are included in this thesis and respective parts clearly marked as such in the text and figure legends.

The group previously identified OTUD6B as a novel vulnerability and oncogene in MM. The loss of this DUB lead to a defect in the G1/S-transition of the cell cycle (Paulmann et.al. under review). Furthermore, the RNA-binding protein LIN28B (Heo et al. 2009; Balzeau et al. 2017) could be identified as a direct deubiquitylation substrate. The stabilizing effect of OTUD6B on its substrate was shown to be timed to the G1/S-transition, most probably by a not further specified phosphorylation event on the LIN28B side (Paulmann et.al. under review). Important questions at the time included, whether LIN28B was indeed the direct deubiquitylation substrate of OTUD6B responsible for the observed cell cycle arrest, thereby mediating the phenotype of OTUD6B loss *in vitro* and *in vivo* (Paulmann et.al. under review). Additionally, the molecular mechanism of OTUD6B regulation remained elusive, as neither the phosphorylation event which facilitates the DUB-substrate interaction nor the mode of OTUD6B activation were investigated to this date. To answer these questions, a rescue experiment was established in which the inability of OTUD6B depleted MM cells to leave G1-phase could be rescued by induced re-expression of LIN28B, further solidifying the importance of the OTUD6B-LIN28B-MYC axis for the entry of S-phase in MM. To further characterize the active OTUD6B complex, two different mass-spectrometric screens were set up to first identify possible phosphorylation sites on LIN28B and second to connect the responsible kinase with the phosphorylation event in an unbiased interactome screen of the substrate protein.

7.1. Ectopic expression of LIN28B rescues the G1/S transition defect in OTUD6B depleted cells

In order to verify that LIN28B was indeed the deubiquitylation substrate of OTUD6B responsible for the G1/S arrest, a rescue experiment was conducted. Therefore, MM1.S cells were lentivirally transfected with pTRIPZ-RFP or pTRIPZ-LIN28B, which allow for doxycycline induced transgene expression. Cells were selected for the expression vector by puromycin and tested for transgene induction by doxycycline addition. The resulting MM1.S-pTRIPZ-RFP (EV) or -LIN28B were lentivirally transduced with shRNA constructs targeting OTUD6B or non-targeting controls. The next day, a double thymidine block was started to arrest cells at the G1/S-cell cycle transition, during which transgene expression was induced in the four different conditions by doxycycline addition. The G1/S-arrested cells were subsequently released and samples collected for PI-staining and WB analysis 0 and 8 hrs after the wash out. The analysis of the cellular DNA-content by PI-staining and flow cytometry, revealed a high number of cells at the G1/S-transition in every condition and an almost complete release of cells from the cell cycle block for the shCtrl transduced cells, irrespective of LIN28B or RFP overexpression (Fig. 42A).

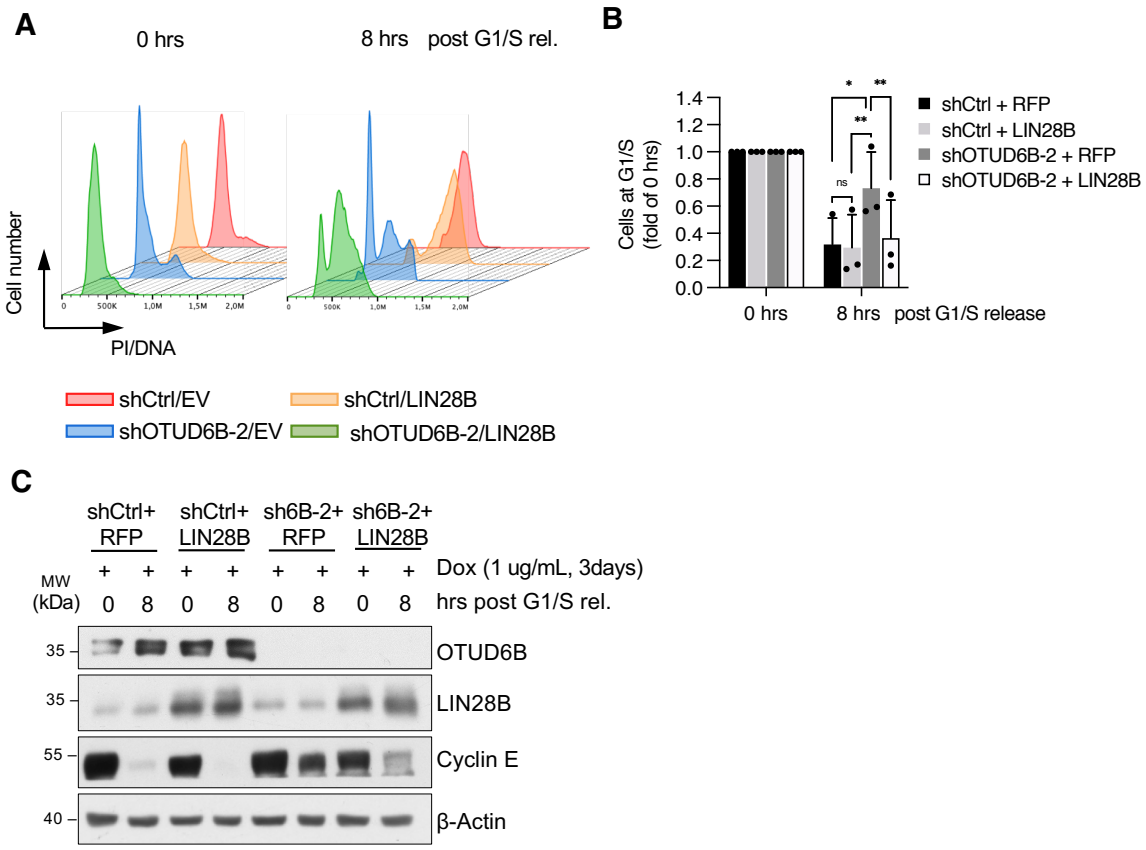

Figure 42: LIN28B is the deubiquitylation substrate of OTUD6B which mediates the entry into S-phase in MM cells. A-C, Cell cycle analysis of MM1.S cells with doxycycline induced overexpression of RFP (EV) or LIN28B expressing the indicated shRNAs before and after G1/S release. MM1.S cells stably expressing doxycycline inducible RFP or LIN28B were transduced with either shCtrl or shOTUD6B. Cells were then synchronized at G1/S by double thymidine block and transgene expression induced for 3 days by doxycycline (1 µg/mL) addition. Samples were taken at the indicated time points before and after thymidine wash out. **A,** Analysis of the cell cycle distribution before and 8 hrs after wash out by PI staining and flow cytometry. Results are depicted as histograms of FL2-A (PI) signal intensity. **B**, Quantification of the cell cycle distribution as depicted in (A) normalized to cells at G1/S before release per condition (n = 3 independent experiments. Values represent mean ± S.D.; *, $P < 0.05$; **, $P < 0.01$; by paired Student's *t*-test corrected for multiple testing). **C,** Immunoblot based cell cycle analysis of MM1.S treated as described above. WCEs were analyzed by immunoblotting using the indicated antibodies. ß-Actin served as loading control.

In line with previous data, OTUD6B depletion in MM1.S cells led to an impaired progression from G1/S block in combination with induced RFP-overexpression. The ectopic re-expression of LIN28B reduced the progression defect caused by OTUD6B depletion significantly, validating LIN28B as a deubiquitylation target responsible for the OTUD6B phenotype in MM1.S cells (Fig. 42A, B). The corresponding protein samples were also lysed and analyzed by immunoblot to validate the OTUD6B-knock down and the induced overexpression of LIN28B. Furthermore, probing of the G1/S marker protein Cyclin E validated the partial rescue seen by flow cytometry, as the ectopic expression of LIN28B led to a stronger downregulation after thymidine wash than in the RFP-overexpressing OTUD6B depleted cells (Fig. 42C). These data indicate that LIN28B is the deubiquitylation substrate of OTUD6B responsible for the defect in G1/S-transition in OTUD6B depleted cells.

7.2 LIN28B binding at the G1/S transition determines OTUD6B activity

Data by Carmen Paulmann (Paulmann et. al., under review) showed an almost complete loss of interaction between OTUD6B and LIN28B in mitosis as compared to asynchronous cells. However, how OTUD6B activity was timed to the G1/S-transition remained elusive. To investigate if the differential binding also occurred in G1/S arrested versus released MM1.S cells, lentivirally transduce MM1.S cells stably expressing FLAG-EV or -OTUD6B were arrested at the G1/S transition by two sequential thymidine blocks. Protein samples were collected before and 12 hrs after thymidine wash out and subjected to FLAG-IP. Immunoblotting revealed a distinct interaction between LIN28B and FLAG-OTUD6B which was reduced after cells progressed from G1/S towards mitosis. Synchronization in and the release from G1/S was verified by probing the WCE before and after wash out for Cyclin E and the G2/M specific expressed Cyclin B (Fig. 43A).

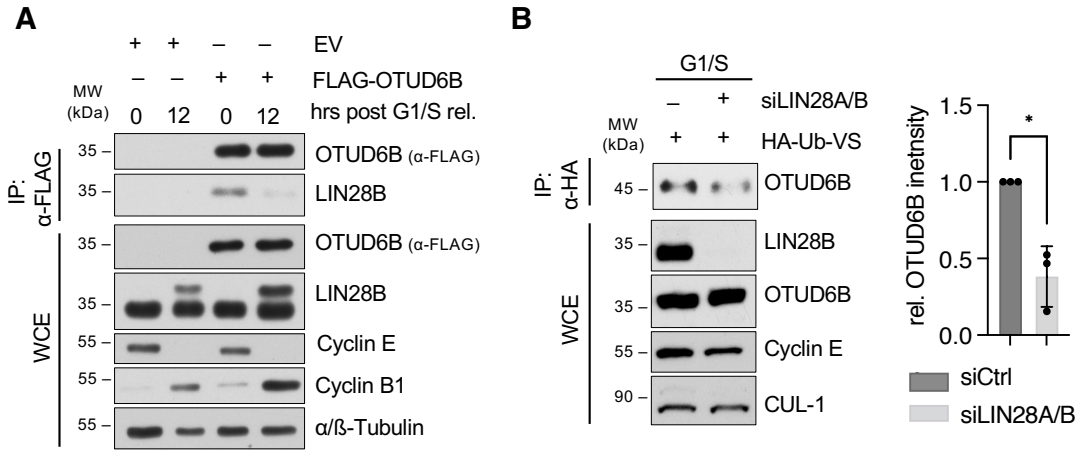

Figure 43. LIN28B binds and activates OTUD6B at the G1/S transition. A, Co-IP of FLAG-OTUD6B with endogenous LIN28B from MM1.S cells at G1/S and 12 hrs post release. MM1.S cells stably expressing FLAG-OTUD6B or FLAG-EV were synchronized at G1/S and harvested at the indicated time points after release. IPs were performed and analyzed together with WCE by immunoblotting. **B,** DUB activity assay for OTUD6B in G1/S- synchronized A549 cells with LIN28A/B knockdown using HA-ubiquitin vinyl-sulfone to isolate active forms of DUBs. Analysis was performed by immunoblotting using the indicated antibodies (left). Loading control Densitometry quantification of HA-ubiquitin vinyl-sulfone bound OTUD6B from three independent experiments (right). Data are mean ± S.D. *, P < 0.05 by paired Student's t-test.

Next, the hypothesis was tested whether the presence of LIN28B enabled OUTUD6B enzymatic activity at the G1/S transition. To this end, A549 cells were transfected with siRNAs targeting either LIN28A/B or siCtrl and arrested in G1/S using a double thymidine block. Pellets were lysed in DUB-activity-assay buffer without protease inhibitors and equal amounts of protein incubated with 1 µM of the DUB-activity probe HA-ubiquitin vinyl-sulfone for 30 min at 37°C. This ubiquitin variant is covalently bound to the active site cysteine of DUBs during attempted ubiquitin cleavage and can then be immunoprecipitated together with active DUBs by HA-pulldown.

When immunoblotting the resulting HA-IPs for OTUD6B, a reduced pulldown of the DUB could be detected in the LIN28A/B depleted condition, implicating a reduction in the enzyme's activity upon substrate depletion in G1/S arrested cells (Fig. 43B). These results showed that LIN28B not only bound to OTUD6B specifically at the G1/S-transition and early S-phase but also that LIN28B-OTUD6B interaction might activate the DUB.

7.3 Identification and characterization of LIN28B phosphorylation sites

Events with cell cycle context are often coordinated by protein phosphorylation (Fisher et al. 2012), as is the binding between OTUD6B and LIN28B (Paulmann et. al., under review). Interestingly, and in contrast to many other DUB-substrates pairs described (Dietachmayr et al. 2020; O. W. Huang et al. 2012; Jaynes et al. 2020), the LIN28B side was found to be in need of phosphorylation to ensure interaction (Fig. 44A) (Paulmann et. al., under review). In order to identify the corresponding kinase and phosphorylation site, two different MS-based approaches were set up.

First, MM1.S cells stably expressing FLAG-tagged LIN28B or -EV control were created. For the analysis of differentially phosphorylated amino acid residues, 10^8 FLAG-LIN28B expressing MM1.S cells per condition were left untreated (DMSO), incubated for 18 hrs with the AKT-inhibitor MK2206, synchronized at the G1/S transition by double thymidine block or in G2/M by sequential thymidine and nocodazole treatment. The snap frozen cell pellets were lysed and subjected to FLAG-IP followed by elution of bead bound proteins with acidified 0.2M glycine. After TCA precipitation and lyophilization of the eluted proteins, 2.5% were separated by SDS-PAGE and silver stained to verify target protein enrichment (Fig. 44B).
The remaining samples were sent to Jana Zecha/Julia Mergner at the chair of Proteomics and Bioanalytics (TUM) for further processing. Samples were separated by Nu-PAGE gradient gel, the LIN28B bands of approximately 35 kDa cut out and used for in-gel trypsin digestion. MS/MS measurement of the resulting peptides was carried out and the MaxQuant software (V 1.6.3.3) was used for peptide identification with variable modifications enabled (Oxidation (M); Acetyl (Protein N-term); Phospho (STY); GlyGly (K)). The bait protein coverage of LIN28B was determined to be 72.5%. The Perseus (V 1.6.14.0) and Skyline software (V 20.2.0.343) were used for phospho-mapping and peptide intensity normalization to determine the phosphorylated residues and their relative abundance per condition.

In total five phosphorylated residues were overserved within the covered sequence of LIN28B (Fig. 44C). Two of them – Serine (S) 218 and S221 – could not be distinguished from one another due to ambiguous spectra produced by the two possible phospho-peptides. The intensity of the VTGPGGpSPCLGSER (S105) phosphopeptide was higher in G2/M arrested cells, while all the other phosphorylation sites showed no clear differences in abundance in the different conditions tested (Fig. 44C). The analysis of LIN28B by MS resulted in the detection of phosphorylated residues but none of them were detected with a differential abundance in G1/S arrested cells, which could explain the dependence of the LIN28B-OTUD6B interaction on the post translational modification as well as the G1/S specific binding.

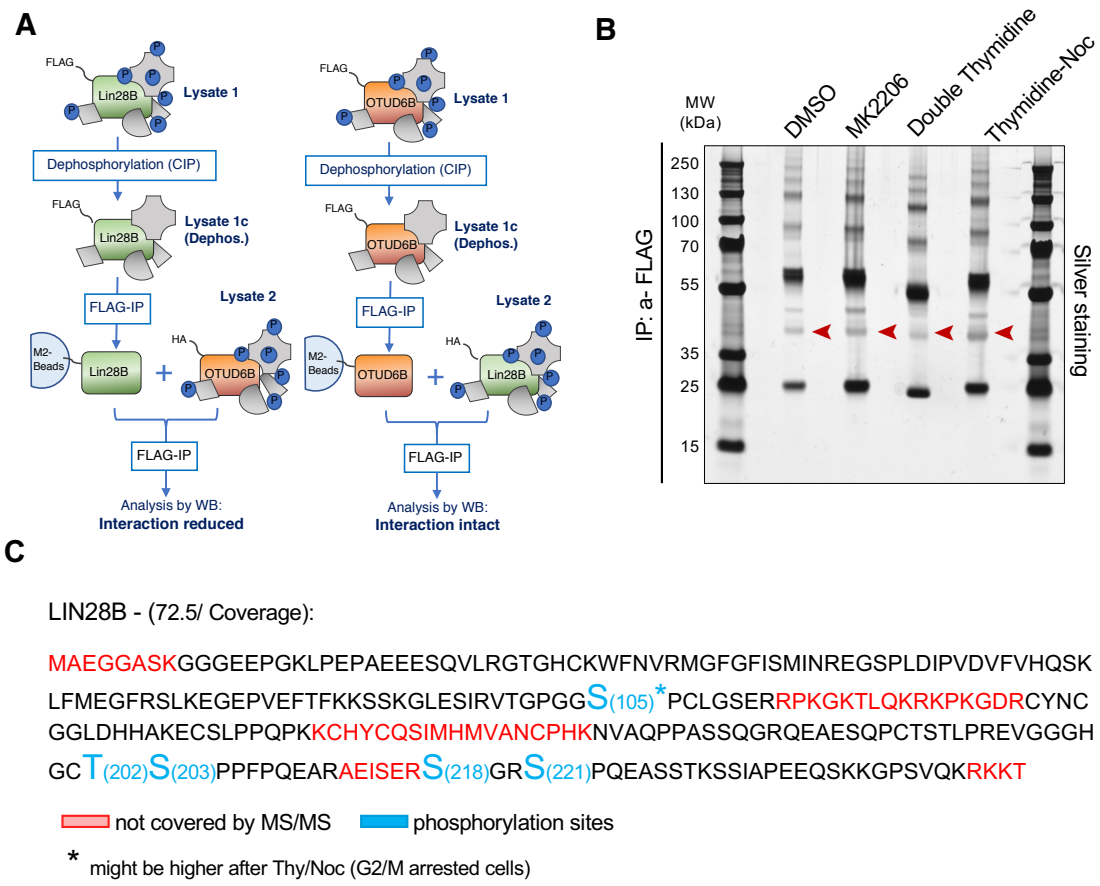

Figure 44. LIN28B is phosphorylated at multiple residues. A, Schematic overview of the OTUD6B-LIN28B binding studies, indicating that LIN28B is phosphorylated to enable OTUD6B binding. **B**, Silver gel analysis of FLAG-purified LIN28B. MM1.S cells were transduced with pHIV-FLAG-LIN28B and selected for expression by puromycin addition. The resulting MM1.S cells were expanded to 10^8 per condition and either supplemented with DMSO, MK2066 (10 µM), synchronized at the G1/S by double thymidine or in G2/M by sequential thymidine and nocodazole treatment. WCEs were subjected to FLAG-IP with FLAG-M2-Affinity gel, which were eluted using acidified glycine. 2.5% of each condition were separated by SDS-PAGE and subjected to silver staining. The remaining TCA precipitated proteins were sent to Jana Zecha/Julia Mergner at the chair of Proteomics and Bioanalytics (TUM). Red arrowheads mark FLAG-purified LIN28B **C,** Representation of the LIN28B sequence including the detected phosphorylation sites. The phosphorylated residues are indicated in blue and their position within the protein indicated by the number in brackets. Residues not detected by MS due to trypsin cleavage sides are marked in red. [MS data provided by J. Zecha/J. Mergner and Prof. B. Küster].

Next, point mutants of FLAG-tagged LIN28B were created in which all amino acids shown to be phosphorylated by MS were exchanged to alanine by side directed mutagenesis. The side chain of this amino acid cannot be phosphorylated and the interaction between the DUB and its substrate should thus be impaired upon the mutagenesis, if one of the sites was indeed phosphorylated to broker the binding.

The resulting mutants of LIN28B were ectopically expressed alongside the FLAG-tagged WT protein and empty vector control in HEK293T. Lysates were then subjected to FLAG-IP and the resulting purifications analyzed for co-IP of endogenous OTUD6B by immunoblotting. This revealed that none of the mutants interacted less with OTUD6B than LIN28B WT (Fig. 45A). The exchange of threonine 203 (T203) and serine 221 (S221) with alanine lead to the reduction of the upper band detected by the FLAG-antibody in LIN28B overexpression samples. This shift in size has been shown by C. Paulmann to be a phosphorylation event, that occurs in the G2/M phase of the cell cycle in which OTUD6B and LIN28B do not interact (Paulmann et. al. under review). This led to the hypothesis that phosphorylation on multiple specific sides might be necessary for the DUB-substrate pair to

interact. Thus, another set of FLAG-LIN28B mutant were created by replacing either T203 and S221 (double mutant) or the remaining phosphorylation sites (triple mutant) with alanine. In addition, a mutant was created by side directed mutagenesis, in which all detected phosphorylation sides were mutated to completely impair phosphorylation of the protein. Again, these mutants were expressed alongside the WT protein and empty vector control in HEK293T, followed by lysis and FLAG-IP. Analysis by immunoblotting revealed, that neither the loss of all detected LIN28B phosphorylation sites nor the tested combinations reduced the binding to OTUD6B (Fig. 45B).

These data lead to the conclusion that either the relevant phosphorylation site was not detected by MS due to incomplete sequence coverage, the loss of the phosphorylation sites becomes relevant only in G1/S arrested cells or LIN28B is not directly phosphorylated to induce the binding.

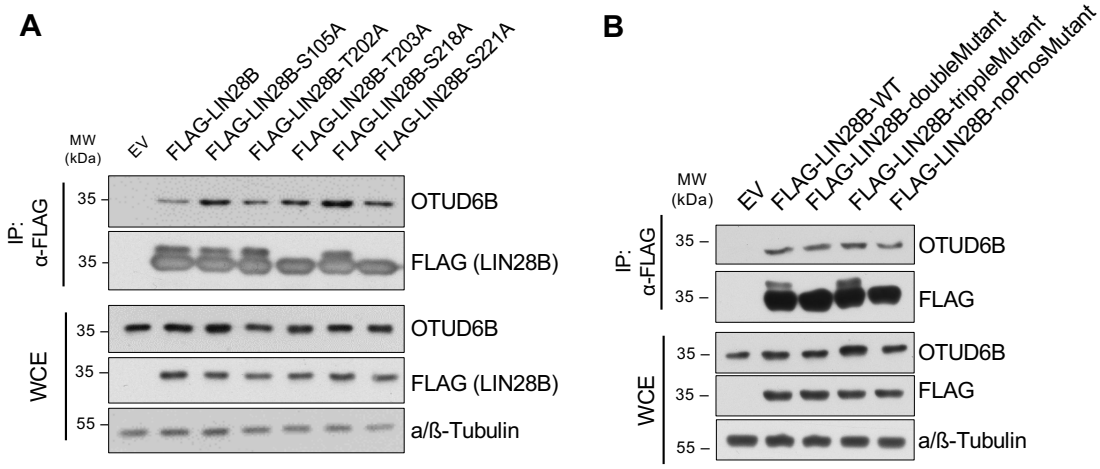

Figure 45. LIN28B binds to OTUD6B independent of the phosphorylation status at the identified sites. **A, B,** Immunoblot analysis of OTUD6B-LIN28B binding studies using LIN28B-WT or non-phosphorylatable mutants. Individual **(A)** or combinations of **(B)** S/T to A mutations of the residues found to be phosphorylated by MS were created in FLAG-tagged LIN28B and the resulting mutants expressed alongside the WT protein in HEK293T using lipofectamine2000. WCEs were subjected to FLAG-IP and both analyzed by immunoblotting using the indicated antibodies. Double Mutant (T203A and S221); Triple mutant (S105A, T202A and S218A); noPhos Mutant (T203A, S221, S105A, T202A and S218A). a/ß-Tubulin served as loading control. S- Serine, T-Threonine, A-Alanine.

7.4 CDK9 activity mediates LIN28B and OTUD6B interaction

Another intriguing question was, which kinase was responsible for the described G1/S transition specific phosphorylation leading to the OTUD6B-LIN28B interaction. To address this, the MM1.S cells stably expressing FLAG-EV or FLAG-LIN28B described above were used for a MS-based interactome analysis of LIN28B in G1/S arrested versus asynchronous cells. Snap frozen cell pellets of MM1.S pHIV-FLAG-EV or -LIN28B, which were synchronized in G1/S by double thymidine block or left asynchronous, were lysed, subjected to FLAG-IP and proteins eluted as described before. Dried protein samples were sent to Jana Zecha/Julia Mergner at the chair of Proteomics and Bioanalytics (TUM) for further processing, mass spectrometric measurement and data evaluation.

A total of 725 protein groups were identified over all conditions with 516 detected in all of them. But only 8 proteins were exclusively detected in the LIN28B G1/S arrested (double

thymidine, dT) sample (Fig. 46A, Figure provided by J. Mergner). If no valid intensity for a protein was detected by MS/MS in one condition, a constant value of 20 was imputed after log2 transformation of the LFQ intensities. When screening the list of potential interactors for kinases or kinase related proteins, CDK9 was the only kinase detected more than two-fold enriched in the G1/S-synchronized LIN28B sample, when compared to the respective empty vector control (EV_dT). Additionally, the enrichment of CDK9 was lower in the asynchronous LIN28B pulldown samples, hinting towards a stronger binding at the G1/S-transition (Fig. 46B).

A

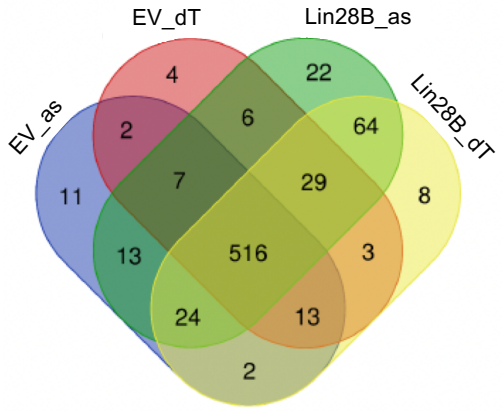

B

Protein names	Gene names	log2 (LIN28B/EV_as)	log2 (LIN28B/EV_dT)	log2(dtLIN28B/ dtEV)- log2(as LIN28B/asEV)
Protein lin-28 homolog B	LIN28B	10.672	8.332	-2.340
Period circadian protein homolog 2	PER2	-5.496	1.165	6.661
Cyclin-dependent kinase 9	CDK9	0.318	1.040	0.722
Serine-threonine kinase receptor-associated protein	STRAP	0.094	0.596	0.502
Ser/thr-protein phosphatase PP1-alpha/beta catalytic subur	PPP1CA/B	-0.408	0.293	0.700
MOB kinase activator 2	MOB2	-0.207	0.114	0.321
Fructose-2,6-bisphosphatase	PFKFB3	-0.779	0.083	0.862
cAMP-dependent protein kinase catalytic subunit gamma	PRKACG	-4.289	0.070	4.359
Cyclin-K	CCNK	4.293	0.000	-4.293
Phosphatidylinositol 4-kinase alpha	PI4KA	3.734	-0.026	-3.760
Mitogen-activated protein kinase kinase kinase 7	MAP3K7	0.050	-0.071	-0.121
TGF-beta-activated kinase 1/MAP3K7-binding protein 2	TAB2	0.020	-0.093	-0.113
Dual specificity protein kinase CLK4	CLK4	0.160	-0.141	-0.301

Bait – LIN28B
Kinases and Kinase-subunits
Phosphatases and Phosphatase-subunits
Kinase binding proteins

Figure 46. Unbiased LIN28B MS-based interactome analysis identifies CDK9 as a potential kinase. Results of a MS-based LIN28B interaction screen in asynchronous and G1/S arrested MM1.S cells stably expressing pHIV-EV or pHIV-FLAG-LIN28B were expanded to 10^8 per condition and either harvested as an asynchronous (as) population or synchronized at the G1/S by double thymidine (dT) treatment beforehand. WCEs were subjected to FLAG-IP with FLAG-M2-Affinity gel, which were eluted using acidified glycine. After quality control, TCA precipitated proteins were sent to Jana Zecha/Julia Mergner at the chair of Proteomics and Bioanalytics (TUM) and analyzed by MS. Missing values of proteins, which were only detected in one sample, were replaced by 1000 in the respective other sample (imputed intensities). **A,** Venn diagram representing the measured interactome data. The numbers per field indicate the amount of proteins identified in a single or multiple sample. Data analysis and visualization by J. Mergner. **B,** List of interactors identified by MS which potentially influence LIN28B phosphorylation e.g. kinases and phosphatases. Values represent Log2 transformed ratios of LFQ intensities of proteins identified in FLAG-LIN28B vs EV control from asynchronous or double thymidine treated cells and differences thereof. [MS data provided by J. Zecha/J. Mergner and Prof. B. Küster].

CDK9, also known as PITALRE, is a proline directed serine/threonine kinase (Garriga et al. 1996), which would match several of the detected phospho-sites detected on LIN28B (Fig. 44C). The binding of CDK9 to LIN28B was thus validated. The MM1.S cell lines used for MS-based screening were either harvested asynchronous or after arrest in G1/S as described previously. Cells were lysed and subjected to FLAG-IP followed by immunoblot analysis. Precipitated FLAG-LIN28B was indeed found to pull down endogenous CDK9, which was even more profound in G1/S arrested cells (Fig. 47A).

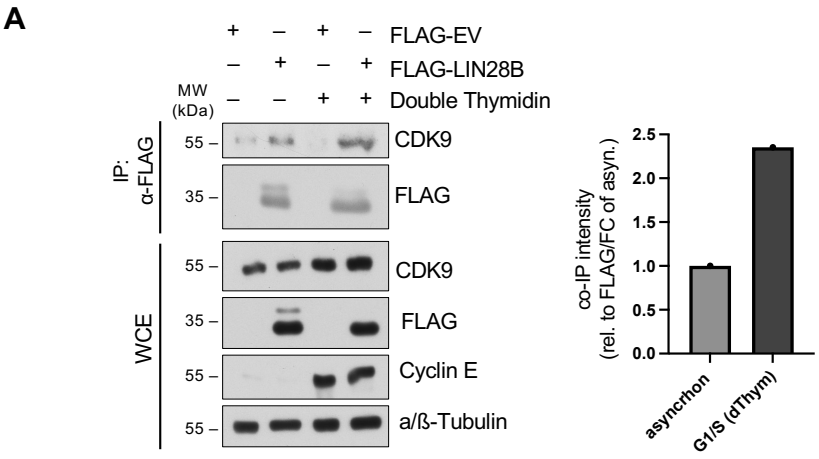

Figure 47. Enhanced CDK9 binding to LIN28B at the G1/S transition. A, Immunoprecipitation of FLAG-LIN28B from asynchronous or G1/S synchronized MM1.S cells. Cells stably expression pHIV-FLAG-EV or –LIN28B were either left untreated or synchronized at the G1/S transition using a double thymidine block. WCEs were subjected to FLAG-IP and immunoblot analysis using the indicated antibodies. a/ß-tubulin served as a loading control. Densitometry quantification of the co-IP intensity relative to the detected FLAG signal, plotted as fold of asynchronous cells.

To further analyze the function behind the interaction of CDK9 and LIN28B, LDC067, a specific CDK9 inhibitor, was used to inhibit the kinase in G1/S arrested MM1.S cells stably expressing FLAG-EV or -OTUD6B. Cells were treated for 18 hrs with 5 µM LDC067 or DMSO during the second incubation with thymidine before sample collection and FLAG-IP.

Immunoblot of IP and WCE revealed an MCL-1 and CDK9 reduction upon inhibitor addition in WCEs, confirming functional CDK9-inhibiton. Furthermore, an attenuated interaction of the DUB-substrate pair upon CDK9 inhibition was detected (Fig. 48A). As the Cyclin E levels were higher in WCEs of LDC067 treated cells, the question arose whether the inhibition of CDK9 interfered with the synchronization of the cells. PI-staining and flow cytometric analysis of the DNA content of samples taken in parallel to collection of immunoblot samples showed a comparably good arrest of the cells at the G1/S transition, dismissing the hypothesis that the reduction in interaction was due to synchronization difficulties (Fig. 48B).
As small molecule kinase inhibitors can have effects on multiple targets (Klaeger et al. 2017), shRNAs targeting CDK9 were designed to investigate, if the depletion of the kinase had a similar effect on the OTUD6B-LIN28B interaction as LCD067 treatment. Control or CDK9 targeting shRNA constructs were lentivirally delivered to MM1.S stably expressing FLAG-EV or -OTUD6B. Half of the cells were left untreated while the rest of the cells were synchronized in G1/S by sequential thymidine block. After samples collection, cells were lysed and subjected to FLAG-IP with subsequent immunoblot analysis.

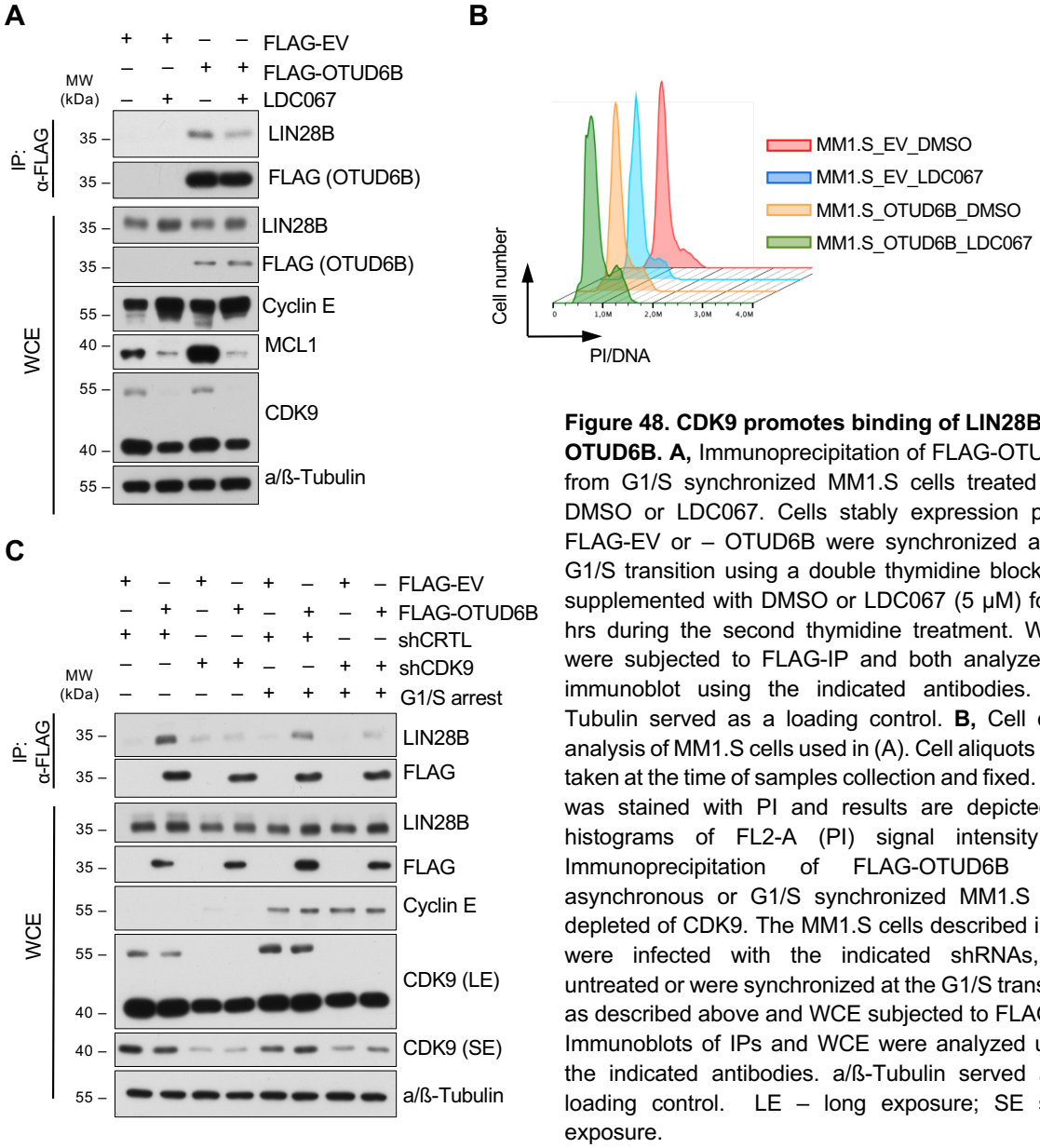

Figure 48. CDK9 promotes binding of LIN28B and OTUD6B. A, Immunoprecipitation of FLAG-OTUD6B from G1/S synchronized MM1.S cells treated with DMSO or LDC067. Cells stably expression pHIV-FLAG-EV or – OTUD6B were synchronized at the G1/S transition using a double thymidine block and supplemented with DMSO or LDC067 (5 µM) for 18 hrs during the second thymidine treatment. WCEs were subjected to FLAG-IP and both analyzed by immunoblot using the indicated antibodies. a/ß-Tubulin served as a loading control. **B,** Cell cycle analysis of MM1.S cells used in (A). Cell aliquots were taken at the time of samples collection and fixed. DNA was stained with PI and results are depicted as histograms of FL2-A (PI) signal intensity. **C,** Immunoprecipitation of FLAG-OTUD6B from asynchronous or G1/S synchronized MM1.S cells depleted of CDK9. The MM1.S cells described in (A) were infected with the indicated shRNAs, left untreated or were synchronized at the G1/S transition as described above and WCE subjected to FLAG-IP. Immunoblots of IPs and WCE were analyzed using the indicated antibodies. a/ß-Tubulin served as a loading control. LE – long exposure; SE short exposure.

The following immunoblot confirmed the desired CDK9 knock down in the WCEs of the respective samples, while the interaction analysis showed a reduced binding of OTUD6B to LIN28B upon CDK9 depletion in asynchronous as well as G1/S arrested cells (Fig. 48C).

Together these results indicate that CDK9 binds to LIN28B and that its activity promotes the interaction between LIN28B and OTUD6B. If LIN28B is directly phosphorylated by CDK9 and a potential phosphorylation site remains to be investigated.

8. Discussion OTUD6B

The deubiquitylase OTUD6B was described as a novel targetable oncogene and central regulator of LIN28B and MYC activity in MM by Paulmann and colleagues (Paulmann et. al. under review). The identification of the RNA binding protein LIN28B presents the first description of a deubiquitylation target of OTUD6B, contradicting the hypothesis that OTUD6B

was inactive (Paulmann et. al. under review) (Mevissen et al. 2013). Furthermore, the unique expression pattern of LIN28B indicates that OTUD6B inhibition by small molecules might have a favorable therapeutic window, as the protein is highly expressed in embryonic stem cells, but is downregulated in differentiated cells and becomes re-expressed in a subset of tumors, including MM (Balzeau et al. 2017; Manier et al. 2017; Shyh-Chang and Daley 2013; Jin Zhang et al. 2016; Viswanathan, Daley, and Gregory 2008). Targeting OTUD6B pharmacologically would therefore allow the reactivation of lethal 7 (let-7) microRNAs which in turn inhibit MYC activity, making the TF targetable by small molecules in cancers with active OTUD6B-LIN28B axis. During the pre-clinical screening of compound libraries for potent inhibitors of enzymatic activity, the establishment of a reliable high throughput assay is key (Harrigan et al. 2018). Therefore, it seemed utterly important to understand how OTUD6B activity was timed to the G1/S transition, especially which kinase was responsible for the phosphorylation event on LIN28B necessary for the interaction with OTUD6B.

After having established that the destabilization of LIN28B was indeed significantly contributing to the G1/S transition defects in OTUD6B depleted MM cells (Fig. 42), the binding of LIN28B to OTUD6B could be timed to the G1/S transition (Fig. 43A) in a process that seemed to rely on the phosphorylation of LIN28B (Paulmann et. al. under review). While activatory phosphorylation events on DUBs are well described(Ling Song and Rape 2008; Mevissen and Komander 2017), this presented the intriguing possibility that a post translational modification (PTM) other than ubiquitylation on a substrate was responsible for the activation of an otherwise inactive DUB. This hypothesis was further solidified, as cells depleted of the substrate LIN28B showed a decrease in OTUD6B DUB activity (Fig. 43B). There are several possibilities on how LIN28B promotes the catalytic activity of OTUD6B.

First, the binding of one or multiple phosphorylated LIN28B molecules might trigger a conformational change in OTUD6B to allow the active site cysteine to effectively hydrolyze the isopeptide bond linking the Ubiquitin chain to LIN28B as well as the HA-Ubi-vinyl-sulfone suicide probe. In contrast to DUB activation by Ubiquitin binding, as described for the catalytic center of UCH-L1 (Boudreaux et al. 2010), it seems that the binding of (polyubiquitylated) LIN28B is necessary for the activation. Second, phosphorylated LIN28B might recruit additional binding partners which are essential for the activity of OTUD6B in a similar fashion as seen for USP1 and its cofactor USP1-associated factor 1 (UAF1). The recruitment of this activator is not mediated by substrate but USP1 phosphorylation at Ser313, which leads to a change in subcellular localization and enhances DUB activity up to 36-fold (Das et al. 2020; Cohn et al. 2007). In order to determine how LIN28B activates OTUD6B, solving the crystal structure of the DUB alone and in combination with its (ubiquitylated) substrate might be key.

In order to identify the amino acid residue of LIN28B, that needs to be phosphorylated to allow OTUD6B binding, LIN28B was purified from MM1.S cells synchronized in different cell cycle phases and analyzed by MS/MS. With roughly 72% of the protein sequence covered, five different phosphorylation sites were detected (Fig. 44C) but none of them showed a higher abundance in G1/S synchronized cells, what would be expected if the site was responsible for the specific OTUD6B recruitment at this point during the cell cycle. When the Serine or Threonine residues identified as phosphorylated by MS were mutated to Alanine, which renders them un-phosphorylatable, the resulting LIN28B mutants did not lose the ability to bind to OTUD6B (Fig. 45A). Additionally, the removal of specific subsets as well as all detected phosphorylation sites within LIN28B did not lead to a reduction in OTUD6B co-purification. This indicates that the relevant phosphorylation takes place on a stretch of LIN28B that was not detected by MS after the trypsin digest. To enhance sequence coverage, purified LIN28B could be digested with protease generating different peptides like chymotrypsin (Giansanti et al.

2016). Additionally, the loss of this specific phosphorylation might only become relevant at the G1/S transition and was therefore not detected in asynchronous HEK293T cells. Thus, the LIN28B mutants are currently being tested for their ability to interact with OTUD6B in synchronized cells. Another possibility is that overexpressed mutant LIN28B interacts with a sufficient amount of the WT protein for example by dimerization or in a complex to mask the effect of point mutations. Lastly, the phosphorylation inducing LIN28B binding to OTUD6B might not occur on the substrate directly but on one or multiple proteins in a multi-subunit DUB complex similar to for example USP8 in the SAGA complex (Mevissen and Komander 2017). This complex might be disassembling upon dephosphorylation. To test this hypothesis, LIN28B complex formation with and without dephosphorylation and upon CDK9-inhibition (further discussed below) should be evaluated by mass spectrometry.

In an attempt to identify the kinase responsible for the phosphorylation event, the LIN28B interaction landscape from asynchronous and G1/S synchronized cells was analyzed (Fig. 46). Among the kinases and kinase related proteins, only CDK9 was detected in both pull downs and was enriched upon G1/S synchronization (Fig. 46B). This interaction dynamics could be verified by immunoblot (Fig. 47) and the reduction of CDK9 activity by pharmacological inhibition as well as by shRNA mediated depletion of the protein lead to decrease in interaction of LIN28B and OTUD6B (Fig. 48). The proline directed kinase CDK9, sometimes referred to as PITALRE(Falco and Giordano 1998; Garriga et al. 1996), was identified as a part of the Positive Transcription Elongation Factor (P-TEFb), which is essential for productive transcription elongation by phosphorylating the carboxyl terminal domain (CTD) on a RNA polymerase II (RNAP II) subunit (Morales and Giordano 2016; Anshabo et al. 2021; Franco et al. 2018). In contrast to other Cyclin dependent kinases, CDK9 and its Cyclin partners T and K are not expressed differentially throughout the cells cycle, but are recruited to the DNA by BRD4 to mitotic chromosomes to enable productive transcription of important G1 genes in the next cell cycle phase. Therefore, downregulation of CDK9 as well as BRD4 is described to result in a G1 cell cycle arrest and apoptosis (Anshabo et al. 2021). Although, CDK9s role in complex with Cyclin T upon recruitment to the DNA is well established, it has been shown that the kinase together with Cyclin K is tethered to a promotor by RNA (X. Lin et al. 2002). Importantly, Cyclin K instead of T was detected by MS, indicating that the RNA-interacting form of the P-TEFb complex might have been co-purified with LIN28B. This provides a direct link to the RNA-binding protein LIN28B. Additionally, this particular CDK9/Cyclin complex has been shown to have transcription independent cellular functions, for example in the DNA damage response (D. S. Yu et al. 2010; Liu et al. 2010).

The very dominant influence of CDK9 on transcriptional control poses a challenge for the investigation into its role in the phosphorylation dependent interaction between LIN28B and OTUD6B. In a cellular context, it seems almost impossible to differentiate between a direct phosphorylation of LIN28B and the indirect effects of impaired transcription upon CDK9 inactivation. As exemplified for MCL1 (Fig. 48A), short lived proteins will be severely reduced upon CDK9 inhibition (Phillips et al. 2020), indicating that any of those proteins could be responsible for the reduced interaction of the DUB-substrate pair seen in the interaction studies. The next steps in deciphering the role of CDK9 in the regulation of OTUD6B activity will therefore be carried out in a fully or partially reconstituted setting using commercially available CDK9/Cyclin K purified from insect cells. In a cellular context further validation experiments will include the depletion of Cyclin K instead of CDK9 to discriminate between the two CDK9 complexes and their functions.

9. Results FBXO21

The results presented below are part of a project of the group of Prof. F. Bassermann, which was initially conducted by B. Targosz and U. Baumann. For a comprehensive understanding of this project, data generated by Targosz and Baumann are presented first (Figure 49). The contributions to this project by collaborators are indicated in the text and figure legends.

9.1 Previous Data FBXO21

The cleaved form of NF-κB1 - p50 has been described to be degraded in an ubiquitin-proteasome-dependent manner in BCL3 knock out MEFs (Carmody et al. 2007), but the responsible ubiquitin ligase has not been identified. In search for the corresponding ubiquitin ligase/s, an unbiased proteome wide mass spectrometry-based interaction screen was conducted by B. Targosz using Strep-FLAG-tagged p50 immunoprecipitated from HEK293T cells as bait (Fig. 49A). After multiple filtering steps to remove background contaminants, the interactome analysis revealed only one potential E3 ubiquitin ligase, namely the orphan FBOX protein FBXO21 (Fig. 49B). Follow up interaction studies were conducted by B. Targosz as well as U. Baumann to verify the binding between BCL-3, FBXO21 and p50 by immunoprecipitation (IP) from HEK293T cells. For this, GFP-FBXO21 and FLAG-p50 were co-overexpressed, while FLAG-FBXO21 was overexpressed individually for co-immunoprecipitation of endogenous interaction partners. Following the IP, interaction was confirmed by analysis via immunoblot. A co-purification was repeatedly observed, especially in the double-over-expression setting. Treatment of the cells with lipopolysaccharides (LPS) prior to lysis increased FBXO21 pull down of BCL-3 and p50, respectively (Fig. 49C, D). Furthermore, an *in vivo* ubiquitylation assay was performed by U. Baumann to investigate whether FBXO21 had an influence on p50 ubiquitylation. An increased polyubiquitin signal was detected compared to empty-vector- or GFP-FBXO25-control, when overexpressing GFP-FBXO21 together with HA-ubiquitin and FLAG-p50 (Fig. 49E).

These data suggested FBXO21 as a potential E3 ubiquitin ligase for p50 ubiquitylation and degradation. Therefore, the aim of this project was to characterize the role of FBXO21 in the UPS dependent degradation of p50.

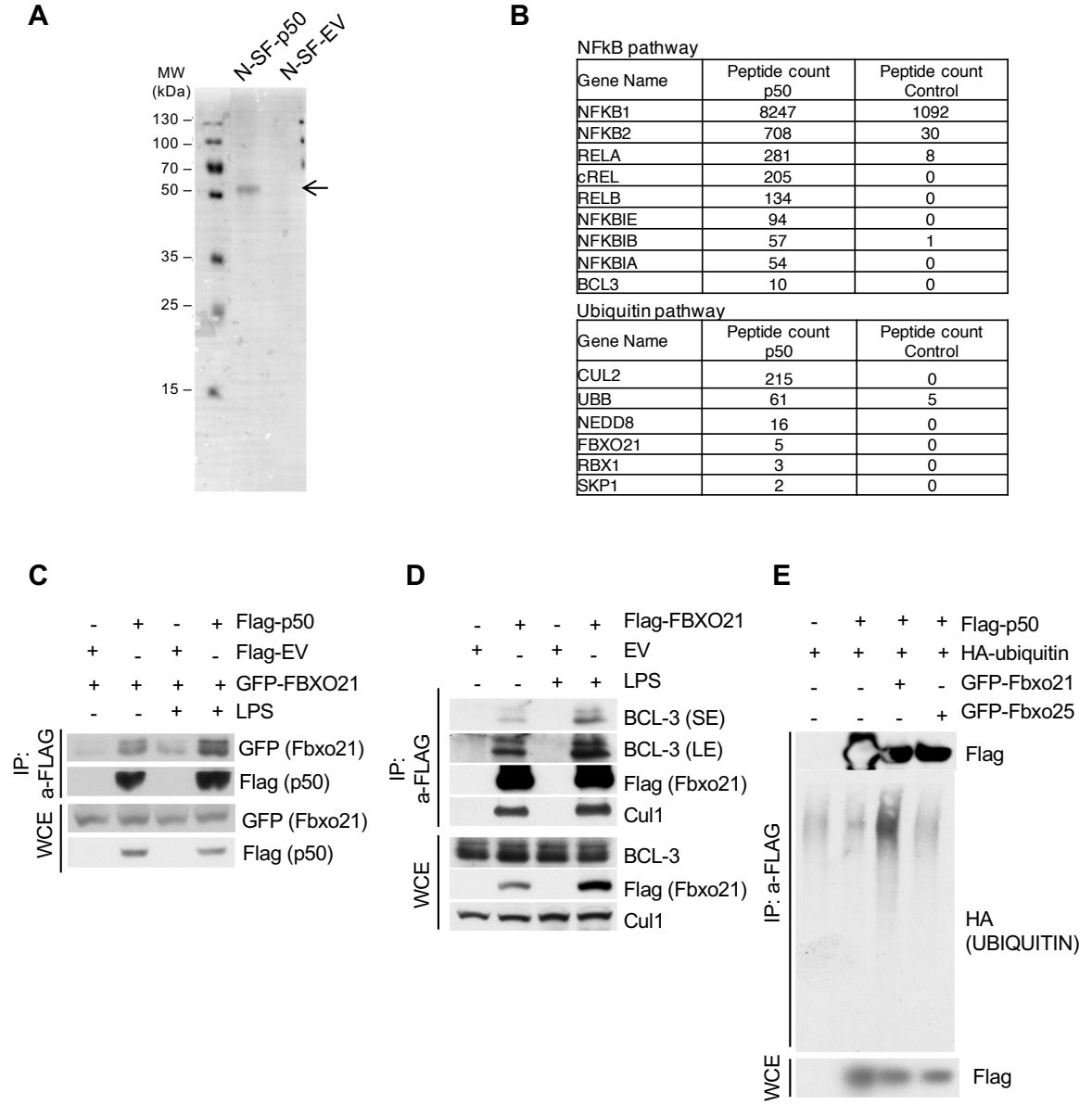

Figure 49. Identification of FBXO21 as a potential E3 ubiquitin ligase of NF-κB1/p50. A, Silver gel analysis of purified p50 protein. N-terminally Strep-FLAG-tagged p50 (N-SF-p50) or empty vector control (N-SF-EV) was expressed in $5x10^9$ HEK293T cells each and the resulting WCEs subjected to a sequential purification approach. First, tagged proteins were immobilized on Strep-Tactin beads, washed and eluted with desthiobiotin, before immunoprecipitation with anti-FLAG M2 gel and elution with 3x-FLAG-peptide. The eluted proteins were separated by SDS-PAGE and analyzed by mass spectrometry. The depicted silver stained gel contained 5% of the eluates and the arrow indicates a band at the expected molecular weight of STREP-FLAG-p50. **B,** Filtered and categorized interactors of p50 detected by mass spectrometry analysis of the purification experiment described in (A). **C,** Co-immunoprecipitation of FLAG-FBXO21 and GFP-p50 from cells treated with or without LPS. HEK293T cells were transfected with the indicated combinations of expression vectors and treated with vehicle or LPS prior to cell lysis. WCEs were subjected to FLAG-IP and immunoblot analysis using the indicated antibodies. **D,** Co-immunoprecipitation of FLAG-FBXO21 and endogenous BCL3 from cells treated as in (C). **E**, *In vivo* ubiquitylation assay of p50. HEK293T cells were transfected with indicated combinations of Flag-tagged p50, HA-ubiquitin and GFP-FBXO21 or GFP-FBXO25 (control). Following 3 hrs of treatment with MG132 (10 μM), WCEs were prepared and subjected to FLAG-immunoprecipitations (IP) under denaturing conditions. WCE and IPs were analyzed by immunoblotting using the indicated antibodies. SE - short exposure, LE – Long exposure. Data in A and B were provided by B. Targosz; C-E were provided by U. Baumann.

9.2 p50 does not interact with FBXO21 and is not destabilized upon cycloheximide treatment

In order to further verify the interaction between FBXO21 and p50, but also to identify factors that might play an important role in their crosstalk as described for other FBOX-proteins like ß-TrCP and PARP11 (Guo et al. 2019; Skaar, Pagan, and Pagano 2013), a second mass spectrometry-based screen for interaction partners of FBXO21 was conducted. In this case FBXO21 was used as bait. A tandem affinity purification (TAP) of STREP-FLAG-tagged FBXO21 and empty-vector control from about $3x10^9$ HEK293T cells per condition was performed. To visualize target protein enrichment, 2.5% of the precipitated eluates were subjected to SDS-PAGE followed by silver staining (Fig. 50A) and the remaining samples send for processing and mass spectrometry analysis to S. Klaeger at the Chair of Proteomics and Bioanalytics (TUM).

After bioinformatic workup, removal of known contaminants from the list of proteins identified by MS/MS, only a very limited number of proteins, mainly SCF-complex components (CUL1, SKP1) and chaperones like HSPs, remained as potential interactors (Fig. 50B).

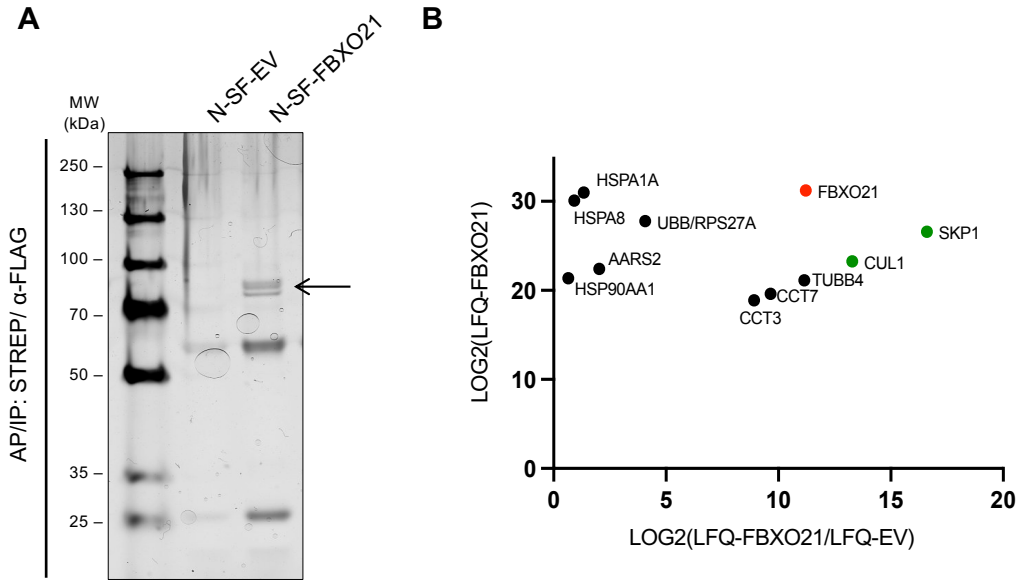

Figure 50. Mass spectrometry analysis of TAP purified FBXO21. A, Silver gel analysis of purified FBXO21 protein. N-terminally Strep-FLAG-tagged FBXO21 (N-SF-FBXO21) or empty vector control (N-SF-EV) was expressed in $3x10^9$ HEK293T cells each and the resulting WCEs subjected to a sequential purification approach. First, tagged proteins were bound to Strep-Tactin beads, washed and eluted with desthiobiotin, before immunoprecipitation with anti-FLAG M2 gel and elution with 3x-FLAG-peptide. The eluted proteins were separated by SDS-PAGE and analyzed by mass spectrometry (MS). The depicted silver stained gel contained 2.5% of the eluates and the arrow indicates a band at the expected molecular weight of STREP-FLAG-FBXO21. **B,** Mass spectrometric analysis of samples from (A). Co-purified proteins were identified by MS and log2 transformed ratios of FBXO21/EV LFQ intensity values were blotted against the logs2 transformed values of the FBXO21 sample. FBXO21 (bait) is marked in red and SCF-complex subunits in green. Data for B provided by S. Klaeger and B. Kuster (Chair of Proteomics and Bioanalytics, TUM).

To increase the number of potential interactors, FLAG-FBXO21 was purified from HEK293T cells (~$5x10^8$ cells per condition) stimulated with vehicle or tumor necrosis factor alpha (TNF-α) to induce NF-κB signaling in a subset of samples. Again, 2.5% per elution were TCA precipitated separately, target protein enrichment verified by SDS-PAGE and silver staining and the remaining samples send for MS/MS analysis to S. Klaeger (Fig. 51A). After the reduction from two to a single affinity purification step, this second screen identified a total of 2221 (untreated) and 2361 protein groups (TNF-α treated) in the different sample sets. The

intensity was set to 1000 to enable the calculation of a fold change when a protein was only identified in one of the samples. These proteins can be seen as the straight lines in the scatter blots (Fig. 51B).

The calculation of the fold changes in label free quantification (LFQ) intensities identified 936 (untreated) and 1527 (TNF-α treated) proteins that were enriched more than 2-fold in the FBXO21 purifications when compared to the respective empty vector control, with SCF-complex components and EID1, a known FBXO21 interactor (Watanabe, Yumimoto, and Nakayama 2015), among the top hits (Fig. 51B). The list of potential interactors contained some proteins well-known for their involvement in NF-κB regulation like COMMD-proteins and CCDC22 (Maine and Burstein 2007; Bartuzi, Hofker, and Van de Sluis 2013), TAX1BP1 (Shembade, Ma, and Harhaj 2010) and CHUK (Ghosh and Karin 2002; Kanayama et al. 2004). However, this affinity screen did not identify NF-κB1/p50 as interaction partner of FBXO21 (Fig 51B).

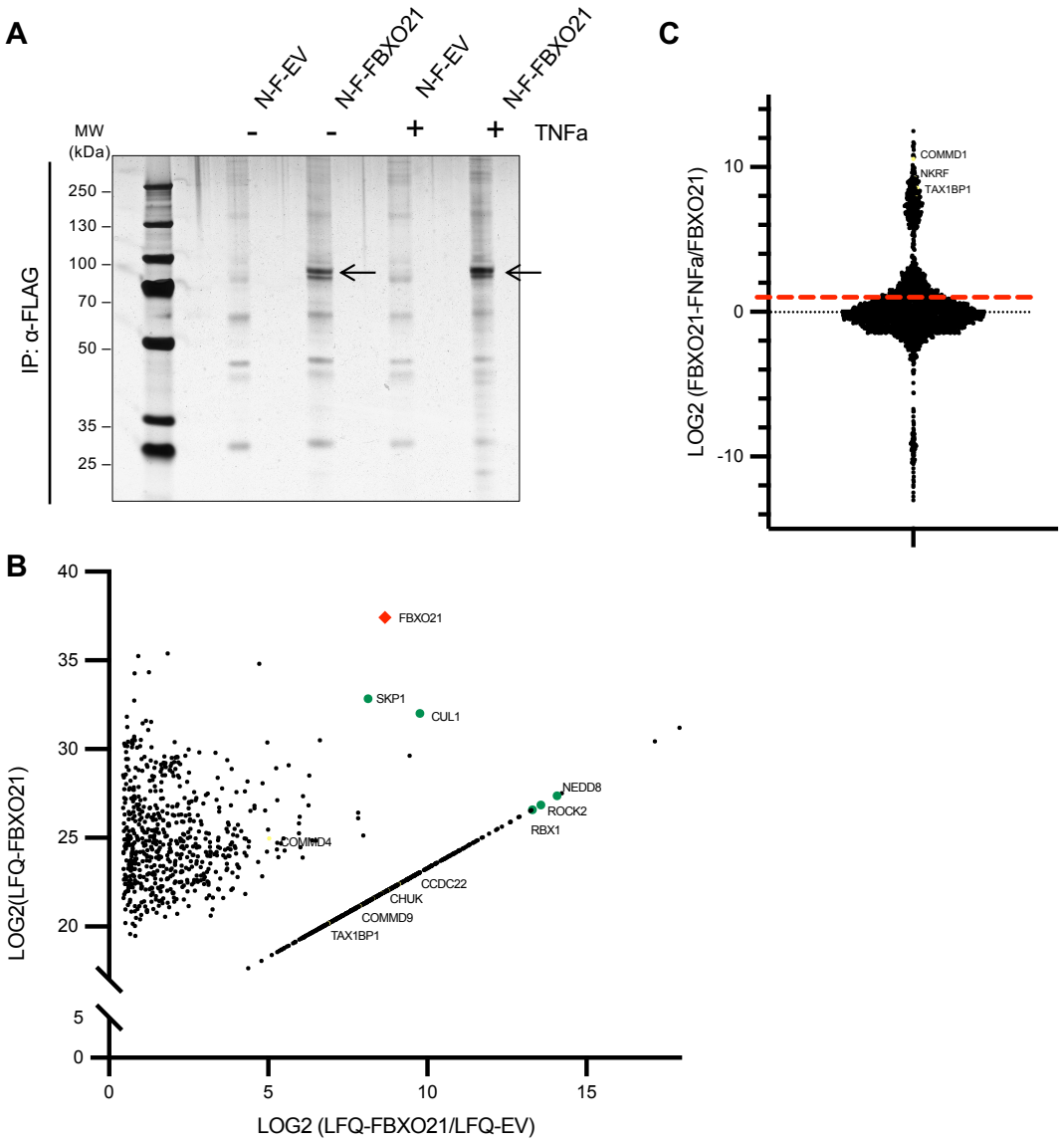

Figure 51. Mass spectrometry analysis of FLAG-purified FBXO21. A, Silver gel analysis of FLAG-purified FBXO21 protein. N-terminally FLAG-tagged FBXO21 (N-F-FBXO21) or empty vector control (N-F-EV) was expressed in $5x10^8$ HEK293T cells each and treated with TNF-α or not (2 hrs, 10 ng/mL) prior to samples collection. WCEs were subjected to immunoprecipitation using FLAG M2 affinity gel and subsequent elution with 3x-FLAG-peptide. The eluted proteins were separated by SDS-PAGE and analyzed by mass spectrometry (MS). The depicted silver stained gel contained 2.5% of the eluates and the arrows indicate the bands at the expected molecular weight of FLAG-FBXO21. **B,** Mass spectrometric analysis of the untreated samples from (A). Proteins co-purified with FBXO21 were identified by MS and log2 transformed ratios of FBXO21/EV LFQ intensity values were blotted against the logs2 transformed values of the FBXO21 sample. In case a protein group was only detected in one sample, an intensity of 1000 was imputed in the respective other sample. FBXO21 (bait) is marked in red, SCF-complex subunits in green and potential NF-κB regulators in yellow. **C,** Comparison of proteins co-purified with FBXO21 from untreated and TNF-α stimulated cells identified by mass spectrometric analysis from (A). Ratios of the LFQ intensity values of proteins identified in the FBXO21 untreated and TNF-a treated samples were log2 transformed and blotted by their enrichment rank. The red line indicates a two-fold enrichment and potential NF-κB regulators in yellow. Data for B and C provided by S. Klaeger and B. Kuster (Chair of Proteomics and Bioanalytics, TUM).

As the interaction between FBXO21 and NF-κB1/p50 presented in Figure 51 was not confirmed by this mass spectrometry interactome analyses for FBXO21, previous experiments were repeated and reproduced the interaction of the two proteins in a double overexpression setting using FLAG-tagged p50 as bait and GFP-tagged FBXO21 as the designated prey followed by FLAG-IP and analyzed by immunoblot (Fig. 52A).

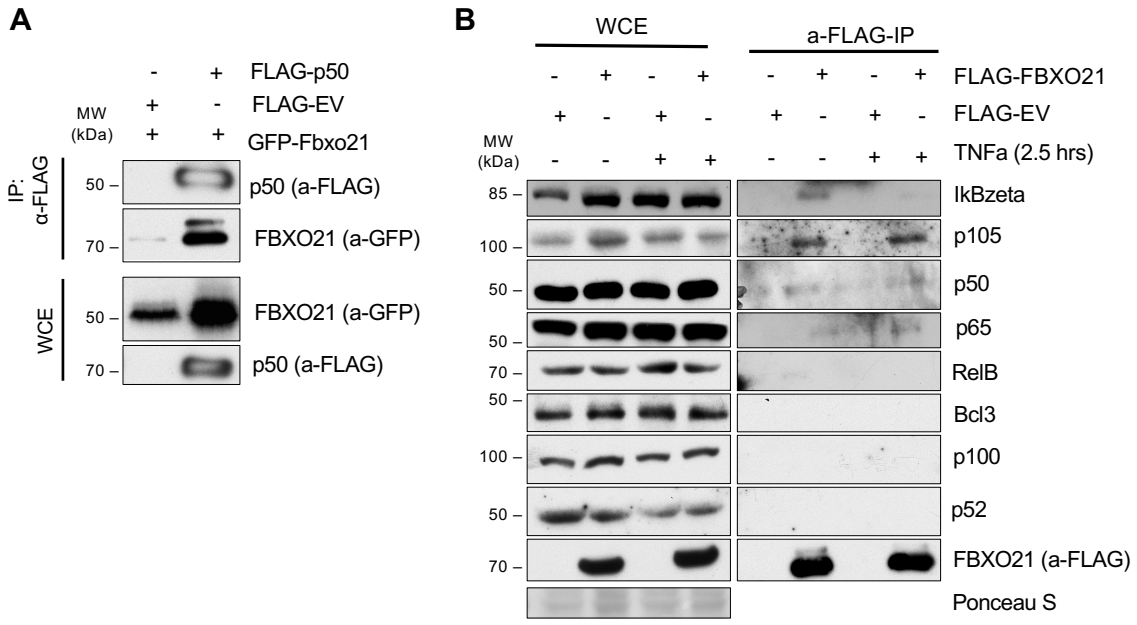

Figure 52. Semi-endogenous co-IP cannot reproduce FBXO21-p50 interaction. A, Co-immunoprecipitation of GFP-FBXO21 and FLAG-p50. HEK293T cells were transfected with the indicated combinations of expression vectors and WCEs subjected to FLAG-IP and immunoblot analysis using the indicated antibodies. **B,** Co-immunoprecipitation of FLAG-FBXO21 and various endogenous proteins of the NF-κB pathway. MCF-7 cells were transfected with FLAG-FBXO21 or empty vector control using Lipofectamnine2000 and supplemented with TNF-α (10 ng/mL; 2.5 hrs) or left untreated 24 hrs. WCE were subjected to FLAG-IPs and both analyzed by immunoblotting using the indicated antibodies. Ponceau S staining of the membrane was used as a loading control.

As HEK293T cells are not a very well established NF-κB model system, the experiments for endogenous and semi-endogenous interaction studies were carried out in the estrogen receptor positive (ER+) epithelial breast cancer cell line MCF-7, which is commonly used for studying NF-κB signaling (Khan et al. 2013; Faggioli et al. 1996). When transiently overexpressing FLAG-FBXO21 and immunoprecipitating it from MCF-7 cells with and without

TNF-α treatment, a weak but distinct interaction of FBXO21 with endogenous p105 and IκBzeta but not with p50 could be observed by immunoblotting (Fig. 52B). Treatment with TNF-α reduced the co-immunoprecipitation of IκBzeta but did not show any influence on the p105, p50 or p65 pulldown (Fig. 52B).

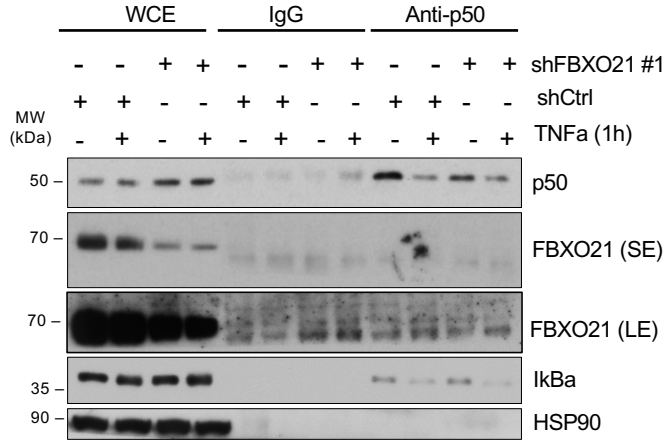

Figure 53. Endogenous p50 and FBXO21 do not interact. Co-immunoprecipitation of p50 and FBXO21 in an endogenous system. MCF-7 cells stably expressing the indicated shRNAs were supplemented with TNF-α (10 ng/mL; 1 h) or left untreated and WCE subjected to immunoprecipitation with anti-p50-antibody or the respective IgG control (both 1 µg/mL) and Protein-A agarose. WCEs and IPs were analyzed by immunoblotting using the indicated antibodies. HSP90 served as loading control. SE - short exposure, LE – Long exposure.

Next, endogenous p50 was immunoprecipitated from MCF-7 cells stably expressing a shRNA constructs targeting FBXO21 or the respective control construct let untreated or stimulated with TNF-α. Cleared lysates were incubated with anti-p50 antibody or the corresponding control IgG at 4°C overnight and incubated with Protein-A beads for 1.5 hrs to purify the antibody-protein complexes. After washing and SDS-PAGE, samples were subjected to immunoblot analysis. As expected, p50 interacted specifically with its well described repressor IκBα. However, no interaction of p50 with endogenous FBXO21 occurred (Fig. 53).

Having established, that FBXO21 was not interacting with p50 we next investigated whether FBXO21 was influencing p50 or its stability indirectly, irrespective of the two protein's interaction. A well-established method to probe for a protein's stability is the stalling of translation by inhibition of the ribosome using cycloheximide (CHX) in a time dependent manner(Fung et al. 2018; Dietachmayr et al. 2020). Immunoblot analysis of a treatment time course in HEK293T with or without overexpression of FBXO21 revealed that p50, as well as its precursor protein p105, were stable for at least 4 hrs of ribosomal inhibition, while the short lived, cell cycle regulated proteins CENTRIN-3 and PLK-1 (Dietachmayr et al. 2020) were decreased over time (Fig 54A). The degradation of the control proteins could be reversed by the simultaneous inhibition of the proteasome by MG132. This experiment also showed that endogenous as well as ectopically expressed FBXO21 was subjected to proteasomal degradation in a similar extend as the proteins included as controls (Fig. 54A, B). In order to check whether the degradation of p50 was stimulation dependent, MCF-7 cells with shRNA-mediated knock down, endogenous levels or stable lentiviral overexpression of FBXO21 were subjected to CHX treatment for up to 4 hrs. One sample set was simultaneously supplemented with TNF-α to trigger canonical NF-κB signaling. While the positive control CENTRIN-3 was readily degraded in the unstimulated samples, p50 and its precursor p105 protein levels were stable irrespective of the FBXO21 levels of the cells (Fig. 54B upper panel).

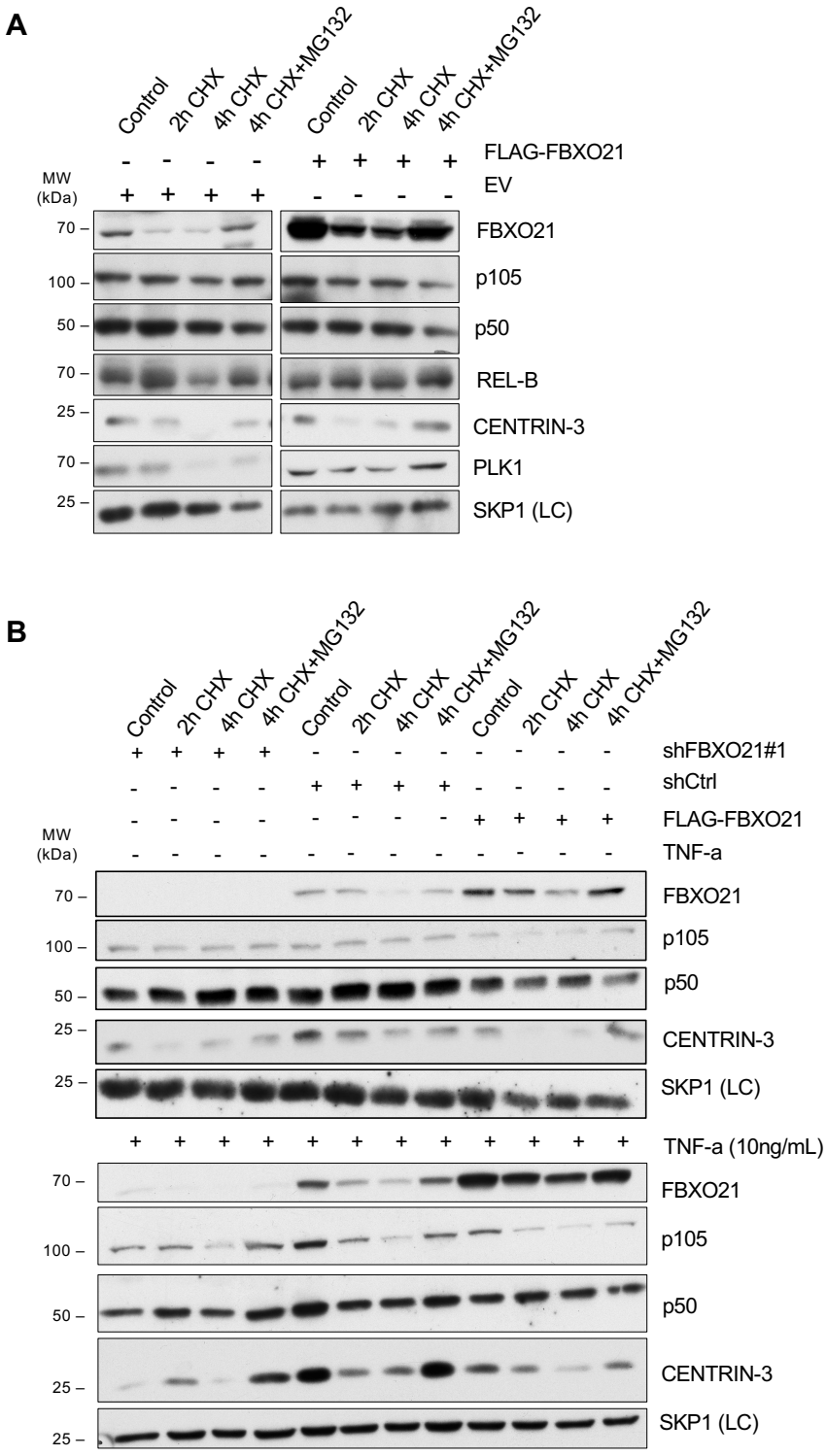

Figure 54: p50 is stable upon CHX treatment. A Immunoblot analysis of CHX treatment time course in HEK293T cells. Cells were transfected with FLAG-EV or FLAG-FBXO21 expression constructs and 24 hrs later treated with 200 µg/mL cycloheximide (CHX) and MG132 (10 µM) as indicated. Sample were harvested at the indicated time points and WCEs were subjected to immunoblot analysis using the indicated antibodies. SKP1 served as a loading control. **B** Immunoblot analysis of CHX treatment time course in MCF-7 cells. Cells stably expressing untagged FBXO21, a control shRNA or a shRNA directed against FBXO21 were treated with 200 µg/mL cycloheximide (CHX) and MG132 (10 µM) as indicated. A subset of samples was supplemented with TNF-α (10 ng/mL; lower panel). Sample were harvested at the indicated time points after treatment start and WCEs subjected to immunoblot analysis using the indicated antibodies. SKP1 served as a loading control (LC).

The addition of TNF-α induced degradation of NF-κB1/p50 precursor protein p105 when translation was inhibited by CHX addition. However, the degradation occurred independently of FBXO21 as knock down or overexpression did not alter p105 degradation and did not result in changes in p50 protein levels, when compared to the loading control (LC) (Fig. 54B, lower panel).

It is well described that the expression of and cleavage from its precursor p105 influence p50 protein levels. On the other hand, dynamic shuttling in and out of the nucleus with subsequent DNA binding is the step that allows the NF-κB transcription factor subunits to actually exert their function. Additionally, Carmody *et. al.* described the amount of DNA bound p50 to be altered in cells of BCL3 knock out mice in great details (Carmody et al. 2007). Therefore, p50 degradation might only occur in the nuclear compartment or in the proteins DNA bound state as described for p65 (Saccani et al. 2004; H. Li et al. 2012) and the analysis of whole cell lysates might thus be insufficient to detect changes in p50 protein levels. To analyze the stability of the nuclear/DNA bound p50, MCF-7 cells stably expressing shFBXO21 or shCtrl were subjected to a CHX time course over 4 hrs including a condition where MG132 was added for proteasomal inhibition. Extracted protein samples were separated into cytosolic and chromatin fractions and subsequently analyzed by immunoblotting (Fig. 55A left panel).

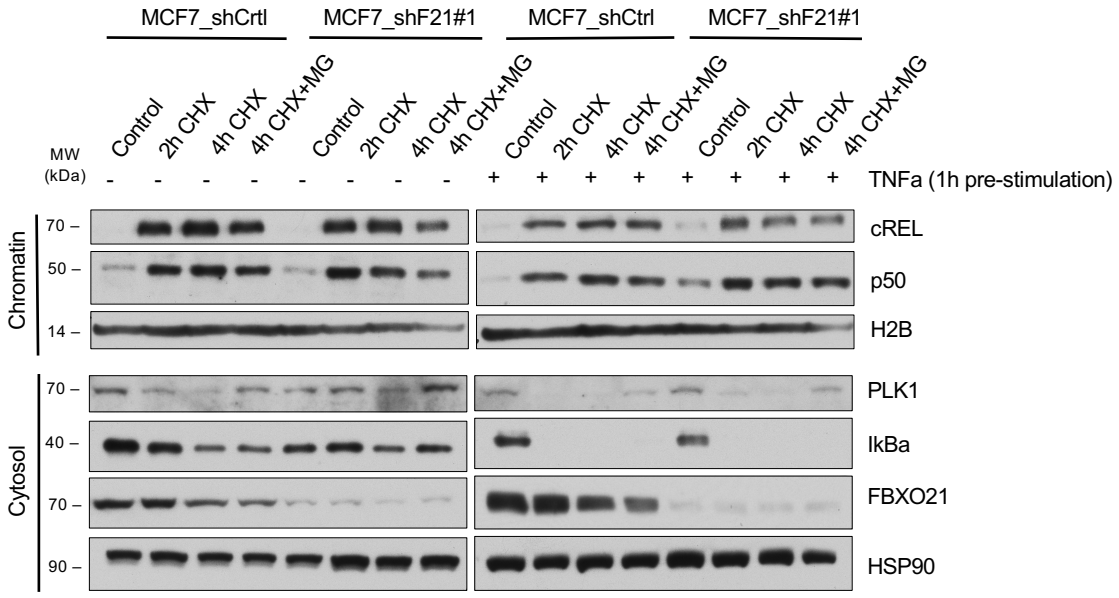

Figure 55: Levels of DNA bound p50 are stable upon CHX-treatment. Immunoblot analysis of MCF-7 chromatin fractions upon CHX and TNF-α treatment. MCF-7 cells stably expressing a control shRNA directed against FBXO21 were either left unstimulated (left panel) or supplemented with TNF-a (10 ng/mL, right panel). After 1 h of stimulation, cells were incubated with 200 µg/mL cycloheximide (CHX) and MG132 (10 µM) as indicated for different durations. Immediately after sample collection, pellets were fractionated into cytosolic and chromatin containing lysates and subjected to immunoblot analysis using the indicated antibodies. HSP90 and H2B served as the respective loading controls.

To control for pure subcellular fractions, Histone H2B was used as a chromatin specific loading control and the transcription factor c-REL for NF-κB specific comparison. Incubation with CHX alone was sufficient to induce degradation of IκBα in the cytoplasm with subsequent nuclear translocation and DNA binding of p50 as well as c-REL indicating an artificial, partial NF-κB response without a prior stimulus. The levels of p50 in untreated control chromatin fractions were very similar in FBXO21 knock down and control samples, as well as the amount of p50 that bound after 2 hrs of CHX incubation. After 4 hrs of ribosomal inhibition, no p50

destabilization was observed in either shFBXO21 or shCtrl samples. This protein distribution and stability were reflected by c-REL protein levels in the respective samples (Fig. 55 left panel). In order to induce NF-κB signaling and thereby the translocation of p50 as well as c-REL to the nucleus, cells were stimulated with TNF-α in presence of CHX (Fig. 55 right panel) and processed and analyzed as described above. Rapid IκBα degradation occurred in response to TNF-α stimulation, which implies a strong and persisting NF-κB activation in these samples, including the translocation of p50 and c-REL to the nucleus. Levels of chromatin bound p50 as well as c-REL were higher in the FBXO21 knock down samples before addition of CHX but no degradation of the two transcription factors or a difference in stability between FBXO21 knock down and control samples were observed over the time course of 4 hrs (Fig. 55 right panel).

As the observed translocation of p50 (and c-REL) to the nucleus upon ribosomal inhibition was not the result of genuine NF-κB and might have resulted in artificial effects, we aimed to study the chromatin bound p50 levels in steady state or after TNF-α induced translocation and the influence of FBXO21 knock down upon them. Thus, MCF-7 cells with or without lentiviral-induced depletion of FBXO21 were stimulated with TNF-α for the indicated time points. In a subset of samples, the proteasome was inhibited by addition of MG132 to check whether an accumulation of p50 occurred, which would be expected if this fraction was degraded in an UPS dependent manner. The fractionation and subsequent immunoblot analysis of these samples revealed no changes in p50 levels under steady state (no TNF-α treatment) conditions in either the cytosolic or nuclear compartment of the cell upon FBXO21 knock down or/and proteasomal inhibition (Fig. 56A).

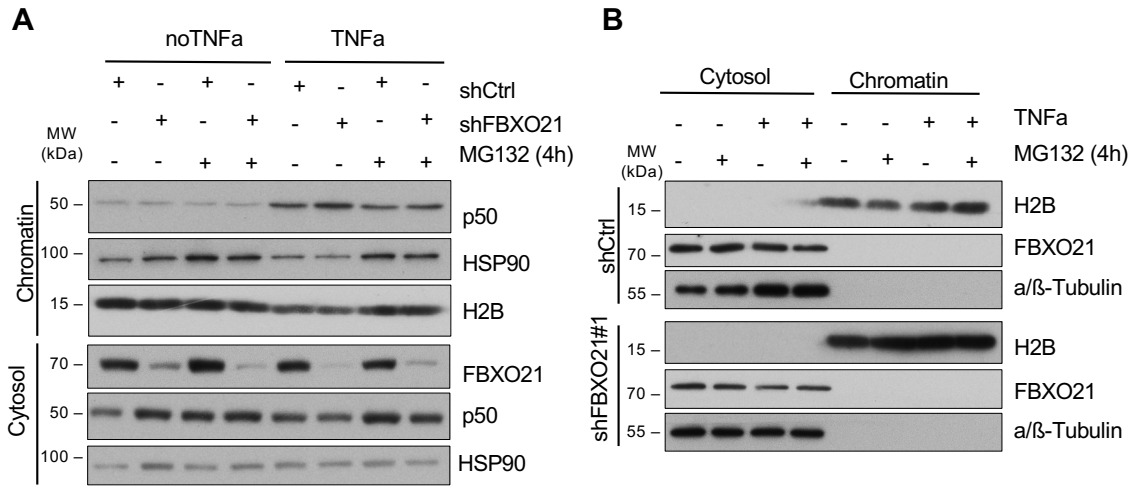

Figure 56: DNA bound p50 does not accumulate upon proteasomal inhibition. A Immunoblot analysis of MCF-7 chromatin fractions upon MG132 and TNF-α treatment. MCF-7 cells stably expressing a control shRNA or shRNA directed against FBXO21 were either left unstimulated or supplemented with TNF-α (10 ng/mL). After 1 h of stimulation, cells were incubated with MG132 (10 μM) for 4 hrs. Immediately after sample collection, pellets were fractionated into cytosolic and chromatin containing lysates and subjected to immunoblot analysis using the indicated antibodies. HSP90 and H2B served as the respective loading controls. **B**, Samples generated in (A) analyzed by immunoblot using the indicated antibodies in a revised order to serve as fractionation controls.

The nuclear translocation of p50 was robustly induced by 1 hrs TNF-α stimulation but did not change upon FBXO21 depletion. Additional inhibition of the proteasome did not lead to an accumulation of the protein in its DNA bound state independent of the cellular FBXO21 levels. Immunoblot analysis of the samples further showed a very good separation of the sub-cellular fractions (Fig. 56B) as neither a/ß-Tubulin was detected in the chromatin nor H2B in the

cytosolic fractions, making it unlikely any effects were masked by technical inadequacies. It was noticed that FBXO21 was exclusively detected in the cytosol.

9.3 NF-κB1/p50 is not ubiquitylated or degraded in murine BCL-3-/- cells

As the experiments in human cell lines irrespective of their FBXO21 levels did not reveal any effect on p50 or its degradation, the next step was to validate the data published by Carmody et. al. and others (Carmody et al. 2007; Liang Song et al. 2016). A special focus was on the ubiquitylation experiments in BCL3 knock out cells, as these data initiated the search for an E3-ubiquitn ligase at the very beginning of the project.

For this purpose, we obtained murine embryonic fibroblasts (MEFs) from BCL3 knock out (Bcl-3-/-) or wild type (Bcl-3+/+) mice from AG Algül (TUM). After confirming the BCL-3 knock out by immunoblot analysis (Fig. 57A), CHX chase experiments were preformed to determine the p50 half-life time in BCL-3 knock out cells. Immunoblotting of the samples revealed that NF-κB1/p50 was stable over a 24 hrs period of ribosomal inhibition, even if cells were treated with murine TNF-α simultaneously, while CENTRIN3, which served as a control protein, was degraded readily in a proteasome dependent manner (Fig. 57B).

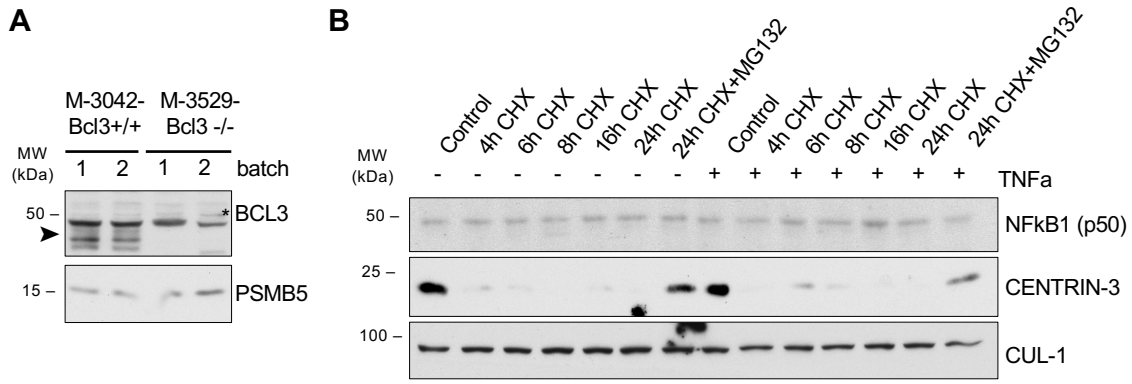

Figure 57. p50 levels are stable upon CHX treatment in BCL3 -/- MEFs. A Immunoblot analysis of two different batches of BCL3 WT and knock out murine embryonic fibroblasts (MEFs). BCL3 WT and knock out MEFs obtained from AG Algül (TUM) were tested for their BCL-3 expression by immunoblot using the indicated antibodies. The arrow indicates the band of expected size of BCL3 and the star an unspecific band produced by the BCL-3 antibody. PSMB5 served as a loading control. **B**, Immunoblot analysis of a CHX time course treatment in BCL-3 -/- cells. BCL-3 knock out MEFs were either left unstimulated or supplemented with TNF-a (10 ng/mL). After 1 h of stimulation, cells were incubated with 200 µg/mL cycloheximide (CHX) and MG132 (10 µM) as indicated for different durations. WCEs were analyzed by immunoblot using the indicated antibodies. CUL-1 served as a loading control.

In order to investigate if p50 was actually ubiquitylated in BCL-3-/- cells, an *in vivo* ubiquitylation assay was performed. Therefore, the indicated combinations of plasmids encoding for HA-Ubiquitin, empty vector control and murine FLAG-tagged p50 or -IKKα were transfected into BCL-3-/- cells. Before lysis, the cells were supplemented with MG132 for 4 hrs to enrich for ubiquitylated proteins, that might otherwise be degraded by the proteasome, and subjected to FLAG-IP under denaturing conditions. The analysis by immunoblotting revealed a strong HA-Ubiquitin signal for the IP of the positive control IKKα. This signal showed the characteristic laddering pattern from approximately the size of the protein towards higher molecular weights, representing polyubiquitylation forms of the immunoprecipitated protein (Fig 58, very right lane). This pattern could also be detected in longer exposures of the corresponding FLAG-

blot, indicating that the detected HA signal indeed represents covalently modified FLAG-IKKα. For p50 on the other hand, no such characteristic signal could be detected on either of the immunoblots (Fig. 58, second lane from the right), arguing against a polyubiquitylation of p50 in whole cell lysates.

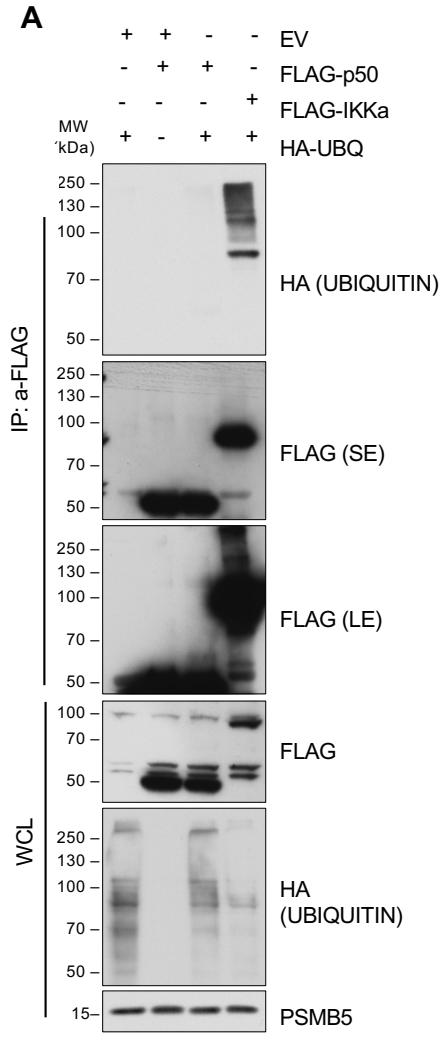

Figure 58. p50 lacks polyubiquitylation in BCL-3 knock out cells. *In vivo* ubiquitylation assay of p50 in BCL-3-/- MEFs. BCL-3 knock out cells were transfected with indicated combinations of Flag-tagged p50, HA-ubiquitin, FLAG-IKKa and EV-control using Lipofectamine2000. After 24 hrs cells were treated for 3 hrs of with MG132 (10 μM), WCEs were prepared and subjected to FLAG-immunoprecipitations (IP) under denaturing conditions. WCE and IPs were analyzed by immunoblotting using the indicated antibodies. SE - short exposure, LE – Long exposure. PSMB5 served as a loading control.

Next, the ubiquitylation of chromatin bound p50 protein was examined (Fig. 59). Therefore, another *in vivo* ubiquitylation assay was performed in BCL-3 -/- MEFs as described above, including a TNF-α stimulated condition. The resulting cell pellets were fractionated before denaturation of the chromatin fractions. Samples were then split in half to perform FLAG-IPs (Fig. 59A) and HA-IPs (Fig. 59B) under denaturing conditions which were subsequently analyzed by immunoblot. The quality of the fractionation was tested for every sample by immunoblot (Fig. 59C) and was, according to the marker proteins tested, considered sufficient to rule out an impact of cytosolic contamination on the results.

The IP of IKKα from these chromatin fractions produced the expected HA- and FLAG-signal pattern (Fig.59A, very right lane), comparable to protein purified from WCEs (Fig. 58A). FLAG-p50 was immunoprecipitated to a much greater extent than the positive control FLAG-IKKα. On longer exposures of the FLAG-blot, a distinct laddering of FLAG-signal above 50 kDa was observed irrespective of the co-overexpression of HA-ubiquitin or TNF-α addition and also in lanes containing FLAG-IKKα, indicating that the upwards shift detected for FLAG-p50 was an artefact of the anti-FLAG antibody.

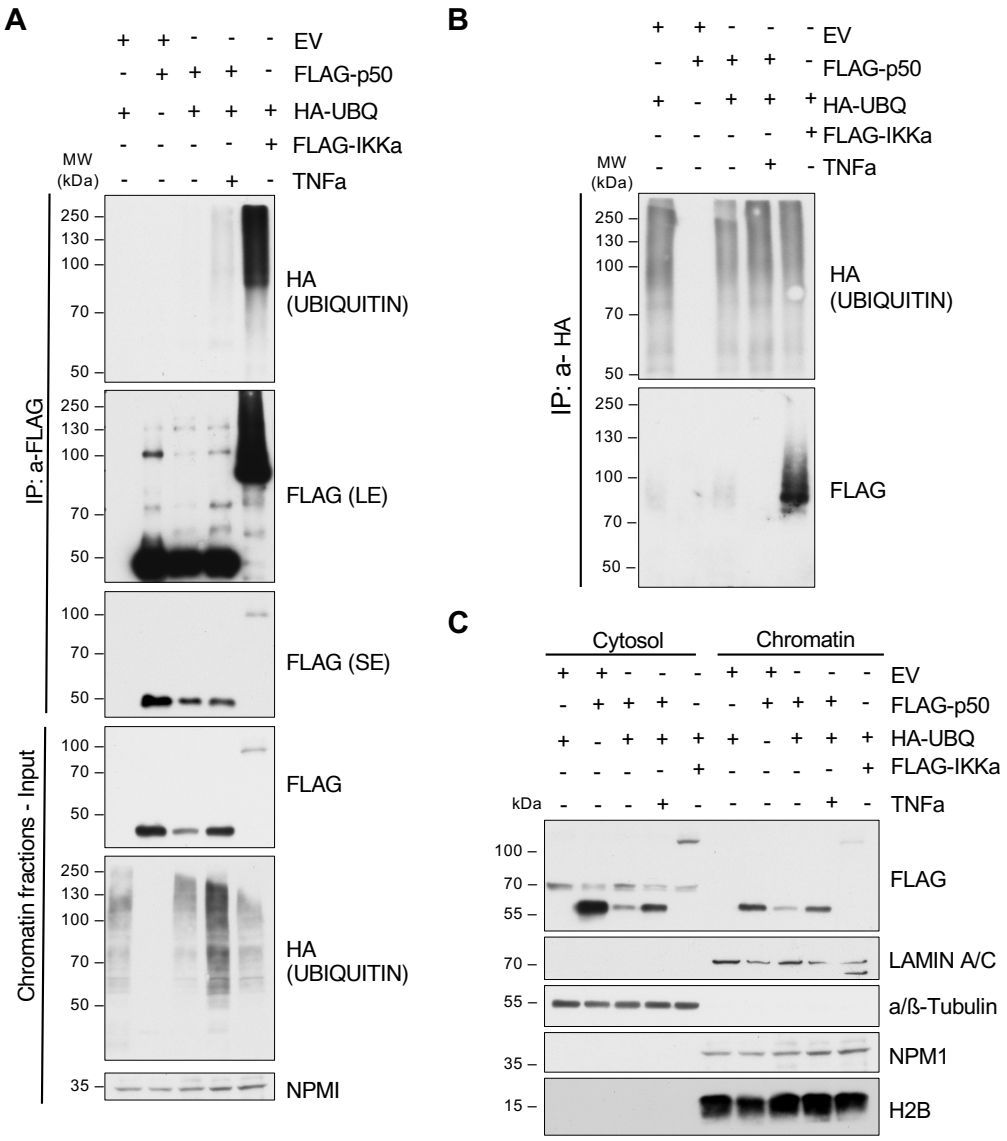

Figure 59. Chromatin bound p50 is not polyubiquitylated in BCL-3 knock out cells. A, B, *In vivo* ubiquitylation assay of chromatin bound p50 in BCL-3 -/- MEFs. BCL-3 knock out cells were transfected with indicated combinations of Flag-tagged p50, HA-ubiquitin, FLAG-IKKα and EV-control using Lipofectamine2000. After 24 hrs cells were either left untreated or treated with murine TNF-α (10 ng/mL) for 1 h, before addition of MG132 (10 μM) for 3 hrs. Immediately after sample collection, pellets were fractionated into cytosolic and chromatin containing lysates. **A**, Half of the Chromatin fraction were subjected to FLAG-IP under denaturing conditions and both analyzed by immunoblotting using the indicated antibodies. SE - short exposure, LE – Long exposure. NPMI served as a loading control. **B,** The remaining half of the chromatin fractions were subjected to HA-IP under denaturing conditions and analyzed by immunoblot using the indicated antibodies. **C,** Fractionation controls of the lysates used in (A) and (B). The cytosolic and chromatin fractions of the experiment described above were analyzed by immunoblot using the indicated antibodies.

The corresponding HA blots revealed a faint signal for HA-ubiquitin in the TNF-α treated p50 sample, which corresponded to much higher HA-ubiquitin levels in the input sample (Fig. 59A). The HA-IP performed with the other half of the lysates revealed that ubiquitylated FLAG-IKKα could be co-purified with HA-tagged ubiquitin but no specific signal for FLAG-p50 could be detected (Fig. 59B).

From this data we concluded that NF-κB1/p50 is neither polyubiquitylated nor degraded in BCL3 knock out cells.

9.4 FBXO21 does not influence NF-κB activity in MCF-7 cells

Even though p50 was neither found to be ubiquitylated nor degraded regardless of FBXO21 or BCL-3 levels protein levels within a cell, interactome analysis of FBXO21 by mass spectrometry identified a variety of NF-κB regulators as potential substrates. We therefore hypothesized that FBXO21 might influence NF-κB signaling in a p50 independent manner.

First, we checked whether NF-κB promotor occupancy was altered using an electrophoretic mobility shift assay (EMSA) with cleared nuclear extracts from MCF-7 cells stably expressing shRNA constructs targeting FBXO21 or the respective non-targeting control (Fig. 60). Again, a subset of samples was stimulated with TNF-α prior to fractionation. Equal amounts of cleared lysates were incubated with biotinylated dsDNA-probes specific for NF-κB (Saccani et al. 2004). An additional sample was supplemented with a 10-fold excess of unlabeled DNA-probe to verify the specificity of the detected signal. After native PAGE and crosslinking, the biotin coupled to the DNA-probes was detected using specific antibodies as described for immunoblotting. The detected signal seemed specific, as the biotinylated probe was easily outcompeted by its unlabeled counterpart (Fig. 60, very right lane) and minor differences were visible between FBXO21 depleted and control samples, irrespective of TNF-α treatment (Fig. 60).

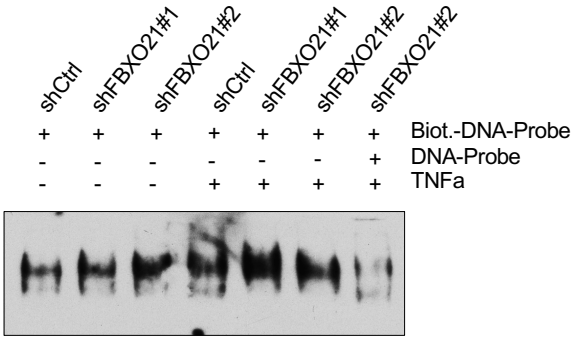

Figure 60. Amounts of NF-κB subunits bound to DNA upon FBXO21 knock down. Electrophoretic Mobility-Shift Assay (EMSA) using NF-κB-specific DNA-probes. MCF-7 cells stably expressing control or different FBXO21 targeting shRNA constructs were treated with TNF-α (10 ng/mL) for 1 h or left untreated. Immediately after sample collection, pellets were fractionated into cytosolic and nuclear lysates. The nuclear fractions were used as input material for an EMSA using NF-κB-specific biotinylated DNA-probes. As a specificity control, one sample was supplemented with 10-fold excess of unlabeled probe as indicated. Results were analyzed by native PAGE followed by immunoblot with an anti-biotin antibody.

Second, to follow up the EMSA results and investigate whether the differences in DNA occupancy resulted in altered NF-κB promotor activity, a commercially available dualGlow NF-κB-specific luciferase assay was performed (Fig. 61). For that, MCF-7 cells were transfected with either siCtrl or siFBXO21 using RNAiMAX and seeded 24 hrs later into a 96-well plate together with two different luciferase constructs according to the manufacturers' instructions. The day after, cells were stimulated with TNF-α for the indicated times in triplicates and the luminescence signal measured and analyzed (Fig. 61A). The analysis of the relative luminescence revealed no change in NF-κB promotor activity upon FBXO21 depletion irrespective of TNF-α stimulation. An immunoblot from cells harvested from additional wells of the 96-well plate prior to the luciferase detection confirmed the knock down of FBXO21 and the NF-κB stimulation (Fig. 61B).

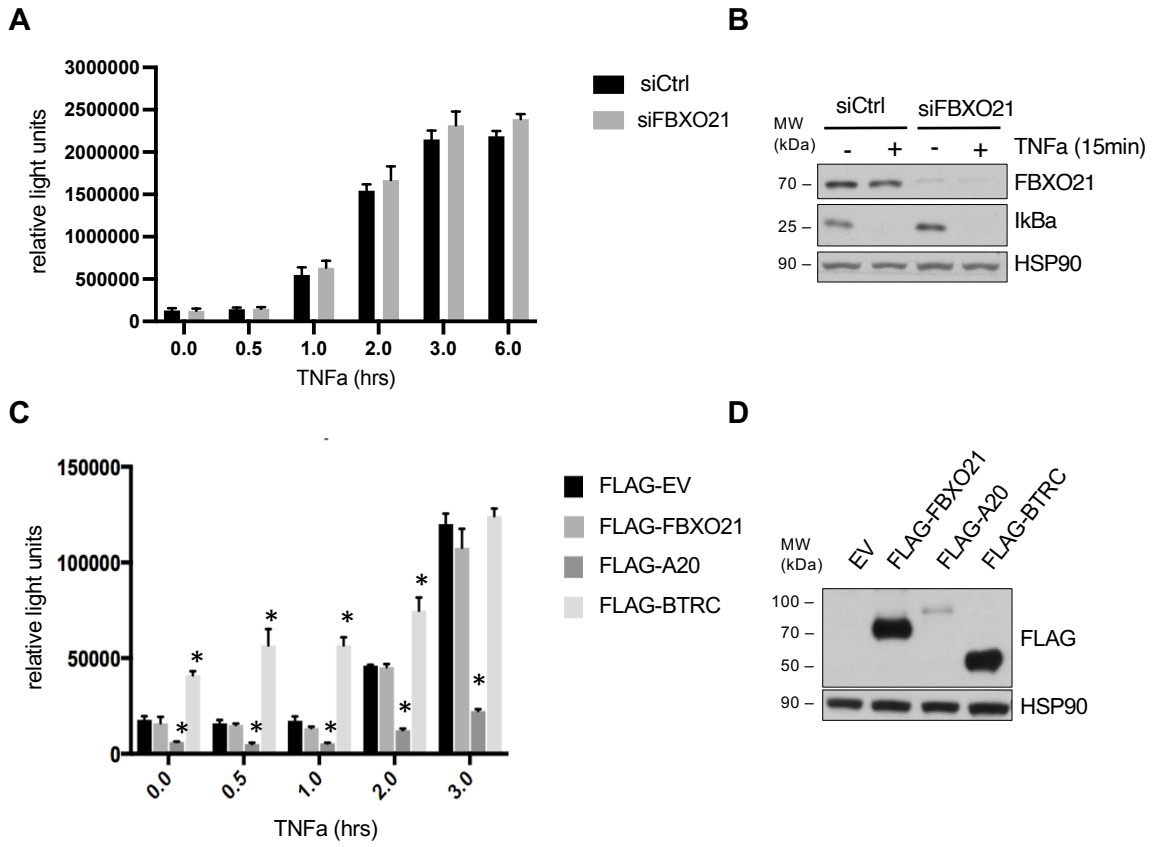

Figure 61. NF-κB reporter activity is independent of FBXO21. A, NF-κB luciferase reporter assay in FBXO21 knock down cells. MCF-7 cells were transfected with either siCtrl or siFBXO21 using RNAiMAX and seeded into a 96 well plate 24 hrs later. The wells contained two different luciferase constructs expressing the nanoLuc luciferase under the control of a constant PGK promotor and the fire-fly luciferase under the control of a NF-κB response element complexed with Lipofectmanine2000 in a reverse transfection setting. Another 24 hrs later three wells per condition were treated with TNF-α (10 ng/mL) for the indicated durations. The expression of the two different luciferases was measured by chemiluminescence signal detection using in a two-step process according to the manufacturer's instruction. The light units emitted by the inducible fire fly luciferase were normalized to emission by the PGK-driven one and plotted as relative light units per condition. **B,** Immunoblot analysis of cells used in (A) from additional wells of the 96-well plate prior to the luciferase detection using the indicated antibodies. HSP90 served as a loading control. **C**, NF-κB luciferase reporter assay in FBXO21 overexpressing cells. MCF-7 cells were seeded into a 96 well plate and transfected with the two different luciferase constructs described in (A) and an expression vector for either FLAG-EV, -FBXO21, -A20 or -BTRC using Lipofectamine2000. Cells were subjected to a TNF-α treatment time course followed by luciferase activity measurement as described in (A). Results were normalized and plotted as relative light units. *, P≤ 0.05 by Students T-test, corrected for multiple testing. **D,** Immunoblot analysis of cells used in (C) from additional wells of the 96-well plate prior to the luciferase detection using the indicated antibodies. HSP90 served as a loading control.

In case an increase in FBXO21 instead of a knock down would alter NF-κB signaling, FBXO21 was also overexpressed alongside ß-TrCP, A20 and an empty-vector control together with the two luciferase expression constructs in MCF-7 cells in a 96-well format (Fig. 61C). The day after transfection, three wells per condition/overexpression construct were stimulated with TNF-α for the indicated time points and the luciferase assay performed and analyzed according to the manufacturer's instructions. As expected, overexpression of A20 not only significantly reduced NF-κB promotor activity in unstimulated cells but significantly interfered with its induction by TNF-α, while overexpression of ß-TrCP had the opposite effect on promotor activity in the luciferase assay (Fig. 61C). Between empty vector control and FBXO21 overexpression, no significant difference was detected in unstimulated cells or upon TNF-α stimulation. To confirm that all constructs were properly expressed, three additional

unstimulated wells per condition were harvested and analyzed by immunoblot, revealing the expression of all three FLAG-tagged transgenes (Fig.61D).

The measurement of promotor activity in this type of assay is dependent on the transcription of luciferase which might be influenced by additional factors. Additionally, it does not depict the very early time points of the signaling cascade. We thus used MCF7 cells transfected with either siCtrl or siFBXO21 and performed a TNF-α stimulation time course and analyzed different time points by immunoblotting (Fig. 62). The blots revealed IKKα phosphorylation and IκBα degradation as early as 15 min after stimulation but did not reveal any changes in the activation dynamics when comparing FBXO21 depleted versus control cells. IκBα protein expression was reestablished 60 min after stimulation in both conditions.

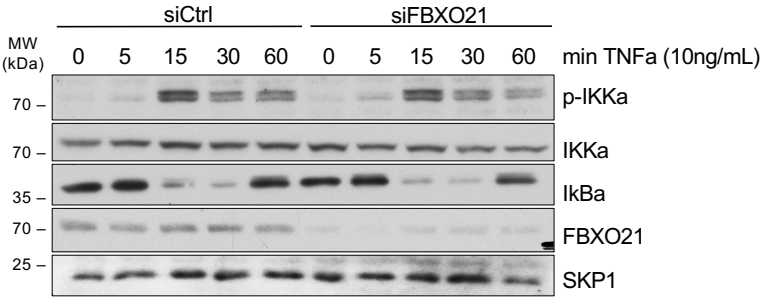

Figure 62 IKKα phosphorylation and IκBα degradation is independent of FBXO21. Immunoblot analysis of MCF-7 cells depleted of FBXO21 upon TNF-α treatment. MCF-7 cells transfected with either siCtrl or siFBXO21 using RNAiMAX were left unstimulated or supplemented with TNF-α (10 ng/mL) 48 hrs after transfection. Samples were collected at the indicated time points and WCEs subjected to immunoblot using the indicated antibodies. SKP1 served as a loading control.

In conclusion, these results show that FBXO21 is not a regulator of NF-κB signaling in the cell lines and conditions tested.

10. Discussion FBXO21

For over 30 years (Sen and Baltimore 1986b) NF-κB-signaling has been studied extensively and was found to be present in virtually every cell type and can be triggered by a variety of stimuli (Karin and Ben-Neriah 2000). Before stimulation the NF-κB transcription factors reside mainly in the cytoplasm due to their interaction with members of the IκB family. One of the central processes in which canonical NF-κB signaling converges is the ubiquitylation and subsequent degradation of the classical IκBs – IκBα, IκBβ and IκBeε – by the proteasome upon stimulation of the IKK complex through different stimuli (Hayden and Ghosh 2008). This rapid degradation process allows various NF-κB transcription factor dimers to translocate to the nucleus and modulate a transcriptional response (Q. Zhang, Lenardo, and Baltimore 2017). To halt transcription and prevent cellular exhaustion or hypo-responsiveness, IκBa and IκBe are able to bind to the DNA-bound transcription factors and shuttle them back to the cytoplasm(Hayden and Ghosh 2008). Another concept for the termination of NF-κB responses has emerged around the polyubiquitylation and subsequent proteasomal degradation of the nuclear fraction of the NF-κB-subunit p65 (Ryo et al. 2003) for which several E3-ligases have been described over the years (Tanaka, Grusby, and Kaisho 2007; Shin et al. 2017; Maine et al. 2007; Jodo et al. 2020). The same concept of nuclear proteasomal

degradation was proposed for the removal of transcription inhibiting p50:p50 homodimers from the DNA, which was described to be hindered by its interaction with the nuclear IκB BCL3 (Carmody et al. 2007; Collins, Kiely, and Carmody 2014). This study was thus set up to find a E3-ligase responsible for the ubiquitylation and degradation of the processed NF-κB-subunit p50.

Even though the back-then orphan E3-ligase FBXO21 was identified in a mass spectrometry based interactome screen using p50 as bait, no involvement of the E3-ligase in the protein's ubiquitylation or NF-κB signaling per se could be confirmed. Furthermore, no conclusive poly-ubiquitylation and no proteasomal degradation of p50 could be detected in BCL3 WT or knock out cells.

10.1 Endogenous p50 does interact with FBXO21

The emerging concept of ubiquitylation and proteasomal degradation for p65 as an additional means to tailor and restrict NF-κB signaling (Ryo et al. 2003; Tanaka, Grusby, and Kaisho 2007), prompted the question whether similar mechanisms applied for the remaining NF-κB subunits after they translocated to the nucleus. Carmody et. al. presented data showing the involvement of the UPS in the removal of the cleaved form of NF-κB1/p50 from the DNA. Even though the concept suggested by Carmody et al. evolved from BCL-3-knock out cells, they showed that ectopically expressed XP-tagged p50 was readily poly-ubiquitylated and degraded in HEK293T cells. The responsible, so far unidentified E3-ubiqiuitin ligase should therefore be detectable not only in the BCL3-knock out context.

Thus, the mass spectrometry based interactome screen using p50 as bait was performed in HEK293T and the co-purification of a wide variety of NF-κB pathway components validated the quality of the interaction screen (data by B. Targosz, Fig 49A-B). FBXO21 was co-purified as the only potential E3-ligase for p50 and therefore investigated further. First validation experiments were also conducted in HEK293T cells in a co-overexpression setting, which was shown to be affected by LPS stimulation (data by U. Baumann, Fig. 49C-D). This seemed counter intuitive, as HEK293T are described to lack the TLR4 receptor protein, which is necessary for LPS recognition and the respective downstream signaling. If used to explore signaling events upon LPS stimulation, these cells are transfected with the respective cell surface receptors (Tsukamoto et al. 2018), as even the electroporation with LPS failed to create a cellular response (Shi et al. 2014). It therefore seems not plausible that the binding between FBXO21 and p50 and/or BCL-3 was affected by the incubation with the compound.

The stimulus used to trigger canonical NF-κB signaling was therefore changed to TNF-a treatment, which verifiably resulted in IκBα degradation and translocation of NF-κB subunits to the nucleus (Fig. 55, 56, 60-62). The two mass-spectrometry based interaction screens, using FBXO21 as bait and including the activation of NF-κB signaling, identified up to 1527 protein groups in a single sample set (Fig. 51). Still, NF-κB1/p50 could not be detected. In three independent publications that propose substrates for FBXO21, interactome or 'ubiquitome' purifications in form of di-Gly/TUBE followed by MS were utilized to identify candidates. None of the screens detected an FBXO21/p50 interaction or differential ubiquitylation of NF-κB1 (Y. Yoshida et al. 2015; Watanabe, Yumimoto, and Nakayama 2015; Z. Lin et al. 2021). Immunoblot based interaction studies to follow up the initial MS finding in HEK293T and MCF-7 cells in the semi-endogenous and endogenous setting did not confirm specific interaction either (Fig. 52-53). If anything, there seemed to be an interaction with the NF-κB-precursor p105 (Fig. 52B), which reportedly resides in the cytoplasm (Cartwright, Perkins, and L Wilson 2016). While the cleaved NF-κB1-subunit p50 can translocate to the nucleus and is described to be endogenously ubiquitylated in its DNA bound state (Carmody

et al. 2007), FBXO21 could not be detected in nuclear or chromatin fractions (Fig. 56). These findings recapitulate published data for the FBOX protein's role in the ubiquitylation of EID1, which itself can translocate to the nucleus, but interacts with FBXO21 exclusively in the cytoplasm (Watanabe, Yumimoto, and Nakayama 2015).

After all, FBXO21 might have been co-purified with p50 because it is part of an (unrelated) SCF-complex (Pierce et al. 2013) and the central role of the UPS in NF-κB-signaling, especially the ß-TrCP mediated degradation of the IκBs and the processing of the NF-κB-precursor proteins (Karin and Ben-Neriah 2000).

10.2 FBXO21 does not influence p50 protein levels or NF-κB signaling

As interactions between a E3-ligase and one of its substrates might be too transient to detect, the question remained whether FBXO21 had an influence on the stability of endogenous p50 protein. Using cycloheximide to repress protein re-synthesis, various experiments showed that endogenous and overexpressed FBXO21 was degraded by the proteasome. In contrast, p50 remained stable, independent of (pre-)stimulation with TNF-α and up- or downregulation of FBXO21 over the time course of 4 hrs (Fig. 54,55), which covers the timeframe that was reported as the half-life for endogenous p50(Carmody et al. 2007). The analysis showing p50 degradation presented by Carmdoy et.al. shows the ^{35}S-methionine signal emitted by IPs of overexpressed or endogenous p50 from samples taken at different time points after pulse-labeling with ^{35}S-methionine. The IP levels of total p50 (and BCL-3) protein, which would be crucial to control for differences in the ^{35}S-methionine-signals, cannot be found in the publication (Carmody et al. 2007). This fact interferes with the conclusive interpretation of the results presented, especially when looking at the half-life time endogenous p50, where the ^{35}S-methionine-signals increase before restoring the initial levels.

The missing reduction of p50 levels when looking at whole cell lysates as presented in Figure 54 on the other hand, might be due to the limited proteolysis from its precursor p105, which keeps whole cell levels of p50 constant (Hayden and Ghosh 2008). Importantly, the constitutive processing of p105 is reported to take place at least in part co-translationally (L. Lin and Kobayashi 2003; Sun 2011), which is prevented by the applied cycloheximide treatment. Therefore, it seems unlikely that the processing of the precursor protein influenced whole-cell levels of p50 under steady state conditions to a greater extend, even though this was not ruled out experimentally. In addition to the co-translational processing, the limited proteolysis of p105 is enhanced upon NF-κB stimulation (Sun 2011; Cartwright, Perkins, and L Wilson 2016). In the data presented, a reduction of p105 during cycloheximide mediated inhibition of translation in combination with TNF-α stimulation was detected (Fig. 54B, lower panel), indicating that the protein might indeed be processed to p50. Another possibility explaining the reduction of p105 is that the entire 105 kDa precursor protein was degraded by ß-TrCP-mediated proteasomal degradation, a phenomenon reported to take place after stimulation of the NF-κB-pathway (Kravtsova-Ivantsiv et al. 2015).

A similar issue arises with DNA-bound p50 subunits. NF-κB transcription factor subunits are known to shuttle in and out of the nucleus dynamically (Karin and Ben-Neriah 2000) and the stability of a given subunit bound to DNA might therefore be hard to determine without the complete inhibition of nuclear import and export (Tanaka, Grusby, and Kaisho 2007; Saccani et al. 2004). To control for these general changes in subunit export and import, when assessing the stability/shuttling dynamics of DNA bound p50, c-Rel was used as a NF-κB specific control (Fig. 55). Importantly, the two proteins showed almost identical behavior over time independent of the FBXO21 levels within the cell, indicating no specific regulation of

cleaved NF-κB1/p50. Furthermore, the nuclear export of DNA-bound NF-κB-subunits is attributed to newly synthesized IκBα and IκBβ (Ruland 2011; Ghosh and Karin 2002), a process that is inhibited by cycloheximide treatment, and might therefore not conceal changes in p50 levels bound to DNA. Together with the lack of differences in DNA-bound p50 upon MG132 treatment, which blocks the degradation of the cytoplasmic IκBs and therefore most of the TF factor shuttling (Kanarek and Ben-Neriah 2012), this led us to believe that FBXO21 does not influence p50 stability or dynamics and p50 appeared stable throughout all experiments performed.

Even though a specific interaction between FBXO21 and p50 could not be confirmed experimentally, the E3-ligase pulled down a variety of NF-κB-regulators (Fig. 51). This led to the hypothesis that it might still influence NF-κB signaling. To test this hypothesis, a variety of NF-κB read out systems, including EMSAs (Fig. 60), NF-κB luciferase reporter assays (Fig. 61) and immunoblot based pathway analysis (Fig. 62), were used in addition to subcellular fractionations to monitor NF-KB-subunit shuttling (Fig. 55, 56).

All of these experiments failed to show a modulation of the signaling pathway by FBXO21. In order to trigger NF-κB signaling, TNF-α was applied to cells, which produced a very robust canonical NF-κB-response. If FBXO21 targeted an NF-κB effector for ubiquitylation, which was not related to TNF-receptor/TLR4 signaling but upstream of the IKK complex, known to be the essential for signal integration of the canonical pathway(Neil D. Perkins 2007), it effects might have been missed in those assays. When looking at the pathway modulators present in the MS-hit list though, all possible candidates were either involved in the negative or down-regulation of the canonical signaling pathway in a stimulus independent fashion like the COMMD-proteins and CCDC22 (Maine and Burstein 2007; Bartuzi, Hofker, and Van de Sluis 2013). Furthermore, FBXO21 did not score in a CRISPR-Cas9 based loss of function drop out screen performed in the NF-κB-driven ABC-type DLBCL cell line Oci-LY10 (data R. Spallek, not part of this thesis) and in a genome-wide siRNA screen for NF-κB modulators using the Epstein–Barr virus (EBV) latent membrane protein 1 (LMP1) as an activation signal (Gewurz et al. 2012). A study by Yu et al. that describes FBXO21 as an E3-ligase for ASK1 and its role in the antiviral immune response, specifically investigated the proteins role in NF-κB signaling and did not report an effect on the pathways activity in steady state or upon viral infection (Z. Yu et al. 2016). The other described ubiquitylation substrates of FBXO21 namely NR2F2 (Jiang et al. 2021), TARS (Y. Yoshida et al. 2015), EID1 (Watanabe, Yumimoto, and Nakayama 2015; Y. Yoshida et al. 2015) and P-glycoprotein (Ravindranath et al. 2015) are also not proposed to have a direct influence of NF-κB-signaling.

Due to the lack of evidence that FBXO21 was involved in NF-κB-signaling, other potential ubiquitylation substrates identified by mass-spectrometry were not followed up upon.

10.3 p50 is not polyubiquitylated in BCL-3 knock out cells

After being unbale to confirm the degradation of p50 in BCL-3 WT cells, BCL-3 knock out MEFs were used to reproduce the data of the publication reporting the p50 polyubiquitylation(Carmody et al. 2007). Carmody et al. found the degradation of endogenous p50 protein to depend on the absence or low expression of the nuclear IκB BCL-3, which they reasoned would otherwise stabilize the inhibitory homodimer in its DNA bound state (Carmody et al. 2007). Others reported that BCL-3 removed the p50:p50 dimer from IκB-promotor sites to allow activating dimers like p65:p50 to access the respective stretches of DNA or even described the atypical IκB to be a transcriptional co-activator for p50 and p52 homodimers, that lack a transactivation domain (TAD) (Perkins 2006; Hayden and Ghosh 2004). To this day,

the role of BCL-3 in the regulation of NF-κB-signaling remains debated (Truscott and Sinclair 2019; Schuster et al. 2013).

In vivo ubiquitylation assays in both WCEs and chromatin fractions of BCL-3-KO MEFs did not confirm that p50 is polyubiquitylated (Fig. 58, 59) and p50 was stable over a period of 24 hrs irrespective of NF-κB stimulation (Fig. 57). Importantly, to this day no E3-ubiquitin ligase for the polyubiquitylation of p50 has been proposed. Recently, the BARD1/BRCA1 complex has been reported to mono-ubiquitylate p50 upon ATR stimulation and during S-phase to promote its stability (Wu et al. 2020). The ubiquitylation assays performed by Wu et al. additionally produced a poly-ubiquitin banding pattern upon overexpression of the ligase complex. This might stem from background binding of other ubiquitylated proteins though, as the IPs were not conducted under denaturing conditions. In line with that, an *in vitro* ubiquitylation assay by Wu and colleagues using recombinant proteins shows HIS-tagged p50 to be mono-ubiquitylation in but fail to produce a poly-ubiquitin pattern as seen in the cellular assays (Wu et al. 2020).

Therefore, we conclude that p50 is not polyubiquitylated and degraded by the proteasome under the applied conditions.

11. Acknowledgments

The projects presented in this thesis would not have been possible without the scientific and moral support of many people.

First of all, I want to thank my supervisor Prof. Dr. Florian Bassermann for giving me the opportunity to conduct the research leading to this dissertation in his laboratory, countless fruitful scientific discussions and support throughout! Second, I want to thank my second thesis advisory committee member and collaborator Prof. Dr. Bernhard Kuster and his team – especially Jana Zecha, Susan Klaeger, Piero Giansanti and Julia Mergner – for their invaluable support by providing and discussing mass spectrometry data that were crucial for all three projects. A big thank you also goes to Andreas Kratzert, Iana Gadjalova and Selina Keppler for providing me with murine B-cell and B-cell lymphoma samples, the knowledge on how to conduct and interpret experiments with them and for solving a lot of my FACS-related issues! Additionally, I want to thank all the current and former members of the Bassermann lab for the countless hours spend in the lab together, especially Carmen Paulmann for her introduction to the world of DUBs and cell cycle biology, Petra Schenk and Isabell Schäffer for an unprecedented amount of technical and moral support, Oleksandra Karpiuk for being a great mentor and David Brockelt for the encouragement, important scientific advice in difficult times and being a great friend.

Finally, I would like to thank my family and friends for their support, understanding and patience during the last six years.

12. Publication

Carmen Paulmann*, Ria Spallek*, Oleksandra Karpiuk, Michael Heider, Isabell Schäffer, Jana Zecha, Susan Klaeger, Michaela Walzik, Rupert Öllinger, Thomas Engleitner, Matthias Wirth, Ulrich Keller, Jan Krönke, Martina Rudelius, Susanne Kossatz, Roland Rad, Bernhard Kuster, Florian Bassermann. “The OTUD6B-LIN28B-MYC axis determines the proliferative state in multiple myeloma”. Manuscript under review

*Equal contribution

13. References

Adams, Richard R., Mar Carmena, and William C. Earnshaw. 2001. “Chromosomal Passengers and the (Aurora) ABCs of Mitosis.” *Trends in Cell Biology* 11 (2): 49–54. https://doi.org/10.1016/S0962-8924(00)01880-8.

Alexandrov, Ludmil B., Serena Nik-Zainal, David C. Wedge, Samuel A.J.R. Aparicio, Sam Behjati, Andrew V. Biankin, Graham R. Bignell, et al. 2013. “Signatures of Mutational Processes in Human Cancer.” *Nature* 500 (7463): 415–21. https://doi.org/10.1038/nature12477.

Alizadeh, Ash A., Michael B. Elsen, R. Eric Davis, Ch L. Ma, Izidore S. Lossos, Andreas Rosenwald, Jennifer C. Boldrick, et al. 2000. “Distinct Types of Diffuse Large B-Cell Lymphoma Identified by Gene Expression Profiling.” *Nature* 403 (6769): 503–11. https://doi.org/10.1038/35000501.

Anshabo, Abel Tesfaye, Robert Milne, Shudong Wang, and Hugo Albrecht. 2021. “CDK9: A Comprehensive Review of Its Biology, and Its Role as a Potential Target for Anti-Cancer Agents.” *Frontiers in Oncology* 11 (May): 1–24. https://doi.org/10.3389/fonc.2021.678559.

Asante, David, Nicola L. Stevenson, and David J. Stephens. 2014. “Subunit Composition of the Human Cytoplasmic Dynein-2 Complex.” *Journal of Cell Science* 127 (21): 4774–87. https://doi.org/10.1242/jcs.159038.

Bai, Chang, Partha Sen, Kay Hofmann, Lei Ma, Mark Goebl, J.Wade Harper, and Stephen J. Elledge. 1996. “SKP1 Connects Cell Cycle Regulators to the Ubiquitin Proteolysis Machinery through a Novel Motif, the F-Box.” *Cell* 86 (2): 263–74. https://doi.org/10.1016/S0092-8674(00)80098-7.

Balzeau, Julien, Miriam R. Menezes, Siyu Cao, and John P. Hagan. 2017. “The LIN28/Let-7 Pathway in Cancer.” *Frontiers in Genetics* 8 (MAR): 1–16. https://doi.org/10.3389/fgene.2017.00031.

Bard, Jared A M, Ellen A Goodall, Eric R Greene, Erik Jonsson, Ken C Dong, and Andreas Martin. 2018. “Structure and Function of the 26S Proteasome.” *Annual Review of Biochemistry* 87 (June): 697–724. https://doi.org/10.1146/annurev-biochem-062917-011931.

Barnum, Kevin J, and Matthew J O’Connell. 2014. “Cell Cycle Regulation by Checkpoints.” *Methods in Molecular Biology (Clifton, N.J.)* 1170: 29–40. https://doi.org/10.1007/978-1-4939-0888-2_2.

Barr, Alexis R., and Fanni Gergely. 2007. “Aurora-A: The Maker and Breaker of Spindle Poles.” *Journal of Cell Science* 120 (17): 2987–96. https://doi.org/10.1242/jcs.013136.

Bartek, Jiri, and Jiri Lukas. 2003. “Chk1 and Chk2 Kinases in Checkpoint Control and Cancer.” *Cancer Cell* 3 (5): 421–29. https://doi.org/10.1016/S1535-6108(03)00110-7.

Bartuzi, Paulina, Marten H. Hofker, and Bart Van de Sluis. 2013. “Tuning NF-KB Activity: A Touch of COMMD Proteins.” *Biochimica et Biophysica Acta - Molecular Basis of Disease* 1832 (12): 2315–21. https://doi.org/10.1016/j.bbadis.2013.09.014.

Bassermann, Florian, Ruth Eichner, and Michele Pagano. 2014. “The Ubiquitin Proteasome System - Implications for Cell Cycle Control and the Targeted Treatment of Cancer.” *Biochimica et Biophysica Acta - Molecular Cell Research* 1843 (1): 150–62. https://doi.org/10.1016/j.bbamcr.2013.02.028.

Bassermann, Florian, Christine von Klitzing, Silvia Münch, Ren-Yuan Bai, Hiroyuki Kawaguchi, Stephan W. Morris, Christian Peschel, and Justus Duyster. 2005. “NIPA Defines an SCF-Type Mammalian E3 Ligase That Regulates Mitotic Entry.” *Cell* 122 (1): 45–57. https://doi.org/10.1016/j.cell.2005.04.034.

Basso, Katia, and Riccardo Dalla-Favera. 2015. “Germinal Centres and B Cell Lymphomagenesis.” *Nature Reviews Immunology* 15 (3): 172–84. https://doi.org/10.1038/nri3814.

Baumann, Ursula, Vanesa Fernández-Saíz, Martina Rudelius, Simone Lemeer, Roland Rad, Anna Maria Knorn, Jolanta Slawska, et al. 2014. “Disruption of the PRKCD-FBXO25-HAX-1 Axis Attenuates the Apoptotic Response and Drives Lymphomagenesis.” *Nature Medicine* 20 (12): 1401–9. https://doi.org/10.1038/nm.3740.

Berland, Robert, and Henry H Wortis. 2002. “Origins and Functions of B-1 Cells with Notes on the Role of CD5.” *Annual Review of Immunology* 20 (1): 253–300. https://doi.org/10.1146/annurev.immunol.20.100301.064833.

Bettencourt-Dias, Mónica, and David M. Glover. 2007. “Centrosome Biogenesis and Function: Centrosomics Brings New Understanding.” *Nature Reviews Molecular Cell Biology* 8 (6): 451–63. https://doi.org/10.1038/nrm2180.

Bianchi, Giada, Laura Oliva, Paolo Cascio, Niccolò Pengo, Francesca Fontana, Fulvia Cerruti, Andrea Orsi, et al. 2009. “The Proteasome Load versus Capacity Balance Determines Apoptotic Sensitivity of Multiple Myeloma Cells to Proteasome Inhibition.” *Blood* 113 (13): 3040–49. https://doi.org/10.1182/blood-2008-08-172734.

Blanc, Pascal, Ludovic Moro-Sibilot, Lucas Barthly, Ferdinand Jagot, Sebastien This, Simon De Bernard, Laurent Buffat, et al. 2016. “Mature IgM-Expressing Plasma Cells Sense Antigen and Develop Competence for Cytokine Production upon Antigenic Challenge.” *Nature Communications* 7. https://doi.org/10.1038/ncomms13600.

Blom, Bianca, and Hergen Spits. 2006. “Development of Human Lymphoid Cells.” *Annual Review of Immunology* 24 (1): 287–320. https://doi.org/10.1146/annurev.immunol.24.021605.090612.

Bonelli, Mara, Silvia La Monica, Claudia Fumarola, and Roberta Alfieri. 2019. “Multiple Effects of CDK4/6 Inhibition in Cancer: From Cell Cycle Arrest to Immunomodulation.” *Biochemical Pharmacology* 170 (December): 113676. https://doi.org/10.1016/j.bcp.2019.113676.

Borg, Natalie A., and Vishva M. Dixit. 2017. “Ubiquitin in Cell-Cycle Regulation and Dysregulation in Cancer.” *Annual Review of Cancer Biology* 1 (1): 59–77. https://doi.org/10.1146/annurev-cancerbio-040716-075607.

Boudreaux, David A, Tushar K Maiti, Christopher W Davies, and Chittaranjan Das. 2010. “Ubiquitin Vinyl Methyl Ester Binding Orients the Misaligned Active Site of the Ubiquitin Hydrolase UCHL1 into Productive Conformation.” *Proceedings of the National Academy of Sciences* 107 (20): 9117 LP – 9122. https://doi.org/10.1073/pnas.0910870107.

Buetow, Lori, and Danny T. Huang. 2016. “Structural Insights into the Catalysis and Regulation of E3 Ubiquitin Ligases.” *Nature Reviews Molecular Cell Biology* 17 (10): 626–42. https://doi.org/10.1038/nrm.2016.91.

Busino, Luca, Maddalena Donzelli, Massimo Chiesa, Daniele Guardavaccaro, Dvora Ganoth, N. Valerio Dorrello, Avram Hershko, Michele Pagano, and Giulio F. Draetta. 2003. “Degradation of Cdc25A by β-TrCP during S Phase and in Response to DNA Damage.” *Nature*

426 (6962): 87–91. https://doi.org/10.1038/nature02082.

Cai, Yuqi, Yuehong Yang, Minhong Shen, and Tianhua Zhou. 2009. “Inhibition of Cytokinesis by Overexpression of NudCL That Is Localized to the Centrosome and Midbody.” *Cell Research* 19 (11): 1305–8. https://doi.org/10.1038/cr.2009.118.

Calame, K. L. 2001. “Plasma Cells: Finding New Light at the End of B Cell Development.” *Nature Immunology* 2 (12): 1103–8. https://doi.org/10.1038/ni1201-1103.

Canning, Peter, Christopher D.O. Cooper, Tobias Krojer, James W. Murray, Ashley C.W. Pike, Apirat Chaikuad, Tracy Keates, et al. 2013. “Structural Basis for Cul3 Protein Assembly with the BTB-Kelch Family of E3 Ubiquitin Ligases.” *Journal of Biological Chemistry* 288 (11): 7803–14. https://doi.org/10.1074/jbc.M112.437996.

Cardozo, Timothy, and Michele Pagano. 2004. “The SCF Ubiquitin Ligase: Insights into a Molecular Machine.” *Nature Reviews Molecular Cell Biology* 5 (9): 739–51. https://doi.org/10.1038/nrm1471.

Carlton, Jez G., and Juan Martin-Serrano. 2007. “Parallels between Cytokinesis and Retroviral Budding: A Role for the ESCRT Machinery.” *Science* 316 (5833): 1908–12. https://doi.org/10.1126/science.1143422.

Carmody, Ruaidhrí J, Qingguo Ruan, Scott Palmer, Brendan Hilliard, and Youhai H Chen. 2007. “Negative Regulation of Toll-like Receptor Signaling by NF-KB P50 Ubiquitination Blockade.” *Science* 317 (5838): 675–78. https://doi.org/10.1126/science.1142953.

Carrasco, Daniel R., Kumar Sukhdeo, Marina Protopopova, Raktim Sinha, Miriam Enos, Daniel E E. Carrasco, Mei Zheng, et al. 2007. “The Differentiation and Stress Response Factor XBP-1 Drives Multiple Myeloma Pathogenesis.” *Cancer Cell* 11 (4): 349–60. https://doi.org/10.1016/j.ccr.2007.02.015.

Cartwright, Tyrell, Neil D. Perkins, and Caroline L Wilson. 2016. “NFKB1: A Suppressor of Inflammation, Ageing and Cancer.” *The FEBS Journal* 283 (10): 1812–22. https://doi.org/10.1111/febs.13627.

Cassimere, Erica K., Claire Mauvais, and Catherine Denicourt. 2016. “P27Kip1 Is Required to Mediate a G1 Cell Cycle Arrest Downstream of ATM Following Genotoxic Stress.” *PLoS ONE* 11 (9): 1–20. https://doi.org/10.1371/journal.pone.0162806.

Chan, Fong Chun, Emilia Lim, Robert Kridel, and Christian Steidl. 2018. “Novel Insights into the Disease Dynamics of B-Cell Lymphomas in the Genomics Era.” *Journal of Pathology* 244 (5): 598–609. https://doi.org/10.1002/path.5043.

Chan, Ying Wai, Kasper Fugger, and Stephen C. West. 2018. “Unresolved Recombination Intermediates Lead to Ultra-Fine Anaphase Bridges, Chromosome Breaks and Aberrations.” *Nature Cell Biology* 20 (1): 92–103. https://doi.org/10.1038/s41556-017-0011-1.

Chao, Hui Xiao, Cere E. Poovey, Ashley A. Privette, Gavin D. Grant, Hui Yan Chao, Jeanette G. Cook, and Jeremy E. Purvis. 2017. “Orchestration of DNA Damage Checkpoint Dynamics across the Human Cell Cycle.” *Cell Systems* 5 (5): 445-459.e5. https://doi.org/10.1016/j.cels.2017.09.015.

Chaplin, David D. 2010. “Overview of the Immune Response.” *Journal of Allergy and Clinical Immunology* 125 (2 SUPPL. 2): S3–23. https://doi.org/10.1016/j.jaci.2009.12.980.

Chapuy, Bjoern, Chip Stewart, Andrew Dunford, Jaegil Kim, Atanas Kamburov, Robert Redd,

Mike Lawrence, et al. 2018. “Molecular Subtypes of Diffuse Large B-Cell Lymphoma Are Associated with Distinct Pathogenic Mechanisms and Outcomes.” *Nature Medicine* 24 (May): In press. https://doi.org/10.1038/s41591-018-0016-8.

Chen, Jie, Yuhui Ou, Yanyan Yang, Wen Li, Ye Xu, Yuntao Xie, and Ying Liu. 2018. “KLHL22 Activates Amino-Acid-Dependent MTORC1 Signalling to Promote Tumorigenesis and Ageing.” *Nature* 557 (7706): 585–89. https://doi.org/10.1038/s41586-018-0128-9.

Chen, Zheng, Miaoxing Wu, and Jiahua Liu. 2020. “Kelch-like Protein 14 Promotes Proliferation and Migration of Ovarian Cancer Cells.” *International Journal of Clinical and Experimental Pathology* 13 (12): 2950–61. http://www.ncbi.nlm.nih.gov/pubmed/33425096%0Ahttp://www.pubmedcentral.nih.gov/articlerender.fcgi?artid=PMC7791369.

Choi, Jaewoo, Kyutae Lee, Kristin Ingvarsdottir, Roberto Bonasio, Anita Saraf, Laurence Florens, Michael P. Washburn, Saber Tadros, Michael R. Green, and Luca Busino. 2018. “Loss of KLHL6 Promotes Diffuse Large B-Cell Lymphoma Growth and Survival by Stabilizing the MRNA Decay Factor Roquin2.” *Nature Cell Biology* 20 (5): 586–96. https://doi.org/10.1038/s41556-018-0084-5.

Choi, Jaewoo, James D Phelan, George W Wright, Björn Häupl, Da Wei Huang, Arthur L Shaffer, Ryan M Young, et al. 2020. “Regulation of B Cell Receptor-Dependent NF-KB Signaling by the Tumor Suppressor KLHL14.” *Proceedings of the National Academy of Sciences* 117 (11): 6092 LP – 6102. https://doi.org/10.1073/pnas.1921187117.

Ciccia, Alberto, and Stephen J. Elledge. 2010. “The DNA Damage Response: Making It Safe to Play with Knives.” *Molecular Cell* 40 (2): 179–204. https://doi.org/10.1016/j.molcel.2010.09.019.

Ciechanover, Aaron, and Ronen Ben-Saadon. 2004. “N-Terminal Ubiquitination: More Protein Substrates Join In.” *Trends in Cell Biology* 14 (3): 103–6. https://doi.org/10.1016/j.tcb.2004.01.004.

Cimprich, Karlene A., and David Cortez. 2008. “ATR: An Essential Regulator of Genome Integrity.” *Nature Reviews Molecular Cell Biology* 9 (8): 616–27. https://doi.org/10.1038/nrm2450.

Clague, Michael J., Judy M. Coulson, and Sylvie Urbé. 2012. “Cellular Functions of the DUBs.” *Journal of Cell Science* 125 (2): 277–86. https://doi.org/10.1242/jcs.090985.

Cohn, Martin A., Przemyslaw Kowal, Kailin Yang, Wilhelm Haas, Tony T. Huang, Steven P. Gygi, and Alan D. D’Andrea. 2007. “A UAF1-Containing Multisubunit Protein Complex Regulates the Fanconi Anemia Pathway.” *Molecular Cell* 28 (5): 786–97. https://doi.org/10.1016/j.molcel.2007.09.031.

Collins, Patricia E., Patrick A. Kiely, and Ruaidhrí J. Carmody. 2014. “Inhibition of Transcription by B Cell Leukemia 3 (Bcl-3) Protein Requires Interaction with Nuclear Factor KB (NF-KB) P50.” *Journal of Biological Chemistry* 289 (10): 7059–67. https://doi.org/10.1074/jbc.M114.551986.

Coutinho, Antonio, Eva Gronowicz, Wesley W Bullock, and Göran Möller. 1974. “MECHANISM OF THYMUS-INDEPENDENT IMMUNOCYTE TRIGGERING.” *Journal of Experimental Medicine* 139 (1): 74–92. https://doi.org/10.1084/jem.139.1.74.

Coux, O, K Tanaka, and A L Goldberg. 1996. “Structure and Functions of the 20S and 26S Proteasomes.” *Annual Review of Biochemistry* 65: 801–47.

https://doi.org/10.1146/annurev.bi.65.070196.004101.

Crasta, Karen, Neil J. Ganem, Regina Dagher, Alexandra B. Lantermann, Elena V. Ivanova, Yunfeng Pan, Luigi Nezi, Alexei Protopopov, Dipanjan Chowdhury, and David Pellman. 2012. "DNA Breaks and Chromosome Pulverization from Errors in Mitosis." *Nature* 482 (7383): 53–58. https://doi.org/10.1038/nature10802.

Credendino, Sara Carmela, Nicole Lewin, Miriane De Oliveira, Swaraj Basu, Barbara D'Andrea, Elena Amendola, Luigi Di Guida, et al. 2017. "Tissue- and Cell Type-Specific Expression of the Long Noncoding RNA Klhl14-AS in Mouse." *International Journal of Genomics* 2017. https://doi.org/10.1155/2017/9769171.

Cresson, Charlotte, Sophie Péron, Laura Jamrog, Nelly Rouquié, Nais Prade, Marine Dubois, Sylvie Hébrard, et al. 2018. "PAX5A and PAX5B Isoforms Are Both Efficient to Drive B Cell Differentiation." *Oncotarget* 9 (67): 32841–54. https://doi.org/10.18632/oncotarget.26003.

Cuadrado, Myriam, Paula Gutierrez-Martinez, Aneta Swat, Angel R. Nebreda, and Oscar Fernandez-Capetillo. 2009. "P27Kip1 Stabilization Is Essential for the Maintenance of Cell Cycle Arrest in Response to DNA Damage." *Cancer Research* 69 (22): 8726–32. https://doi.org/10.1158/0008-5472.CAN-09-0729.

Das, Tanuza, Sang Chul Shin, Eun Joo Song, and Eunice Eunkyeong Kim. 2020. "Regulation of Deubiquitinating Enzymes by Post-Translational Modifications." *International Journal of Molecular Sciences* 21 (11): 1–18. https://doi.org/10.3390/ijms21114028.

David, Yael, Nicola Ternette, Mariola J. Edelmann, Tamar Ziv, Batya Gayer, Rotem Sertchook, Yakir Dadon, Benedikt M. Kessler, and Ami Navon. 2011. "E3 Ligases Determine Ubiquitination Site and Conjugate Type by Enforcing Specificity on E2 Enzymes." *Journal of Biological Chemistry* 286 (51): 44104–15. https://doi.org/10.1074/jbc.M111.234559.

David, Yael, Tamar Ziv, Arie Admon, and Ami Navon. 2010. "The E2 Ubiquitin-Conjugating Enzymes Direct Polyubiquitination to Preferred Lysines." *Journal of Biological Chemistry* 285 (12): 8595–8604. https://doi.org/10.1074/jbc.M109.089003.

Davies, Andrew, Thomas E. Cummin, Sharon Barrans, Tom Maishman, Christoph Mamot, Urban Novak, Josh Caddy, et al. 2019. "Gene-Expression Profiling of Bortezomib Added to Standard Chemoimmunotherapy for Diffuse Large B-Cell Lymphoma (REMoDL-B): An Open-Label, Randomised, Phase 3 Trial." *The Lancet Oncology* 20 (5): 649–62. https://doi.org/10.1016/S1470-2045(18)30935-5.

Davis, R Eric, Vu N Ngo, Georg Lenz, Pavel Tolar, Ryan Young, Paul B. Romesser, Holger Kohlhammer, et al. 2010. "Chronic Active B Cell Receptor Signaling in Diffuse Large B Cell Lymphoma." *Nature* 463 (7277): 88–92. https://doi.org/10.1038/nature08638.Chronic.

Demchenko, Yulia N., and W. Michael Kuehl. 2010. "A Critical Role for the NFκB Pathway in Multiple Myeloma." *Oncotarget* 1 (1): 59–68. https://doi.org/10.18632/oncotarget.109.

Demidenko, Z. N., S. Kalurupalle, C. Hanko, C-u Lim, E. Broude, and M. V. Blagosklonny. 2008. "Mechanism of G1-like Arrest by Low Concentrations of Paclitaxel: Next Cell Cycle P53-Dependent Arrest with Sub G1 DNA Content Mediated by Prolonged Mitosis." *Oncogene* 27 (32): 4402–10. https://doi.org/10.1038/onc.2008.82.

Denicourt, Catherine, and Steven F. Dowdy. 2004. "Cip/Kip Proteins: More than Just CDKs Inhibitors." *Genes and Development* 18 (8): 851–55. https://doi.org/10.1101/gad.1205304.
Dewhurst, Sally M. 2020. "Chromothripsis and Telomere Crisis: Engines of Genome Instability." *Current Opinion in Genetics & Development* 60: 41–47.

https://doi.org/https://doi.org/10.1016/j.gde.2020.02.009.

Dietachmayr, Michael, Abirami Rathakrishnan, Oleksandra Karpiuk, Felix von Zweydorf, Thomas Engleitner, Vanesa Fernández-Sáiz, Petra Schenk, et al. 2020. “Antagonistic Activities of CDC14B and CDK1 on USP9X Regulate WT1-Dependent Mitotic Transcription and Survival.” *Nature Communications* 11 (1): 1–12. https://doi.org/10.1038/s41467-020-15059-5.

Duijf, Pascal H.G., Nikolaus Schultz, and Robert Benezra. 2013. “Cancer Cells Preferentially Lose Small Chromosomes.” *International Journal of Cancer* 132 (10): 2316–26. https://doi.org/10.1002/ijc.27924.

Durand, J K, and A S Baldwin. 2017. “Targeting IKK and NF-KB for Therapy.” In *Advances in Protein Chemistry and Structural Biology*, 1st ed., 107:77–115. Elsevier Inc. https://doi.org/10.1016/bs.apcsb.2016.11.006.

Durie, B G, and S E Salmon. 1975. “A Clinical Staging System for Multiple Myeloma.” *Cancer* 36 (3): 842–54. https://doi.org/10.1002/1097-0142(197509)36:3<842::AID-CNCR2820360303>3.0.CO;2-U.

Durie, Prof Brian G M, Cedars-sinai Samuel Oschin, Los Angeles, Antje Hoering, Muneer H Abidi, Spectrum Health, Grand Rapids, et al. 2018. “VRD versus RD” 389 (10068): 519–27. https://doi.org/10.1016/S0140-6736(16)31594-X.Bortezomib.

Dutertre, Stéphanie, Simon Descamps, and Claude Prigent. 2002. “On the Role of Aurora-A in Centrosome Function.” *Oncogene* 21 (4): 6175–83. https://doi.org/10.1038/sj.onc.1205775.
Eichner, Ruth. 2016. “Functional Characterization of Cereblon , the Molecular Target of Immunomodulatory Drugs.”

Elbashir, Sayda M., Jens Harborth, Winfried Lendeckel, Abdullah Yalcin, Klaus Weber, and Thomas Tuschl. 2001. “Duplexes of 21-Nucleotide RNAs Mediate RNA Interference in Cultured Mammalian Cells.” *Nature* 411 (6836): 494–98. https://doi.org/10.1038/35078107.
Elgueta, Raul, Micah J. Benson, Victor C. De Vries, Anna Wasiuk, Yanxia Guo, and Randolph J. Noelle. 2009. “Molecular Mechanism and Function of CD40/CD40L Engagement in the Immune System.” *Immunological Reviews* 229 (1): 152–72. https://doi.org/10.1111/j.1600-065X.2009.00782.x.

Faggioli, Laura, Chiara Costanzo, Marcello Merola, Ercolina Bianchini, Adriana Furia, Antonclla Carsana, and Marta Palmieri. 1996. “Nuclear Factor KB (NF-KB), Nuclear Factor Interleukin-6 (NFIL-6 or C/EBPβ) and Nuclear Factor Interleukin-6β (NFIL6-β or C/EBPδ) Are Not Sufficient to Activate the Endogenous Interleukin-6 Gene in the Human Breast-Carcinoma Cell Line MCF-7. Comparative An.” *European Journal of Biochemistry* 239 (3): 624–31. https://doi.org/10.1111/j.1432-1033.1996.0624u.x.

Falck, Jacob, Julia Coates, and Stephen P. Jackson. 2005. “Conserved Modes of Recruitment of ATM, ATR and DNA-PKcs to Sites of DNA Damage.” *Nature* 434 (7033): 605–11. https://doi.org/10.1038/nature03442.

Falco, Giulia D E, and Antonio Giordano. 1998. “CDK9 (PITALRE): A Multifunctional Cdc2-Related Kinase” 506 (June): 501–6.

Fededa, Juan Pablo, and Daniel W. Gerlich. 2012. “Molecular Control of Animal Cell Cytokinesis.” *Nature Cell Biology* 14 (5): 440–47. https://doi.org/10.1038/ncb2482.

Fero, Matthew L., Erin Randel, Kay E. Gurley, James M. Roberts, and Christopher J. Kemp. 1998. “The Murine Gene P27Kip1 Is Haplo-Insufficient for Tumour Suppression.” *Nature* 396

(6707): 177–80. https://doi.org/10.1038/24179.

Fisher, Daniel, Liliana Krasinska, Damien Coudreuse, and Béla Novák. 2012. “Phosphorylation Network Dynamics in the Control of Cell Cycle Transitions.” *Journal of Cell Science* 125 (20): 4703–11. https://doi.org/10.1242/jcs.106351.

Fong, Chii Shyang, Gregory Mazo, Tuhin Das, Joshua Goodman, Minhee Kim, Brian P. O’Rourke, Denisse Izquierdo, and Meng Fu Bryan Tsou. 2016. “53BP1 and USP28 Mediate P53- Dependent Cell Cycle Arrest in Response to Centrosome Loss and Prolonged Mitosis.” *ELife* 5 (2016JULY): 1–18. https://doi.org/10.7554/eLife.16270.

Fonseca, Rafael, Richard J. Bailey, Gregory J. Ahmann, S. Vincent Rajkumar, James D. Hoyer, John A. Lust, Robert A. Kyle, Morie A. Gertz, Philip R. Greipp, and Gordon W. Dewald. 2002. “Genomic Abnormalities in Monoclonal Gammopathy of Undetermined Significance.” *Blood* 100 (4): 1417–24. https://doi.org/10.1182/blood.v100.4.1417.h81602001417_1417_1424.

Franco, Lia Carolina, Fátima Morales, Silvia Boffo, and Antonio Giordano. 2018. “CDK9: A Key Player in Cancer and Other Diseases.” *Journal of Cellular Biochemistry* 119 (2): 1273–84. https://doi.org/10.1002/jcb.26293.

Frontzek, Fabian, and Georg Lenz. 2019. “Novel Insights into the Pathogenesis of Molecular Subtypes of Diffuse Large B-Cell Lymphoma and Their Clinical Implications.” *Expert Review of Clinical Pharmacology* 12 (11): 1059–67. https://doi.org/10.1080/17512433.2019.1683447.

Fung, Ella, Carmen Richter, Hong-Bin Yang, Isabell Schäffer, Roman Fischer, Benedikt M Kessler, Florian Bassermann, and Vincenzo D’Angiolella. 2018. “ FBXL 13 Directs the Proteolysis of CEP 192 to Regulate Centrosome Homeostasis and Cell Migration .” *EMBO Reports* 19 (3): 1–16. https://doi.org/10.15252/embr.201744799.

Garriga, Judit, Edy Segura, Xavier Mayol, Charles Grubmeyer, and Xavier Graña. 1996. “Phosphorylation Site Specificity of the CDC2-Related Kinase PITALRE.” *Biochemical Journal* 320 (3): 983–89. https://doi.org/10.1042/bj3200983.

Gatta, Alberto T, and Jeremy G Carlton. 2019. “The ESCRT-Machinery: Closing Holes and Expanding Roles.” *Current Opinion in Cell Biology* 59: 121–32. https://doi.org/https://doi.org/10.1016/j.ceb.2019.04.005.

Genschik, Pascal, Izabela Sumara, and Esther Lechner. 2013. “The Emerging Family of CULLIN3-RING Ubiquitin Ligases (CRL3s): Cellular Functions and Disease Implications.” *The EMBO Journal* 32 (17): 2307–20. https://doi.org/10.1038/emboj.2013.173.

Gewurz, Benjamin E, Fadi Towfic, Jessica C Mar, Nicholas P Shinners, Kaoru Takasaki, Bo Zhao, Ellen D Cahir-McFarland, John Quackenbush, Ramnik J Xavier, and Elliott Kieff. 2012. “Genome-Wide SiRNA Screen for Mediators of NF-KB Activation.” *Proceedings of the National Academy of Sciences of the United States of America* 109 (7): 2467–72. https://doi.org/10.1073/pnas.1120542109.

Ghosh, Sankar, and Michael Karin. 2002. “Missing Pieces in the NF-Kappa B Puzzle.” *Cell* 109: S81–96.

Giam, Maybelline, and Giulia Rancati. 2015. “Aneuploidy and Chromosomal Instability in Cancer: A Jackpot to Chaos.” *Cell Division* 10 (1): 1–12. https://doi.org/10.1186/s13008-015-0009-7.

Giansanti, Piero, Liana Tsiatsiani, Teck Yew Low, and Albert J.R. Heck. 2016. “Six Alternative

Proteases for Mass Spectrometry-Based Proteomics beyond Trypsin." *Nature Protocols* 11 (5): 993–1006. https://doi.org/10.1038/nprot.2016.057.

Giles, Lisa M., Lian Li, and Lih Shen Chin. 2009. "Printor, a Novel TorsinA-Interacting Protein Implicated in Dystonia Pathogenesis." *Journal of Biological Chemistry* 284 (32): 21765–75. https://doi.org/10.1074/jbc.M109.004838.

Giunta, Simona, and Stephen P. Jackson. 2011. "Give Me a Break, but Not in Mitosis: The Mitotic DNA Damage Response Marks DNA Double Strand Breaks with Early Signaling Events." *Cell Cycle* 10 (8): 1215–21. https://doi.org/10.4161/cc.10.8.15334.

Gloeckner, Christian Johannes, Karsten Boldt, Annette Schumacher, Ronald Roepman, and Marius Ueffing. 2007. "A Novel Tandem Affinity Purification Strategy for the Efficient Isolation and Characterisation of Native Protein Complexes." *Proteomics* 7 (23): 4228–34. https://doi.org/10.1002/pmic.200700038.

Gomes, Edgar R., Shantanu Jani, and Gregg G. Gundersen. 2005. "Nuclear Movement Regulated by Cdc42, MRCK, Myosin, and Actin Flow Establishes MTOC Polarization in Migrating Cells." *Cell* 121 (3): 451–63. https://doi.org/10.1016/j.cell.2005.02.022.

Gouveia, Susana Montenegro, Sihem Zitouni, Dong Kong, Paulo Duarte, Beatriz Ferreira Gomes, Ana Laura Sousa, Erin M. Tranfield, Anthony Hyman, Jadranka Loncarek, and Monica Bettencourt-Dias. 2019. "PLK4 Is a Microtubule-Associated Protein That Self-Assembles Promoting de Novo MTOC Formation." *Journal of Cell Science* 132 (4). https://doi.org/10.1242/jcs.219501.

Graham, F L, and A.J Van der EB. 1973. "A New Technique for the Assay Adenovirus of Infectivity of Human Adenovirus 5 DNA." *Virology* 467 (52): 456–67.

Greipp, Philip R., Jesus San Miguel, Brian G.M. Dune, John J. Crowley, Bart Barlogie, Joan Bladé, Mario Boccadoro, et al. 2005. "International Staging System for Multiple Myeloma." *Journal of Clinical Oncology* 23 (15): 3412–20. https://doi.org/10.1200/JCO.2005.04.242.

Guerrero-Garcia, Thomas A, Sara Gandolfi, Jacob P Laubach, Teru Hideshima, Dharminder Chauhan, Constantine Mitsiades, Kenneth C Anderson, and Paul G Richardson. 2018. "The Power of Proteasome Inhibition in Multiple Myeloma." *Expert Review of Proteomics* 15 (12): 1033–52. https://doi.org/10.1080/14789450.2018.1543595.

Gundersen, Gregg G., and Howard J. Worman. 2013. "Nuclear Positioning." *Cell* 152 (6): 1376–89. https://doi.org/10.1016/j.cell.2013.02.031.

Guo, Tingting, Yibo Zuo, Liping Qian, Jin Liu, Yukang Yuan, Kailin Xu, Ying Miao, et al. 2019. "ADP-Ribosyltransferase PARP11 Modulates the Interferon Antiviral Response by Mono-ADP-Ribosylating the Ubiquitin E3 Ligase β-TrCP." *Nature Microbiology* 4 (11): 1872–84. https://doi.org/10.1038/s41564-019-0428-3.

Gutiérrez, N. C., M. E. Sarasquete, I. Misiewicz-Krzeminska, M. Delgado, J. De Las Rivas, F. V. Ticona, E. Fermĩán, et al. 2010. "Deregulation of MicroRNA Expression in the Different Genetic Subtypes of Multiple Myeloma and Correlation with Gene Expression Profiling." *Leukemia* 24 (3): 629–37. https://doi.org/10.1038/leu.2009.274.

Han, Xuesong, Briseis Kilfoy, Tongzhang Zheng, Theodore R. Holford, Zhang Yawei, Cairong Zhu, Cairong Zhu, and Yong Zhu. 2008. "Lymphoma Survival Patterns by WHO Subtype in the United States, 1973-2003." *Cancer Causes Control* 19: 841–58. https://doi.org/10.1007/s 10552-008-9 147-4.

Harhaj, Edward W., and Vishva M. Dixit. 2012. “Regulation of NF-KB by Deubiquitinases.” *Immunological Reviews* 246 (1): 107–24. https://doi.org/10.1111/j.1600-065X.2012.01100.x.
Harrigan, Jeanine A., Xavier Jacq, Niall M. Martin, and Stephen P. Jackson. 2018. “Deubiquitylating Enzymes and Drug Discovery: Emerging Opportunities.” *Nature Reviews Drug Discovery* 17 (1): 57–77. https://doi.org/10.1038/nrd.2017.152.

Hatch, Emily M., Andrew H. Fischer, Thomas J. Deerinck, and Martin W. Hetzer. 2013. “Catastrophic Nuclear Envelope Collapse in Cancer Cell Micronuclei.” *Cell* 154 (1): 47. https://doi.org/10.1016/j.cell.2013.06.007.

Hayashi, M T, and J Karlseder. 2013. “DNA Damage Associated with Mitosis and Cytokinesis Failure.” *Oncogene* 32 (39): 4593–4601. https://doi.org/10.1038/onc.2012.615.

Hayashi, Makoto T., Anthony J. Cesare, Teresa Rivera, and Jan Karlseder. 2015. “Cell Death during Crisis Is Mediated by Mitotic Telomere Deprotection.” *Nature* 522 (7557): 492–96. https://doi.org/10.1038/nature14513.

Hayden, Matthew S., and Sankar Ghosh. 2008. “Shared Principles in NF-KB Signaling.” *Cell* 132 (3): 344–62. https://doi.org/10.1016/j.cell.2008.01.020.

Hayden, Matthew S, and Sankar Ghosh. 2004. “Signaling to NF- □ B,” 2195–2224. https://doi.org/10.1101/gad.1228704.bone.

Heesbeen, Roy G.H.P. van, Jonne A. Raaijmakers, Marvin E. Tanenbaum, Vincentius A. Halim, Daphne Lelieveld, Cor Lieftink, Albert J.R. Heck, David A. Egan, and René H. Medema. 2017. “Aurora A, MCAK, and Kif18b Promote Eg5-Independent Spindle Formation.” *Chromosoma* 126 (4): 473–86. https://doi.org/10.1007/s00412-016-0607-4.

Heo, Inha, Chirlmin Joo, Young Kook Kim, Minju Ha, Mi Jeong Yoon, Jun Cho, Kyu Hyeon Yeom, Jinju Han, and V. Narry Kim. 2009. “TUT4 in Concert with Lin28 Suppresses MicroRNA Biogenesis through Pre-MicroRNA Uridylation.” *Cell* 138 (4): 696–708. https://doi.org/10.1016/j.cell.2009.08.002.

Hershko, Avram, and Aaron Ciechanover. 1998. “THE UBIQUITIN SYSTEM.” *Annual Review of Biochemistry* 67 (1): 425–79. https://doi.org/10.1146/annurev.biochem.67.1.425.

Herzog, Sebastian, Michael Reth, and Hassan Jumaa. 2009. “Regulation of B-Cell Proliferation and Differentiation by Pre-B-Cell Receptor Signalling.” *Nature Reviews Immunology* 9 (3): 195–205. https://doi.org/10.1038/nri2491.

Hideshima, Teru, Constantine Mitsiades, Giovanni Tonon, Paul G. Richardson, and Kenneth C. Anderson. 2007. “Understanding Multiple Myeloma Pathogenesis in the Bone Marrow to Identify New Therapeutic Targets.” *Nature Reviews Cancer* 7 (8): 585–98. https://doi.org/10.1038/nrc2189.

Higginbotham, Holden R., and Joseph G. Gleeson. 2007. “The Centrosome in Neuronal Development.” *Trends in Neurosciences* 30 (6): 276–83. https://doi.org/10.1016/j.tins.2007.04.001.

Hobeika, E, S Thiemann, B Storch, H Jumaa, P J Nielsen, R Pelanda, and M Reth. 2006. “Testing Gene Function Early in the B Cell Lineage in Mb1-Cre Mice.” *Proceedings of the National Academy of Sciences of the United States of America* 103 (37): 13789–94. https://doi.org/10.1073/pnas.0605944103.

Hobeika, Elias, Ella Levit-Zerdoun, Vasiliki Anastasopoulou, Roland Pohlmeyer, Simon Altmeier, Ameera Alsadeq, Marc-Werner Dobenecker, Roberta Pelanda, and Michael Reth.

2015. “CD19 and BAFF-R Can Signal to Promote B-Cell Survival in the Absence of Syk.” *The EMBO Journal* 34 (7): 925–39. https://doi.org/10.15252/embj.201489732.

Hochegger, Helfrid, Shunichi Takeda, and Tim Hunt. 2008. “Cyclin-Dependent Kinases and Cell-Cycle Transitions: Does One Fit All?” *Nature Reviews Molecular Cell Biology* 9 (11): 910–16. https://doi.org/10.1038/nrm2510.

Hodgkin, Philip D, Nin Fei Go, James E Cupp, and Maureen Howard. 1991. “Interleukin-4 Enhances Anti-IgM Stimulation of B Cells by Improving Cell Viability and by Increasing the Sensitivity of b Cells to the Anti-IgM Signal.” *Cellular Immunology* 134 (1): 14–30. https://doi.org/https://doi.org/10.1016/0008-8749(91)90327-8.

Hodkinson, Brendan P., Michael Schaffer, Joshua D. Brody, Wojciech Jurczak, Cecilia Carpio, Dina Ben-Yehuda, Irit Avivi, et al. 2021. “Biomarkers of Response to Ibrutinib plus Nivolumab in Relapsed Diffuse Large B-Cell Lymphoma, Follicular Lymphoma, or Richter’s Transformation.” *Translational Oncology* 14 (1): 100977. https://doi.org/10.1016/j.tranon.2020.100977.

Hoffmann, Anja, Sheena Kerr, Julia Jellusova, Jiquan Zhang, Florian Weisel, Ute Wellmann, Thomas H. Winkler, Burkhard Kneitz, Paul R. Crocker, and Lars Nitschke. 2007. “Siglec-G Is a B1 Cell-Inhibitory Receptor That Controls Expansion and Calcium Signaling of the B1 Cell Population.” *Nature Immunology* 8 (7): 695–704. https://doi.org/10.1038/ni1480.

Huang, Oscar W., Xiaolei Ma, Jianping Yin, Jeremy Flinders, Till Maurer, Nobuhiko Kayagaki, Qui Phung, et al. 2012. “Phosphorylation-Dependent Activity of the Deubiquitinase DUBA.” *Nature Structural and Molecular Biology* 19 (2): 171–76. https://doi.org/10.1038/nsmb.2206.

Huang, Xiao Dong, Matthew K. Summers, Victoria Pham, Jennie R. Lill, Jinfeng Liu, Gwanghee Lee, Donald S. Kirkpatrick, Peter K. Jackson, Guowei Fang, and Vishva M. Dixit. 2011. “Deubiquitinase USP37 Is Activated by CDK2 to Antagonize APCCDH1 and Promote S Phase Entry.” *Molecular Cell* 42 (4): 511–23. https://doi.org/10.1016/j.molcel.2011.03.027.

Hwang, Harry C., and Bruce E. Clurman. 2005. “Cyclin E in Normal and Neoplastic Cell Cycles.” *Oncogene* 24 (17): 2776–86. https://doi.org/10.1038/sj.onc.1208613.

Ikeda, Fumiyo, and Ivan Dikic. 2008. “Atypical Ubiquitin Chains: New Molecular Signals. ‘Protein Modifications: Beyond the Usual Suspects’ Review Series.” *EMBO Reports* 9 (6): 536–42. https://doi.org/10.1038/embor.2008.93.

Inuzuka, Hiroyuki, Hidefumi Fukushima, Shavali Shaik, and Wenyi Wei. 2010. “Novel Insights into the Molecular Mechanisms Governing Mdm2 Ubiquitination and Destruction.” *Oncotarget* 1 (7): 685–90. https://doi.org/10.18632/oncotarget.202.

Izzo, Franco, and Dan A. Landau. 2016. “Genetic and Epigenetic Determinants of B-Cell Lymphoma Evolution.” *Current Opinion in Hematology* 23 (4): 392–401. https://doi.org/10.1097/MOH.0000000000000258.

Janssen, Aniek, Marja Van Der Burg, Karoly Szuhai, Geert J.P.L. Kops, and René H. Medema. 2011. “Chromosome Segregation Errors as a Cause of DNA Damage and Structural Chromosome Aberrations.” *Science* 333 (6051): 1895–98. https://doi.org/10.1126/science.1210214.

Jaynes, Patrick William, Prasanna Vasudevan Iyengar, Sarah Kit Leng Lui, Tuan Zea Tan, Natali Vasilevski, Sarah Christine Elizabeth Wright, Giuseppe Verdile, Anand D. Jeyasekharan, and Pieter Johan Adam Eichhorn. 2020. “OTUD4 Enhances TGFβ Signalling through Regulation of the TGFβ Receptor Complex.” *Scientific Reports* 10 (1): 1–13.

https://doi.org/10.1038/s41598-020-72791-0.

Jiang, Yannan, Xinyu Liu, Renbin Shen, Xinhua Gu, and Weifeng Qian. 2021. “Fbxo21 Regulates the Epithelial-to-Mesenchymal Transition through Ubiquitination of Nr2f2 in Gastric Cancer.” *Journal of Cancer* 12 (5): 1421–30. https://doi.org/10.7150/JCA.49674.

Jin, Jianping, Timothy Cardozo, Ruth C. Lovering, Stephen J. Elledge, Michele Pagano, and J. Wade Harper. 2004. “Systematic Analysis and Nomenclature of Mammalian F-Box Proteins.” *Genes and Development* 18 (21): 2573–80. https://doi.org/10.1101/gad.1255304.

Jodo, Aya, Azusa Shibazaki, Asuka Onuma, Tsuneyasu Kaisho, and Takashi Tanaka. 2020. “PDLIM7 Synergizes With PDLIM2 and P62/Sqstm1 to Inhibit Inflammatory Signaling by Promoting Degradation of the P65 Subunit of NF-KB.” *Frontiers in Immunology* 11 (August). https://doi.org/10.3389/fimmu.2020.01559.

Joukov, Vladimir, and Arcangela De Nicolo. 2018. “Aurora-PLK1 Cascades as Key Signaling Modules in the Regulation of Mitosis.” *Science Signaling* 11 (543): 1–26. https://doi.org/10.1126/scisignal.aar4195.

Joukov, Vladimir, Johannes C. Walter, and Arcangela De Nicolo. 2014. “The Cep192-Organized Aurora A-Plk1 Cascade Is Essential for Centrosome Cycle and Bipolar Spindle Assembly.” *Molecular Cell* 55 (4): 578–91. https://doi.org/10.1016/j.molcel.2014.06.016.

Kanarek, N, and Y Ben-Neriah. 2012. “Regulation of NF-KappaB by Ubiquitination and Degradation of the IkappaBs.” *Immunological Reviews* 246 (1): 77–94. https://doi.org/10.1111/j.1600-065X.2012.01098.x.

Kanayama, Atsuhiro, Rashu B. Seth, Lijun Sun, Chee Kwee Ea, Mei Hong, Abdullah Shaito, Yu Hsin Chiu, Li Deng, and Zhijian J. Chen. 2004. “TAB2 and TAB3 Activate the NF-KB Pathway through Binding to Polyubiquitin Chains.” *Molecular Cell* 15 (4): 535–48. https://doi.org/10.1016/j.molcel.2004.08.008.

Kang, Min H., and C. Patrick Reynolds. 2009. “Bcl-2 Inhibitors: Targeting Mitochondrial Apoptotic Pathways in Cancer Therapy.” *Clinical Cancer Research* 15 (4): 1126–32. https://doi.org/10.1158/1078-0432.CCR-08-0144.

Karin, Michael, and Yinon Ben-Neriah. 2000. “PHOSPHORYLATION MEETS UBIQUITINATION : The Control of NF-KB Activity.” *Annual Review of Immunology*, 621–63. https://doi.org/DOI: 10.1146/annurev.immunol.18.1.621.

Kastan, Michael B., and Jiri Bartek. 2004. “Cell-Cycle Checkpoints and Cancer.” *Nature* 432 (7015): 316–23. https://doi.org/10.1038/nature03097.

Kazazian, Karineh, Yosr Haffani, Deanna Ng, Chae Min Michelle Lee, Wendy Johnston, Minji Kim, Roland Xu, et al. 2020. “FAM46C/TENT5C Functions as a Tumor Suppressor through Inhibition of Plk4 Activity.” *Communications Biology* 3 (1): 1–14. https://doi.org/10.1038/s42003-020-01161-3.

Khan, Shagufta, Zenaida Lopez-Dee, Raj Kumar, and Jun Ling. 2013. “Activation of NFkB Is a Novel Mechanism of Pro-Survival Activity of Glucocorticoids in Breast Cancer Cells.” *Cancer Letters* 337 (1): 90–95. https://doi.org/10.1016/j.canlet.2013.05.020.

Khodadadi, Laleh, Qingyu Cheng, Andreas Radbruch, and Falk Hiepe. 2019. “The Maintenance of Memory Plasma Cells.” *Frontiers in Immunology* 10 (April). https://doi.org/10.3389/fimmu.2019.00721.

King, Rebecca L., and Adam Bagg. 2014. “Genetics of Diffuse Large B-Cell Lymphoma: Paving a Path to Personalized Medicine.” *Cancer Journal (United States)* 20 (1): 43–47. https://doi.org/10.1097/PPO.0000000000000014.

Kingston, Robert E., Claudia A. Chen, and Hiroto Okayama. 1999. “Calcium Phosphate Transfection.” *Current Protocols in Immunology* 31 (1): 27–30. https://doi.org/10.1002/0471142735.im1013s31.

Kisselev, A F, T N Akopian, K M Woo, and A L Goldberg. 1999. “The Sizes of Peptides Generated from Protein by Mammalian 26 and 20 S Proteasomes. Implications for Understanding the Degradative Mechanism and Antigen Presentation.” *The Journal of Biological Chemistry* 274 (6): 3363–71. https://doi.org/10.1074/jbc.274.6.3363.
Klaeger, Susan, Stephanie Heinzlmeir, Mathias Wilhelm, Harald Polzer, Binje Vick, Paul Albert Koenig, Maria Reinecke, et al. 2017. “The Target Landscape of Clinical Kinase Drugs.” *Science* 358 (6367). https://doi.org/10.1126/science.aan4368.

Knies, Nathalie, Begüm Alankus, Andre Weilemann, Alexandar Tzankov, Kristina Brunner, Tanja Ruff, Marcus Kremer, Ulrich B Keller, Georg Lenz, and Jürgen Ruland. 2015. “Lymphomagenic CARD11/BCL10/MALT1 Signaling Drives Malignant B-Cell Proliferation via Cooperative NF-KB and JNK Activation.” *Proceedings of the National Academy of Sciences* 112 (52): E7230–38. https://doi.org/10.1073/pnas.1507459112.

Kobayashi, Akira, Moon-Il Kang, Hiromi Okawa, Makiko Ohtsuji, Yukari Zenke, Tomoki Chiba, Kazuhiko Igarashi, and Masayuki Yamamoto. 2004. “Oxidative Stress Sensor Keap1 Functions as an Adaptor for Cul3-Based E3 Ligase to Regulate Proteasomal Degradation of Nrf2.” *Molecular and Cellular Biology* 24 (16): 7130–39. https://doi.org/10.1128/MCB.24.16.7130-7139.2004.

Komander, David. 2009. “The Emerging Complexity of Protein Ubiquitination.” *Biochemical Society Transactions* 37 (5): 937–53. https://doi.org/10.1042/BST0370937.

Komander, David, Michael J. Clague, and Sylvie Urbé. 2009. “Breaking the Chains: Structure and Function of the Deubiquitinases.” *Nature Reviews Molecular Cell Biology* 10 (8): 550–63. https://doi.org/10.1038/nrm2731.

Komander, David, and Michael Rape. 2012. “The Ubiquitin Code.” *Annual Review of Biochemistry* 81 (1): 203–29. https://doi.org/10.1146/annurev-biochem-060310-170328.

Kooten, Cees Van, Jacques Banchereau, and C D L Gene. 2000. “CD40-CD40 Ligand” 67 (January).

Kraus, Petra, V. Sivakamasundari, Victoria Olsen, Victoria Villeneuve, Abbey Hinds, and Thomas Lufkin. 2019. “Klhl14 Antisense RNA Is a Target of Key Skeletogenic Transcription Factors in the Developing Intervertebral Disc.” *Spine* 44 (5): E260–68. https://doi.org/10.1097/BRS.0000000000002827.

Kravtsova-Ivantsiv, Yelena, Inna Shomer, Victoria Cohen-Kaplan, Berend Snijder, Giulio Superti-Furga, Hedva Gonen, Thomas Sommer, et al. 2015. “KPC1-Mediated Ubiquitination and Proteasomal Processing of Nf-Kb1 P105 to P50 Restricts Tumor Growth.” *Cell* 161 (2): 333–47. https://doi.org/10.1016/j.cell.2015.03.001.

Krupina, Ksenia, Charlotte Kleiss, Thibaud Metzger, Sadek Fournane, Stephane Schmucker, Kay Hofmann, Benoit Fischer, et al. 2016. “Ubiquitin Receptor Protein UBASH3B Drives Aurora B Recruitment to Mitotic Microtubules.” *Developmental Cell* 36 (1): 63–78. https://doi.org/10.1016/j.devcel.2015.12.017.

Kuehl, W. Michael, and P. Leif Bergsagel. 2002. “Multiple Myeloma: Evolving Genetic Events and Host Interactions.” *Nature Reviews Cancer* 2 (3): 175–87. https://doi.org/10.1038/nrc746.

Kumar, Shaji K., Vincent Rajkumar, Robert A. Kyle, Mark Van Duin, Pieter Sonneveld, María Victoria Mateos, Francesca Gay, and Kenneth C. Anderson. 2017. “Multiple Myeloma.” *Nature Reviews Disease Primers* 3. https://doi.org/10.1038/nrdp.2017.46.

Küppers, Ralf. 2005. “Mechanisms of B-Cell Lymphoma Pathogenesis.” *Nature Reviews Cancer* 5 (4): 251–62. https://doi.org/10.1038/nrc1589.

Kyle, R. A., and S. V. Rajkumar. 2009a. “Criteria for Diagnosis, Staging, Risk Stratification and Response Assessment of Multiple Myeloma.” *Leukemia* 23 (1): 3–9. https://doi.org/10.1038/leu.2008.291. 2009b. “Criteria for Diagnosis, Staging, Risk Stratification and Response Assessment of Multiple Myeloma.” *Leukemia* 23 (1): 3–9. https://doi.org/10.1038/leu.2008.291.

Lampson, Michael A., and Iain M. Cheeseman. 2011. “Sensing Centromere Tension: Aurora B and the Regulation of Kinetochore Function.” *Trends in Cell Biology* 21 (3): 133–40. https://doi.org/10.1016/j.tcb.2010.10.007.

Lange, Jonas, Georg Lenz, and Birgit Burkhardt. 2017. “Mature Aggressive B-Cell Lymphoma across Age Groups–Molecular Advances and Therapeutic Implications.” *Expert Review of Hematology* 10 (2): 123–35. https://doi.org/10.1080/17474086.2017.1271318.

Lara-Gonzalez, Pablo, Frederick G. Westhorpe, and Stephen S. Taylor. 2012. “The Spindle Assembly Checkpoint.” *Current Biology* 22 (22): R966–80. https://doi.org/10.1016/j.cub.2012.10.006.

Leber, Blanka, Bettina Maier, Florian Fuchs, Jing Chi, Phillip Riffel, Simon Anderhub, Ludmila Wagner, et al. 2010. “Proteins Required for Centrosome Clustering in Cancer Cells.” *Science Translational Medicine* 2 (33). https://doi.org/10.1126/scitranslmed.3000915.

Leggett, Susan E., Alex M. Hruska, Ming Guo, and Ian Y. Wong. 2021. “The Epithelial-Mesenchymal Transition and the Cytoskeleton in Bioengineered Systems.” *Cell Communication and Signaling* 19 (1): 1–24. https://doi.org/10.1186/s12964-021-00713-2.

Lenz, Georg, R. Eric Davis, Vu N. Ngo, Lloyd Lam, Thaddeus C. George, George W. Wright, Sandeep S. Dave, et al. 2008. “Oncogenic CARD11 Mutations in Human Diffuse Large B Cell Lymphoma.” *Science* 319 (5870): 1676–79. https://doi.org/10.1126/science.1153629.

Levine, Michelle S., and Andrew J. Holland. 2018. “The Impact of Mitotic Errors on Cell Proliferation and Tumorigenesis.” *Genes and Development* 32 (9–10): 620–38. https://doi.org/10.1101/gad.314351.118.

Li, H., T. Wittwer, A. Weber, H. Schneider, R. Moreno, G. N. Maine, M. Kracht, M. L. Schmitz, and E. Burstein. 2012. “Regulation of NF-B Activity by Competition between RelA Acetylation and Ubiquitination.” *Oncogene* 31 (5): 611–23. https://doi.org/10.1038/onc.2011.253.

Li, Shuyin, Jun Liu, Qing Min, Tomokatsu Ikawa, Shoya Yasuda, Yang Yang, Yan Qing Wang, Takeshi Tsubata, Yaofeng Zhao, and Ji Yang Wang. 2018. “Kelch-like Protein 14 Promotes B-1a but Suppresses B-1b Cell Development.” *International Immunology* 30 (7): 311–18. https://doi.org/10.1093/intimm/dxy033.

Lin, Li, and Minae Kobayashi. 2003. “Stability of the Rel Homology Domain Is Critical for Generation of NF-KB P50 Subunit.” *Journal of Biological Chemistry* 278 (34): 31479–85. https://doi.org/10.1074/jbc.M304140200.

Lin, Xin, Ran Taube, Koh Fujinaga, and B. Matija Peterlin. 2002. “P-TEFb Containing Cyclin K and Cdk9 Can Activate Transcription via RNA.” *Journal of Biological Chemistry* 277 (19): 16873–78. https://doi.org/10.1074/jbc.M200117200.

Lin, Zhiming, Jianing Miao, Tao Zhang, Ming He, Ziyuan Wang, Xinyuan Feng, and Lunhao Bai. 2021. “JUNB-FBXO21-ERK Axis Promotes Cartilage Degeneration in Osteoarthritis by Inhibiting Autophagy.” *Aging Cell* 20 (2): 1–15. https://doi.org/10.1111/acel.13306.

Liontos, Michalis, Georgia Velimezi, Ioannis S. Pateras, Roxani Angelopoulou, Athanasios G. Papavassiliou, Jiri Bartek, and Vassilis G. Gorgoulis. 2010. “The Roles of P27Kip1 and DNA Damage Signalling in the Chemotherapy-Induced Delayed Cell Cycle Checkpoint.” *Journal of Cellular and Molecular Medicine* 14 (9): 2264–67. https://doi.org/10.1111/j.1582-4934.2010.01145.x.

Liu, Hongbing, Christine H Herrmann, Karen Chiang, Tzu-Ling Sung, Sung-Hwan Moon, Lawrence A Donehower, and Andrew P Rice. 2010. “55K Isoform of CDK9 Associates with Ku70 and Is Involved in DNA Repair.” *Biochemical and Biophysical Research Communications* 397 (2): 245–50. https://doi.org/10.1016/j.bbrc.2010.05.092.

Lollo, V. Di, A. Canciello, M. Orsini, N. Bernabò, M. Ancora, M. Di Federico, V. Curini, et al. 2020. “Transcriptomic and Computational Analysis Identified LPA Metabolism, KLHL14 and KCNE3 as Novel Regulators of Epithelial-Mesenchymal Transition.” *Scientific Reports* 10 (1): 1–13. https://doi.org/10.1038/s41598-020-61017-y.

Lowry, O. H., N. J. Rosebrough, A. L. Farr, and R. J. RandallL. 1951. “Protein Measurement with the Folin Phenol Reagent.” *The Journal of Biological Chemistry* 193 (1): 265–75. https://doi.org/10.1016/s0021-9258(19)52451-6.

Lu, Mingfang, and Robert Munford. 2016. “LPS Stimulates IgM Production in Vivo without Help from Non-B Cells.” *Innate Immunity* 22 (5): 307–15. https://doi.org/10.1177/1753425916644675.

Lüders, Jens. 2021. “Nucleating Microtubules in Neurons: Challenges and Solutions.” *Developmental Neurobiology*. https://doi.org/10.1002/dneu.22751.

Maciejowski, John, Yilong Li, Nazario Bosco, Peter J. Campbell, and Titia De Lange. 2015. “Chromothripsis and Kataegis Induced by Telomere Crisis.” *Cell* 163 (7): 1641–54. https://doi.org/10.1016/j.cell.2015.11.054.

Maerki, Sarah, Michael H. Olma, Titu Staubli, Patrick Steigemann, Daniel W. Gerlich, Manfredo Quadroni, Izabela Sumara, and Matthias Peter. 2009. “The Cul3-KLHL21 E3 Ubiquitin Ligase Targets Aurora B to Midzone Microtubules in Anaphase and Is Required for Cytokinesis.” *Journal of Cell Biology* 187 (6): 791–800. https://doi.org/10.1083/jcb.200906117.

Maine, Gabriel N., and Ezra Burstein. 2007. “COMMD Proteins and the Control of the NFκB Pathway.” *Cell Cycle* 6 (6): 672–76. https://doi.org/10.4161/cc.6.6.3989.

Maine, Gabriel N., Xicheng Mao, Christine M. Komarck, and Ezra Burstein. 2007. “COMMD1 Promotes the Ubiquitination of NF-KB Subunits through a Cullin-Containing Ubiquitin Ligase.” *EMBO Journal* 26 (2): 436–47. https://doi.org/10.1038/sj.emboj.7601489.

Malumbres, Marcos, and Mariano Barbacid. 2009. “Cell Cycle, CDKs and Cancer: A Changing Paradigm.” *Nature Reviews Cancer* 9 (3): 153–66. https://doi.org/10.1038/nrc2602.

Manchado, E., M. Guillamot, and M. Malumbres. 2012. “Killing Cells by Targeting Mitosis.” *Cell*

Death and Differentiation 19 (3): 369–77. https://doi.org/10.1038/cdd.2011.197.

Mandelbaum, Jonathan, Govind Bhagat, Hongyan Tang, Tongwei Mo, Manisha Brahmachary, Qiong Shen, Amy Chadburn, et al. 2010. "BLIMP1 Is a Tumor Suppressor Gene Frequently Disrupted in Activated B Cell-like Diffuse Large B Cell Lymphoma." *Cancer Cell* 18 (6): 568–79. https://doi.org/10.1016/j.ccr.2010.10.030.

Manfrini, Nicola, Marilena Mancino, Annarita Miluzio, Stefania Oliveto, Matteo Balestra, Piera Calamita, Roberta Alfieri, et al. 2020. "FAM46C and FNDC3A Are Multiple Myeloma Tumor Suppressors That Act in Concert to Impair Clearing of Protein Aggregates and Autophagy." *Cancer Research* 80 (21): 4693 LP – 4706. https://doi.org/10.1158/0008-5472.CAN-20-1357.

Manier, S., J. T. Powers, A. Sacco, S. V. Glavey, D. Huynh, M. R. Reagan, K. Z. Salem, et al. 2017. "The LIN28B/Let-7 Axis Is a Novel Therapeutic Pathway in Multiple Myeloma." *Leukemia* 31 (4): 853–60. https://doi.org/10.1038/leu.2016.296.

McCabe, Michael T., Heidi M. Ott, Gopinath Ganji, Susan Korenchuk, Christine Thompson, Glenn S. Van Aller, Yan Liu, et al. 2012. "EZH2 Inhibition as a Therapeutic Strategy for Lymphoma with EZH2-Activating Mutations." *Nature* 492 (7427): 108–12. https://doi.org/10.1038/nature11606.

McCarthy, Philip L., Sarah A. Holstein, Maria Teresa Petrucci, Paul G. Richardson, Cyrille Hulin, Patrizia Tosi, Sara Bringhen, et al. 2017. "Lenalidomide Maintenance after Autologous Stem-Cell Transplantation in Newly Diagnosed Multiple Myeloma: A Meta-Analysis." *Journal of Clinical Oncology* 35 (29): 3279–89. https://doi.org/10.1200/JCO.2017.72.6679.

McMahon, Michael, Ken Itoh, Masayuki Yamamoto, and John D Hayes. 2003. "Keap1-Dependent Proteasomal Degradation of Transcription Factor Nrf2 Contributes to the Negative Regulation of Antioxidant Response Element-Driven Gene Expression." *The Journal of Biological Chemistry* 278 (24): 21592–600. https://doi.org/10.1074/jbc.M300931200.

Meka, Durga Praveen, Robin Scharrenberg, and Froylan Calderon de Anda. 2020. "Emerging Roles of the Centrosome in Neuronal Development." *Cytoskeleton* 77 (3–4): 84–96. https://doi.org/10.1002/cm.21593.

Melchers, Fritz. 2015. "Checkpoints That Control B Cell Development Find the Latest Version : Checkpoints That Control B Cell Development." *The Journal of Clinical Investigation* 125 (6): 2203–10. https://doi.org/10.1172/JCI78083.In.

Mevissen, Tycho E.T., Manuela K. Hospenthal, Paul P. Geurink, Paul R. Elliott, Masato Akutsu, Nadia Arnaudo, Reggy Ekkebus, et al. 2013. "OTU Deubiquitinases Reveal Mechanisms of Linkage Specificity and Enable Ubiquitin Chain Restriction Analysis." *Cell* 154 (1): 169–84. https://doi.org/10.1016/j.cell.2013.05.046.

Mevissen, Tycho E.T., and David Komander. 2017. "Mechanisms of Deubiquitinase Specificity and Regulation." *Annual Review of Biochemistry* 86 (May): 159–92. https://doi.org/10.1146/annurev-biochem-061516-044916.

Meyer, Stefanie N., Sanjay Koul, and Laura Pasqualucci. 2021. "Mouse Models of Germinal Center Derived B-Cell Lymphomas." *Frontiers in Immunology* 12 (August): 1–19. https://doi.org/10.3389/fimmu.2021.710711.

Michel, Martin A, Kirby N Swatek, David Komander, Martin A Michel, Kirby N Swatek, Manuela K Hospenthal, and David Komander. 2017. "Ubiquitin Linkage-Specific Affimers Reveal Insights Resource Ubiquitin Linkage-Specific Affimers Reveal Insights into K6-Linked Ubiquitin Signaling." *Molecular Cell* 68 (1): 1–14. https://doi.org/10.1016/j.molcel.2017.08.020.

Mikhael, Joseph, Nofisat Ismaila, Matthew C. Cheung, Caitlin Costello, Madhav V. Dhodapkar, Shaji Kumar, Martha Lacy, et al. 2019. “Treatment of Multiple Myeloma: ASCO and CCO Joint Clinical Practice Guideline.” *Journal of Clinical Oncology* 37 (14): 1228–63. https://doi.org/10.1200/JCO.18.02096.

Miki, Toshio, Thomas Lehmann, Hongbo Cai, Donna B. Stolz, and Stephen C. Strom. 2005. “Stem Cell Characteristics of Amniotic Epithelial Cells.” *Stem Cells* 23 (10): 1549–59. https://doi.org/10.1634/stemcells.2004-0357.

Molina, Oscar, Meritxell Vinyoles, Isabel Granada, Heleia Roca-Ho, Francisco Gutierrez-Agüera, Luis Valledor, Carlos M. López-López, et al. 2020. “Impaired Condensin Complex and Aurora B Kinase Underlie Mitotic and Chromosomal Defects in Hyperdiploid B-Cell ALL.” *Blood* 136 (3): 313–27. https://doi.org/10.1182/blood.2019002538.

Mombaerts, P, J Iacomini, R S Johnson, K Herrup, S Tonegawa, and V E Papaioannou. 1992. “RAG-1-Deficient Mice Have No Mature B and T Lymphocytes.” *Cell* 68 (5): 869–77. https://doi.org/10.1016/0092-8674(92)90030-g.

Morales, Fatima, and Antonio Giordano. 2016. “Overview of CDK9 as a Target in Cancer Research.” *Cell Cycle* 15 (4): 519–27. https://doi.org/10.1080/15384101.2016.1138186.

Morton, Lindsay M., Sophia S. Wang, Susan S. Devesa, Patricia Hartge, Dennis D. Weisenburger, and Martha S. Linet. 2006. “Lymphoma Incidence Patterns by WHO Subtype in the United States, 1992-2001.” *Blood* 107 (1): 265–76. https://doi.org/10.1182/blood-2005-06-2508.

Mroczek, Seweryn, Justyna Chlebowska, Tomasz M. Kuliński, Olga Gewartowska, Jakub Gruchota, Dominik Cysewski, Vladyslava Liudkovska, Ewa Borsuk, Dominika Nowis, and Andrzej Dziembowski. 2017. “The Non-Canonical Poly(A) Polymerase FAM46C Acts as an Onco-Suppressor in Multiple Myeloma.” *Nature Communications* 8 (1). https://doi.org/10.1038/s41467-017-00578-5.

Muroyama, Andrew, and Terry Lechler. 2017. “Microtubule Organization, Dynamics and Functions in Differentiated Cells.” *Development (Cambridge)* 144 (17): 3012–21. https://doi.org/10.1242/dev.153171.

Negrini, Simona, Vassilis G. Gorgoulis, and Thanos D. Halazonetis. 2010. “Genomic Instability an Evolving Hallmark of Cancer.” *Nature Reviews Molecular Cell Biology* 11 (3): 220–28. https://doi.org/10.1038/nrm2858.

Nery, Flavia C., Cintia C. da Hora, Nadia A. Atai, Edward Y. Kim, Jasmin Hettich, Thorsten R. Mempel, Xandra O. Breakefield, and Daniel Irimia. 2014. “Microfluidic Platform to Evaluate Migration of Cells from Patients with DYT1 Dystonia.” *Journal of Neuroscience Methods* 232: 181–88. https://doi.org/10.1016/j.jneumeth.2014.05.027.

Nigg, Erich A., and Jordan W. Raff. 2009. “Centrioles, Centrosomes, and Cilia in Health and Disease.” *Cell* 139 (4): 663–78. https://doi.org/10.1016/j.cell.2009.10.036.

Nikesitch, Nicholas, James M. Lee, Silvia Ling, and Tara Laurine Roberts. 2018. “Endoplasmic Reticulum Stress in the Development of Multiple Myeloma and Drug Resistance.” *Clinical and Translational Immunology* 7 (1): 1–13. https://doi.org/10.1002/cti2.1007.

Nikonova, Anna S., Igor Astsaturov, Ilya G. Serebriiskii, Roland L. Dunbrack, and Erica A. Golemis. 2013. “Aurora A Kinase (AURKA) in Normal and Pathological Cell Division.” *Cellular and Molecular Life Sciences* 70 (4): 661–87. https://doi.org/10.1007/s00018-012-1073-7.

Nitta, Masayuki, Osamu Kobayashi, Shinobu Honda, Toru Hirota, Shinji Kuninaka, Tomotoshi Marumoto, Yukitaka Ushio, and Hideyuki Saya. 2004. “Spindle Checkpoint Function Is Required for Mitotic Catastrophe Induced by DNA-Damaging Agents.” *Oncogene* 23 (39): 6548–58. https://doi.org/10.1038/sj.onc.1207873.

O’Connor, Brian P., Michael W. Gleeson, Randolph J. Noelle, and Loren D. Erickson. 2003. “The Rise and Fall of Long-Lived Humoral Immunity: Terminal Differentiation of Plasma Cells in Health and Disease.” *Immunological Reviews* 194: 61–76. https://doi.org/10.1034/j.1600-065X.2003.00055.x.

Obeng, Esther A., Louise M. Carlson, Delia M. Gutman, William J. Harrington, Kelvin P. Lee, and Lawrence H. Boise. 2006. “Proteasome Inhibitors Induce a Terminal Unfolded Protein Response in Multiple Myeloma Cells.” *Blood* 107 (12): 4907–16. https://doi.org/10.1182/blood-2005-08-3531.

Oranger, Angela, Claudia Carbone, Maddalena Izzo, and Maria Grano. 2013. “Cellular Mechanisms of Multiple Myeloma Bone Disease.” *Clinical and Developmental Immunology* 2013. https://doi.org/10.1155/2013/289458.

Palmer, Scott, and Youhai H. Chen. 2008. “Bcl-3, a Multifaceted Modulator of NF-KB-Mediated Gene Transcription.” *Immunologic Research* 42 (1–3): 210–18. https://doi.org/10.1007/s12026-008-8075-4.

Palumbo, Antonio, and Kenneth C. Anderson. 2011. “Multiple Myeloma.” *The New England Journal of Medicine* 364 (11): 1046–60. https://doi.org/10.1056/NEJMra1011442.

Palumbo, Antonio, Hervé Avet-Loiseau, Stefania Oliva, Henk M. Lokhorst, Hartmut Goldschmidt, Laura Rosinol, Paul Richardson, et al. 2015. “Revised International Staging System for Multiple Myeloma: A Report from International Myeloma Working Group.” *Journal of Clinical Oncology* 33 (26): 2863–69. https://doi.org/10.1200/JCO.2015.61.2267.

Perkins, N. D. 2006. “Post-Translational Modifications Regulating the Activity and Function of the Nuclear Factor Kappa B Pathway.” *Oncogene* 25 (51): 6717–30. https://doi.org/10.1038/sj.onc.1209937.

Perkins, Neil D. 2007. “Integrating Cell-Signalling Pathways with NF-KappaB and IKK Function.” *Nature Reviews. Molecular Cell Biology* 8 (1): 49–62. https://doi.org/10.1038/nrm2083.

Petroski, Matthew D., and Raymond J. Deshaies. 2005. “Function and Regulation of Cullin-RING Ubiquitin Ligases.” *Nature Reviews Molecular Cell Biology* 6 (1): 9–20. https://doi.org/10.1038/nrm1547.

Phelan, James D., Ryan M. Young, Daniel E. Webster, Sandrine Roulland, George W. Wright, Monica Kasbekar, Arthur L. Shaffer, et al. 2018. “A Multiprotein Supercomplex Controlling Oncogenic Signalling in Lymphoma.” *Nature* 560 (7718): 387–91. https://doi.org/10.1038/s41586-018-0290-0.

Phillips, Darren C., Sha Jin, Gareth P. Gregory, Qi Zhang, John Xue, Xiaoxian Zhao, Jun Chen, et al. 2020. “A Novel CDK9 Inhibitor Increases the Efficacy of Venetoclax (ABT-199) in Multiple Models of Hematologic Malignancies.” *Leukemia* 34 (6): 1646–57. https://doi.org/10.1038/s41375-019-0652-0.

Pierce, Nathan W., J. Eugene Lee, Xing Liu, Michael J. Sweredoski, Robert L.J. Graham, Elizabeth A. Larimore, Michael Rome, et al. 2013. “Cand1 Promotes Assembly of New SCF

Complexes through Dynamic Exchange of F Box Proteins." *Cell* 153 (1): 206–15. https://doi.org/10.1016/j.cell.2013.02.024.

Pinto, Dora, Erica Montani, Martin Bolli, Guido Garavaglia, Federica Sallusto, Antonio Lanzavecchia, and David Jarrossay. 2013. "A Functional BCR in Human IgA and IgM Plasma Cells." *Blood* 121 (20): 4110–14. https://doi.org/10.1182/blood-2012-09-459289.

Podar, Klaus, Yu Tzu Tai, Faith E. Davies, Suzanne Lentzsch, Martin Sattler, Teru Hideshima, Boris K. Lin, et al. 2001. "Vascular Endothelial Growth Factor Triggers Signaling Cascades Mediating Multiple Myeloma Cell Growth and Migration." *Blood* 98 (2): 428–35. https://doi.org/10.1182/blood.V98.2.428.

Pohl, Christian, and Stefan Jentsch. 2009. "Midbody Ring Disposal by Autophagy Is a Post-Abscission Event of Cytokinesis." *Nature Cell Biology* 11 (1): 65–70. https://doi.org/10.1038/ncb1813.

Potapova, Tamara, and Gary J. Gorbsky. 2017. "The Consequences of Chromosome Segregation Errors in Mitosis and Meiosis." *Biology* 6 (1): 1–33. https://doi.org/10.3390/biology6010012.

Raab, Marc S., Klaus Podar, Iris Breitkreutz, Paul G. Richardson, and Kenneth C. Anderson. 2009. "Multiple Myeloma." *The Lancet* 374 (9686): 324–39. https://doi.org/10.1016/S0140-6736(09)60221-X.

Rajkumar, S. Vincent, and Shaji Kumar. 2016. "Multiple Myeloma: Diagnosis and Treatment." *Mayo Clinic Proceedings* 91 (1): 101–19. https://doi.org/10.1016/j.mayocp.2015.11.007.

Ramadan, Kristijan, Roland Bruderer, Fabio M. Spiga, Oliver Popp, Tina Baur, Monica Gotta, and Hemmo H. Meyer. 2007. "Cdc48/P97 Promotes Reformation of the Nucleus by Extracting the Kinase Aurora B from Chromatin." *Nature* 450 (7173): 1258–62. https://doi.org/10.1038/nature06388.

Ravindranath, Abhilash K, Swayamjot Kaur, Roman P Wernyj, Muthu N. Kumaran, Karl E. Miletti-Gonzalez, Rigel Chan, Elaine Lim, Kiran Madura, and Lorna Rodriguez-Rodriguez. 2015. "CD44 Promotes Multi-Drug Resistance by Protecting P-Glycoprotein from FBXO21-Mediated Ubiquitination." *Oncotarget* 6 (28): 26308–21. https://doi.org/10.18632/oncotarget.4763.

Reddy, Anupama, Jenny Zhang, Nicholas S. Davis, Andrea B. Moffitt, Cassandra L. Love, Alexander Waldrop, Sirpa Leppa, et al. 2017. "Genetic and Functional Drivers of Diffuse Large B Cell Lymphoma." *Cell* 171 (2): 481-494.e15. https://doi.org/10.1016/j.cell.2017.09.027.

Revilla-I-Domingo, Roger, Ivan Bilic, Bojan Vilagos, Hiromi Tagoh, Anja Ebert, Ido M Tamir, Leonie Smeenk, et al. 2012. "The B-Cell Identity Factor Pax5 Regulates Distinct Transcriptional Programmes in Early and Late B Lymphopoiesis." *EMBO Journal* 31 (14): 3130–46. https://doi.org/10.1038/emboj.2012.155.

Rickert, R C, J Roes, and K Rajewsky. 1997. "B Lymphocyte-Specific, Cre-Mediated Mutagenesis in Mice." *Nucleic Acids Research* 25 (6): 1317–18. https://doi.org/10.1093/nar/25.6.1317.

Ripon, Md Kamal Hossain, Hyun Sook Lee, Raju Dash, Ho Jin Choi, Diyah Fatimah Oktaviani, Il Soo Moon, and Md Nazmul Haque. 2020. "N-Acetyl-D-Glucosamine Kinase Binds Dynein Light Chain Roadblock 1 and Promotes Protein Aggregate Clearance." *Cell Death and Disease* 11 (8). https://doi.org/10.1038/s41419-020-02862-7.

Ritorto, Maria Stella, Richard Ewan, Ana B. Perez-Oliva, Axel Knebel, Sara J. Buhrlage, Melanie Wightman, Sharon M. Kelly, et al. 2014. “Screening of DUB Activity and Specificity by MALDI-TOF Mass Spectrometry.” *Nature Communications* 5. https://doi.org/10.1038/ncomms5763.

Rolink, Antonius G., Jan Andersson, and Fritz Melchers. 1998. “Characterization of Immature B Cells by a Novel Monoclonal Antibody, by Turnover and by Mitogen Reactivity.” *European Journal of Immunology* 28 (11): 3738–48. https://doi.org/10.1002/(SICI)1521-4141(199811)28:11<3738::AID-IMMU3738>3.0.CO;2-Q.

Ron, David, and Peter Walter. 2007. “Signal Integration in the Endoplasmic Reticulum Unfolded Protein Response.” *Nature Reviews Molecular Cell Biology* 8 (7): 519–29. https://doi.org/10.1038/nrm2199.

Roodman, G. D. 2009. “Pathogenesis of Myeloma Bone Disease.” *Leukemia* 23 (3): 435–41. https://doi.org/10.1038/leu.2008.336.

Rosenbaum, Marc, Andreas Gewies, Konstanze Pechloff, Christoph Heuser, Thomas Engleitner, Torben Gehring, Lara Hartjes, et al. 2019. “Bcl10-Controlled Malt1 Paracaspase Activity Is Key for the Immune Suppressive Function of Regulatory T Cells.” *Nature Communications* 10 (1): 2352. https://doi.org/10.1038/s41467-019-10203-2.

Ruchaud, Sandrine, Mar Carmena, and William C. Earnshaw. 2007. “Chromosomal Passengers: Conducting Cell Division.” *Nature Reviews Molecular Cell Biology* 8 (10): 798–812. https://doi.org/10.1038/nrm2257.

Ruland, Jürgen. 2011. “Return to Homeostasis: Downregulation of NF-KB Responses.” *Nature Immunology* 12 (8): 709–14. https://doi.org/10.1038/ni.2055.

Ryo, Akihide, Futoshi Suizu, Yasuhiro Yoshida, Kilian Perrem, Yih Cherng Liou, Gerburg Wulf, Robert Rottapel, Shoji Yamaoka, and Kun Ping Lu. 2003. “Regulation of NF-KB Signaling by Pin1-Dependent Prolyl Isomerization and Ubiquitin-Mediated Proteolysis of P65/RelA.” *Molecular Cell* 12 (6): 1413–26. https://doi.org/10.1016/S1097-2765(03)00490-8.

Saavedra-Garcia, Paula, Francesca Martini, and Holger W. Auner. 2019. “Proteasome Inhibition in Multiple Myeloma - Lessons for Other Cancers.” *American Journal of Physiology-Cell Physiology*. https://doi.org/10.1152/ajpcell.00286.2019.

Saccani, Simona, Ivan Marazzi, Amer A. Beg, and Gioacchino Natoli. 2004. “Degradation of Promoter-Bound P65/RelA Is Essential for the Prompt Termination of the Nuclear Factor KB Response.” *Journal of Experimental Medicine* 200 (1): 107–13. https://doi.org/10.1084/jem.20040196.

Sahni, Vibhu, Yasuhiro Itoh, Sara J. Shnider, and Jeffrey D. Macklis. 2021. “Crim1 and Kelch-like 14 Exert Complementary Dual-Directional Developmental Control over Segmentally Specific Corticospinal Axon Projection Targeting.” *Cell Reports* 37 (3): 109842. https://doi.org/10.1016/j.celrep.2021.109842.

Sahni, Vibhu, Sara J. Shnider, Denis Jabaudon, Janet H.T. Song, Yasuhiro Itoh, Luciano C. Greig, and Jeffrey D. Macklis. 2021. “Corticospinal Neuron Subpopulation-Specific Developmental Genes Prospectively Indicate Mature Segmentally Specific Axon Projection Targeting.” *Cell Reports* 37 (3): 109843. https://doi.org/10.1016/j.celrep.2021.109843.

Sahtoe, Danny D., and Titia K. Sixma. 2015. “Layers of DUB Regulation.” *Trends in Biochemical Sciences* 40 (8): 456–67. https://doi.org/10.1016/j.tibs.2015.05.002.

Sanchez, Ariana D., and Jessica L. Feldman. 2017. “Microtubule-Organizing Centers: From the Centrosome to Non-Centrosomal Sites.” *Current Opinion in Cell Biology* 44: 93–101. https://doi.org/10.1016/j.ceb.2016.09.003.

Sansregret, Laurent, and Charles Swanton. 2017. “The Role of Aneuploidy in Cancer Evolution.” *Cold Spring Harbor Perspectives in Medicine* 7 (1): 1–18. https://doi.org/10.1101/cshperspect.a028373.

Sarikas, Antonio, Thomas Hartmann, and Zhen Qiang Pan. 2011. “The Cullin Protein Family.” *Genome Biology* 12 (4): 1–12. https://doi.org/10.1186/gb-2011-12-4-220.

Saunders, Cosmo A., Nathan J. Harris, Patrick T. Willey, Brian M. Woolums, Yuexia Wang, Alex J. McQuown, Amy Schoenhofen, et al. 2017. “TorsinA Controls TAN Line Assembly and the Retrograde Flow of Dorsal Perinuclear Actin Cables during Rearward Nuclear Movement.” *The Journal of Cell Biology* 216 (3): 657–74. https://doi.org/10.1083/jcb.201507113.

Schatten, Heide. 2008. “The Mammalian Centrosome and Its Functional Significance.” *Histochemistry and Cell Biology* 129 (6): 667–86. https://doi.org/10.1007/s00418-008-0427-6.
Scheffner, Martin, Ulrike Nuber, and Jon M. Huibregtse. 1995. “Protein Ubiquitination Involving an E1–E2–E3 Enzyme Ubiquitin Thioester Cascade.” *Nature* 373 (6509): 81–83. https://doi.org/10.1038/373081a0.

Scherer, D C, J A Brockman, Z Chen, T Maniatis, and D W Ballard. 1995. “Signal-Induced Degradation of I Kappa B Alpha Requires Site-Specific Ubiquitination.” *Proceedings of the National Academy of Sciences of the United States of America* 92 (24): 11259–63. https://doi.org/10.1073/pnas.92.24.11259.

Schmitz, R., G. W. Wright, D. W. Huang, C. A. Johnson, J. D. Phelan, J. Q. Wang, S. Roulland, et al. 2018. “Genetics and Pathogenesis of Diffuse Large B-Cell Lymphoma.” *New England Journal of Medicine* 378 (15): 1396–1407. https://doi.org/10.1056/NEJMoa1801445.

Schuster, Marc, Michaela Annemann, Carlos Plaza-Sirvent, and Ingo Schmitz. 2013. “Atypical IκB Proteins - Nuclear Modulators of NF-KB Signaling.” *Cell Communication and Signaling* 11 (1): 1–11. https://doi.org/10.1186/1478-811X-11-23.

Sen, Ranjan, and David Baltimore. 1986a. “Inducibility of κ Immunoglobulin Enhancer-Binding Protein NF-KB by a Posttranslational Mechanism.” *Cell* 47 (6): 921–28. https://doi.org/10.1016/0092-8674(86)90807-X———. 1986b. “Multiple Nuclear Factors Interact with the Immunoglobulin Enhancer Sequences.” *Cell* 46 (5): 705–16. https://doi.org/10.1016/0092-8674(86)90346-6.

Shembade, Noula, Averil Ma, and Edward W. Harhaj. 2010. “Inhibition of NF-KB Signaling by A20 Through Disruption of Ubiquitin Enzyme Complexes” 327 (February): 1135–40.

Shi, Jianjin, Yue Zhao, Yupeng Wang, Wenqing Gao, Jingjin Ding, Peng Li, Liyan Hu, and Feng Shao. 2014. “Inflammatory Caspases Are Innate Immune Receptors for Intracellular LPS.” *Nature* 514 (7521): 187–92. https://doi.org/10.1038/nature13683.

Shin, Chanyoung, Yuma Ito, Shota Ichikawa, Makio Tokunaga, Kumiko Sakata-Sogawa, and Takashi Tanaka. 2017. “MKRN2 Is a Novel Ubiquitin E3 Ligase for the P65 Subunit of NF-KB and Negatively Regulates Inflammatory Responses.” *Scientific Reports* 7 (April): 1–10. https://doi.org/10.1038/srep46097.

Shyh-Chang, Ng, and George Q. Daley. 2013. “Lin28: Primal Regulator of Growth and Metabolism in Stem Cells.” *Cell Stem Cell* 12 (4): 395–406. https://doi.org/10.1016/j.stem.2013.03.005.

Siegel, Rebecca L., Kimberly D. Miller, and Ahmedin Jemal. 2016. “Cancer Statistics, 2016.” *CA: A Cancer Journal for Clinicians* 66 (1): 7–30. https://doi.org/10.3322/caac.21332.———. 2019. “Cancer Statistics, 2019.” *CA: A Cancer Journal for Clinicians* 69 (1): 7–34. https://doi.org/10.3322/caac.21551.

Silva, Nilushi S. De, and Ulf Klein. 2015. “Dynamics of B Cells in Germinal Centres.” *Nature Reviews Immunology* 15 (3): 137–48. https://doi.org/10.1038/nri3804.

Skaar, Jeffrey R., Julia K. Pagan, and Michele Pagano. 2013. “Mechanisms and Function of Substrate Recruitment by F-Box Proteins.” *Nature Reviews Molecular Cell Biology* 14 (6): 369–81. https://doi.org/10.1038/nrm3582.
Skaar, Jeffrey R., and Michele Pagano. 2009. “Control of Cell Growth by the SCF and APC/C Ubiquitin Ligases.” *Current Opinion in Cell Biology* 21 (6): 816–24. https://doi.org/10.1016/j.ceb.2009.08.004.

Skowyra, Dorota, Karen L. Craig, Mike Tyers, Stephen J. Elledge, and J. Wade Harper. 1997. “F-Box Proteins Are Receptors That Recruit Phosphorylated Substrates to the SCF Ubiquitin-Ligase Complex.” *Cell* 91 (2): 209–19. https://doi.org/10.1016/S0092-8674(00)80403-1.

Smale, Stephen T. 2012. “Dimer-Specific Regulatory Mechanisms within the NF-KB Family of Transcription Factors.” *Immunological Reviews* 246 (1): 193–204. https://doi.org/10.1111/j.1600-065X.2011.01091.x.

Sobol, Anna, Caroline Askonas, Sara Alani, Megan J. Weber, Vijayalakshmi Ananthanarayanan, Clodia Osipo, and Maurizio Bocchetta. 2017. “Deubiquitinase OTUD6B Isoforms Are Important Regulators of Growth and Proliferation.” *Molecular Cancer Research* 15 (2): 117–27. https://doi.org/10.1158/1541-7786.MCR-16-0281-T.

Solecki, David J., Eve Ellen Govek, Toshifumi Tomoda, and Mary E. Hatten. 2006. “Neuronal Polarity in CNS Development.” *Genes and Development* 20 (19): 2639–47. https://doi.org/10.1101/gad.1462506.

Soltes, Garner, Eric Muller, and Teresa G. D’Aversa. 2011. “Ubiquitin, Ubiquitination, and Proteasomal Degradation in the Eukaryotic Cell: A Review.” *BIOS* 82 (3): 64–71. https://doi.org/10.1893/011.082.0303.

Song, Liang, Sonja Wörmann, Jiaoyu Ai, Patrick Neuhöfer, Marina Lesina, Kalliope N. Diakopoulos, Dietrich Ruess, et al. 2016. “BCL3 Reduces the Sterile Inflammatory Response in Pancreatic and Biliary Tissues.” *Gastroenterology* 150 (2): 499-512.e20. https://doi.org/10.1053/j.gastro.2015.10.017.

Song, Ling, and Michael Rape. 2008. “Reverse the Curse-the Role of Deubiquitination in Cell Cycle Control.” *Current Opinion in Cell Biology* 20 (2): 156–63. https://doi.org/10.1016/j.ceb.2008.01.012.

Spencer, Erika, Jin Jiang, and Zhijian J. Chen. 1999. “Signal-Induced Ubiquitination of IκBα by the F-Box Protein Slimb/β- TrCP.” *Genes and Development* 13 (3): 284–94. https://doi.org/10.1101/gad.13.3.284.

Stebegg, Marisa, Saumya D. Kumar, Alyssa Silva-Cayetano, Valter R. Fonseca, Michelle A. Linterman, and Luis Graca. 2018a. “Regulation of the Germinal Center Response.” *Frontiers in Immunology* 9 (OCT): 1–13. https://doi.org/10.3389/fimmu.2018.02469. 2018b. “Regulation of the Germinal Center Response.” *Frontiers in Immunology* 9 (OCT): 1–13. https://doi.org/10.3389/fimmu.2018.02469.

Steigemann, Patrick, Claudia Wurzenberger, Michael H.A. Schmitz, Michael Held, Julien Guizetti, Sandra Maar, and Daniel W. Gerlich. 2009. “Aurora B-Mediated Abscission Checkpoint Protects against Tetraploidization.” *Cell* 136 (3): 473–84. https://doi.org/10.1016/j.cell.2008.12.020.

Stewart, Daniel P., Brian Koss, Madhavi Bathina, Rhonda M. Perciavalle, Kristen Bisanz, and Joseph T. Opferman. 2010. “Ubiquitin-Independent Degradation of Antiapoptotic MCL-1.” *Molecular and Cellular Biology* 30 (12): 3099–3110. https://doi.org/10.1128/mcb.01266-09.

Stewart, Scott, and Guowei Fang. 2005. “Destruction Box-Dependent Degradation of Aurora B Is Mediated by the Anaphase-Promoting Complex/Cyclosome and Cdh1.” *Cancer Research* 65 (19): 8730–35. https://doi.org/10.1158/0008-5472.CAN-05-1500.

Stogios, Peter J., Gregory S. Downs, Jimmy J.S. Jauhal, Sukhjeen K. Nandra, and Gilbert G. Privé. 2005. “Sequence and Structural Analysis of BTB Domain Proteins.” *Genome Biology* 6 (10): 1–18. https://doi.org/10.1186/gb-2005-6-10-r82.

Stucki, Manuel, Julie A. Clapperton, Duaa Mohammad, Michael B. Yaffe, Stephen J. Smerdon, and Stephen P. Jackson. 2005. “MDC1 Directly Binds Phosphorylated Histone H2AX to Regulate Cellular Responses to DNA Double-Strand Breaks.” *Cell* 123 (7): 1213–26. https://doi.org/10.1016/j.cell.2005.09.038.

Sumara, Izabela, Manfredo Quadroni, Claudia Frei, Michael H. Olma, Grzegorz Sumara, Romeo Ricci, and Matthias Peter. 2007. “A Cul3-Based E3 Ligase Removes Aurora B from Mitotic Chromosomes, Regulating Mitotic Progression and Completion of Cytokinesis in Human Cells.” *Developmental Cell* 12 (6): 887–900. https://doi.org/10.1016/j.devcel.2007.03.019.

Sun, Shao-Cong. 2011. “Non-Canonical NF-KB Signaling Pathway.” *Cell Research* 21 (1): 71–85. https://doi.org/10.1038/cr.2010.177.

Swatek, Kirby N., and David Komander. 2016. “Ubiquitin Modifications.” *Cell Research* 26 (4): 399–422. https://doi.org/10.1038/cr.2016.39.

Tai, Yu-tzu, and Kenneth C Anderson. 2012. “Bruton ’s Tyrosine Kinase : Oncotarget in Myeloma MM Stem Cell Osteoblast Tumor BM Stromal Cells Osteoclast Precursors Osteoclasts.” *Oncotarget* 3 (9): 913–14.

Tai, Yu Tzu, Chirag Acharya, Gang An, Michele Moschetta, Mike Y. Zhong, Xiaoyan Feng, Michele Cea, et al. 2016. “APRIL and BCMA Promote Human Multiple Myeloma Growth and Immunosuppression in the Bone Marrow Microenvironment.” *Blood* 127 (25): 3225–36. https://doi.org/10.1182/blood-2016-01-691162.

Tanaka, Takashi, Michael J. Grusby, and Tsuneyasu Kaisho. 2007. “PDLIM2-Mediated Termination of Transcription Factor NF-KB Activation by Intranuclear Sequestration and Degradation of the P65 Subunit.” *Nature Immunology* 8 (6): 584–91. https://doi.org/10.1038/ni1464.

Tchakarska, Guergana, and Brigitte Sola. 2020. “The Double Dealing of Cyclin D1.” *Cell Cycle* 19 (2): 163–78. https://doi.org/10.1080/15384101.2019.1706903.

Thompson, Ruth, Rachel Gatenby, and Samuel Sidi. 2019. “How Cells Handle DNA Breaks during Mitosis: Detection, Signaling, Repair, and Fate Choice.” *Cells* 8 (9): 1049. https://doi.org/10.3390/cells8091049.

Tietsche de Moraes Hungria, Vania, Carlos Chiattone, Miguel Pavlovsky, Lina M. Abenoza,

Gladys P. Agreda, Jorge Armenta, Celso Arrais, et al. 2019. “Epidemiology of Hematologic Malignancies in Real-World Settings: Findings From the Hemato-Oncology Latin America Observational Registry Study.” *Journal of Global Oncology* 5: 1–19. https://doi.org/10.1200/JGO.19.00025.

Tillery, Marisa, Caitlyn Blake-Hedges, Yiming Zheng, Rebecca Buchwalter, and Timothy Megraw. 2018. “Centrosomal and Non-Centrosomal Microtubule-Organizing Centers (MTOCs) in Drosophila Melanogaster.” *Cells* 7 (9): 121. https://doi.org/10.3390/cells7090121.

Tomko, Robert J Jr, and Mark Hochstrasser. 2013. “Molecular Architecture and Assembly of the Eukaryotic Proteasome.” *Annual Review of Biochemistry* 82: 415–45. https://doi.org/10.1146/annurev-biochem-060410-150257.

Trivedi, Prasad, and P. Todd Stukenberg. 2020. “A Condensed View of the Chromosome Passenger Complex.” *Trends in Cell Biology* 30 (9): 676–87. https://doi.org/10.1016/j.tcb.2020.06.005.

Truscott, T.G., and R.S. Sinclair. 2019. *Structural Immunology*. Edited by Tengchuan Jin and Qian Yin. *Advances in Experimental Medicine and Biology*. Vol. 1172. Advances in Experimental Medicine and Biology. Singapore: Springer Singapore. https://doi.org/10.1007/978-981-13-9367-9.

Tsou, Meng Fu Bryan, and Tim Stearns. 2006. “Mechanism Limiting Centrosome Duplication to Once per Cell Cycle.” *Nature* 442 (7105): 947–51. https://doi.org/10.1038/nature04985.

Tsukamoto, Hiroki, Shino Takeuchi, Kanae Kubota, Yohei Kobayashi, Sao Kozakai, Ippo Ukai, Ayumi Shichiku, et al. 2018. “Lipopolysaccharide (LPS)-Binding Protein Stimulates CD14-Dependent Toll-like Receptor 4 Internalization and LPS-Induced TBK1-IKKα-IRF3 Axis Activation.” *Journal of Biological Chemistry* 293 (26): 10186–201. https://doi.org/10.1074/jbc.M117.796631.

Uetake, Yumi, and Greenfield Sluder. 2010. “Prolonged Prometaphase Blocks Daughter Cell Proliferation despite Normal Completion of Mitosis.” *Current Biology* 20 (18): 1666–71. https://doi.org/10.1016/j.cub.2010.08.018.

Urbé, Sylvie, Han Liu, Sebastian D. Hayes, Claire Heride, Daniel J. Rigden, and Michael J. Clague. 2012. “Systematic Survey of Deubiquitinase Localization Identifies USP21 as a Regulator of Centrosome-and Microtubule-Associated Functions.” *Molecular Biology of the Cell* 23 (6): 1095–1103. https://doi.org/10.1091/mbc.E11-08-0668.

Utley, Adam, Brittany Lipchick, Kelvin P. Lee, and Mikhail A. Nikiforov. 2020. “Targeting Multiple Myeloma through the Biology of Long-Lived Plasma Cells.” *Cancers* 12 (8): 1–17. https://doi.org/10.3390/cancers12082117.

Valastyan, Julie S., and Susan Lindquist. 2011. “Torsina and the Torsina-Interacting Protein Printor Have No Impact on Endoplasmic Reticulum Stress or Protein Trafficking in Yeast.” *PLoS ONE* 6 (7). https://doi.org/10.1371/journal.pone.0022744.

Vallabhapurapu, Sivakumar, Atsushi Matsuzawa, Wei Zhou Zhang, Ping Hui Tseng, Jonathan J. Keats, Haopeng Wang, Dario A.A. Vignali, P. Leif Bergsagel, and Michael Karin. 2008. “Nonredundant and Complementary Functions of TRAF2 and TRAF3 in a Ubiquitination Cascade That Activates NIK-Dependent Alternative NF-KB Signaling.” *Nature Immunology* 9 (12): 1364–70. https://doi.org/10.1038/ni.1678.

Vater, I, M. Montesinos-Rongen, M Schlesner, A Haake, F Purschke, R Sprute, N Mettenmeyer, et al. 2015. “The Mutational Pattern of Primary Lymphoma of the Central

Nervous System Determined by Whole-Exome Sequencing." *Leukemia* 29 (3): 677–85. https://doi.org/10.1038/leu.2014.264.

Viswanathan, Srinivas R., George Q. Daley, and Richard I. Gregory. 2008. "Selective Blockade of MicroRNA Processing by Lin28." *Science* 320 (5872): 97–100. https://doi.org/10.1126/science.1154040.

Wang, Bin, Zuliang Jie, Donghyun Joo, Alban Ordureau, Pengda Liu, Wenjian Gan, Jianping Guo, et al. 2017a. "TRAF2 and OTUD7B Govern a Ubiquitin-Dependent Switch That Regulates MTORC2 Signalling." *Nature* 545 (7654): 365–69. https://doi.org/10.1038/nature22344.
———. 2017b. "TRAF2 and OTUD7B Govern a Ubiquitin-Dependent Switch That Regulates MTORC2 Signalling." *Nature* 545 (May): 365. https://doi.org/10.1038/nature22344.

Wang, Peng, Marcos Malumbres, and Vincent Archambault. 2014. "The Greatwall-PP2A Axis in Cell Cycle Control." *Methods in Molecular Biology (Clifton, N.J.)* 1170: 99–111. https://doi.org/10.1007/978-1-4939-0888-2_6.

Wang, Won Jing, Rajesh Kumar Soni, Kunihiro Uryu, and Meng Fu Bryan Tsou. 2011. "The Conversion of Centrioles to Centrosomes: Essential Coupling of Duplication with Segregation." *Journal of Cell Biology* 193 (4): 727–39. https://doi.org/10.1083/jcb.201101109.

Watanabe, Koki, Kanae Yumimoto, and Keiichi I. Nakayama. 2015. "FBXO21 Mediates the Ubiquitylation and Proteasomal Degradation of EID1." *Genes to Cells* 20 (8): 667–74. https://doi.org/10.1111/gtc.12260.

Wei, Wenyi, Nagi G. Ayad, Yong Wan, Guo-Jun Zhang, Marc W. Kirschner, and William G. Kaelin. 2004. "Degradation of the SCF Component Skp2 in Cell-Cycle Phase G1 by the Anaphase-Promoting Complex." *Nature* 428 (6979): 194–98. https://doi.org/10.1038/nature02381.
Wiedemann, Annika, Marie Lettau, Ina Wirries, Annemarie Jungmann, Abdulrahman Salhab, Gilles Gasparoni, Henrik E. Mei, et al. 2021. "Human IgA-Expressing Bone Marrow Plasma Cells Characteristically Upregulate Programmed Cell Death Protein-1 Upon B Cell Receptor Stimulation." *Frontiers in Immunology* 11 (February): 1–11. https://doi.org/10.3389/fimmu.2020.628923.

Willems, Andrew R., Michael Schwab, and Mike Tyers. 2004. "A Hitchhiker's Guide to the Cullin Ubiquitin Ligases: SCF and Its Kin." *Biochimica et Biophysica Acta - Molecular Cell Research* 1695 (1–3): 133–70. https://doi.org/10.1016/j.bbamcr.2004.09.027.

Willems, Estelle, Matthias Dedobbeleer, Marina Digregorio, Arnaud Lombard, Paul Noel Lumapat, and Bernard Rogister. 2018. "The Functional Diversity of Aurora Kinases: A Comprehensive Review." *Cell Division* 13 (1): 1–17. https://doi.org/10.1186/s13008-018-0040-6.

Williams, Lauren K., Douglas R. Mackay, Madeline A. Whitney, Genevieve C. Couldwell, Wesley I. Sundquist, and Katharine S. Ullman. 2021. "Identification of Abscission Checkpoint Bodies as Structures That Regulate Escrt Factors to Control Abscission Timing." *ELife* 10: 1–24. https://doi.org/10.7554/ELIFE.63743.

Wirth, Matthias, Markus Schick, Ulrich Keller, and Jan Krönke. 2020. "Ubiquitination and Ubiquitin-like Modifications in Multiple Myeloma: Biology and Therapy." *Cancers* 12 (12): 1–19. https://doi.org/10.3390/cancers12123764.

Wortis, Henry H., Mark Teutsch, Mindy Higer, Jenny Zheng, and David C. Parker. 1995. "B-Cell Activation by Crosslinking of Surface IgM or Ligation of CD40 Involves Alternative Signal

Pathways and Results in Different B-Cell Phenotypes." *Proceedings of the National Academy of Sciences of the United States of America* 92 (8): 3348–52. https://doi.org/10.1073/pnas.92.8.3348.

Wu, Longtao, Clayton D. Crawley, Andrea Garofalo, Jackie W. Nichols, Paige Ashley Campbell, Galina F. Khramtsova, Olufunmilayo I. Olopade, Ralph R. Weichselbaum, and Bakhtiar Yamini. 2020. "P50 Mono-Ubiquitination and Interaction with BARD1 Regulates Cell Cycle Progression and Maintains Genome Stability." *Nature Communications* 11 (1). https://doi.org/10.1038/s41467-020-18838-2.

Xu, Lai, Yue Wei, Jerome Reboul, Philippe Vaglio, Tae Ho Shin, Marc Vidal, Stephen J. Elledge, and J. Wade Harper. 2003. "BTB Proteins Are Substrate-Specific Adaptors in an SCF-like Modular Ubiquitin Ligase Containing CUL-3." *Nature* 425 (6955): 316–21. https://doi.org/10.1038/nature01985.

Yilmaz, Mahmut, and Gerhard Christofori. 2009. "EMT, the Cytoskeleton, and Cancer Cell Invasion." *Cancer and Metastasis Reviews* 28 (1–2): 15–33. https://doi.org/10.1007/s10555-008-9169-0.

Yoshida, Taketoshi, Henrik Mei, Thomas Dörner, Falk Hiepe, Andreas Radbruch, Simon Fillatreau, and Bimba F. Hoyer. 2010. "Memory B and Memory Plasma Cells." *Immunological Reviews* 237 (1): 117–39. https://doi.org/10.1111/j.1600-065X.2010.00938.x.

Yoshida, Yukiko, Yasushi Saeki, Arisa Murakami, Junko Kawawaki, Hikaru Tsuchiya, Hidehito Yoshihara, Mayumi Shindo, and Keiji Tanaka. 2015. "A Comprehensive Method for Detecting Ubiquitinated Substrates Using TR-TUBE." *Proceedings of the National Academy of Sciences* 112 (15): 4630–35. https://doi.org/10.1073/pnas.1422313112.

Young, Ryan M., Arthur L. Shaffer, James D. Phelan, and Louis M. Staudt. 2015. "B-Cell Receptor Signaling in Diffuse Large B-Cell Lymphoma." *Seminars in Hematology* 52 (2): 77–85. https://doi.org/10.1053/j.seminhematol.2015.01.008.

Young, Ryan M., and Louis M. Staudt. 2013. "Targeting Pathological B Cell Receptor Signalling in Lymphoid Malignancies." *Nature Reviews Drug Discovery* 12 (3): 229–43. https://doi.org/10.1038/nrd3937.

Yu, David S., Runxiang Zhao, Emory L. Hsu, Jennifer Cayer, Fei Ye, Yan Guo, Yu Shyr, and David Cortez. 2010. "Cyclin-dependent Kinase 9–Cyclin K Functions in the Replication Stress Response." *EMBO Reports* 11 (11): 876–82. https://doi.org/10.1038/embor.2010.153.

Yu, Zhou, Taoyong Chen, Xuelian Li, Mingjin Yang, Songqing Tang, Xuhui Zhu, Yan Gu, et al. 2016. "Lys29-Linkage of ASK1 by Skp1-Cullin 1-Fbxo21 Ubiquitin Ligase Complex Is Required for Antiviral Innate Response." *ELife* 5 (APRIL2016): 1–23. https://doi.org/10.7554/eLife.14087.

Zhang, Cheng Zhong, Alexander Spektor, Hauke Cornils, Joshua M. Francis, Emily K. Jackson, Shiwei Liu, Matthew Meyerson, and David Pellman. 2015. "Chromothripsis from DNA Damage in Micronuclei." *Nature* 522 (7555): 179–84. https://doi.org/10.1038/nature14493.

Zhang, Jin, Sutheera Ratanasirintrawoot, Sriram Chandrasekaran, Zhaoting Wu, Scott B. Ficarro, Chunxiao Yu, Christian A. Ross, et al. 2016. "LIN28 Regulates Stem Cell Metabolism and Conversion to Primed Pluripotency." *Cell Stem Cell* 19 (1): 66–80. https://doi.org/10.1016/j.stem.2016.05.009.

Zhang, Juliet, Jarret A.P. Weinrich, Jeffrey B. Russ, John D. Comer, Praveen K. Bommareddy, Richard J. DiCasoli, Christopher V.E. Wright, Yuqing Li, Peter J. van Roessel, and Julia A.

Kaltschmidt. 2017a. “A Role for Dystonia-Associated Genes in Spinal GABAergic Interneuron Circuitry.” *Cell Reports* 21 (3): 666–78. https://doi.org/10.1016/j.celrep.2017.09.079.———. 2017b. “A Role for Dystonia-Associated Genes in Spinal GABAergic Interneuron Circuitry.” *Cell Reports* 21 (3): 666–78. https://doi.org/10.1016/j.celrep.2017.09.079.

Zhang, Qian, Michael J Lenardo, and David Baltimore. 2017. “30 Years of NF-KB: A Blossoming of Relevance to Human Pathobiology.” *Cell*. Elsevier. https://doi.org/10.1016/j.cell.2016.12.012.

Zhang, Shizhen, Yanwen Shen, Hua Li, Chao Bi, Yilun Sun, Xiufang Xiong, Wenyi Wei, and Yi Sun. 2020. “The Negative Cross-Talk between SAG/RBX2/ROC2 and APC/C E3 Ligases in Regulation of Cell Cycle Progression and Drug Resistance.” *Cell Reports* 32 (10): 108102. https://doi.org/10.1016/j.celrep.2020.108102.

Zhou, Bin-bing S, and Stephen J Elledge. 2000. “Checkpoints in Perspective.” *Nature* 408 (November): 433–39.

Zhou, Tianhua, Wendy Zimmerman, Xiaoqi Liu, and Raymond L. Erikson. 2006. “A Mammalian NudC-like Protein Essential for Dynein Stability and Cell Viability.” *Proceedings of the National Academy of Sciences of the United States of America* 103 (24): 9039–44. https://doi.org/10.1073/pnas.0602916103.

Zhuang, Min, Matthew F. Calabrese, Jiang Liu, M. Brett Waddell, Amanda Nourse, Michal Hammel, Darcie J. Miller, et al. 2009. “Structures of SPOP-Substrate Complexes: Insights into Molecular Architectures of BTB-Cul3 Ubiquitin Ligases.” *Molecular Cell* 36 (1): 39–50. https://doi.org/10.1016/j.molcel.2009.09.022.